Universidad del País Vasco
Euskal Herriko Unibertsitatea

Technical School of Engineering of Bilbao

Electronic Technology Department

PhD Thesis

Modular Multilevel Converters for Medium Voltage Applications: Low Switching Frequency Modulation Strategies and Circulating Current Control Techniques

Author: Ángel Luis Pérez Basante

Thesis Directors: Íñigo Martínez de Alegría Mancisidor, Salvador Ceballos Recio

Bilbao, May 2017

Mis padres
Santos y Esperanza

y mi mujer
Inés

Acknowledgements

A José Luis y Jaime, por darme la oportunidad de iniciar mi camino como investigador.

A mis directores de tesis, Salva e Íñigo, por todo lo que me han enseñado a lo largo de estos años y sin cuya ayuda no hubiera sido posible realizar esta tesis. ¡Gracias por vuestra paciencia!

A Jon e Íñigo y a todo el grupo APERT por todo lo que me habéis ayudado. ¡Me he sentido como en casa!

A mis compañeros de APERT, Víctor, Asier, Julen, Oier, Igor, Naiara, Itxaso, Estefi, Edorta, Iraide y David, por todos los consejos y momentos de apoyo y por los buenos ratos que hemos pasado juntos a lo largo de estos años. ¡Que sepáis que guardo el elefante rosa!

A Tecnalia, en especial a Salva, a Pedro, a Susana, a Jorge, a Maite y a Igor, por todo su apoyo y por darme la oportunidad de investigar y de trabajar con un grupo de personas tan válido.

A Georgios, thank you very much for your help!

A Inés, por animarme cada día y porque sin su ayuda y apoyo la realización de esta tesis no hubiera sido posible.

A mis padres, Inés madre, familiares y amigos, por todos sus consejos y ayuda durante estos años.

Muchas gracias a todos.

Bilbao, 2017.

Resumen

Los convertidores de media tensión han adquirido una gran relevancia en aplicaciones industriales y de tracción de alta potencia, así como en energías renovables. Esta tesis proporciona un estudio de los diferentes tipos de convertidores de media tensión, centrándose en el convertidor multinivel modular (MMC), debido a las ventajas que ofrece con respecto a otros convertidores. En concreto, debido a su utilidad en diferentes tipos de aplicaciones de media tensión, se ha elegido la topología MMC indirecta. Por lo tanto, se han estudiado su principio de funcionamiento, las distintas técnicas de modulación y de control existentes, los diferentes algoritmos de equilibrado de la tensión de los sub-módulos, así como el dimensionamiento de sus componentes.

El rendimiento de los MMCs en aplicaciones de media tensión (MV), en las que el número de sub-módulos (SMs) necesarios no es muy alto, se puede mejorar usando modulaciones de baja frecuencia de conmutación, tal como selective harmonic elimination-pulse width modulation (SHE-PWM), que proporciona un control estricto de los armónicos de orden inferior y pérdidas de conmutación bajas.

Se tienen que cumplir dos objetivos para utilizar SHE-PWM con la topología MMC indirecta. En primer lugar, es necesario el control de un alto número de armónicos en todo el rango del índice de modulación. De esta forma, se puede utilizar un amplio rango de frecuencias fundamentales, usando una frecuencia de conmutación similar, para diferentes valores de índice de modulación. Por lo tanto, sería conveniente desarrollar un nuevo método que simplifique el proceso de cálculo de los ángulos de disparo y que permita calcular un alto número de ellos. En segundo lugar, es necesario controlar la corriente circulante con el objetivo de reducir el rizado de la tensión de los condensadores de los SMs, así como las pérdidas del MMC.

En esta tesis se propone un método de cálculo, que se basa en dos nuevas formulaciones que permiten resolver el problema de SHE-PWM con simetría de cuarto

de onda (QW) y de media onda (HW), respectivamente. En concreto, se han considerado MMCs con (N+1) y (2N+1) niveles de tensión de salida de cada fase, obteniendo formas de onda (N+1) SHE-PWM y (2N+1) SHE-PWM, respectivamente, donde N es el número de SMs en cada rama del MMC. Este método de cálculo utiliza un sistema de ecuaciones único que es válido para cualquier forma de onda posible. Por lo tanto, es capaz de calcular simultáneamente, sin formas de onda predefinidas, tanto los patrones de conmutación como los ángulos de disparo asociados que resuelven el problema de SHE-PWM. En consecuencia, el proceso de búsqueda de los ángulos disparo se simplifica y se optimiza significativamente.

Además, esta tesis propone también dos técnicas de control de corriente circulante que se pueden aplicar junto con (N+1) SHE-PWM y (2N+1) SHE-PWM, respectivamente. Las técnicas de control propuestas no distorsionan la tensión de salida de la fase.

Finalmente, se han obtenido distintos resultados de simulación que han permitido validar las nuevas formulaciones propuestas para SHE-PWM con simetrías QW y HW, además de las técnicas de control de la corriente circulante propuestas para (N+1) SHE-PWM y (2N+1) SHE-PWM. Por otro lado, se han obtenido resultados experimentales, a partir de un prototipo de MMC con una sola fase, que han permitido validar la formulación con simetría QW y el control de la corriente circulante propuesto para (2N+1) SHE-PWM.

Laburpena

Erdi-tentsio bihurgailuek garrantzi handia lortu dute aplikazio industrialetan eta trakziokoetan, baita energia berriztagarrietan ere. Tesi honek mota desberdinen erdi-tentsio bihurgailuen ikerketa egiten du, *modular multilevel converter* (MMC)-n arreta ipiniz, beste bihurgailuekin konparatuta eskaintzen dituen abantailengatik. Hain zuzen ere, erdi-tentsio aplikazioetan hainbat erabilgarritasunengatik, zeharkako MMC topologia aukeratu da. Beraz, ikasi dira bere funtzionamendu-jatorria, modulazioko eta kontroleko teknika ezberdinak, azpimoduluen tentsioko orekatze algoritmoak, baita bere osagaien baloreak ere.

Erdi-Tentsioko (MV) aplikazioetan MMC-ren errendimendua hobe daiteke, beharrezko azpi-moduluko (SM) kopurua oso altua ez denean, kommutazioko behe-maiztasuneko modulazioak erabiliz. Esate baterako, *selective harmonic elimination-pulse width modulation* (SHE-PWM) modulazioa, beheko harmonikoen kontrol zorrotza eta kommutazio-galera baxuak ematen ditu.

Bi helburu bete behar dira SHE-PWM-a zeharkako MMC topologiarekin erabiltzeko. Lehenik, harmoniko askoren kontrola beharrezkoa da modulazio indize maila guztian. Horrela, funtsezko maiztasun ugari erabil daiteke, antzeko kommutazio maiztasuna erabilita, modulazio indizeko balio desberdinetarako. Beraz, egokia izango litzateke angeluen kalkulu prozesua sinplifikatzen duen, eta haietako kopuru handia kalkulatzea baimentzen duen, metodo berria garatzea. Bigarrenik, beharrezkoa da, SM-ko kondentsadoreen tentsioaren kizkurtzea txikiagotzeko, korronte zirkulatzailea kontrolatzea, baita MMC-ren galerak ere.

Tesi honetan kalkulu metodo bat proposatzen da, uhin laurden (QW) eta uhin erdiko (HW) simetria duen SHE-PWM arazoa konpontzea baimentzen duten bi formulazio berritan oinarritzen dena. Zehazki, kontuan hartu dira MMC-n (N+1) eta (2N+1) irteera tentsio mailak fase bakoitzeko, (N+1) SHE-PWM eta (2N+1) SHE-PWM uhin formak lortuz (N, MMC-ren adar bakoitzeko SM kopurua da). Kalkulu-metodo honek edozein uhin forma posibletarako den ekuazio-sistema

bakarra erabiltzen du. Beraz, gai da kalkulatzeko, bai kommutazio-patroiak, bai SHE-PWM arazoa konpontzen duten angeluak, guzti hau aurredefinitutako uhin-formarik gabe. Hori dela eta, angeluen bilaketa prozesua sinplifikatzen eta optimizatzen da.

Gainera, tesi honek korronte zirkulatzailearen kontroleko bi teknika ere proposatzen ditu, batera (N+1) SHE-PWM-rekin eta (2N+1) SHE-PWM-rekin erabili daitekeena. Proposatutako kontrol-teknikek ez dute fasearen tentsio irteera distortsionatzen.

Azkenik, lortu dira, QW eta HW simetriekin SHE-PWM-rako, proposatutako formulazio berriak baliozkotzea baimendu duten emaitza desberdinak, baita proposatutako korronte zirkulatzailearen kontrolak (N+1) SHE-PWM eta (2N+1) SHE-PWM-rako ere. Bestalde, emaitza esperimentalak lortu dira, fase bakarrarekiko MMC-ko prototipo batean, (2N+1) SHE-PWM-rako QW simetriarekiko formulazioa eta proposatutako korronte zirkulatzailearen kontrola baliozkotzea baimendu duena.

Abstract

Medium voltage converters have acquired a high relevance for high power industrial and traction applications as well as regenerative energy sources. This thesis provides an outcome of different kinds of medium voltage converters, focusing on the modular multilevel converter (MMC) due to its advantages with respect to other converters. In particular, due to its usefulness in different kinds of medium voltage applications, the indirect MMC topology has been selected. Therefore, the operating principle, modulations, control techniques, balancing algorithms and component sizing of indirect MMCs are studied.

The performance of modular multilevel converters (MMCs) in medium voltage (MV) applications, where the number of required sub-modules (SMs) is not high, can be improved utilizing low switching frequency modulations such as selective harmonic elimination-pulse width modulation (SHE-PWM), which provides tight control of lower order harmonics and low switching losses.

Two main challenges must be met to utilize SHE-PWM with indirect MMCs. Firstly, a high number of harmonics must be controlled throughout the modulation index range. In this way, a wide range of fundamental frequencies, using similar switching frequency and different modulation index values can be employed. Therefore, a new method which simplifies the process to calculate a high number of firing angles would be desirable. Secondly, the circulating current must be controlled with the aim of reducing the SM capacitor voltage ripple and the MMC losses.

This thesis proposes a calculation method, which is based on a novel formulation, to solve the SHE-PWM problem with quarter wave (QW) and half wave (HW) symmetries. In particular, MMCs with (N+1) and (2N+1) phase output voltage levels are considered, obtaining (N+1) and (2N+1) SHE-PWM waveforms, respectively, where N is the number of SMs at each arm. This method utilizes a unique system of equations which is valid for any possible waveform. There-

fore, it is able to calculate simultaneously, without predefined waveforms, both the switching patterns and the associated firing angles that solve the SHE-PWM problem. Consequently, the search process is simplified and optimized.

Furthermore, this thesis also proposes two circulating current control techniques which can be applied along with (N+1) SHE-PWM and (2N+1) SHE-PWM, respectively. The proposed control techniques do not disturb the phase output voltage.

Finally, simulation results have validated the proposed SHE-PWM formulations, with QW and HW symmetries, besides the circulating current control techniques proposed for (N+1) SHE-PWM and (2N+1) SHE-PWM. In addition, experimental results, obtained from a prototype of single-phase MMC, have validated the formulation with QW symmetry and the circulating current control proposed for (2N+1) SHE-PWM.

Content

List of figures

List of tables

Nomenclature

a_n	Fourier series coefficient, a_n
b_n	Fourier series coefficient, b_n
C	Sub-module capacitance [F]
Δv_c	Sub-module capacitor voltage ripple [V]
ΔW_{arm}	Arm energy variation [W]
ϵ_n	Normalized amplitude error of harmonic n
ϵ_{an}	Normalized amplitude error for a_n
ϵ_{bn}	Normalized amplitude error for b_n
F	Objective function
f	Fundamental frequency [Hz]
f_c	Carrier frequency [Hz]
f_{k-low}	Step sign at lower arm
f_{k-up}	Step sign at upper arm
$f_{sampling}$	Sampling frequency [Hz]
$f_{sw-effective}$	Effective switching frequency [Hz]
$f_{sw-(N+1)SHE-PWM}$	Effective switching frequency of (N+1) SHE-PWM [Hz]
$f_{sw-(2N+1)SHE-PWM}$	Effective switching frequency of (2N+1) SHE-PWM [Hz]
$f_{sw-IPD-PWM}$	Effective switching frequency of IPD-PWM [Hz]
$f_{sw-PD-PWM}$	Effective switching frequency of PD-PWM [Hz]
f_{valid}	Validation function
i_{circ}	Circulating current [A]
$i_{circ-2f}$	Second harmonic component of circulating Current [A]
$i_{circ,pos}$	Circulating current with positive sequence[A]
$i_{circ,neg}$	Circulating current with negative sequence[A]
i_a	Phase Output Current [A]
$\widehat{I}_a$	Phase Output Current Amplitude [A]
i_{comm}	Common mode current [A]
i_l	Lower Arm Current [A]
i_u	Upper Arm Current [A]
k_r	Normalized sub-module capacitor voltage ripple
l	Number of firing angles in the first quarter wave
L	Arm inductance [H]
L	Number of levels of modular multilevel converter
L_k	Voltage level after step k
L_L	Minimum allowed voltage level [V]
$L_{initial}$	Initial voltage level [V]
L_{final}	Final voltage level [V]
m_1	Modulation index 1
m_2	Modulation index 2
m_a	Modulation index
m_{a-low}	Modulation index in the lower arm
m_{a-up}	Modulation index in the upper arm
m_k	Sign of every voltage step
N	Number of sub-modules at every arm of MMC

p_u	Upper arm power [VA]
p_l	Lower arm power [VA]
P_S	Apparent power [VA]
ϕ	Output current phase [rad]
ϕ_1	Fundamental phase of output voltage [rad]
θ	Firing angle [rad]
$\theta_{virtual}$	Virtual firing angle [rad]
U_L	Maximum allowed voltage level [V]
v_{a0}	Phase Output Voltage [V]
V_c	Sub-module capacitor averaged voltage [V]
v_c	Sub-module capacitor voltage [V]
v_{cm}	Common mode voltage [V]
v_{diff}	Differential Voltage [V]
v_{dc}	DC bus voltage [V]
V_L	Step voltage amplitude [V]
V_{ref}	Reference voltage [V]
$\widehat{V}_{upper,2}$	Second harmonic of upper arm voltage amplitude [V]
ω	Angular fundamental frequency [rad/s]
ω_{cm}	Angular frequency of common mode voltage [rad/s]

List of acronyms

APERT *Applied Electronics Research Team*

AC *Alternate Current*

APOD-PWM *Alternative Phase Opposition Disposition Pulse Width Modulation*

CSC *Current Source Converter*

CCC *Capacitor Commutated Converter*

CD *Clamped Doubled*

CFBC *Cascaded Full-Bridge Converter*

CTV *Convergence Threshold Value*

DC *Direct Current*

DE *Differential Evolution Algorithms*

FCC *Flying Capacitor Converter*

FOC *Field Oriented Control*

FPGA *Field Programmable Gate Array*

FB *Full-Bridge*

GA *Genetic Algorithm*

GHNN *Generalized Hopfield Neural Network*

HB *Half-Bridge*

HDF *Harmonic Distortion Factor*

HLF *Harmonic Loss Factor*

HV *High Voltage*

HVDC *High Voltage Direct Current*

HW *Half-Wave*

HMMC *Hybrid Modular Multilevel Converter*

IGBT *Insulated Gate Bipolar Transistor*

IGCT *Integrated Gate Commutated Thyristor*

IPD *Initial Population Definition*

IPD-PWM *Interleaving Phase Disposition Pulse Width Modulation*

IPM *Instantaneous Power Mode*

LCC *Line Commutated Converter*

LCI *Line Commutated Inverter*

LFM *Low Frequency Mode*

LV *Low Voltage*

LVAC *Low Voltage Alternate Current*

LVDC *Low Voltage Direct Current*

MMC *Modular Multilevel Converter*

MPC *Model Predictive Control*

MPM *Mean Power Mode*

MV *Medium Voltage*

MVAC *Medium Voltage Alternate Current*

MVDC *Medium Voltage Direct Current*

MTDC *Multi-Terminal Direct Current*

MVSC *Multilevel Voltage Source Converter*

MVSI *Multilevel Voltage Source Inverter*

NLC *Nearest Level Control*

NPCC *Neutral-Point Clamped Converter*

NSV *Nearest Space Vector*

OP *Optimization Process*

PI *Proportional-Integral*

PLL *Phase-Locked Loop*

PWM *Pulse Width Modulation*

PD-PWM *Phase Disposition Pulse Width Modulation*

POD-PWM *Phase Opposition Disposition Pulse Width Modulation*

PS-PWM *Phase Shifted Pulse Width Modulation*

PSO *Particle Swarm Optimization Algorithms*

QW *Quarter-Wave*

SHE-PWM *Selective Harmonic Elimination - Pulse Width Modulation*

SHM *Selective Harmonic Mitigation*

SM *Sub-module*

SPWM *Sinusoidal Pulse Width Modulation*

STATCOM *Static Synchronous Compensator*

SVM *Space Vector Modulation*

SVC *Space Vector Control*

THD *Total Harmonic Distortion*

THDM *Total Harmonic Distortion Minimization*

VOC *Voltage Oriented Control*

VSC *Voltage Source Converter*

VSI *Voltage Source Inverter*

ZCS *Zero Current Switching*

ZVS *Zero Voltage Switching*

Chapter 1

Introduction

1.1 Context of the Thesis

This work has been realized in the Applied Electronic Research Team (APERT), at the Electronic Technology Department of the University of the Basque Country (UPV/EHU), in collaboration with Tecnalia Research & Innovation. In particular, this work is included in the research line related to medium voltage (MV) converters. This line studies the different kinds of medium voltage converters and their possible applications, such as medium voltage drives or medium voltage direct current (MVDC) distribution and collection (in offshore wind farms) networks, focusing on the development of new topologies and control techniques which reduce the cost and improve the efficiency.

This thesis has been supported by Zabalduz program, a UPV/EHU PhD scholarship funding and has been developed within the following set of projects developed by the Applied Electronic Research Team (APERT) and Tecnalia Research & Innovation:

- FUTUREGRIDS-2020: New technology offer for smart grids by 2020. Offshore HVDC and LV networks operation (IE14-389). Funded by Basque Government within the research program ETORTEK
- HVDCLINK1, HVDCLINK2 (KK-2015/00091-HVDCL-1, KK-2016/00038-HVDCL-2) and HVDCLINK3. HVDC link for extraction of marine energy. Funded by Basque Government within the research program ELKARTEK

1.2 Background

Medium voltage converters have acquired high relevance for high power industrial and traction applications as well as renewable energy sources [1–3]. In case of direct conversion, cycloconverter is the most utilized topology, providing high efficiency and power flow in both directions. However, this technology provides a limited dynamic performance. This issue can be addressed utilizing voltage source converters (VSCs) or current source converters (CSCs). CSCs are classified in line commutated converters (LCCs) and pulse width modulation - current source converters (PWM-CSCs). Comparing CSCs and VSCs, the latter, which are based on insulated gate bipolar transistors (IGBTs), have experienced a higher market penetration and a higher development over last years [2]. In particular, VSCs provide lower losses than PWM-CSCs, due to the lower number of semiconductors connected in series. On the other hand, VSCs provide smaller footprint, reduced harmonic content, bi-directional active and reactive power flow, insensitivity to the strength of the ac network or extended operating range, with respect to LCCs.

Regarding VSCs, the multilevel concept provides a lower effective switching frequency than its two-level counterpart. The effective switching frequency of multilevel voltage source converters (MVSCs) is inversely proportional to the number of levels [4], endowing MVSCs with higher efficiency than two-level converters. Moreover, lower total harmonic distortion (THD) is obtained due to the multilevel characteristic, which allows the converters to follow the reference signal more accurately and with lower dV/dt, facilitating the use of smaller harmonic filters and reducing the insulation requirements [2, 5, 6].

Among the different MVSC topologies, the modular multilevel converter (MMC) [7], presents higher scalability and reliability [5]. In addition, the absence of a common dc bus capacitor [8] and the use of capacitor voltage balancing algorithms, which are able to balance the sub-module (SM) capacitor voltages under any working condition, are also advantages of MMCs. Therefore, the utilization of MMCs in MV applications is currently being explored [9, 10]. In particular, the indirect MMC topology is studied in this thesis due to its possible applications, such as medium voltage drives or medium voltage direct current (MVDC) networks.

One of the main goals of new modulation and control techniques for indirect MMCs is the improvement of its efficiency. In this way, low switching frequency modulations, such as selective harmonic elimination - pulse width modulation (SHE-PWM), are suitable to reduce simultaneously the switching losses and the harmonic content, when the number of SMs is not too high [11, 12].

The main challenges which must be met to apply SHE-PWM to indirect MMCs is the simplification of the calculation method to obtain the firing angles and the control of the circulating current. The latter improves the operation of the converter. In addition, controlling a high number of harmonics would be desirable to obtain a low total harmonic distortion and a wide range of fundamental frequencies. In this way, a research effort should be applied to address both issues.

1.3 Objectives of the Study

With the aim of improving the efficiency of converters which operate in medium voltage applications, this thesis aims to address the following objectives:

- State of the art of medium voltage converters: The existing medium voltage converters are studied and their main features are compared
- Study of the operation of indirect modular multilevel converters (MMCs): Due to their advantages with respect to other multilevel converters, the operation of MMCs and their possible MV applications will be studied in depth.
- Contributions to the implementation of SHE-PWM and its application to indirect MMCs, with the aim of increasing the MMC efficiency and reducing its total harmonic distortion:
  - Development of two novel formulations to solve the SHE-PWM problem with quarter (QW) and half-wave (HW) symmetries, respectively. The objective is eliminating the requirement of predefined waveforms to search the firing angles. In this way, the search process would be significantly simplified, with respect to previous methods and a high number of different solutions could be found for every modulation index value.
  - Employing the proposed formulations to solve SHE-PWM, development of a search method, based on genetic algorithms (GAs), to find the firing angles. In particular, the objectives are eliminating a high number of harmonics and finding several different solutions for every modulation index value
  - Development of two novel circulating current controls for indirect MMCs, which can be applied along with (N+1) SHE-PWM and (2N+1) SHE-PWM, respectively. The objective is obtaining simul-

taneously low SM capacitor voltage ripple, low MMC losses and low total harmonic distortion (THD)

1.4 Contents of the Thesis

This document contains 6 chapters and 2 appendixes. Besides the introductory chapter, the contents of the document are as follows:

Chapter 2. **Medium Voltage Power Systems**: This chapter contains the study of the state of the art of medium voltage converters. Because of its advantages, the indirect MMC operation is studied in depth along with its utilization in medium voltage applications. In this way, the operating principle, modulations, control techniques, balancing algorithms and component sizing of indirect MMCs are studied.

Chapter 3. **Selective Harmonic Elimination - Pulse Width Modulation**: Due to its ability to provide simultaneously low switching losses and a tight control of lower order harmonics, this chapter analyses the selective harmonic elimination - pulse width modulation (SHE-PWM) and its application to indirect MMCs. In particular, the different symmetries and its corresponding formulations, besides the different implementations in indirect MMCs, (N+1) SHE-PWM or (2N+1) SHE-PWM, are studied. In addition, the state of the art of the different calculation methods to solve the SHE-PWM problem is studied.

Chapter 4. **Novel Technique to Implement SHE-PWM**: This chapter proposes two formulations for SHE-PWM with quarter-wave (QW) and half-wave (HW) symmetries, respectively, which do not use predefined waveforms to solve the problem, unlike previous formulations. In this way, the search of firing angles is simplified and more solutions could be found for a particular modulation index value. This fact is significantly important in case of multilevel converters, such as MMCs, where a particular waveform could not be useful to find a solution for a determined modulation index value. In addition, in case of multilevel converters, different waveforms are required to find a solution throughout the modulation index range. On the other hand, a search method, based on genetic algorithms, is proposed to calculate the firing angles. In this way, a high number of firing angles can be eliminated. The different solutions obtained with the proposed formulations are analysed and validated by simulation and experimental results.

Chapter 5. **Novel Circulating Current Control Methods for MMC with SHE-PWM**: This chapter proposes two circulating current control techniques for indirect MMCs, which can be applied with (N+1) SHE-PWM and (2N+1) SHE-PWM, respectively, without disturbing the phase output voltage. In this way, the dc component of the circulating current and the energy stored in the different sub-modules (SMs) of the indirect MMC are adjusted to their references. In addition, the energy balance between the upper and lower arms at every phase is maintained. In this way, it is possible to achieve a low SM capacitor voltage ripple and simultaneously to get benefit from the low switching losses and low total harmonic distortion (THD) provided by (N+1) SHE-PWM and (2N+1) SHE-PWM.

Chapter 6. **Conclusions and Future Work**. The chapter included in this part presents the main conclusions and contributions obtained in this thesis. In turn, the main publications provided by this thesis are described and the future research lines derived from this work are detailed.

Appendix A. **Algorithm Results for a Low Number of Controlled Harmonics**: This chapter contains the performance factors provided by the different solutions obtained throughout the modulation index range, when a low number of harmonics is controlled. In particular, six different cases are regarded, where the MMCs provide different number of levels and controlled harmonics, besides different symmetry (QW or HW). The analysis of the results is included in chapter 4.

Appendix B. **Algorithm Results for a High Number of Controlled Harmonics**: This chapter contains different solutions obtained for particular modulation index values when a high number of harmonics is controlled. Both the firing angles and the harmonic content are shown. The obtained results are analysed in chapter 4.

Chapter 2

Medium Voltage Power Systems

2.1 Introduction

Medium voltage converters are gaining very high relevance for high power industrial and traction applications as well as renewable energy sources [1]. This chapter provides an overview of different kinds of medium voltage converters, focusing on the modular multilevel converter (MMC) due to its advantages with respect to other converters, as it is described in next section. In particular, due to its usefulness in different kinds of medium voltage applications, the indirect MMC topology is studied. Therefore, the operating principle [13], modulations, control techniques, balancing algorithms and component sizing of indirect MMCs are studied.

2.2 Medium Voltage (MV) Converters

Different technologies, which are included at Fig. 2.1, can be utilized to implement medium voltage converters [2, 4–6, 14, 14–30]. These technologies are classified into three main families: cycloconverters, current source converters (CSCs) and voltage source converters (VSCs):

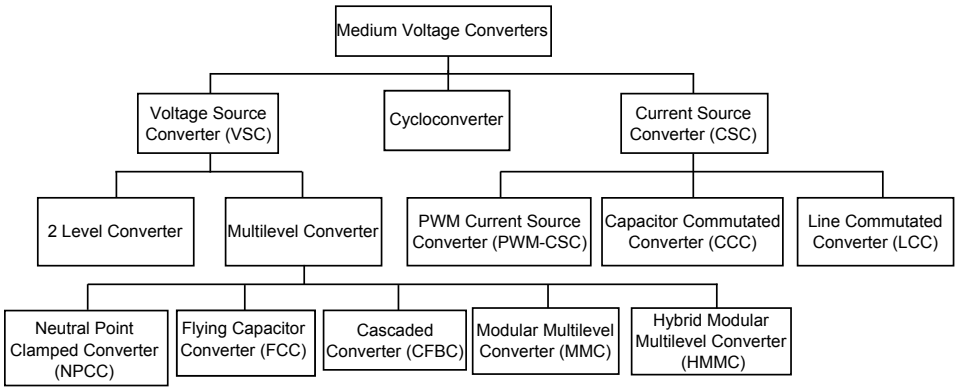

Figure 2.1. Classification of medium voltage converters.

2.2.1 Cycloconverters

The cycloconverter, whose topology is depicted at fig. 2.2, is based on conventional thyristors [1] and is a widely used topology in high-power applications. This converter makes it possible the conversion of a three-phase ac voltage with fixed frequency and magnitude to variable frequency and variable magnitude. Cycloconverters allow the transfer of energy in both directions but with limited dynamic performance [2].

2.2.2 Current Source Converters (CSC)

There are two different kinds of current source converters which have been industrially commercialized [2, 6, 14, 16–18]:

2.2.2.1 Line commutated converter (LCC)

LCCs which are based on thyristors consist on a rectifier stage, a dc link choque and an inverter section which provides a variable magnitude and variable frequency output [16]. On the one hand, its main features are simple topology, low manufacturing cost and reliable operation. On the other hand, its main drawbacks are low input power factor and distorted input current [2].

A relevant topology, based on LCC technology, which is specially suitable for high power applications, is the multi-pulse converter. When it is used as a rectifier,

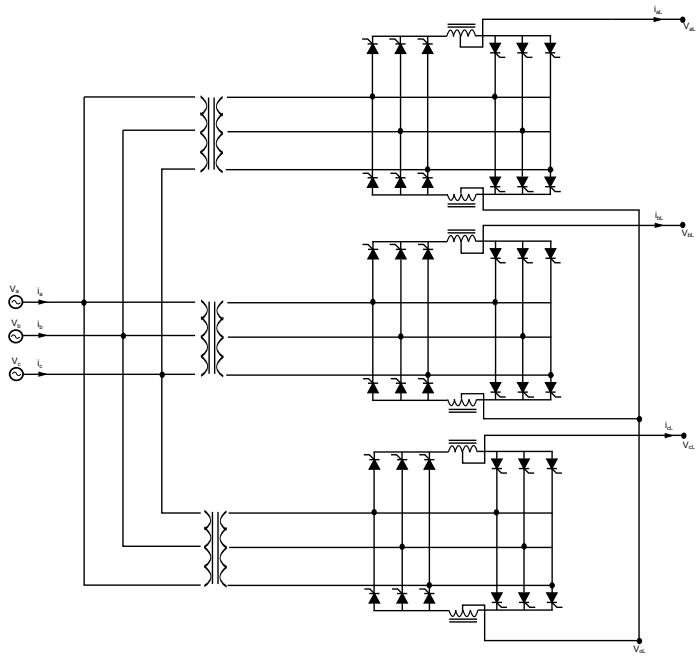

Figure 2.2. Three phase cycloconverter topology.

it offers the possibility to manage a high input voltage and a low level of input-current harmonics. In fig. 2.3-(a) 12, 18 and 24 pulse circuit configurations are depicted [2].

2.2.2.2 Capacitor commutated converters (CCC)

CCCs represented a breakthrough in LCC technology [14]. As it can be seen at fig. 2.3-(b), commutation capacitors, which are placed between the transformer and the thyristor bridge, provides reactive power compensation that is proportional to the load of the converter. Therefore, shunt capacitors are no more required to compensate the reactive power and the AC filters can be only devoted to eliminate undesired harmonics.

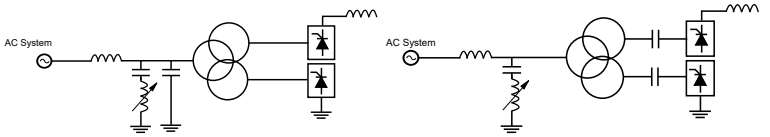

(a) LCC topology. (b) CCC topology.

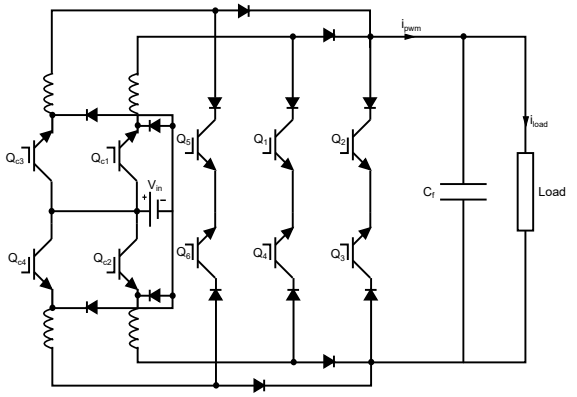

(c) CSC-PWM topology.

Figure 2.3. Current source converters.

2.2.2.3 Current Source Converter - Pulse Width Modulation (CSC-PWM)

This technology is based on power switching devices as IGBTs or MOSFETs in series with diodes, as it is shown in Fig. 2.3-(c). Taking into account the inverter topology, this converter features a capability of short-circuit protection due to its high impedance dc power source, but a protection against open circuit is required to guarantee continuity of the current. The main drawbacks are the utilization of bulky inductors to obtain smooth DC currents, and the discrete diodes connected in series which increase the losses [17]. The latter can be fixed thanks to the emergence of IGBTs with reverse-blocking capability which can be used instead [18]. On the other hand, the current can only be conducted in one direction and therefore, the polarity of the dc voltage must be reversed to obtain power reversal.

Nowadays, despite the fact that current multilevel topologies are available, every cell must be rated at a full ac line-to-line voltage blocking capability, and there-

Table 2.1. High-Power Fully Controlled Semiconductors

Acronym	Type	Full Name
IGBT	Transistor	Insulated Gate Bipolar Transistor
IEGT	Transistor	Injection Enhanced Gate Transistor
GTO	Thyristor	Gate Turn-off Thyristor
IGCT	Thyristor	Integrated Gate Commutated Thyristor
GCT	Thyristor	Gate Commutated Turn-off Thyristor

Table 2.2. IGBTs Rating and Blocking Voltages

Rating Voltage	6.5kV	4.5kV	3.3kV	1.7kV
Blocking Voltage	4.0kV	2.9kV	2.1kV	1.1kV

fore, for medium or high voltage applications a large number of semiconductors connected in series is required. As a result, the efficiency is lower than the one obtained with voltage source converters [6].

2.2.3 Voltage Source Converters (VSC)

VSCs are based on high-voltage high-power fully controlled semiconductors whose implementation can be related to thyristor or transistor technology, as it can be seen in table 2.1 [15].

The first device employed in VSC was the 4.5 kV gate-turn-off thyristor (GTO). Afterwards, the emergence of high-power insulated-gate bipolar transistors (IGBTs) and integrated gate-commutated thyristors (IGCTs) provided the following advantages [2]:

- Superior switching characteristics.
- Reduced power losses.
- Ease of gate control.
- Snubberless operation.

Some of the most used high power semiconductors in VSC converters are IGBT modules, whose rating and blocking voltages are included at table 2.2 and IGCTs with 4.5 kV and 5.5 kV rating voltages [2, 19].

Voltage source converters offer several advantages over line commutated converters [1, 4, 6, 15, 20]:

- Increased availability because of ride-through capability and redundant topologies.
- Improved dynamic performance due to higher switching frequency of PWM. It offers a lower level of harmonics and smaller filters.
- Extended operating range.
- Reduced line harmonics.
- Fast and decoupled control of bi-directional active and reactive power flow.
- Black start capability.
- Smaller station footprint.
- Insensitivity to the strength of the AC network.
- Avoidance of commutation failures because of disturbances in the ac network.
- No requirement of transformers to help the commutation process due to the utilization of fully controlled semiconductors.
- Ability to feed island and passive networks.

The larger size of LCC stations is due to the requirement of large filters and/or the static synchronous compensator (STATCOM) associated, which is in charge of supporting the reactive power control and the voltage needed in the LCC commutation [4]. Otherwise, the main advantages of LCC technology over VSC is a higher power rating or the same rating at lower cost and higher efficiency [1]. However, this difference in efficiency has been reduced by MMCs [4, 31].

There are different kinds of voltage source converters:

2.2.3.1 Two-Level VSCs

Two-level three-phase bridge, whose topology is depicted at Fig. 2.4-(a) is the simplest VSC topology which is employed in low or medium power applications. The anti-parallel diodes ensure four-quadrant operation and the dc bus capacitor provides sufficient energy storage to control the power flow and to filter the dc harmonics [15]. To meet the challenge of managing higher power, many series-connected IGBTs are utilized with the aim of obtaining a higher blocking voltage capability and film capacitors are used in series to reach the required dc-bus voltage [2]. However, the efficiency and the output voltage quality provided by

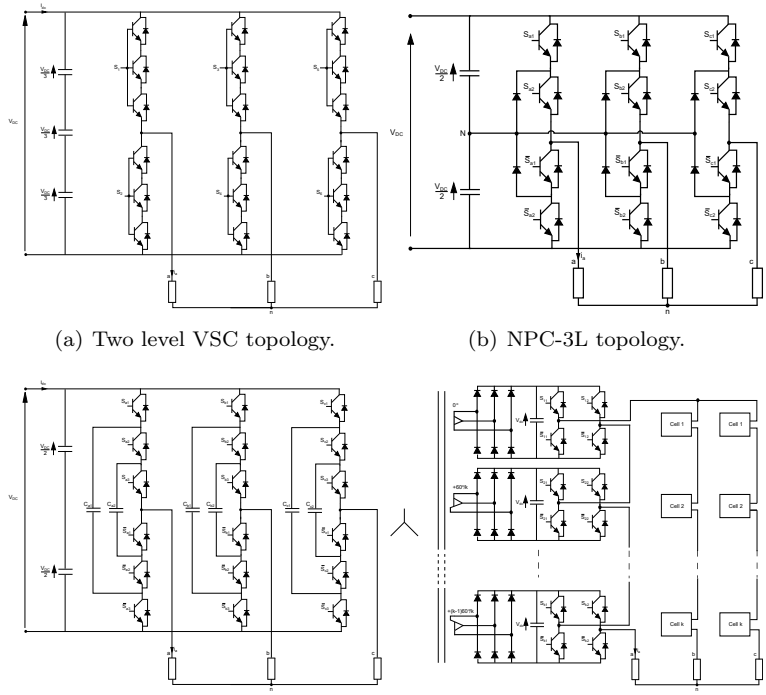

(a) Two level VSC topology. (b) NPC-3L topology.

(c) FC-4L topology. (d) CFBC-(2k+1)L topology.

Figure 2.4. Voltage source converters.

2-level converters are lower than the efficiency and quality provided by multilevel converters [2].

2.2.3.2 Multilevel VSCs

The VSC technology has reached its fourth generation where multilevel topologies are used to manage high power systems [6]. The multilevel concept offers a lower effective switching frequency (1KHz for three-level converters and being reduced as the number of levels increases [4]), than two level converters do, providing a higher efficiency. Moreover, a lower total harmonic distortion is obtained due to the multilevel characteristic, which makes it possible for the converter to follow the reference signal more accurately. In addition, lower dV/dt, lower common-mode voltage, smaller and simpler harmonic filters, together with lower insulation

requirements make the multilevel topologies a suitable option for medium/high voltage applications [2, 5, 6].

Several converters have been industrially commercialized so far [32]. Three level neutral-point clamped converter (NPCC), four level flying capacitor converter and cascaded full-bridge converter of 9, 11 and 13 levels are the most relevant topologies. The voltage covered by them ranges from 2.3 to 13.8 kV and its related apparent power ranges from 0.3 kVA to 32 MVA, respectively [2].

2.2.3.2.1 Three level Neutral-Point Clamped Converters (NPCC)

The operation of the NPCC is based on the utilization of diodes which link the midpoint of the upper and lower arms at every phase to the neutral point of the converter, making a three-level output possible. The main challenge for the correct performance of the converter, which has already been met by different studies, is the control of this neutral point voltage. The topology of this converter, whose scheme is depicted in fig. 2.4-(b), allows every semiconductor to be exposed to half the dc-link voltage. This feature provides the extension of voltage and power ranges compared to two-level converters (for example, NPCCs which provide 2.3-4.16 kV are applied in industrial applications), apart from the reduction of the total harmonic distortion (THD). In case of aiming a higher output voltage, line to line voltages of 4.16-7.2 kV can be achieved using IGCTs of 10kV or series connections of more conventional devices [2].

Despite the fact that more output voltage levels can be generated, these topologies have not found acceptance so far [2]. In case of more than 3 levels, an inherent imbalance appears in the series-connected dc capacitors, and therefore, an external balancing circuit is required, like a buck-boost chopper, between them. Besides this issue, the increment of the number of clamping diodes renders the building of the converter more complex [33]. On the other hand, one of the main issues of NPCCs is the uneven distribution of losses between the IGBTs, which reduces the reliability of the system. However, this problem has been fixed using the active neutral point clamp converter (ANPC) [4] which uses active switches, homogenizing the losses in the semiconductors to increase the allowable converter power throughput [34] or alternatively the switching frequency [2].

2.2.3.2.2 Four-level Flying Capacitor Converters (FCC)

The topology of this converter, depicted in fig. 2.4-(c), is based on the series connection of three commutation cells whose blocking voltage is the third of the dc-bus voltage. Moreover, it offers redundant states with different polarities

in the currents through the flying capacitors which provides the possibility to balance their voltage. Line to line voltage could reach values of 6 kV and 4 MVA, using 6.5 kV 600 A IGBTs [2].

On the other hand, the high cost of flying capacitors at switching frequencies lower than 1kHz represents an important drawback [33]. This technology requires the use of large capacitors with different voltage ratings, which increases the footprint and reduces the level of modularity, finding this technology unsuitable for more than five levels [4]. Despite these problems, currently, a four level FCC is industrially commercialized [34].

2.2.3.2.3 Cascaded Full-Bridge Converters (CFBC)

This converter, represented in fig. 2.4-(d), has been used as a MV high power drive, with voltage, current and power rating of 13.8 kV, 1400 A and 31 MVA, respectively, thanks to its modular topology and power quality operational characteristics. Its structure is based on several sub-modules (SMs) per phase which contain a full-bridge (FB), a dc-link capacitor, a three phase diode rectifier or an active front end (AFE) and an isolated voltage source provided by transformer secondaries or batteries. The secondary windings are phase shifted for input-current harmonics reduction. The increase in the number of SMs improves the input current and output voltage quality [2].

Moreover, the introduction of unequal dc sources in the CFBC provides a reduced converter size and cost, because more output voltage levels can be obtained with a lower number of sub-modules, and consequently a higher reliability besides a reduction of the switching losses with an appropriate control. Particularly, high power cells will operate approximately at fundamental switching frequency and on the other hand, low power cells will operate with high switching frequency modulations, performing a hybrid modulation [2, 6]. However, in this topology the modularity and the redundancy are lost, requiring a special voltage and a special design for every cell, and there is not harmonic cancellation in the input current. On the other hand, using voltage relationships between voltage cells in powers of two offers higher redundancy and reduced switching frequency [2].

The main drawback of cascaded converters is the requirement of multi-winding transformers, which are usually bulky and non-standard and the impossibility of using a single dc source [34].

2.2.3.2.4 Modular Multilevel Converters (MMCs)

The MMC was first presented in [21, 22] as a converter which provides a high quality output voltage waveform and a high efficiency [35]. Therefore, it is suitable for high power and high voltage applications such as HVDC [24], as well as for electric railway supplies and other industrial applications [19]. Its application to high power drives is currently under research [23, 36–40].

Besides the intrinsic advantages associated to multilevel VSCs, MMCs offer a higher degree of scalability than other multilevel converters because of the simplicity of their sub-modules and a higher reliability due to the possibility of bypassing damaged sub-modules (SMs) [5]. These features make it possible to lower the switching losses and the filter requirements due to reduced level of harmonics [4]. Moreover, a common dc bus capacitor can be avoided because of the use of sub-modules which contain smaller capacitors [8] and DC faults can be overcome thanks to the utilization of bipolar sub-modules [6].

MMCs are expected to be the new generation of converters which can be employed in medium or high voltage applications without the requirement of low frequency transformers [41]. These transformers make the converter heavier and bulkier and induce a dc magnetic flux deviation when a single-line-to-ground fault occurs [33]. Therefore, it could be an interesting topology to be used as a MV drive or to obtain MVDC at the output of every offshore wind turbine.

There are 4 main MMC topologies:

- Single-star/Single-delta topologies: These topologies, which are depicted at Fig. 2.5-(a) and 2.5-(b), respectively, can be utilized as a STATCOM [25]. Both converters are able to maintain the capacitor voltages balanced under unbalanced conditions, inserting zero-sequence voltage and current, in case of star and delta configurations, respectively. However, a singularity exists, in case of delta configuration, when the positive and negative sequences of the applied voltage at the converter terminals are equal. For the star case, the singularity exists when the positive and negative sequences of the injected current are equal [42]. Considering this fact, the star topology is suitable, due to the lower number of required SMs, for utility applications which primarily require positive-sequence currents [43]. On the other hand, in case of industrial applications, where for instance flicker mitigation could be necessary, the required negative-sequence current could be high. In this case, the delta configuration must be utilized. In addition, both converters can manage active power in the event of implementing a battery energy storage system. Both topologies require bipolar SMs [25].

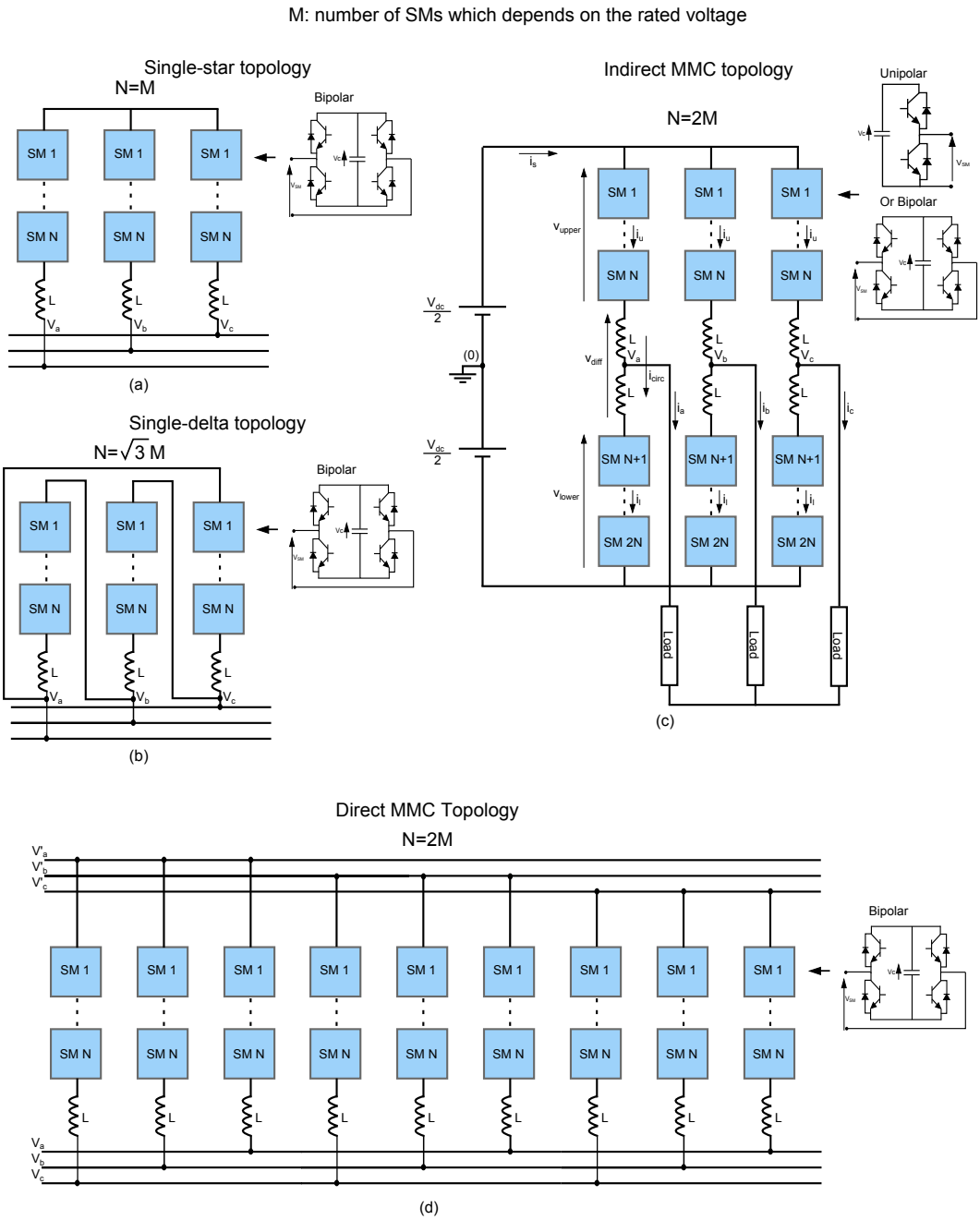

Figure 2.5. Modular multilevel converter (MMC) topologies.

- Indirect (DC/AC or AC/DC) topology: This converter, which is depicted at Fig. 2.5-(c), can be utilized as an inverter, a rectifier or a STATCOM. In the latter case, this converter is able to control negative-sequence reactive power, taking advantage of its circulating current at every phase. On the other hand, the SMs could be unipolar or bipolar. Bipolar SMs provide fault tolerant properties, together with boost or buck functions of the DC bus voltage [25, 29], but higher conduction losses [6].
- Direct (AC/AC) topology: The scheme of this converter is depicted at fig. 2.5-(d), where the SMs must be bipolar. [44] provides two different control modes, mean power mode (MPM) and instantaneous power mode (IPM). The first one is able to balance the SM capacitor voltages at every arm, except for the case where one of the two fundamental frequencies is zero. This drawback can be addressed utilizing IPM. In this way, in case of very low fundamental frequencies, the direct MMC can be operated with lower switching losses than indirect MMC, maintaining a SM capacitor voltage ripple lower than 10% [44].

The main advantage of indirect and direct MMCs with respect to other modular converters such as single-star MMC, single-delta MMC or CFBC is the possibility to transfer active power without using batteries [25] or dc sources isolated by means of a transformer and a rectification stage [21], respectively. Every SM, which is a VSC, contains a capacitor whose voltage will be balanced by the commutation process. On the other hand, using a duality concept, CS sub-modules could be utilized to obtain a multilevel current source converter. However, for MV applications, CS-MMCs provide higher losses than VS converters due to their higher number of semiconductors which are connected in series [6]. Because of this reason, only VS-MMCs are taken into account in this work.

Regarding the DC/AC MMC, this converter presents a great variety of topologies depending on the kinds of SMs and the number of phases used [6]. As it is shown in table 2.3, a great variety of basic SMs have been proposed in the literature. All of them present different features related to complexity, number of voltage levels, conduction losses, number of components, bipolar operation and voltage blocking capability. Unlike in case of DC/AC MMC, AC/AC topology may only use bipolar SMs.

Among all possible SMs, half-bridge (HB) is the simplest topology[28, 29], offering a simple control and the lowest conduction losses. However, unlike it happens with more complex cells, more SMs are required to obtain the same number of levels, increasing the communication load, besides the drawback of not presenting bipolar operation. The latter can be addressed using full-bridge (FB) SMs [45]. However, this increases the conduction losses. These can be reduced using mixed

Scheme	Properties	Scheme	Properties
	• SM: Half-Bridge(HB)[28, 29] • Number of output voltages: 2 • Bipolar operation: No • Control complexity: Low	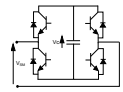	• SM: Full-Bridge(FB)[29, 45] • Number of output voltages: 3 • Bipolar operation: Yes • Control complexity: Low
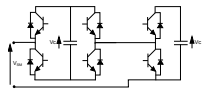	• SM: Mixed (M) [6] • Number of output voltages: 4 • Bipolar operation: Yes • Control complexity: Low	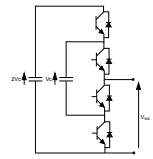	• SM: Flying Capacitor (FC)[26, 27] • Number of output voltages: 3 • Bipolar operation: No • Control complexity: High
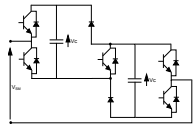	• SM: Clamped-Double(CD)[46, 47] • Number of output voltages: 4 • Bipolar operation: Yes • Control complexity: Low	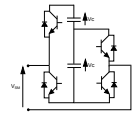	• SM: Asymmetrical (A)[6] • Number of output voltages: 4 • Bipolar operation: Yes • Control complexity: High
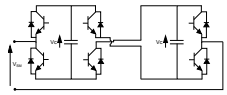	• SM: Cross FB-HB (C-FH)[46] • Number of output voltages: 5 • Bipolar operation: Yes • Control complexity: Low	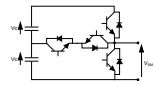	• SM: T connected NPC(T-NPC)[28, 29] • Number of output voltages: 3 • Bipolar operation: No • Control complexity: High

Table 2.3. MMC Sub-modules(SM)

(M) cells between HB and FB SMs [46]. Going further, in case of using crossed cells (C-FH), due to its ability to produce more levels, the number of SMs can be reduced, also reducing the footprint of the converter [46].

Three level NPCC and FCC SMs have also been proposed [6, 26, 27]. They provide a reduction in the number of cells in comparison with HB, although NPCC is not able to achieve a successful capacitor voltage balancing for some operating conditions. Hence, FCC is considered as a better option [26, 27]. Finally, both asymmetrical (A) and clamped-double (CD) SMs offer four voltage levels and a bipolar operation and therefore, they can be regarded as promising topologies in the future [6, 46, 47].

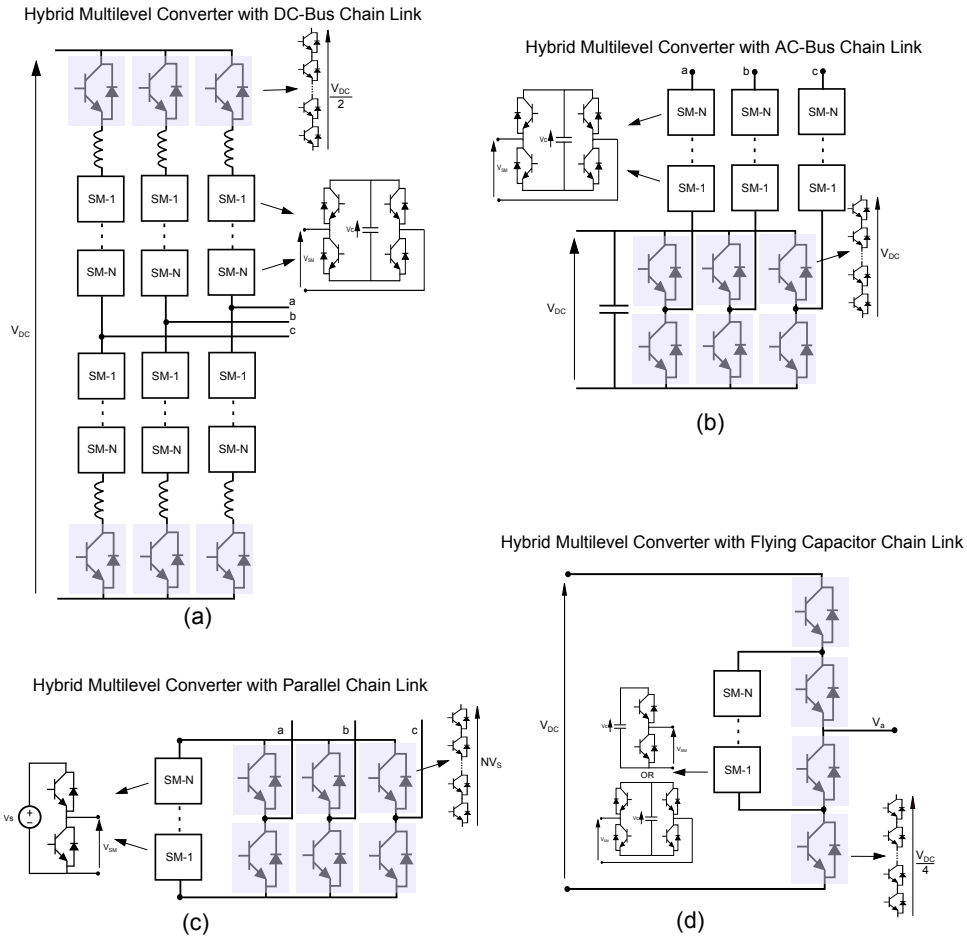

Figure 2.6. Hybrid modular multilevel converters.

2.2.3.2.5 Hybrid Modular Multilevel Converters (HMMCs)

Hybrid converters are based on monolithic and modular structures containing both director switches and chain-links of sub-modules. These director switches consist of series connection of devices and are used to implement a monolithic converter. Therefore, it is possible to obtain a multilevel waveform with less sub-modules and a lower number of switching components than in the conventional MMC topologies [28, 29], offering lower switching losses. However, these

topologies present higher conduction losses because of the employment of director switches which additionally require zero voltage or fundamental switching, resulting in a limited independent active and reactive power control [6]. In addition, in some cases a dc or a small ac filter is required due to an inaccurate synchronization between the director switches and the sub-modules [30]. Different types of hybrid modular converters are depicted at Fig. 2.6.

2.2.4 Market Tendency in High Power - Medium Voltage Drives

Considering the market of high power drives, the largest manufacturers of cycloconverters have been ABB (ACS 6000C) [48], Siemens (SIMOVERT D) [49], Toshiba (Tosvert-μ/S850) and Alstom (ALSPA CL9000) [50]. However, due to the output frequency limitations, high harmonic content and low power factor, currently, in those applications up to 40 MW, the tendency is replacing cycloconverters with medium voltage source inverters (MVSIs) (using a rectifier-MVSI topology with intermediate DC bus) or line commutated inverters (LCIs) [2].

Due to the breakthroughs in new semiconductor technologies and new multilevel topologies, currently, cycloconverters are being replaced with these converter families:

- MVSIs: ACS 6000 of ABB [51], SINAMICS ML-150 of Siemens [52] or Ingedrive MV500 of Ingeteam [53], among others. Additional topologies are offered by Ingeteam for ship propulsion [54].
- LCIs: Megadrive-LCI of ABB [55], Sinamics GL-150 LCI of Siemens [56] or POWERFLEX-7000 of Rockwell automation [57].

LCIs represent the most efficient and reliable alternative to manage power higher than 20 MW [58]. However, the number of installations of VSIs have increased considerably with respect to LCI installations, due to the VSC advantages described in section 2.2.3 [2]. For instance, despite the fact that the largest converter for synchronous machines (100 MW [59]) in 2009 was a LCI, this converter was not selected, due to its high harmonic content and other limitations, to renew the generation and water pumping systems in the hydroelectric power station Grimsel 2 (4 pumps of 80 MW) of Oberhasli Hydroelectric Power Company (KWO). Instead, a VSI with IGCTs was selected [60].

Table 2.4. Proposed and Real MVDC Network Installations

Proposed/Future Installations	MVDC Voltage	Company
MVDC distribution network for high power laboratories	10 kV	RWTH Aachen University, Germany [68]
MVDC distribution network for high power laboratories	5 kV	University of Nottingam, UK [66]
MVDC network for industrial application	7kV	North Carolina State University, US [69]
MVDC distribution network for electric shipboard power systems	12 kV	US Navy [70, 71]
MVDC distribution network for electric shipboard power systems	1.5 kV - 15 kV	Huazhong University, China [61]
MVDC distribution network for electric ship propulsion	-	Royal British Navy [72]
MVDC collection or transmission ($\leq$ 70km) network for offshore wind farms	50 - 80 KV	ABB [63, 64]
MVDC collection Network for offshore Wind Farm	5-40kV	Chalmers University, Denmark [73]
MVDC collection Network for offshore Wind Farm	33kV	University of the Basque Country, Spain [67, 74]
MVDC point to point connection (30 km)	10 kV	RXPE [66]
Reinforcement Link	50 kV	Scottish Power - Anglesey, UK [66]
Real Installations	**MVDC Voltage**	**Company**
MVDC distribution network for high power laboratories	1kV	University of Aberdeen, UK [66]
Onshore Wind Farm (MVDC demonstrator)	9kV	ABB (HVDC Light) [66]

2.3 Medium Voltage (MV) Applications

As it has been detailed in previous sections, regarding the different kinds of medium voltage converters, VSCs provide several advantages with respect to CSCs or cycloconverters. Considering VSCs, MMCs provide several advantages with respect to the rest of multilevel converters, such as higher scalability (providing lower effective switching frequency) and reliability [5], the absence of a common dc bus capacitor [8] and the use of capacitor voltage balancing algorithms, which are able to balance the sub-module (SM) capacitor voltages under any working condition. Due to these reasons, the MMCs have been selected to be utilized in different medium voltage applications. In particular, this thesis focuses on the indirect topology (AC/DC or DC/AC) due to its ability to manage active power and to be connected directly to medium voltage direct current (MVDC) networks. The indirect MMC has been proposed in the technical literature to be used in the following range of MV applications:

- Medium voltage direct current (MVDC) and hybrid networks [61, 62]
- MVDC collector systems for offshore wind farms [63, 64]
- Medium voltage ac applications [9, 37, 65]

Below, a description of these applications and the role of the MMC are given.

2.3.1 Medium Voltage Direct Current (MVDC) Networks

MVDC distribution networks are being studied due to the developments in VSC technology [66]. These networks provide the following advantages [66, 67]:

- No reactive losses
- Lower cable costs
- Lower losses
  - Higher voltage with equal isolation thickness, as it is given by (2.1) [66]. In addition, standard ac cables could be used, increasing the competition in the dc cable supply and therefore, the dc cable cost could be reduced.

$$V_{dc} = 1.41\widehat{V}_{ac}, \tag{2.1}$$

- Asynchronous connection to the grid
- No skin and proximity effects
- Decoupling of both ends of the grid
- No direct effect in the generators in case of
  - Grid voltage dips
  - Grid faults

Examples of different MVDC network projects are included at table 2.4. MVDC distribution networks have been considered for:

- Industrial or laboratory load supply [68, 69]. In particular, when the proportion of dc loads is high (for example: data centres) [66]
- Distribution network reinforcement [66]
- Electrical shipboard power systems supply [61, 70, 71]
- Electrical ship propulsion [39, 40, 72]
- Energy collection inside offshore wind farms [66, 67, 73–75]
- Dc interconnection of HVDC transmission systems [66]
- Scaling of HVDC systems for testing [66]

In case the dc network is multi-terminal (MTDC), this feature provides higher reliability, stability and security but dc circuit breakers are required to manage fault currents [76, 77]. Otherwise, in the point to point links, only ac breakers at both ends are required [76, 77]. Utilizing converters such as indirect MMC with bipolar SMs, provides also dc fault management [29]. Finally, hybrid networks

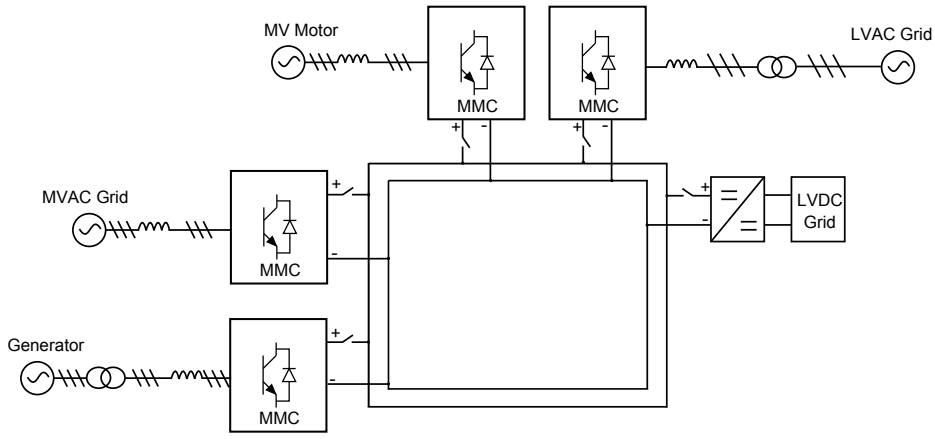

Figure 2.7: Example of MTDC which can be applied in MV applications. This network also provides connections to MVAC, LVAC or LVDC networks.

with MVDC, MVAC, LVDC or LVAC regions, where MMCs may be utilized [61, 62], are also regarded in the technical literature [69, 72]. An example of a MTDC network (utilizing MMCs) with different kinds of loads is depicted at Fig. 2.7. In addition, connections to MVAC, LVAC or LVDC networks are provided.

Regarding offshore wind farms, utilizing dc grids could be interesting for future wind farms if the converter losses and cost are reduced [73, 75]. There are two main dc topologies where the wind turbines are connected in parallel or series, as it is shown in Figs. 2.8-(a) and 2.8-(b), respectively. The first one is more robust but requires high voltage and high power dc/dc converters to obtain high voltage direct current (HVDC) with the aim of transmitting the energy to shore. Additional intermediate dc/dc converters could be utilized to obtain the desired transmission voltage. On the other hand, the series configuration is less reliable and more sensitive to differences in the power and voltage provided by every wind turbine. However, the series connection eliminates the requirement of high power and high voltage dc/dc converters and its corresponding substations, reducing significantly the installation cost [73]. In addition, both topologies utilize a rectifier and a dc/dc converter at the output of every wind turbine to obtain MVDC, as it is depicted at Fig. 2.8.

However, the MVDC installation could be simplified utilizing a medium speed wind turbine [63, 78, 79], a pre-transformer and a MMC with indirect topology, whose scheme is shown at Fig. 2.9. In this way, the number of conversion stages is reduced and therefore, the cost and losses could be also reduced, despite the fact

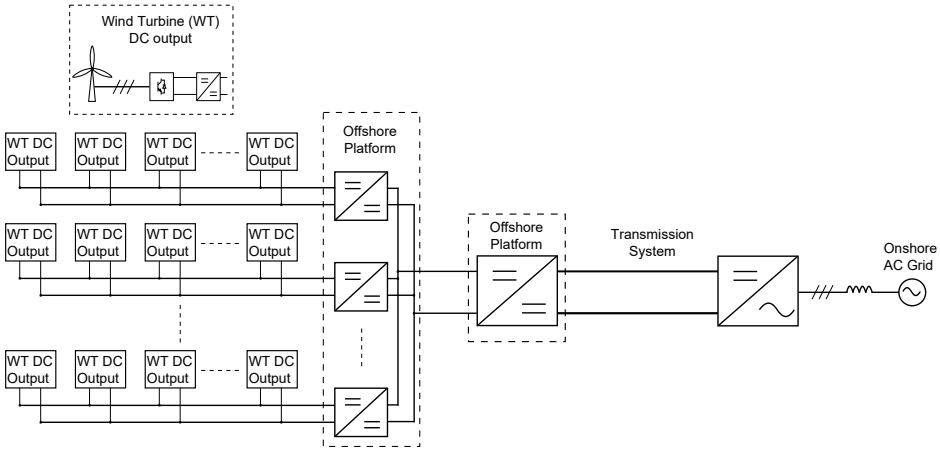

(a) Parallel connection of WTs.

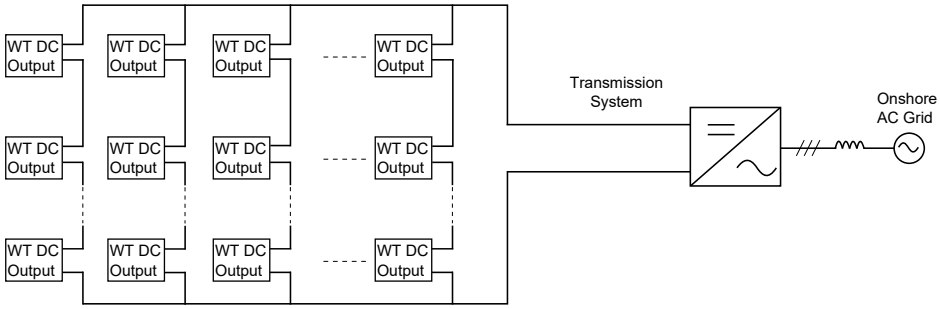

(b) Series connection of WTs.

Figure 2.8: DC networks to transmit offshore wind farm energy, which utilize wind turbine (WT) MVDC output.

that a fundamental frequency transformer is required. This frequency will depend on the medium speed wind turbine utilized, usually somewhere between 60Hz and 84Hz. The design frequency of the transformer would be the maximum operating frequency. In this way, regarding a constant V/f control, when the operating frequency is modified, the flux is maintained constant and the transformer operates correctly [63]. Finally, future wind turbines, regarding the current tendency to provide higher medium output voltage [67], could not require pre-transformers, simplifying further the installation. With the MMC solution, it could be possible to obtain 50-80 kV at the output of the wind turbines, reducing the number of intermediate dc/dc converter stations (or even eliminating it, depending on the

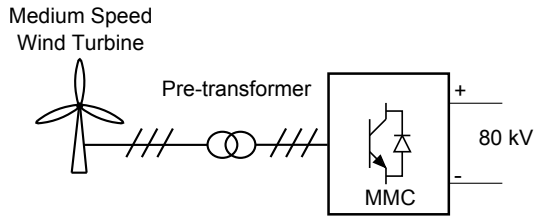

Figure 2.9: Wind turbine with MVDC output, utilizing a pre-transformer and a MMC which operates as a rectifier.

utilized transmission voltage [64]), decreasing significantly the installation costs.

Summarizing, the indirect MMC could be utilized in MVDC networks with different roles (see Figs. 2.7 and 2.9):

- Medium Voltage Inverter/Rectifier (Grid Connection) [61, 62]: MMCs provide the ability to connect directly to MVAC grids form MVDC networks or vice-versa, with high efficiency. In case the ac grid voltage is lower, depending on the voltage ratio and the required grid codes, a low frequency transformer could be required or not.
- Medium Voltage Rectifier (Wind Turbine) [63, 64]: MMCs are able to obtain MVDC at the output of the wind turbine utilizing pre-transformers. This simplifies the number of conversion stages to obtain MVDC in dc wind farm topologies and the number of required dc/dc stations to obtain HVDC at the transmission link. In this way, the installation costs and losses could be reduced. In future wind turbines, where the ac output voltage could be increased, regarding the present tendency, the pre-transformer could not be required.
- Medium Voltage Motor Drive [9, 37]: MMCs could be connected to MVDC networks to operate as a medium voltage motor drive. Medium voltage propulsion provides lower losses than low voltage propulsion. In this way, the application of MMCs in ship propulsion in a near future could be interesting [39, 40].

2.3.2 Medium Voltage Alternate Current (MVAC) Applications

Regarding MVAC networks, the indirect MMC can be used as a back-to-back converter. In this way, it is possible to implement a frequency converter to

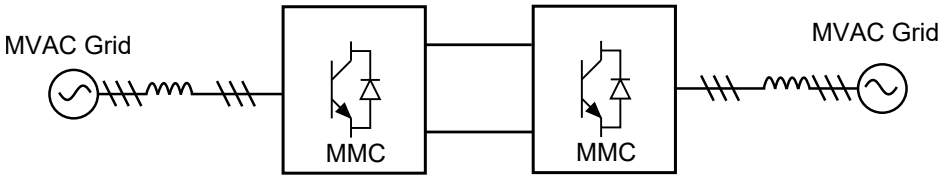

(a) Back-to-Back converter with MMCs to connect two different MVAC grids.

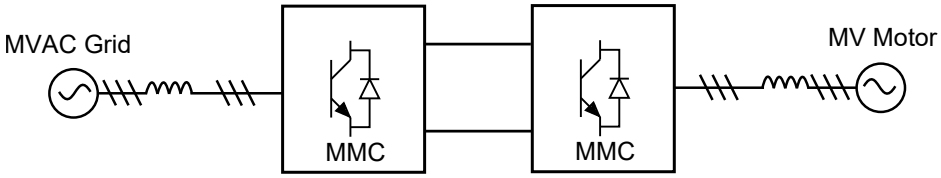

(b) Back-to-Back converter with MMCs which operates as a motor drive.

Figure 2.10. MMCs in medium voltage alternate current (MVAC) applications.

connect two MVAC networks with different operation frequency [65, 80] or a motor drive fed by a MVAC network [81]. The schemes of these applications are depicted at Fig. 2.10

2.4 Modular Multilevel Converter (MMC)

As it has been commented, the indirect MMC will be studied in this thesis due to its advantages and possible applications. Next sections contain the description of the MMC operating principle, existing circulating current controls, balancing algorithms, modulation techniques and passive component sizing, respectively.

2.4.1 Operating Principle

The MMC operating principle has been described in [82] and [13]. Besides this study, other operating principle studies have also been published in the technical literature [7, 83–86].

Although different kinds of SMs can be utilized, half-bridge (HB) SMs have been selected to analyse the MMC operation because this topology is the most widely used due to its simplicity [82]. Every SM contains two IGBTs and one capacitor, as it is shown in Fig. 2.11. In addition, generally, a thyristor is included to

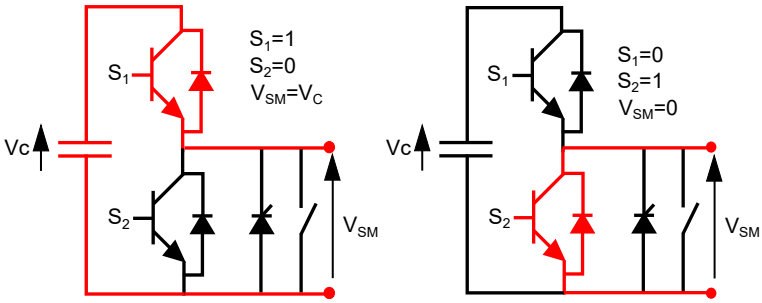

(a) HB SM switching state 1. (b) HB SM switching state 2.

Figure 2.11. Half-bridge (HB) switching states.

protect the IGBTs in case of short circuit in the dc bus, besides a mechanical switch which short-circuits the SM in case it is damaged. The SMs must be initially pre-charged with $v_c = V_{dc}/N$ to operate correctly, where v_c is the SM capacitor voltage, V_{dc} is the dc bus voltage and N is the number of SMs at every arm, regarding the topology depicted at Fig. 2.5-(c). Once the MMC operation has started, the control technique maintains the SM capacitor voltages balanced.

The two states of HB SMs under normal operation are shown at Fig. 2.11. Both IGBTs conduct in a complementary way [29]. In case the upper IGBT is conducting, the SM is inserted, providing a v_c output voltage. When the lower IGBT is conducting, the SM is short-circuited, providing a zero output voltage. In this way, the different levels of the MMC phase output voltage are obtained inserting or short-circuiting the different SMs at every arm.

Fig. 2.12 shows this concept for a single-phase MMC ($N = 4$), generating 5 levels at the output voltage [12]. As it can be noticed, for example, an output level equal to $V_{dc}/4$ requires three SMs inserted in the lower arm and one SM in the upper arm. The phase output voltage, v_{a0} and the upper arm voltage, v_{diff} (the voltage drop in the arm inductances), are given by (2.2) and (2.3), respectively, where v_{upper} and v_{lower} are the upper and lower arm voltages. Once the number of inserted SMs at every arm is determined, a particular selection of inserted SMs is required. This process is implemented by the balancing algorithm, whose different implementations are described in section 2.4.6.

$$v_{a0} = \frac{v_{lower} - v_{upper}}{2}, \tag{2.2}$$

$$v_{diff} = V_{dc} - (v_{lower} + v_{upper}), \tag{2.3}$$

In the example shown at Fig. 2.12, the number of SMs inserted at every phase is N for every output voltage level. However, this fact is not true at every instant and it will depend on the modulation technique utilized and the circulating current, i_{circ}, control [82]. The i_{circ}, which is is depicted at Fig. 2.12-(a), is given by (2.4), where the upper and lower arm currents are given by (2.9) and (2.10), respectively. However, despite the fact that instantaneously the number of inserted SMs could not be equal to N, the i_{circ} control will ensure that, on average over the fundamental period, this number will be equal to N. Otherwise, the arm inductances would be exposed to a dc voltage, preventing the i_{circ} control from operating correctly.

$$i_{circ} = \frac{i_u + i_l}{2}, \tag{2.4}$$

$$i_u = \frac{i_a}{2} + i_{circ}, \tag{2.5}$$

$$i_l = -\frac{i_a}{2} + i_{circ}, \tag{2.6}$$

Table 2.5 extends the concept shown at Fig. 2.12, where the MMC contains 4 SMs at each arm, to MMCs with N SMs at each arm [84]. This table contains the number of SMs which must be inserted inside a particular arm to obtain a determined arm voltage level. On the other hand, for every arm voltage level, table 2.5 contains the number of available redundant switching states. These redundant states will be utilized to balance the SM capacitor voltages at every arm. The voltage levels 0 and V_{dc} do not provide redundant states because all the SMs at upper or lower arms are inserted or short-circuited, respectively. For the rest of voltage levels, the number of redundant states are calculated utilizing the formulations included at table 2.5. For instance, regarding the voltage level $v_{upper} = V_{dc}/N$, only one SM is inserted in the upper arm. Therefore, there are N different possible switching schemes (redundant states) in the upper arm to generate the required voltage. A similar argument can be applied to the rest of voltage levels.

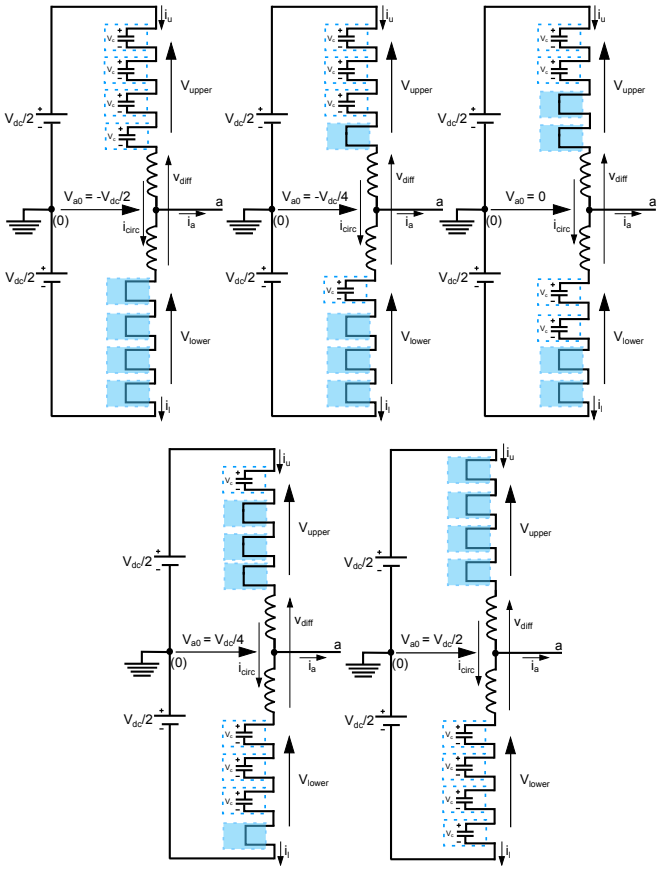

(a) Switching schemes.

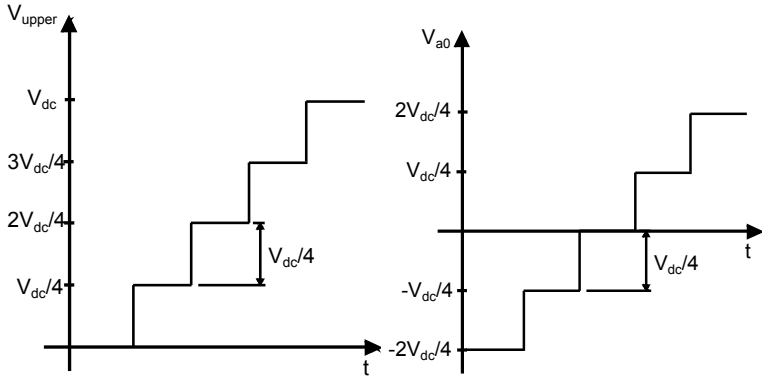

(b) Upper arm voltage levels. (c) Phase output voltage levels.

Figure 2.12: Switching schemes of a MMC with $N = 4$ and their corresponding phase and upper arm voltage levels.

Table 2.5: Number of inserted SMs in a particular arm, arm voltage level and number of redundant states for a MMC with N SMs at each arm.

# of inserted SMs	Arm voltage level	# of redundant states
0	0	0
1	V_{dc}/N	N
2	V_{dc}/N	$\frac{N(N-1)}{2}$
a	aV_{dc}/N	$\frac{N!}{a!(N-a)!}$
-	-	-
N	V_{dc}	0

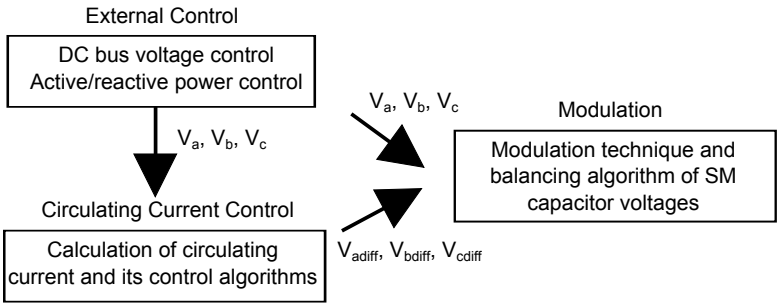

Figure 2.13. MMC control architecture.

2.4.1.1 Control Architecture of MMCs

The control architecture of MMCs can be divided in three different levels, as it can be seen at Fig. 2.13.

- **External control**: This upper control level determines the active and reactive powers injected by the converter, besides the dc bus voltage. The outputs of this control are the phase output voltages (v_a, v_b, v_c) of the MMC. Depending on the application, there are different kinds of controls [23, 37, 65, 87, 88]. Some of these controls are included at section 2.4.4

- **Circulating current control**: The second level provides the i_{circ} value required to obtain a correct operation of the MMC. In this way, the controller utilizes the commands given for (v_a, v_b, v_c) by the upper control level and varies the v_{diff} to obtain the desired i_{circ} value [82]. The operating principle of this control is detailed below, in section 2.4.1.2. In addition, the different kinds of presented i_{circ} controls are included at sections 2.4.2 and 2.4.3. The latter includes the i_{circ} controls utilized for motor drives

- **Modulation technique and balancing algorithm**: Finally, the lowest control level corresponds to the modulation technique [89, 90] and the SM capacitor voltage balancing algorithm [91]. The latter maintains the SM capacitor voltages balanced at every arm. Based on the commands for v_{upper} and v_{lower} provided by the second level, the modulation technique along with the balancing algorithm provide the switching signals for every SM. The different modulation techniques and balancing algorithms are included at sections 2.4.5 and 2.4.6, respectively

2.4.1.2 Circulating Current Reference Definition and Control

Fig. 2.14 shows the operation of one arm of the MMC. Fig. 2.14-(b) shows the voltage generated by the upper arm when nearest level control (NLC) modulation is implemented [92]. As it can be noticed, the upper arm waveform contains both dc and ac components. A similar analysis can be realized for the lower arm. As a consequence, every arm can be represented by the averaged model depicted at Fig. 2.14-(c), where the SMs have been replaced with equivalent ac and dc sources [82, 84]. This model is useful to analyse the power processed by the SMs and to define the required circulating currents which make the MMC operate correctly.

According to Fig. 2.14-(c), the upper and lower arm powers are given by (2.7) and (2.8), where i_u and i_l are the upper and lower arm currents, respectively, V_{dc} is the dc bus voltage and v_{a0} is the phase output voltage [13].

$$p_u = \frac{V_{dc}}{2} i_u - v_{a0} i_u, \tag{2.7}$$

$$p_l = \frac{V_{dc}}{2} i_l + v_{a0} i_l, \tag{2.8}$$

Assuming that i_u and i_l contain common mode and differential mode components, both currents can be represented by (2.9) and (2.10), respectively.

$$i_u = i_{comm} + i_{circ}, \tag{2.9}$$

$$i_l = -i_{comm} + i_{circ}, \tag{2.10}$$

In this way, the upper and lower arm powers can be given by (2.11) and (2.12).

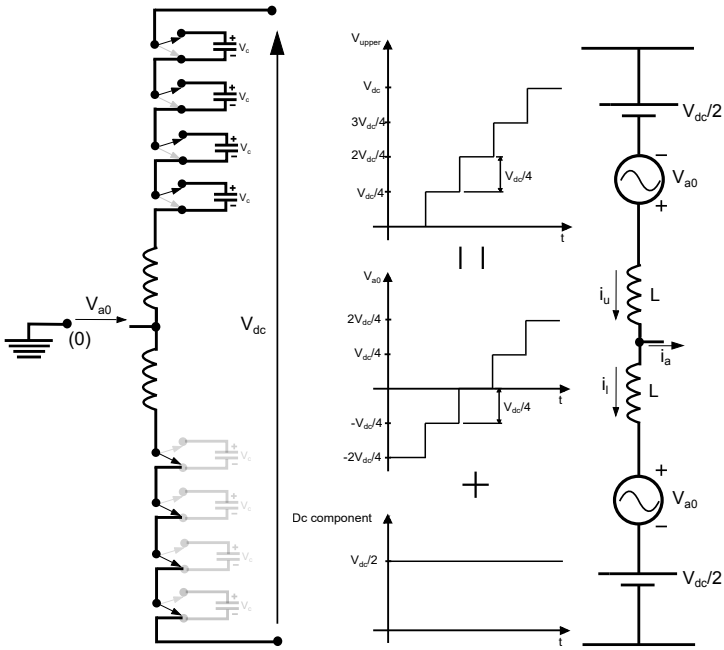

(a) Equivalent MMC switching model. (b) Arm and phase output voltages relationship. (c) Equivalent MMC averaged model.

Figure 2.14. Equivalent MMC models.

$$P_u = \left(\frac{V_{dc}}{2} - v_{a0}\right)(i_{comm} + i_{circ}), \tag{2.11}$$

$$P_l = \left(\frac{V_{dc}}{2} + v_{a0}\right)(-i_{comm} + i_{circ}), \tag{2.12}$$

In addition, according to Fig. 2.14-(c), the common mode current is given by (2.13), where i_a is the phase output current and $\widehat{I}_a$, ϕ and ω are the amplitude, phase and fundamental angular frequency of the phase output current, respectively.

$$i_{comm} = \frac{i_a}{2} = \frac{\widehat{I}_a}{2} cos(\omega t + \phi), \tag{2.13}$$

Assuming the phase output voltage, v_{a0}, is given by (2.14), where m_a is the modulation index and including (2.13) and (2.14) in (2.11) and (2.12), respectively, the upper and lower arm powers are given by (2.15) and (2.16). In this way, (2.15) and (2.16) provide the energy variations in the SMs and therefore, the i_{circ} required to regulate the SM capacitor voltages can be calculated [82, 84].

$$v_{a0} = \frac{m_a V_{dc}}{2} cos(\omega t), \tag{2.14}$$

$$\begin{aligned} p_u = \left(\frac{V_{dc}}{2} - v_a\right) i_u = -\frac{m_a V_{dc} \widehat{I}_a}{8} cos\left(\phi\right) + \frac{V_{dc} \widehat{I}_a}{4} cos\left(\omega t + \phi\right) \\ -\frac{m_a V_{dc} \widehat{I}_a}{8} cos\left(2\omega t + \phi\right) + \frac{V_{dc}}{2} i_{circ} - \frac{m_a V_{dc}}{2} cos\left(\omega t\right) i_{circ}, \end{aligned} \tag{2.15}$$

$$\begin{aligned} p_l = \left(\frac{V_{dc}}{2} + v_a\right) i_l = -\frac{m_a V_{dc} \widehat{I}_a}{8} cos\left(\phi\right) - \frac{V_{dc} \widehat{I}_a}{4} cos\left(\omega t + \phi\right) \\ -\frac{m_a V_{dc} \widehat{I}_a}{8} cos\left(2\omega t + \phi\right) + \frac{V_{dc}}{2} i_{circ} + \frac{m_a V_{dc}}{2} cos\left(\omega t\right) i_{circ}, \end{aligned} \tag{2.16}$$

2.4.1.2.1 DC Circulating Current

The power processed by the SMs, as given by (2.15) and (2.16), contains dc, fundamental and second harmonic components. With the aim of avoiding high fluctuations in the energy stored in the SMs, the dc component must be eliminated. This constraint is given by (2.17) [13, 82].

$$-\frac{m_a V_{dc} \widehat{I}_a}{8} cos(\phi) + \frac{V_{dc}}{2} i_{circ} = 0, \tag{2.17}$$

In this way, the i_{circ} is given by (2.18), providing a steady operation of the MMC. Regarding (2.18), the resulting upper and lower arm powers are given by (2.19) and (2.20).

$$i_{circ} = \frac{m_a \widehat{I}_a}{4} cos\left(\phi\right), \tag{2.18}$$

$$p_u = \frac{V_{dc}\widehat{I}_a}{4} cos\left(\omega t + \phi\right) - \frac{m_a V_{dc}\widehat{I}_a}{8} cos\left(2\omega t + \phi\right) - \frac{m_a^2 V_{dc}\widehat{I}_a}{8} cos\left(\phi\right) cos\left(\omega t\right), \tag{2.19}$$

$$p_l = -\frac{V_{dc}\widehat{I}_a}{4} cos\left(\omega t + \phi\right) - \frac{m_a V_{dc}\widehat{I}_a}{8} cos\left(2\omega t + \phi\right) + \frac{m_a^2 V_{dc}\widehat{I}_a}{8} cos\left(\phi\right) cos\left(\omega t\right), \tag{2.20}$$

As it can be noticed, the dc component in the arm powers has been eliminated and only the fundamental and second harmonic components remain. The average value of these components over the fundamental period is zero. Therefore, the SMs are not providing active power and the capacitors do not charge/discharge. However, the ac components provide voltage oscillations in the capacitor voltages because the instantaneous power is not null. However, the amplitude of these oscillations can be reduced if a second harmonic component is added to i_{circ}, as it will be explained in the next section.

2.4.1.2.2 DC + Second Order Harmonic Circulating Current

As it has been commented, the i_{circ} dc component is required to operate the MMC correctly. Besides this component, it is possible to add a second harmonic component [13]. This component is not crucial for the correct operation of MMCs but provides a reduction of SM capacitor voltage ripple. In the technical literature, several methods have been proposed to calculate this second harmonic component [13, 19, 82, 93, 94]. Among all presented methods, the one presented in [82] has been selected to calculate the i_{circ} reference due to its instantaneous calculation property and its satisfactory results, close to optimum, to reduce the SM capacitor voltage oscillations.

Therefore, in case of introducing a second harmonic in i_{circ}, i_{circ} is given by (2.21).

$$i_{circ} = \frac{m_a \widehat{I}_a}{4} cos\left(\phi\right) + \widehat{I}_a' cos\left(2\omega t + \phi\right), \tag{2.21}$$

In this way, the arm powers are given by (2.22) and (2.23), where $p_u^{'}$ and $p_l^{'}$ are the upper and lower arm powers, including a second harmonic and otherwise, p_u and p_l are the arm powers without a second harmonic. The amplitude of the second harmonic of i_{circ} can be calculated in such a way that the second harmonic component of arm powers is eliminated. The calculated value is given by (2.24) and the resulting arm powers are given by (2.25) and (2.26). Besides the elimination of the second harmonic component, the selected i_{circ} value reduces the amplitude of fundamental harmonic components. As a result, the SM capacitor voltage ripple is also reduced.

$$p_u^{'} = p_u - \frac{m_a V_{dc} \widehat{I_a^{'}}}{4} cos\left(\omega t + \phi\right) + \frac{V_{dc} \widehat{I_a^{'}}}{2} cos\left(2\omega t + \phi\right) - \frac{m_a V_{dc} \widehat{I_a^{'}}}{4} cos\left(3\omega t + \phi\right), \tag{2.22}$$

$$p_l^{'} = p_l + \frac{m_a V_{dc} \widehat{I_a^{'}}}{4} cos\left(\omega t + \phi\right) + \frac{V_{dc} \widehat{I_a^{'}}}{2} cos\left(2\omega t + \phi\right) + \frac{m_a V_{dc} \widehat{I_a^{'}}}{4} cos\left(3\omega t + \phi\right), \tag{2.23}$$

$$\widehat{I_a^{'}} = \frac{m_a \widehat{I_a}}{4}, \tag{2.24}$$

$$p_u^{'} = \frac{V_{dc} \widehat{I_a}}{4} \left(1 - \frac{m_a^2}{2}\right) cos\left(\omega t + \phi\right) - \frac{m_a^2 V_{dc} \widehat{I_a}}{16} cos\left(\omega t - \phi\right) - \frac{m_a^2 V_{dc} \widehat{I_a}}{16} cos\left(3\omega t + \phi\right), \tag{2.25}$$

$$p_l^{'} = -\frac{V_{dc} \widehat{I_a}}{4} \left(1 - \frac{m_a^2}{2}\right) cos\left(\omega t + \phi\right) - \frac{m_a^2 V_{dc} \widehat{I_a}}{16} cos\left(\omega t - \phi\right) + \frac{m_a^2 V_{dc} \widehat{I_a}}{16} cos\left(3\omega t + \phi\right), \tag{2.26}$$

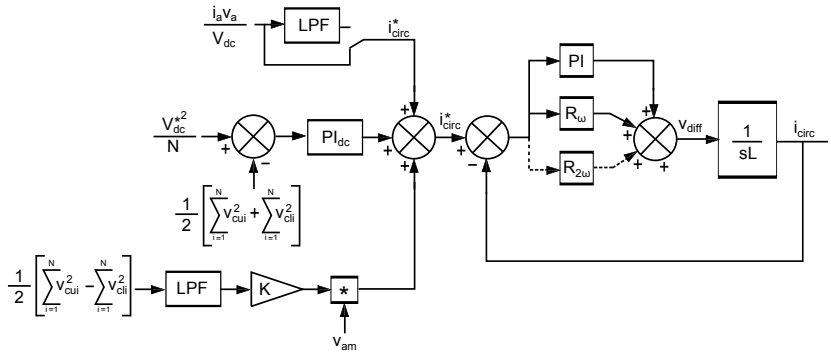

Figure 2.15. Circulating current control for MMC.

Finally, regarding both dc and second harmonic components, the resulting i_{circ} is given by (2.27). As it can be noticed, the i_{circ} value can be calculated instantaneously through the phase output voltage,v_{a0}, the phase output current, i_{a0} and the dc bus voltage. In this way, the real-time implementation is simplified because obtaining the phase or amplitude of any variable is not required [13, 82].

$$i_{circ} = \frac{v_a i_a}{V_{dc}} = \frac{m_a \widehat{I}_a}{4} cos\left(\phi\right) + \frac{m_a \widehat{I}_a}{4} cos\left(2\omega t + \phi\right), \tag{2.27}$$

2.4.1.2.3 Circulating Current Control

The previous section contains the i_{circ} required to obtain a correct operation of MMC. The dc component will be obtained naturally [29] by the converter, even if there is not any regulator. However, undesired harmonics appear in i_{circ} in case a control is not used, increasing the losses and the SM capacitor voltage ripple and therefore, incrementing the rating of the MMC. With the aim of adjusting the value of i_{circ} to its reference, the controller shown at Fig. 2.15 can be utilized for every phase of the MMC [82].

As it can be noticed at Fig. 2.15, the i_{circ} reference contains three different components:

- Component I: This component, given by (2.27), maintains the balance between the ac and dc sizes of the MMC and the desired energy stored in the capacitors of every phase (assuming no losses in the MMC). In addition, the second harmonic of i_{circ} reduces the SM capacitor voltage ripple.

Regarding the trade-off between the losses and the SM capacitor voltage ripple, the second harmonic of i_{circ} can be eliminated utilizing a low pass filter, as it is shown at Fig. 2.15, obtaining the i_{circ} given by (2.18) [82]. In this way, it is possible to minimize the MMC losses. This value is valid for MMCs which operate as PQ node or control the grid voltage in an offshore wind farm. In case the MMC controls the dc bus voltage, the dc component in i_{circ} will be obtained by other method. In this latter case, the dc bus current is measured and divided by 3 [95]. This value is utilized as reference for every phase. In this way, the three phases will contain the same dc component.

- Component II: The first component provides the theoretical i_{circ} required to maintain stable the charge of every SM, when the efficiency of the MMC is 100%. However, regarding the losses of the converter, a second component is required to maintain the energy, stored in the SMs of every phase, adjusted to its reference. This component is calculated utilizing the error between the real and reference energy values. This error is eliminated through a PI control [82].

- Component III: This component introduces a fundamental harmonic component which is used to exchange energy between the upper and lower arms of every phase. Therefore, this component balances the energy stored in both arms. In addition, the fundamental harmonic must be synchronized with the phase output voltage, v_{a0}. This component is not crucial to operate the MMC because both energies are balanced naturally [29]. However, it is useful to improve the MMC balancing dynamic. Finally, this component is provided by a proportional controller. In this way, if the arms are completely balanced, the component will be null.

The generated circulating current reference, i^*_{circ}, is an input of the controller depicted at Fig. 2.15. In a general case, the i_{circ} will contain dc, fundamental and second harmonic components. Therefore, [82] proposed a regulator which utilizes two resonant controllers at f and $2f$, respectively, besides a PI control. The output of the regulator is the v_{diff} required to control the i_{circ}. This voltage, besides v_{a0}, will be utilized to calculate the number of SMs which must be inserted at every moment.

2.4.1.2.4 Analysis and Simulation Results

Expressions (2.18) and (2.27) have been validated through a model, implemented with MATLAB/SIMULINK, of a three-phase MMC with 4 SMs at every arm [13]. Fig. 2.16 shows the simulation results. In particular, Fig. 2.16-(a), 2.16-(c) and

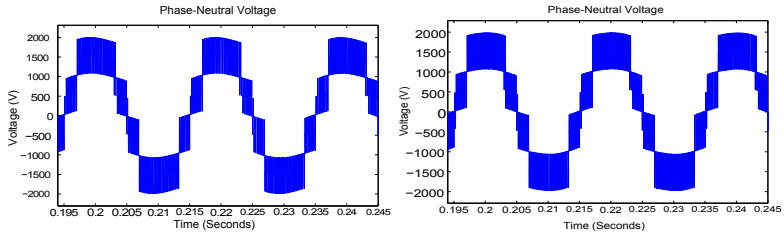

(a) Phase neutral voltage with dc i_{circ}. (b) Phase neutral voltage with dc+2^{nd} i_{circ}.

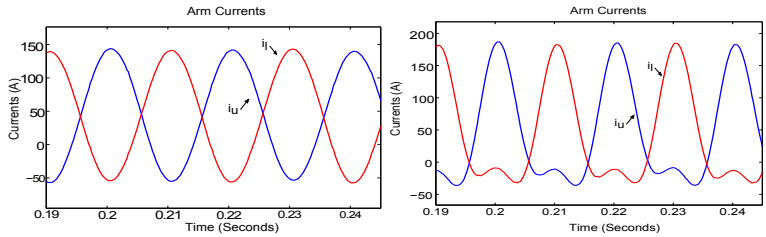

(c) Arm currents with dc i_{circ}. (d) Arm currents with dc+2^{nd} i_{circ}.

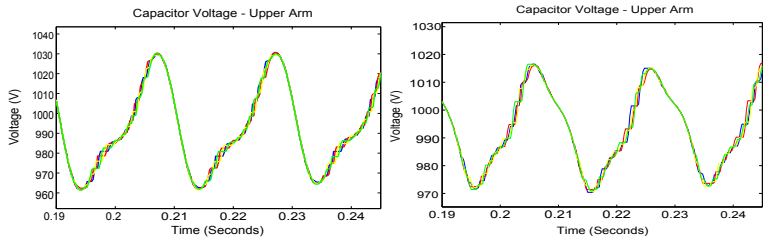

(e) SM capacitor voltages with dc i_{circ}. (f) SM capacitor voltages with dc+2^{nd} i_{circ}.

Figure 2.16. MMC simulation results with phase disposition (PD)-PWM.

2.16-(e) show the v_{a0} voltage, the upper and lower (i_u and i_l) arm currents and the SM capacitor voltages of the upper arm, respectively. These waveforms have been obtained when i_{circ} only contains the dc component given by (2.18). As it can be noticed, despite the oscillations, the SM capacitor voltages are balanced around 1000V.

Figs. 2.16-(b), 2.16-(d) and 2.16-(f) show the same waveforms but utilizing the dc and second harmonic components of i_{circ} given by (2.27). Comparing the Figs. 2.16-(e) and 2.16-(f), the reduction of the SM capacitor voltage ripple utilizing

a second harmonic can be noticed. However, the second harmonic increases the peak value of the arm currents, as it can be noticed at Figs. 2.16-(c) and 2.16-(d), providing higher losses.

Fig 2.16 shows the MMC magnitudes for a particular operating point. With the aim of generalizing this study for any operating point, Figs. 2.17 and 2.18 have been obtained. Fig. 2.17-(a) shows the normalized value of the SM capacitor voltage ripple throughout the m_a and power factor ranges, utilizing a i_{circ} with only a dc component (given by 2.18). The normalized SM capacitor voltage ripple is given by (2.28) [84], where ΔV_c is the peak-to-peak value of the SM capacitor voltage ripple, I_{RMS} is the RMS value of the upper arm current, f is the fundamental frequency and C is the capacitance of every SM. As it can be noticed, the normalized SM capacitor voltage ripple is directly proportional to the SM capacitor voltage ripple and the fundamental frequency. Otherwise, it is inversely proportional to I_{RMS}. Therefore, Fig 2.17-(a) provides the SM capacitor voltage ripple for any operating point. On the other hand, Fig. 2.17-(b) provides the RMS value of the upper arm current with respect to I_{RMS} for any operating condition and with i_{circ} also given by 2.18.

$$\frac{\Delta v_{cn}}{2} = \frac{\frac{\Delta v_c}{2}}{\frac{I_{RMS}}{fC}}, \tag{2.28}$$

Fig. 2.18 shows the same magnitudes than Fig. 2.17 but utilizing a i_{circ} which contain dc and second harmonic components (given by (2.27)). Comparing both figures, a significant reduction of the SM capacitor voltage ripple can be noticed when a second harmonic is utilized in i_{circ} and m_a is high. However, for these conditions, the RMS value of the arm currents increases approximately a 5%, reducing the efficiency of the converter.

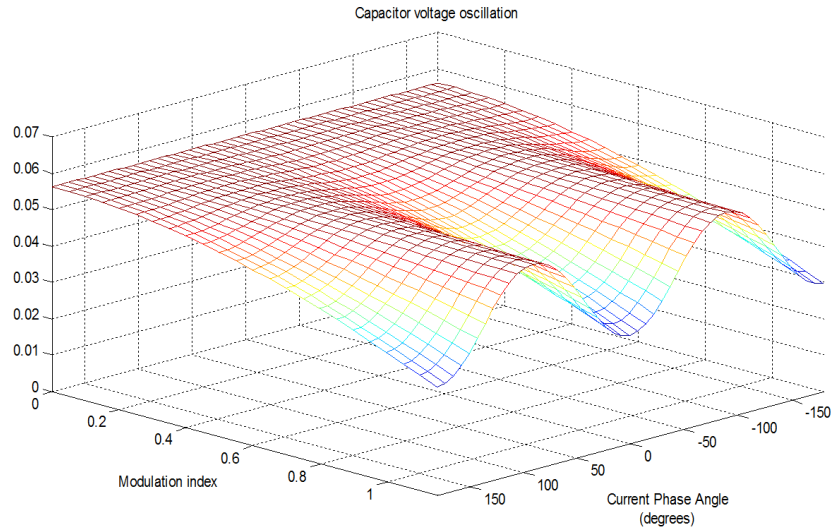

(a) Normalized SM capacitor voltage ripple with dc i_{circ}.

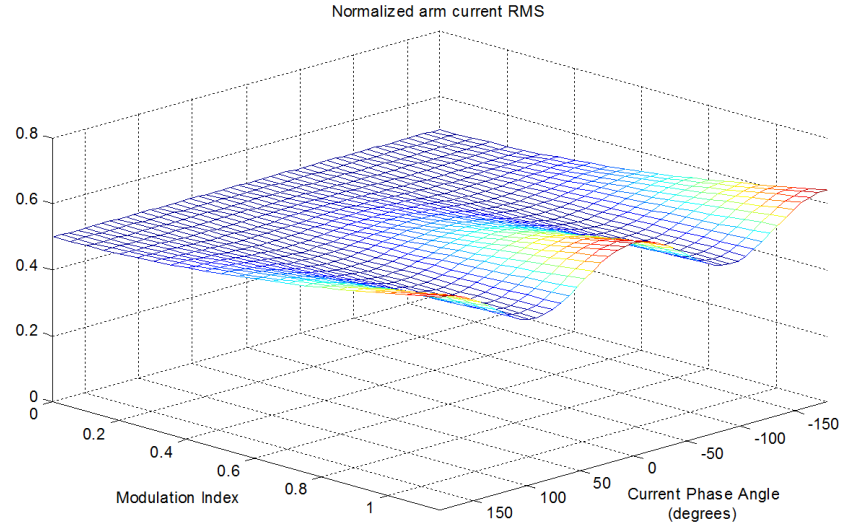

(b) Normalized arm current with dc i_{circ}.

Figure 2.17: Normalized SM capacitor voltage ripple and normalized arm current with dc i_{circ}.

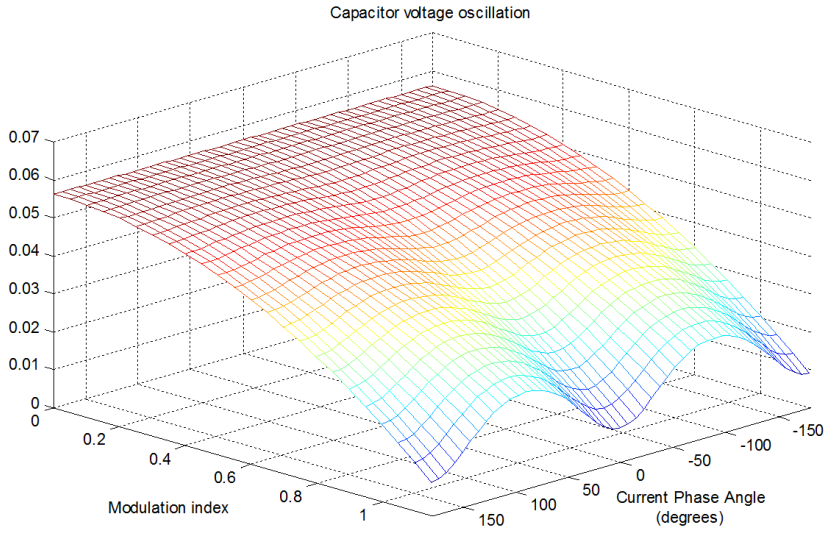

(a) Normalized SM capacitor voltage ripple with dc+2^{nd} i_{circ}.

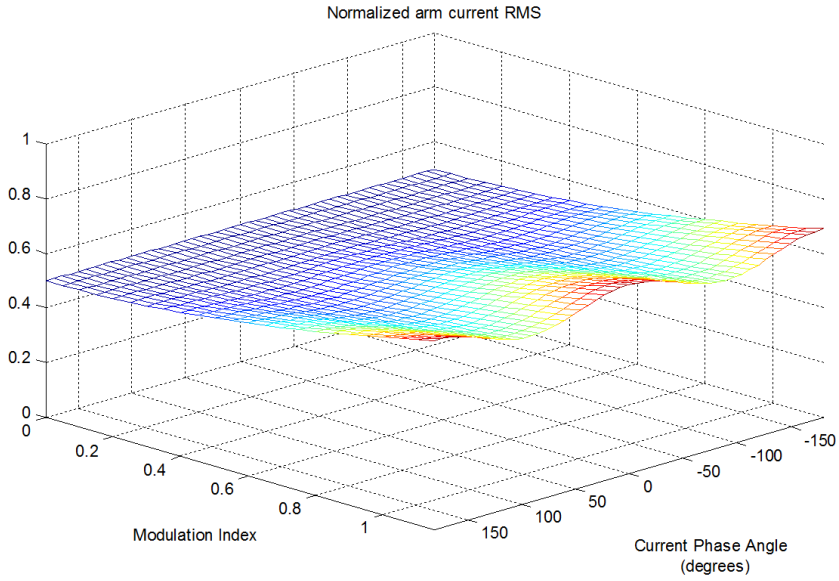

(b) Normalized arm current with dc+2^{nd} i_{circ}.

Figure 2.18: Normalized SM capacitor voltage ripple and normalized arm current with dc+2^{nd} i_{circ}.

Table 2.6. Circulating Current Control Techniques

Closed-loop Circulating Current Control based on Instantaneous References with PD-PWM [82]
Closed-loop Circulating Current Control with PS-PWM [41]
Closed-loop Circulating Current Control with Model Predictive Control [87]
Closed-loop Circulating Current Control for Reduction of SM Capacitor Voltage Ripple with PD-PWM [94]
Closed-loop Circulating Current Suppressing Control based on d-q Model and PS-PWM [88, 98]
Closed-loop Circulating Current Suppressing Control based on $\alpha - \beta$ Model and NLC [99]
Closed-loop Circulating Current Control with SHE-PWM [100]
Closed-loop Circulating Current Control with (2N+1) PWM [101]
Closed-loop Circulating Current Control with Direct Modulation [5]
Open-loop Circulating Current Control with Direct Modulation [24]

2.4.2 Circulating Current Control Techniques

As it has been commented in section 2.4.1, inner controls try to address the main issues associated to MMCs which are the uncontrolled circulating currents and the minimization of the SM capacitors voltage ripple. The first one causes higher power losses, undesired energy transfer between arms, with the resulting imbalance, and the rating of the SMs at higher current. Furthermore, the SM capacitors voltage ripple is increased due to this uncontrolled circulating current. Therefore, i_{circ} must be continuously controlled to meet both challenges, without disturbing the phase output voltage [5].

Section 2.4.1.2 describes a i_{circ} control technique, where the i_{circ} reference is calculated through instantaneous values [13, 82, 96, 97]. This reference is followed using PI and resonant controllers. However, besides this technique, depending on the modulation technique applied, different i_{circ} controls have been proposed in the technical literature, as it is shown in table 2.6. This section includes an overview of these control techniques. Most of them are utilized with high switching frequency modulation techniques and another one has been proposed in case of SHE-PWM. On the one hand, there are i_{circ} controllers which are focused on different components of i_{circ}, such as DC, second harmonic [5, 82, 87] or fourth harmonic [93, 94] components. On the other hand, another controller exists, which monitors every SM capacitor voltage and determines its corresponding switching state with the aim of adjusting its voltage to the reference value [41]. In this way, limiting the SM capacitor voltage ripple, the i_{circ} is also controlled.

- **Closed-loop Circulating Current Control with PS-PWM [41]**

  The stability conditions of an indirect MMC when a PS-PWM (phase shifted - pulse width modulation) is utilized has been analysed in [33, 41]. It was demonstrated, applying the Routh-Hurwitz stability criterion, that with an average control and an individual-balancing control, the MMC can operate only under certain conditions. An arm balancing control was pro-

posed to fix this issue and to meet the challenge of operating correctly for any value of the phase difference between the AC voltage and the load current. Due to the advantages of using PS-PWM, different controls can be implemented modifying the voltage reference of every SM. Particularly, an averaging control, an individual-balancing control and an arm balancing control have been provided. These components modify every SM capacitor voltage reference.

The output voltage contains 2N+1 levels and therefore, its quality is improved [8]. However, the main disadvantages of this control are their limitation to certain PS-PWM methods [102] and a high communication load inherent to feedback controls which can be seriously affected by delays in the measurements in case of a relatively high number of SMs [8].

- **Closed-loop Circulating Current Control with Model Predictive Control [87]**

  A model predictive control (MPC) was proposed by [87]. This technique reduces the capacitor voltage ripple and minimizes the circulating current, utilizing the cost function given by (2.29), where i_a is the phase output current, λ is a proportional coefficient, V_{ci} is the SM_i capacitor voltage and λ_{circ} is a i_{circ} proportional coefficient. For every phase, i_a and i_{circ} are predicted for next sampling time T_s. Regarding these values and the switching redundancies for every output voltage level, the different available configurations are assessed on those predictions and the one which minimizes the cost function given by (2.29), is selected. The main drawback of this method is the requirement of a high switching frequency. On the other hand, another version of this controller has been provided by [103]. In this case, the objective function contains the number of commutations between the current state and the one used in the next sampling time, with the aim of reducing the effective switching frequency without varying the sampling frequency.

$$F = i_a^* - i_a + \lambda \left(\sum_i^N |V_{ci}(t + Ts) - \frac{V_{dc}}{N}| \right) + \lambda_{circ} i_{circ}(t + T_s) \qquad (2.29)$$

- **Closed-loop Circulating Current Control for Reduction of SM Capacitor Voltage Ripple with PD-PWM [94]**

  [94] presented a circulating current control technique which, regarding DC and second harmonic components, reduces the SM capacitor voltage ripple.

The proposed method is based on the averaged MMC model published by [84]. In this way, the averaged SM capacitor voltage ripple is calculated and minimized.

The i_{circ} is controlled, modifying the m_a of the upper and lower arms and therefore, varying v_{diff}, without disturbing the phase output voltage v_a.

On the other hand, besides controlling the second harmonic, the fourth harmonic can be determined with the aim of obtaining a further reduction in the SM capacitor voltage ripple [93]. Both the amplitude and phase values of second and fourth harmonics are calculated through an off-line optimization process.

- **Closed-loop Circulating Current Suppressing Control based on d-q Model and PS-PWM [88, 104]**

  [88, 104] provided a circulating current control technique which is based on a negative-sequence rotational reference frame at double-fundamental frequency. Therefore, the three phase components are transformed into a direct and a quadrature (d-q) components, which are adjusted to their corresponding references utilizing two PI controllers. In this way, this method reduces significantly the circulating current amplitude without disturbing the phase output voltage. The utilized circulating current model and the circulating current suppressing control are depicted at Figs. 2.19-(a) and 2.19-(b), respectively, where v_{diff} is the voltage drop in the arm inductance, $i_{circ-2f}$ is the second harmonic component of the circulating current, $i_{up-phase-j}$ is the upper arm current at phase j and $i_{down-phase-j}$ is the lower arm current at phase j. The proposed control technique has been utilized along with PS-PWM. Finally, this technique can be improved regarding the positive, negative and zero-sequence $i_{circ-2f}$ components under unbalanced grid conditions [105].

- **Closed-loop Circulating Current Suppressing Control based on $\alpha - \beta$ Model and NLC [106]**

  [106] provided a i_{circ} suppressing control based on non-ideal resonant controllers and a $\alpha - \beta$ model. Furthermore, this technique is able to control the positive, negative and zero-sequence i_{circ} components under unbalanced grid conditions. In this way, this method is more simple than other resonant controllers based on *abc* and *dq* models [82, 105]. Moreover, the non-ideal resonant controllers provide a higher robustness under frequency deviations.

- **Closed-loop Circulating Current Control with (N+1) SHE-PWM [107]**

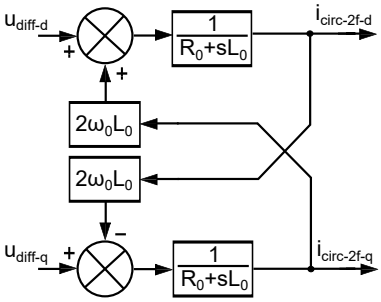

(a) Circulating current model.

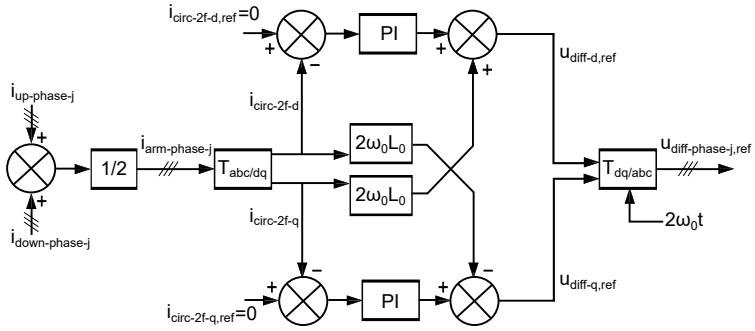

(b) Circulating current suppressing control.

Figure 2.19. Circulating current suppressing control based on d-q model.

[107] developed a i_{circ} control, which can be applied with (N+1) SHE-PWM (described in section 3.2.2), that eliminates the second order harmonic in the MMC i_{circ}, introducing very little disturbances in the phase output voltage. This technique is able to operate with fundamental effective switching frequency, where every SM is operated with a pulse switching pattern whose width is π radians and its central point is γ_k, as it is shown at Fig. 2.20-(a). The angles γ_k, which are calculated through the Newton-Raphson method [108, 109], are utilized to control lower-order harmonics. In this way, the i_{circ} is controlled introducing little variations in the pulse width of every SM. These variations only provide even harmonics in the circulating current. Their effect is studied on both Fourier series a_n and b_n coefficients of the phase output voltage.

Furthermore, in case the required modifications are not significant, the phase output voltage will not be disturbed. Several PI-controllers, which

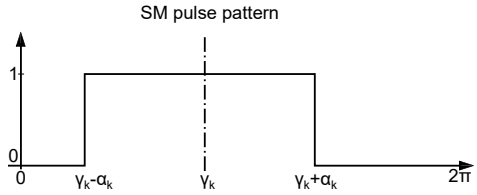

(a) SM pulse pattern for selective harmonic elimination.

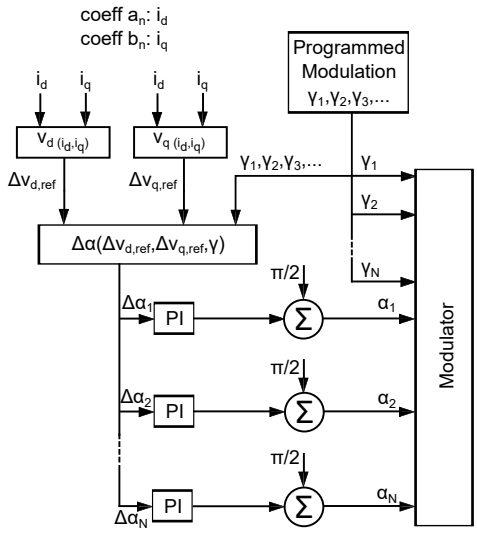

(b) Circulating current control with (N+1) selective harmonic elimination.

Figure 2.20. Circulating current control with (N+1) SHE-PWM.

can be noticed at Fig. 2.20-(b), are utilized to modify the pulse width of every SM. However, the DC component of i_{circ} and the energy stored in the SMs capacitors are not controlled. Furthermore, this technique could insert disturbances in the output voltage in case the variations in the firing angles were significant[110].

- **Closed-loop Circulating Current Control with (2N+1) PWM [111]**

  [111] provided a i_{circ} control utilizing PWM techniques with (2N+1) levels, which can be implemented interleaving the upper and lower arm carriers

or utilizing 2N carriers directly. In this way, several redundant voltage levels are obtained which provide a degree of freedom to control i_{circ}. This technique, despite the fact that it could be utilized with (2N+1) SHE-PWM (described in section 3.2.2), would introduce an uncontrolled i_{circ} ripple due to the low switching frequency and the uneven distance between firing angles, inherent to SHE modulations.

- **Closed-loop Circulating Current Control with Direct Modulation [5]**

  A closed-loop control has been developed by [5]. This method controls the circulating current inside the phases of the MMC and balances the arm voltages for every operating condition. A continuous model that uses direct modulation, with infinity switching frequency and infinity number of SMs per arm, was created for simplicity, avoiding the utilization of averaged models. The continuous model approach was validated against a discrete model.

  In case of utilizing direct modulation without an additional control, i_{circ} will contain a significant second order harmonic. As it has been demonstrated at section 2.4.1, the upper and lower arm powers strongly depend on i_{circ}. In this way, the addition and subtraction of the lower and upper arm powers are realized to calculate the i_{circ} reference. In this way, the i_{circ} is changed manipulating the modulation indexes of both upper and lower arms without disturbing the output voltage. Therefore, the i_{circ} depends on v_{diff} [5, 8, 112].

  As it has also been explained at section 2.4.1, this method injects a dc component and a fundamental component to balance the SM capacitor voltages. As a result, the significant second order harmonic which appears in i_{circ} without control has been eliminated. However, a second order harmonic still remains in the capacitor voltages due to the multiplication of the insertion index and the fundamental frequency component of the arm current[5].

  The main drawback of this method is the addition of harmonics to the output phase voltage [29] due to the utilization of different modulation indexes for the upper and lower arms, respectively. These undesired components are located in high frequencies when a PWM modulation technique is used and therefore, they are negligible. However, in case a fundamental switching frequency modulation is employed with a relatively low number of SMs per arm, the added harmonics would be too close to the fundamental frequency.

- **Open-loop Circulating Current Control with Direct Modulation [24]**

  [24] proposed an open-loop controller, based on the closed-loop controller implemented by [5], which allows reducing the amount of communication systems, although the capacitor voltages still have to be measured because of the utilization of a traditional balancing method. In this way, the sorting algorithm can be executed in a separate processor with parallelization properties, such as FPGAs [8]. An estimation of the stored energy in the upper and lower arms, based on the output voltage reference and the output current, is done. The method is based on a high switching frequency modulation.

  The open-loop control proposed by [24] offers a higher accuracy than the closed-loop proposed by [5] due to lower delays in the communication data. Moreover, the implementation of these two controls over an experimental prototype shows that both are simpler than the one proposed by [41], which is based on PS-PWM, where every SM has its own controller. This fact suggests that the open-loop control best suits the needs of a MMC with a high number of levels [8].

2.4.3 Circulating Current Motor Control Techniques

Regarding the employment of indirect MMC as a variable speed drive, the SM capacitor voltage ripple, as it was shown at section 2.4.1, is inversely proportional to the fundamental frequency and proportional to the output current. Therefore, although the m_a of the output voltage is low at low fundamental frequencies, in case of high starting torque, the available output current will be reduced for a given value of SM capacitance[85]. With the aim of addressing this drawback, several inner control methods which are based on PWM techniques and depend on the motor speed range, have been published in the technical literature.

High, medium and low speed ranges will be considered [37]. As the motor speed changes, in case the fundamental frequency limit between adjacent ranges is exceeded, the switchover of control mode can be implemented utilizing an hysteresis band [113]. On the other hand, the limits of every speed range depend on both the utilized inner and overall control methods. The inner control loop inserts different i_{circ} components, which modify the arm currents and therefore, for a particular motor speed, the available output torque and the SM capacitor voltage ripple will also be different [23, 37]. In this way, the required torque, which is specified by the overall controls, determines if particular motor speeds are available with every inner control technique.

2.4.3.1 Control Methods for High Speed Range

With the aim of reducing the SM capacitor voltage ripple and not exceeding its limit, the standard control techniques described at section 2.4.2 can be applied at high speed ranges, utilizing a i_{circ} with a DC and a second harmonic components [23]. On the other hand, a new control method has been proposed by [37]. This technique, which is utilized along with the control presented at [5] and detailed at section 2.4.2, decreases the averaged SM capacitor voltage when the m_a and the fundamental frequencies are reduced. In this way, it is possible to widen the speed range where the mentioned standard control can be applied, without exceeding the SM capacitor voltage limit.

2.4.3.2 Control Methods for Medium Speed Range

In the medium speed range, the standard control methods, which utilize DC and/or second harmonic i_{circ} components, can be successfully employed to reduce the SM capacitor voltage ripple [23], as in the high speed range. However, the SM capacitors and the arm inductances must be correctly rated, regarding the different operating conditions, as it will be described in section 2.4.7.

With the aim of reducing the SM capacitor voltage ripple or the passive component sizing even more, [37] presented a control technique which introduces a common mode voltage v_{cm} and two i_{circ} components with positive and negative sequence, which are given by (2.30)-(a), (2.30)-(b) and (2.30)-(c), respectively. In this way, it is possible to obtain a i_{circ} component which compensates the fundamental frequency energy fluctuations in the SM capacitors. The values of $\widehat{V}_{cm}$, ω_{cm}, ϕ_{cm}, $\widehat{I}_{circ,pos}$, $\phi_{circ,pos}$, $\widehat{I}_{circ,neg}$ and $\phi_{circ,neg}$ will be determined through an optimization algorithm. Considering the operating conditions, the SM capacitor voltage ripple and the arm currents will be minimized. In addition, the i_{circ} components will not disturb the DC side current.

$$v_{cm} = \widehat{V}_{cm} cos(\omega_{cm} t + \phi_{cm}), \tag{2.30a}$$

$$i_{circ,pos} = \widehat{I}_{circ,pos} cos\left[(\omega_{cm} + \omega_s)\, t + \phi_{circ,pos}\right], \tag{2.30b}$$

$$i_{circ,neg} = \widehat{I}_{circ,neg} cos\left[(\omega_{cm} - \omega_s)\, t + \phi_{circ,neg}\right] \tag{2.30c}$$

However, as the motor speed is reduced, the arm currents are increased due to the higher compensation requirements. In this way, the power losses are also increased. In addition, below a particular fundamental frequency, the SM capacitor

voltage ripple will exceed its maximum allowed value and therefore, another control technique must be utilized or the passive component sizing must be increased [37].

2.4.3.3 Control Method for Standstill and Low Speed Range

[23] proposed a control technique which reduces the SM capacitor voltage ripple in case of standstill and low fundamental frequency operation. This technique requires higher values of i_{circ} than those employed at medium speed range [37]. v_{cm} and i_{circ} components at few hundred Hz are utilized, making the arm powers dependant on this frequency and therefore, reducing the SM capacitor voltage ripple. These components are given by (2.31) and (2.32), respectively, resulting in the arm powers given by (2.33) and (2.34), which only depend on high frequency components. As it can be noticed at (2.31), the first two terms provide the DC and second harmonic components described at section 2.4.1, combining the low frequency mode (LFM) and the standard mode controls.

$$i_{circ} = \frac{v_a i_a}{V_{dc}} + i_a \frac{\frac{2v_a^2}{V_{dc}} - \frac{V_{dc}}{2}}{2v_{cm}}, \tag{2.31}$$

$$v_{cm} = sin(\omega_{cm} t)\sqrt{2} V_{cm,rms} \tag{2.32}$$

$$P_u = v_{cm}\frac{i_a}{2} + \left(\frac{V_{dc}}{2} - v_a\right)\left(i_a \frac{\frac{2v_a^2}{V_{dc}} - \frac{V_{dc}}{2}}{2v_{cm}}\right) + v_{cm}\frac{v_a i_a}{V_{dc}} \tag{2.33}$$

$$P_l = v_{cm}\frac{i_a}{2} + \left(\frac{V_{dc}}{2} + v_a\right)\left(i_a \frac{\frac{2v_a^2}{V_{dc}} - \frac{V_{dc}}{2}}{2v_{cm}}\right) - v_{cm}\frac{v_a i_a}{V_{dc}} \tag{2.34}$$

On the other hand, with the aim of limiting the amplitude of i_{circ} when the values of v_{cm} are closed to zero, i_{circ} will be given by (2.35). In this way, a new residual component will appear in the arm powers at common mode frequency, whose value is not significant.

$$i_{circ} = \frac{v_a i_a}{V_{dc}} + sin(\omega_{cm} t)\sqrt{2} i_a \frac{\frac{2v_a^2}{V_{dc}} - \frac{V_{dc}}{2}}{2V_{cm,rms}}, \tag{2.35}$$

v_{cm} could also be provided by a square waveform, whose frequency is ω_{cm}, with the aim of limiting the amplitude of i_{circ} [81]. However, this technique could generate a zero-sequence current depending on the kind of application or grounding connection and the lifetime of the rotor bearings could be reduced [85]. Therefore, the i_{circ} given by (2.35), which provides a low dv/dt, could address this problem [23].

Utilizing LFM, the available torque is mainly limited by the arm currents and the semiconductor losses. In this way, this torque decreases when the output frequency increases due to the reduction of v_{cm} (caused by the increment of v_a) and the corresponding increment of i_{circ}. Based on this assumption, at medium or high speed range, other control techniques are utilized due to their higher available torque.

2.4.4 External Control Techniques

Once the circulating current control has been implemented, an external MMC control must be defined. This control, which will depend on the application, could be utilized to regulate the dc bus voltage [114], the active and reactive powers injected to the grid [114] or the ac voltage at its output [2, 115]. On the other hand, field-oriented controls and direct-torque controls are suitable in case of machine side converters.

In case of a back-to-back converter implemented with indirect MMCs, an external control has been presented by [65, 87], which was previously used by [116] over an NPC. This technique can be applied to the dynamic analysis and control synthesis, under balanced and unbalanced conditions. On the one hand, the DC-bus voltage can be regulated by a positive-sequence subsystem control. On the other hand, a negative-sequence subsystem is able to eliminate either the DC-bus voltage ripple or the imbalance of the AC-side line currents. Therefore, there is a trade-off between the current and the voltage stress of the converter components.

In the event of motor controls, a constant torque solution throughout the motor speed range has been presented by [37]. On the other hand, a controller which provides a quadratic torque load has been published by [23]. This technique can reduce the upper limit of the low speed range, which has been described at section 2.4.3. In this way, the SM capacitor voltage ripple can be kept constant when

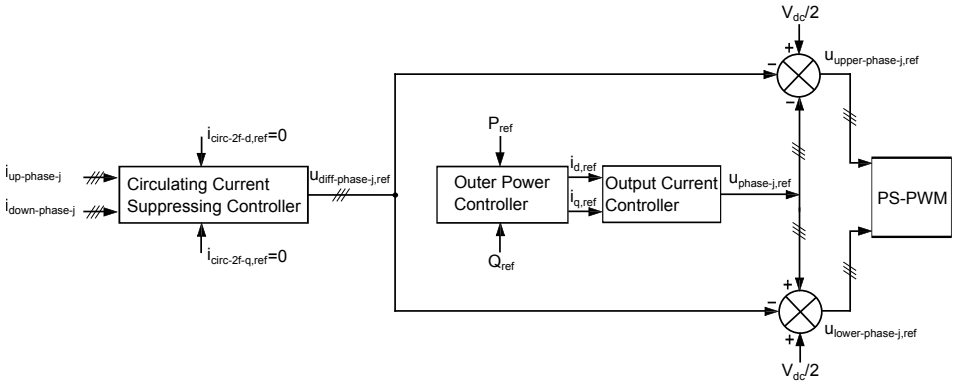

Figure 2.21. Entire MMC control utilizing a d-q model.

the phase output current is proportional to the fundamental frequency. This challenge can be met utilizing a rotor flux which is directly proportional to the square root of the torque [23].

[88] presented a MMC control technique based on a d-q model. Depending on the active and reactive power references and the i_{circ} reference given by the control presented by [88, 104] and detailed at section 2.4.2, the upper and lower arm voltages, v_{upper} and v_{lower}, respectively, are obtained at every phase. The control scheme is depicted at Fig. 2.21. This technique has been implemented along with PS-PWM.

2.4.5 Modulation Techniques

The MMC modulation techniques can be classified depending on the effective switching frequency, as it is depicted at Fig. 2.22. On the one hand, space vector modulation (SVM) and pulse width modulations (PWM) utilize a high effective switching frequency. On the other hand, modulation techniques such as nearest level control (NLC), space vector control (SVC) or selective harmonic elimination (SHE) utilize a low effective switching frequency which can be close to the fundamental frequency [29].

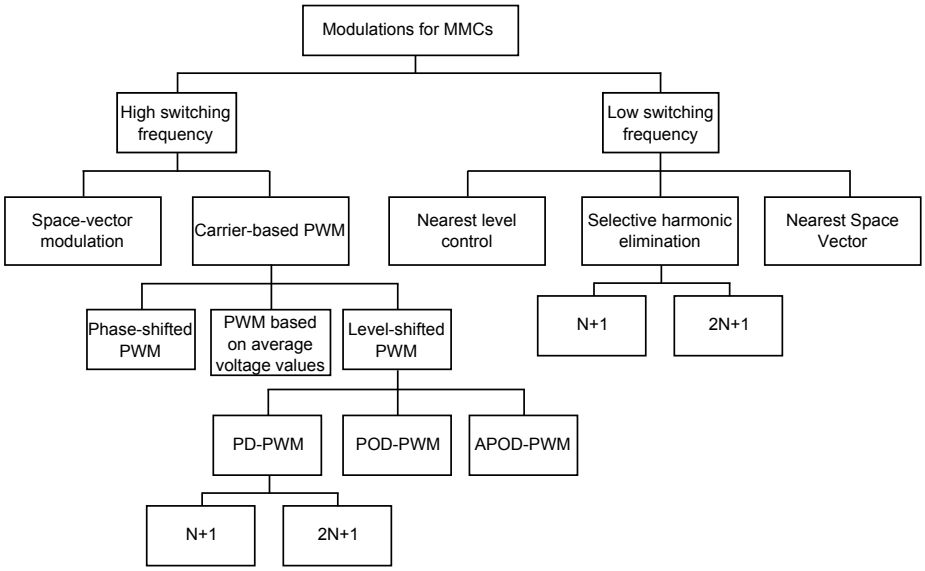

Figure 2.22. Modulation techniques for MMC.

2.4.5.1 High Effective Switching Frequency Modulations

Several high effective switching frequency modulations for MMC have been published in the technical literature [89, 90].

- **Phase Disposition - Pulse Width Modulation (PD-PWM):**

  Different kinds of PD-PWMs have been defined [65, 111, 117–119]. They differ according to the number of carriers and their distribution, as it can be noticed at Fig. 2.23. Regarding N SMs at every arm, phase disposition (PD), phase opposition disposition (POD) and alternative phase opposition disposition (APOD), which utilize N carriers, provide a phase output voltage with N+1 levels. On the other hand, (2N+1) phase disposition and (2N+1) phase disposition with interleaving carriers provide 2N+1 levels because the upper and lower arm commutations are not simultaneous. All of them determine the number of SMs connected at the upper and lower arms depending on the relationship between the carriers and the phase output voltage reference. Finally, the direct modulation (DM) concept, which was presented by [5, 8], depending on whether the carriers for both arms are in phase opposition or not, provides a PD-PWM or a PD-PWM with interleaving, respectively.

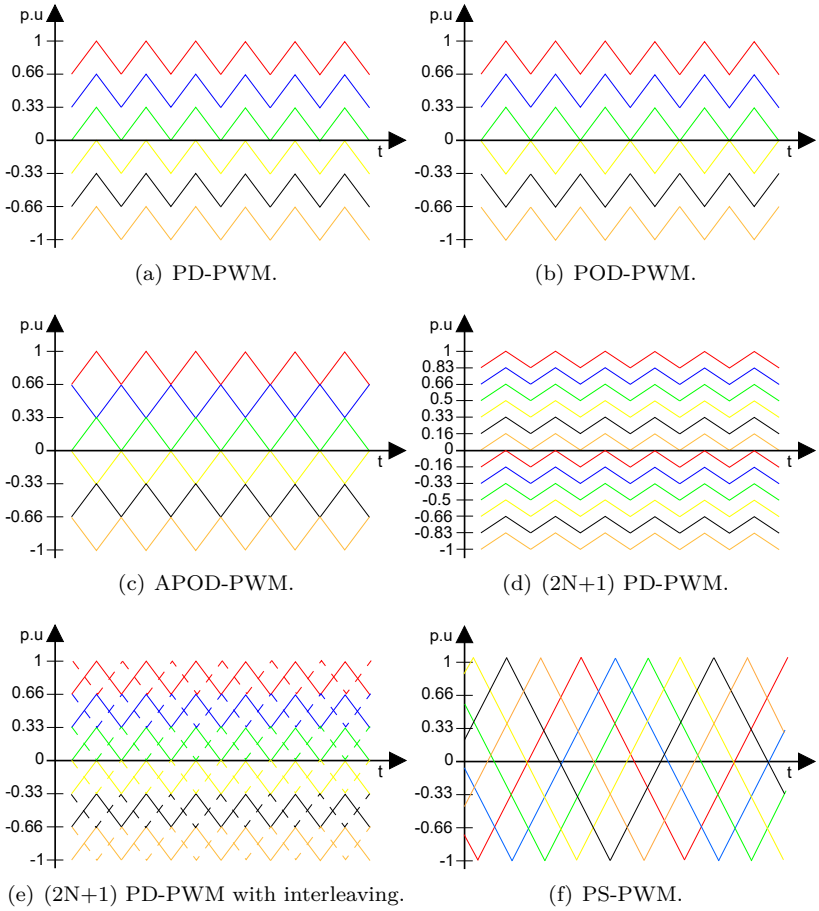

(a) PD-PWM. (b) POD-PWM.

(c) APOD-PWM. (d) (2N+1) PD-PWM.

(e) (2N+1) PD-PWM with interleaving. (f) PS-PWM.

Figure 2.23. PWM carrier arrangements for a MMC with 6 SMs at every arm.

In case of PD, POD and APOD the harmonic content is placed at side bands of the carrier frequency, f_c. Furthermore, regarding a three-phase MMC, where the harmonic located in f_c is eliminated, PD provide the best harmonic content. This feature is relevant when the frequency ratio is low [117]. On the other hand, in case of (2N+1) waveforms, the harmonics are side bands of $2f_c$. As a result, these waveforms provide a lower THD and lower filter requirements but at the expense of a higher i_{circ} ripple [118].

- **Phase Shifted - Pulse Width Modulation (PS-PWM):**

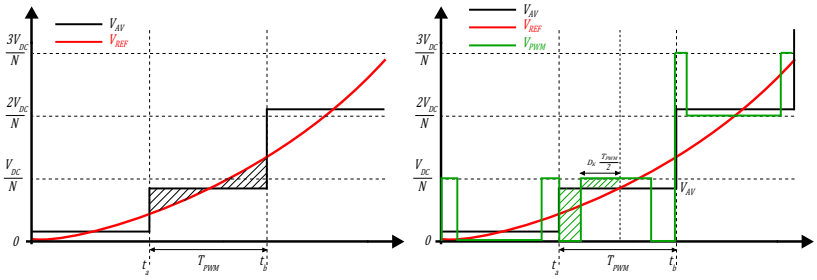

(a) Average voltage. (b) Pulse width modulated voltage.

Figure 2.24. Pulse width modulation based on average voltage value.

PS-PWM provides a (2N+1)-level waveform utilizing $2N$ carriers shifted $\theta = 360°/(2N)$ between each other, as it is shown in Fig. 2.23-(f) [41, 120]. The upper and lower arm references are 180°-shifted [121]. In this way, the phase output voltage contains 2N+1 levels and the harmonic content is located at side bands of $2Nf_c$, where N is the number of SMs at every arm and f_c is the carrier frequency. Finally, comparing the performance of PS-PWM and PD-PWM, the latter provides a lower THD under equivalent effective switching frequency [118, 122]. However, unlike PS-PWM, PD-PWM provides several low-order harmonics, but with very low amplitude and a different conduction period for every SM [120].

- **Pulse Width Modulation based on Average Voltage Value:**

  This technique calculates the medium voltage value of the reference voltage over a carrier frequency period and the duty cycle of the lower and higher voltage levels which are closest to that value. In this way, a triangular carrier is not required. The duty cycle D_k, taking into account the Fig. 2.24, is calculated by (2.36) [34].

$$\begin{aligned} V_{AV} &= \int_{t_a}^{t_b} V_{ref}(t)dt, \quad V_{low} = \left[\frac{V_{AV}}{\frac{V_{dc}}{N}}\right]\frac{V_{dc}}{N}, \\ V_{high} &= V_{low} + \frac{V_{dc}}{N}, \quad D_k = \frac{V_{AV} - V_{low}}{V_{high} - V_{low}}, \end{aligned} \tag{2.36}$$

Two different pulse sequences can be used to approximate the PWM waveform to the reference signal. As it can be seen in fig. 2.24, one possi-

ble configuration would be V_{low}-V_{high}-V_{low} and the other option would be V_{high}-V_{low}-V_{high}.

Once the sequences are defined, it is required to determine which combinations of them will be used over the fundamental period. Three options are considered:

- **Method** α: The sequence is changed every half fundamental period.
- **Method** β: The sequence is changed every carrier period.
- **Method** γ: The sequence is changed every half carrier period.

The methods α and γ offers the lowest THD and WTHD whose values are approximately 10% and 0.3%, respectively [34]. Apart from this result, a study about the current distribution, over one fundamental period, among the IGBTs and diodes of every SM, shows the losses unequally shared between the devices. In particular, one of the IGBTs bear most of the losses.

- **Space Vector Modulation (SVM):**

  SVM provides several output voltage vectors over the plane $\alpha - \beta$, which is depicted at Fig. 2.25. In case of unbalanced systems a third dimension must be used. The number of vectors depends on the number of SMs at every arm. In this way, the main objective is obtaining a combination of output voltage vectors, whose averaged value over the sample period is equal to the reference voltage vector $\widehat{V}_{ref}$. Therefore, the three closest voltage vectors to the reference vector must be selected, as it is shown in Fig. 2.25. Afterwards, the corresponding duty cycles are given by (2.37a) and (2.37b) [29].

$$\widehat{V}_{ref}T_s = t_1\widehat{V}_1 + t_2\widehat{V}_2 + t_3\widehat{V}_3, \tag{2.37a}$$

$$T_s = t_1 + t_2 + t_3, \tag{2.37b}$$

2.4.5.2 Low Effective Switching Frequency Modulations

The main goal of new modulations and control techniques for MMC is the improvement of its efficiency. In this way, low switching frequency modulations are suitable to reduce the switching losses.

- **Nearest Level Control (NLC):**

  The NLC modulation provides a staircase output waveform, which is depicted at Fig. 2.26 [92]. The output voltage is set to the closest level to

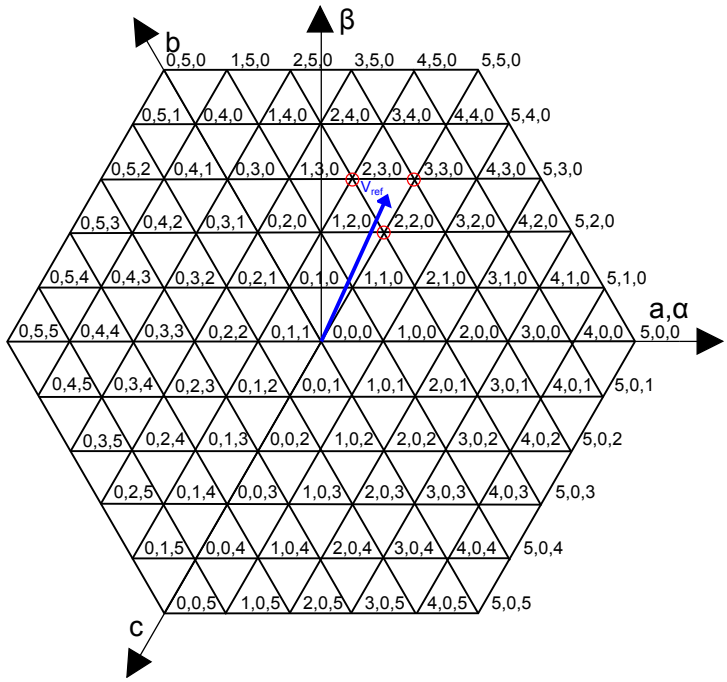

Figure 2.25. Space voltage vectors for a five level MMC.

the reference voltage (V_{ref}). Using that reference and the voltage of each sub-module (V_{sm}), the output voltage level is given by (2.38).

$$n_{nl} = round(\frac{V_{ref}}{V_{sm}}) \tag{2.38}$$

The main advantage of NLC is its simplicity, besides the reduced switching losses due to its fundamental effective switching frequency. Furthermore, in case the MMC has a large number of levels and a high modulation index is employed, the output signal is able to follow the reference signal with high accuracy, obtaining a very low harmonic distortion [123]. Hence, this technique can be applied at high voltage - high power applications. On the other hand, if the modulation index decreases, the number of levels which are utilized is lower, as it can be noticed at Fig. 2.26 and the THD rises. Therefore, NLC is not suitable for motor control stages.

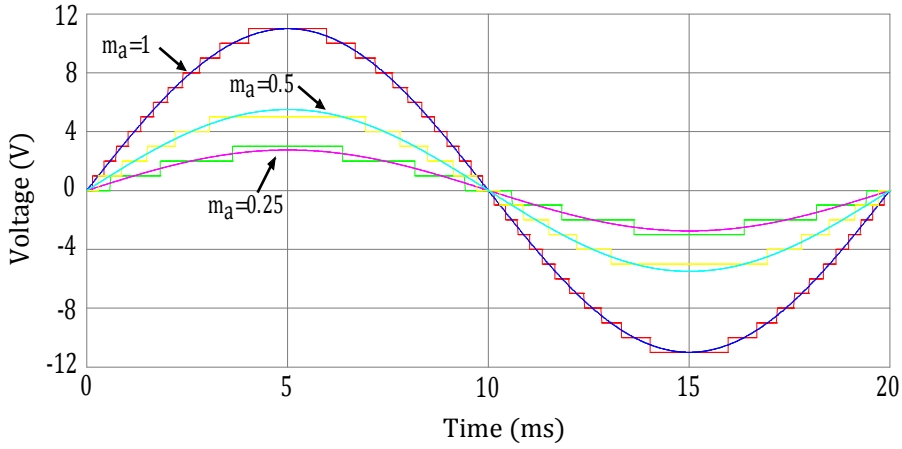

Figure 2.26: Output voltage of 23 level MMC with NLC for $m_a = 1$, 0.5 and 0.25.

Despite the fact that NLC provides fundamental effective switching frequency, comparing with PD-PWM, the latter presents a higher performance under similar switching frequency conditions, due to its lower capacitor voltage ripple and lower weighted total harmonic distortion (WTHD). The difference in performance between PD-PWM and NLC diminishes as the number of SMs increases [91].

- **Nearest Space Vector:**

  This technique is based on the selection of the nearest voltage vector to the reference vector, implementing an accurate approximation in case of converters with a high number of levels [2, 29]. As it can be noticed at Fig. 2.27, the $\alpha - \beta$ space is divided in sections and a threshold is defined with the aim of determining the closest voltage vector to the reference vector.

- **Selective Harmonic Elimination - Pulse Width Modulation (SHE-PWM):**

  SHE-PWM eliminates low-order harmonics for different values of m_a, providing high quality output waveforms with a low effective switching frequency [12]. This technique can be applied in case of MV applications where the number of SMs is not too high [12]. Particularly, in the event of three phase systems where triplen-harmonics are cancelled between phases and controlling them is not required, SHE-PWM provides lower switching losses and lower THD with respect to other modulations [10, 108].

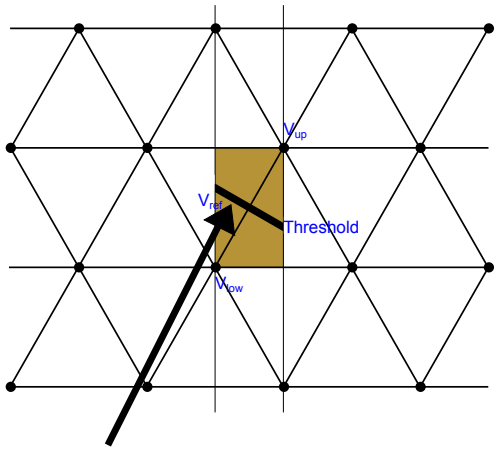

Figure 2.27. Nearest space vector modulation.

SHE is able to control as many harmonics as firing angles are available [108]. In particular, SHE eliminates all the harmonics which must be controlled, except for the fundamental harmonic. Other techniques such as selective harmonic mitigation (SHM) or total harmonic distortion (THD) minimization only control the maximum value of every harmonic with regard to grid codes or the THD, respectively. Therefore, it is possible to control more harmonics with a lower number of firing angles [10, 108]. However, SHM and THD minimization techniques do not eliminate low-order harmonics completely. This drawback, in case of motor drives when low fundamental frequency is employed, could result in low frequency torque which may cause mechanical resonance [124].

Regarding the three-phase MMC scheme depicted at Fig. 2.5-(c), the Fourier series development of the phase output voltage, whose waveform with quarter wave (QW) symmetry is shown at Fig. 2.28, is given by (2.39). The sign $\pm$ indicates whether the step is positive or negative, m is the number of firing angles in the first QW, α_k is the identifier of every firing angle and N is the number of SMs at every arm [125].

$$V_{phase-neutral}(wt) = \sum_{n=1,3,5,\ldots}^{\infty} \frac{4V_{dc}}{n\pi N}(\cos(n\alpha_1) \pm \cos(n\alpha_2) \pm \ldots \pm \cos(n\alpha_m))\sin(nwt) \tag{2.39}$$

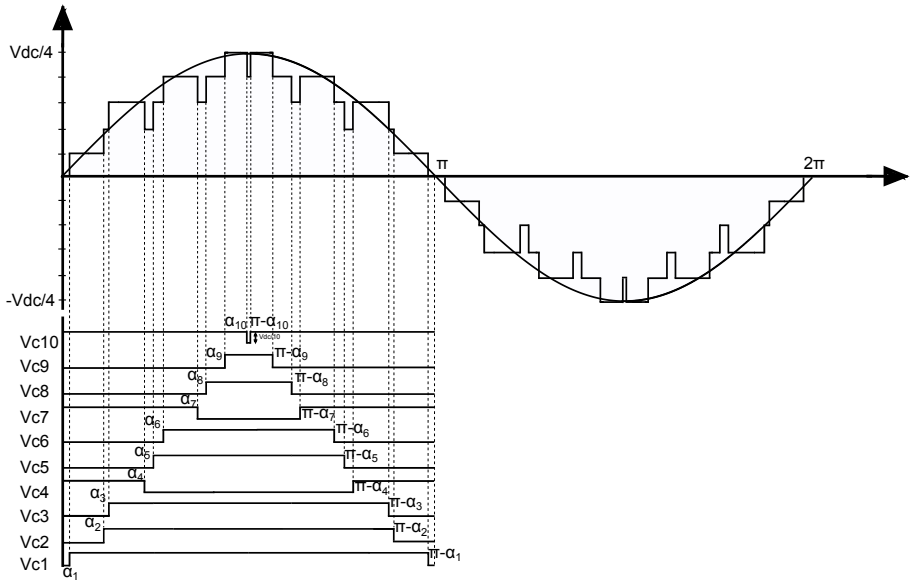

Figure 2.28. SHE-PWM waveform with QW symmetry.

In order to eliminate the closest harmonics to the fundamental frequency, the equation system to be solved is given by (2.40) [125, 126]. The firing angles are inside the range $[0, \pi/2]$ and the modulation index, m_a, range is $[0, 1.14]$. Triplen-harmonics will not be taken into account, since the converter operates in three-phase mode [12].

$$\begin{aligned}
\frac{4V_{dc}}{\pi N}\left(\cos(\alpha_1) \pm \cos(\alpha_2) \pm ... \pm \cos(\alpha_m)\right) &= \frac{m_a}{2} \\
\frac{4V_{dc}}{5\pi N}\left(\cos(5\alpha_1) \pm \cos(5\alpha_2) \pm ... \pm \cos(5\alpha_m)\right) &= 0 \\
\frac{4V_{dc}}{7\pi N}\left(\cos(7\alpha_1) \pm \cos(7\alpha_2) \pm ... \pm \cos(7\alpha_m)\right) &= 0 \\
\frac{4V_{dc}}{11\pi N}\left(\cos(11\alpha_1) \pm \cos(11\alpha_2) \pm ... \pm \cos(11\alpha_m)\right) &= 0 \\
&\vdots \\
\frac{4V_{dc}}{n\pi N}\left(\cos(n\alpha_1) \pm \cos(n\alpha_2) \pm ... \pm \cos(n\alpha_m)\right) &= 0
\end{aligned} \tag{2.40}$$

Table 2.7. Balancing Methods

Balancing Method	Extra switchings	Effective Switching Frequency	Modulation	References
Sorting Balancing Method	Yes/No	High/Low	PD-PWM/NLC/SHE-PWM /(2N+1)SHE-PWM	[138],[29],[135],[136] [24], [5],[1],[12],[91]
Pulse Energy Balancing Method for SHE-PWM	Yes	Low	SHE-PWM	[10]
Balancing Method without Measurements	No	Low	SHE-PWM/NLC	[137]
Balancing Method with Individual References for every SM	No	High	PS-PWM	[41]
Balancing Method based on Pulse Energy for PS-PWM	No	High	PS-PWM	[139]
Balancing Method with Model Predictive Control (MPC)	No	High	MPC	[87]
Predictive Balancing Method	Yes	Low	SHE-PWM/NLC	[140]
Round Robin Balancing Method	No	High	PD-PWM	[141]
Balancing Method based on DC capacitor control	No	Low	Modified NLC	[110]

Several algorithms have been presented in previous works with the aim of solving the non-linear equation system which describes the SHE problem. The most relevant algorithms are iterative approaches, Walsh functions, theory of resultants and optimization algorithms[108, 109, 127–134].

Due to the SHE-PWM advantages, such as tight control of lower order harmonics and low switching losses throughout the m_a range [12], with respect to other modulations, this thesis provides several contributions related to SHE-PWM. Therefore, chapter 3 will describe this modulation in depth.

2.4.6 Balancing Algorithms

Different methods to balance the SM capacitor voltages have been reported in the technical literature, as it can be noticed at table 2.7 [1, 5, 24, 29, 87, 91, 135–137]. All of these methods are based on redundant switching states of the SMs which can be utilized to obtain a particular phase output voltage. This voltage, and therefore, the number of inserted and short-circuited SMs at every arm, will be determined by the utilized modulation technique.

- **Sorting Balancing Method [12, 138]**: This method measures the arm currents at every phase and the capacitor voltages of every SM within the arms. Moreover, an algorithm sorts the SMs which belongs to the same arm, according to their voltage levels. Depending on these measurements and the sign of the arm currents, on the assumption that a positive arm current would charge the corresponding SMs, the number of inserted and short-circuited SMs at every arm will be determined [138]:
  - *Inserted SMs*: In case the arm current is positive, the selected SMs to be inserted will be those with the lowest voltage level. Otherwise, if the arm current is negative, the selected SMs to be inserted will be those with the highest voltage level.

  - *Short-Circuited SMs*: In case the arm current is positive, the selected SMs to be short-circuited will be those with the highest voltage level. Otherwise, if the arm current is negative, the selected SMs to be short-circuited will be those with the lowest voltage level.

  In this way, it is possible to distribute evenly both the stored energy and the power losses among all the SMs at every arm. However, apart from the switchings which are inherent to the modulation technique, this balancing method introduces extra-switchings due to variations in the SM capacitor voltages over the fundamental period. Therefore, the switching frequency could be significantly increased [138]. This problem can be addressed switching the SMs solely in case there is a change in the phase output voltage, at the expense of losing accuracy in the energy distribution [142].

  This algorithm has been used in previous works with different modulation techniques [1, 5, 12, 24, 29, 135, 136, 138]. Furthermore, a new version has been presented in [91], which is recommendable for experimental implementations, where a reduction of conditionals decreases the complexity of the control.

- **Pulse Energy Balancing Method for SHE-PWM [10]**: This technique is designed to operate with standard SHE-PWM, which commutates at every arm simultaneously to maintain the DC bus voltage, and fundamental effective switching frequency. It assumes that every SM is inserted during a pulse of π radians width over the fundamental period. Every pulse will be centred at different angles, γ_k. Depending on, γ_k, the net charge of energy for every SM will be different. Therefore, based on previous fundamental periods, the pulses which provide a higher amount of charge will be assigned to the SMs with the lowest capacitor voltages. If the assignment is maintained invariant, the distribution of energy among the SMs could not be homogeneous. In this way, reassignments are required, which introduce extra-switchings and increase the effective switching frequency. In case these reassignments were done when all the SMs are inserted or short-circuited, this increment of the switching frequency would be avoided. However, this situation only happens at high values of m_a [10].

- **Balancing Method without Measurements [137]**: This method is a modification of the previous ones which does not require the measurement of the SM capacitor voltages. The method is based on a predefined switching pattern, which consists of pulses of π radians width over the fundamental period, that ensures a zero energy exchange for every SM, over few fundamental cycles. This constraint must be satisfied in case of active and reactive power. With this aim, all the pulses are cycled over several

fundamental periods at every SM [137]. A suitable balance, using fundamental switching frequency at every SM, can be achieved with NLC and standard SHE-PWM modulations. The main drawback of this method is its lower robustness against transients and non-idealities than closed-loop methods [10]. Furthermore, it inserts low-frequency ripple, whose frequency is inversely proportional to the number of SMs at every arm, into the SM capacitor voltages. Therefore, the required capacitance in each SM is higher [141].

- **Balancing Method with Individual References for every SM [41, 91]**: This technique is based on the switching redundancy of every output voltage level and the similar conduction times of every SM that Phase-Shifted Pulse Width Modulation (PS-PWM) modulation offers. In this way, the reference of every cell can be adjusted in order to balance the capacitor voltages to the required level [41, 91].

- **Balancing Method based on Pulse Energy for PS-PWM [139]**: This method is based on the switching scheme provided by PS-PWM at every arm. Instead of utilizing different references for every SM, as it is done in previous works [41], the pulses generated at every arm are obtained and classified according to the energy which is charged or discharged from the SMs. In this way, the balancing algorithm sorts both the SM capacitor voltages and the energy associated to every pulse, with the aim of obtaining the best energy distribution [139].

- **Balancing Method with Model Predictive Control (MPC) [87]**: Apart from the switching redundancy, this method is based on an Euler approximation. A prediction, which depends on the phase output current, the SM capacitor voltages and the circulating current, is realized. The MPC strategy determines the most suitable switching combination minimizing a cost function, which includes the circulating current and the error in the prediction of both the output current and the SM capacitor voltages [87]. This technique requires a high sampling rate and therefore, the effective switching frequency could also be high.

- **Predictive Balancing Method [140]**: A predictive model calculates the total positive and negative charges in the SMs at every arm, based on the arm currents, over the previous fundamental period. Afterwards, once the maximum and minimum stored energies have been obtained, the corresponding SM capacitor voltages are calculated. This maximum and minimum voltages are considered as references. Based on the predictive model, the switching combination is determined depending on the relationship between the predicted capacitor voltages at every instant and the aimed reference

voltages. In case of transients, the method is not so accurate, although successful examples have been reported [140]. On the other hand, this method introduces some extra-switchings to follow accurately the reference voltages. This technique can be applied in conjunction with low switching frequency modulations, such as NLC or SHE-PWM.

- **Round Robin Balancing Method [141]**: This technique, which is applied in conjunction with PD-PWM modulation, alternates the switching actions among all the SMs which are included at every arm. Furthermore, with the aim of achieving a correct SM energy balance, time delays, Δt, are applied to the original PD-PWM switching scheme. These delays are executed only at switching instants related to the SMs with the lowest and highest voltage, simplifying the balancing process [141].

- **Balancing Method based on DC capacitor control [110]**: Utilizing fundamental switching frequency at every SM, grouped four pulse patterns are defined. This patterns average the DC and fundamental components in the output voltage of every SM. Furthermore, cycling these pulse patterns at every SM over several fundamental cycles, the SMs can be self-balanced. This method can be applied with a low or a high number of levels, using as many groups of four SMs as it is required. Finally, with the aim of maintaining a correct value of the SM capacitor voltages, a closed-loop control, which considers non-ideal features, reassigns the pulse patterns depending on the sorting of the SM capacitor voltages [110]. As a main drawback, this technique provides a higher THD than NLC and SHE modulations, under equal operating conditions.

Regarding the presented balancing algorithms, the one published by [11, 12] does not introduce extra-switchings. In case the effective switching frequency is close to the fundamental one, several extra-switchings could be required, as it will be detailed in chapter 5. However, other balancing methods which can operate along with SHE-PWM, also introduce extra-switchings [10, 140]. The one presented by [137] does not introduce extra-switchings, but its robustness is lower against transients and non-idealities than closed-loop methods [10]. Furthermore, it inserts low-frequency ripples, whose frequency is inversely proportional to the number of SMs at every arm, into the SM capacitor voltages, requiring a higher capacitance at every SM [141]. In this way, the method presented by [11, 12] has been selected in this thesis to balance the SM capacitor voltages.

2.4.7 Passive Component Sizing

The passive components must be sized with the aim of obtaining a correct MMC operation. In this way, several previous publications have rated both the SM capacitors C and the arm inductances L [7, 29].

2.4.7.1 SM Capacitor Rating

The SM capacitor sizing depends on the arm energy fluctuations over the fundamental period, which can be obtained from the arm powers study described at section 2.4.1. Several methods to size the SM capacitors have been proposed in the technical literature:

- **Method 1**: In case of considering a i_{circ} with only a DC component, whose value is given by 2.18 and where the arm losses are not taken into account, the energy fluctuations are given by 2.41, where V_{dc} is the DC input voltage, P_S is the apparent power of the three-phase MMC, m_a is the modulation index, ω is the fundamental frequency, and $cos(\phi)$ is the power factor [7, 29]. The SM capacitor voltage ripple produced by the arm energy variation is given by (2.42) [7, 84, 86], where N is the number of SMs contained in the arm, V_c is the SM capacitor averaged voltage and C is the SM capacitance. In this way, the SM capacitor voltage v_c is limited by (2.43).

$$\Delta W_{arm} = \frac{2}{3}\frac{P_S}{m_a\omega}\left(1-\left(\frac{m_a cos(\phi)}{2}\right)^2\right)^{\frac{3}{2}}, \tag{2.41}$$

$$k_r = \frac{\Delta W_{arm}}{N2V_c^2C}, \tag{2.42}$$

$$V_c(1-k_r) \leq v_c \leq V_c(1+k_r), \tag{2.43}$$

- **Method 2**: [86] utilized the arm power expressions to calculate the instantaneous arm energy, regarding an i_{circ} with a DC and a second harmonic components, besides a third harmonic common mode voltage v_{cm}. In this way, it is possible to obtain the arm energy ripple ΔW_{arm} over the fundamental period. Finally, the SM capacitor voltage ripple for a particular C value is obtained by (2.42).

- **Method 3**: Utilizing the averaged model developed by [84], the SM capacitor voltage ripple, normalized with respect to the RMS value of i_u, is given by (2.28).

Equations (2.42) and (2.28) provide the possibility to calculate C under the worst case which is given by the maximum i_u, minimum m_a, minimum fundamental frequency and maximum allowed SM capacitor voltage ripple.

The resulting ripple provided by methods 1, 2 and 3 will be an ideal value provided by an infinite switching frequency. Hence, the real SM capacitor voltage ripple will be higher and inversely proportional to the switching frequency [86].

2.4.7.2 Arm Inductance Rating

The arm inductance, L is utilized to eliminate parasitic currents. [143] calculated the L value, considering a i_{circ} with a DC component given by (2.18) and an uncontrolled second order harmonic component. In this way, as it was analysed by [5] and the arm powers study included at section 2.4.1, this i_{circ} generates a second harmonic component at the arm powers and consequently, at the arm voltages. The relevant fluctuation of energy at every MMC phase is given by (2.44), where $\widehat{V}_{upper,2}$ is the second harmonic amplitude of v_{upper}, P_S is the apparent power and ω is the fundamental angular frequency. Regarding (2.44), the relationship between L, C and $\widehat{I}_{circ,2}$ is given by (2.45), where V_c is the SM capacitor averaged voltage and $\widehat{I}_{circ,2}$ is the amplitude of the i_{circ} second harmonic. Therefore, $\widehat{I}_{circ,2}$ can be limited increasing the L value.

$$\Delta W_{phase} = \left(\frac{P_S}{6\omega} + \frac{V_{dc}\widehat{V}_{upper,2}}{8\omega^2 L} \right) sin(2\omega t + \phi), \tag{2.44}$$

$$L = \frac{1}{8\omega^2 C V_c} \left(\frac{P_S}{3\widehat{I}_{circ,2}} + V_{dc} \right), \tag{2.45}$$

On the other hand, L is employed to limit fault currents, as it is done in grid-connected applications [28]. In this way, the relationship between L and the rise rate of the fault current is given by (2.46) [143].

$$\alpha = \frac{di_{circ}}{dt} = \left(\frac{V_{dc}}{2L} \right), \tag{2.46}$$

Both issues, the fault and parasitic currents, have been addressed by [47, 137] utilizing guide L values closed to 0.1 p.u.

2.5 Conclusions

MMC provides several advantages such as low effective switching frequency, low losses, high scalability due to its modularity, requirement of negligible AC filters, mechanical simplicity or transformerless connection. Therefore, it is a suitable converter to be employed with high voltage and high power applications. Furthermore, the utilization of MMCs in medium voltage applications is currently being researched. Particularly, the indirect topology can be employed in different medium voltage applications, such as MVDC networks or MV motor drives. In this way, a low switching frequency modulation such as SHE-PWM can improve the MMC performance, providing simultaneously low switching losses and low THD under different operating conditions. Therefore, this thesis will be focused on applying SHE-PWM to indirect MMCs.

Two main challenges must be met to utilize SHE-PWM with indirect MMCs. Firstly, a high number of harmonics must be controlled throughout the m_a range. In this way, a wide range of fundamental frequencies, utilizing a similar switching frequency and different m_a values can be employed. Therefore, a new method which simplifies the process to calculate a high number of firing angles would be desirable.

Secondly, the i_{circ} must be controlled with the aim of reducing the SM capacitor voltage ripple and the MMC losses. However, the existing i_{circ} controls, which are designed to operate with other modulations such as PWM, provide several drawbacks if they are applied along with (2N+1) SHE-PWM or (N+1) SHE-PWM, which are the two possible SHE-PWM implementations in MMCs (described in section 3.2.2). Several controllers apply different m_a values at each phase arm [5, 82, 85, 87, 93, 96, 103–106, 144–146] or at each SM [41, 104], to follow the i_{circ} reference. However, these techniques would insert significant disturbances at low-order harmonics at the phase output voltage, in case of SHE-PWM modulations [102]. On the other hand, [107] defined a i_{circ} control for (N+1) SHE-PWM which introduces variations in the firing angles at the upper and lower arms. However, this method could insert disturbances at the phase output voltage in case the variations in the firing angles are significant [110]. In addition, this technique is not consistent with (2N+1) SHE-PWM, which alternates the commutations of both phase arms [11, 12]. Finally, [111] provided a i_{circ} control utilizing PWM techniques with (2N+1) levels. In this way, seve-

ral redundant voltage levels are obtained which provide a degree of freedom to control the i_{circ}. This technique, despite the fact that it could be utilized with (2N+1) SHE-PWM, would introduce an uncontrolled i_{circ} ripple due to the low switching frequency and the uneven distance between firing angles, inherent to (2N+1) SHE-PWM.

Therefore, new i_{circ} control methods for SHE-PWM, without disturbing the phase output voltage, must be developed.

This thesis addresses these two challenges. On the one hand, a new method which simplifies the process to calculate the firing angles that solve the SHE-PWM modulation is proposed. On the other hand, new circulating current control methods when the converter is operating under SHE-PWM are presented.

Chapter 3

Selective Harmonic Elimination - Pulse Width Modulation

3.1 Introduction

The utilization of MMCs in MV and high power applications, where the number of required SMs is not high, is currently under research [9, 10, 40, 61, 62]. One of the main goals of new modulations and control techniques for MMC is the improvement of its efficiency. In this way, in MV applications, selective harmonic elimination - pulse width modulation (SHE-PWM) is able to provide lower effective switching frequency and even THD, than high switching frequency modulations such as PWM techniques [12, 108]. In particular, SHE-PWM is attractive in three-phase systems where triplen harmonics are cancelled between phases and controlling them is not required [10, 108]. Therefore, it is an appealing modulation technique to be applied along with grid connected converters or motor drives.

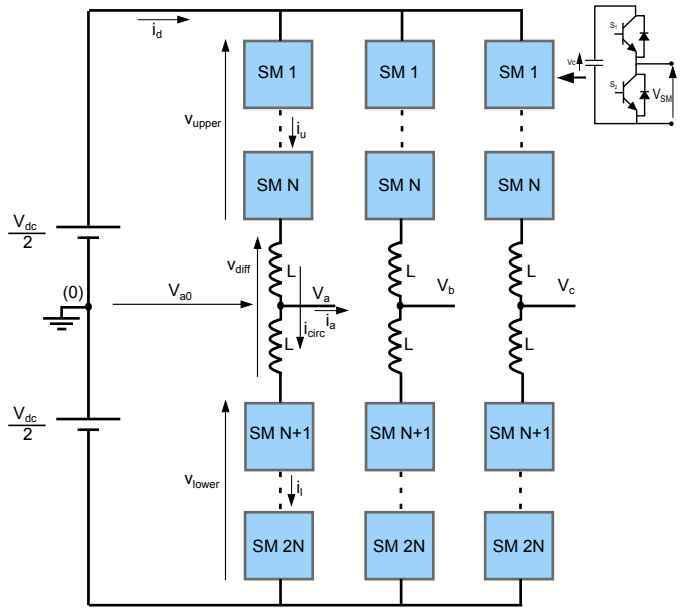

Figure 3.1. Three-phase MMC with HB SMs.

3.2 Formulations

SHE-PWM is able to control as many harmonics as firing angles are available [108]. Therefore, the selected low-order harmonics can be removed and the fundamental frequency may be adjusted to a particular value. As it has been commented in section 2.4.5, there are other techniques such as selective harmonic mitigation (SHM) [147–149] or total harmonic distortion minimization (THDM) [150, 151]. SHM ensures the amplitude of these low-order harmonics to be lower than a particular value according to specific grid codes, instead of completely removing them. THDM, besides considering these grid codes, minimizes the THD. Both SHM and THDM provide the advantage of controlling more harmonics with equal number of firing angles than SHE-PWM [10, 108]. However, they do not eliminate completely low-order harmonics and it could be an important drawback for certain applications such as motor drives. In this case, when low fundamental frequency is employed, it could result in low frequency torque which may cause mechanical resonance [124]. Considering this issue, SHE-PWM will be selected to obtain the phase output voltage, with the aim of eliminating the low-order harmonics completely.

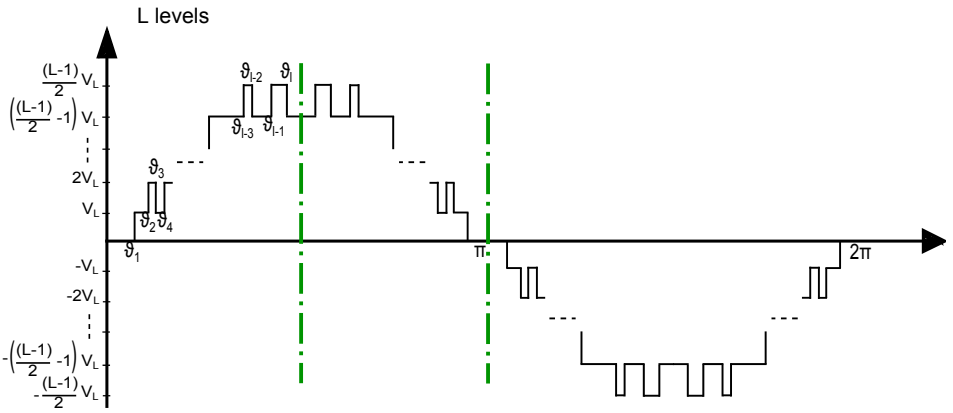

Figure 3.2. Switching scheme of SHE-PWM with QW symmetry.

The different existing formulations for SHE-PWM depend on the utilized symmetry. In addition, in case of MMCs, depicted at Fig. 2.5-(c) and reproduced here for convenience (see Fig. 3.1), the number of phase output voltage levels L provided by the converter and their corresponding amplitude, will depend on the switching scheme employed, $(N+1)$ or $(2N+1)$, being N the number of SMs at every arm. Both issues, the symmetry and the switching schemes are analysed below.

3.2.1 Symmetry

Different kinds of symmetries can be applied to generate the SHE-PWM waveform. Particularly, quarter wave (QW), half wave (HW) or non symmetries could be utilized. In this way, every symmetry requires a different formulation with the aim of solving the SHE-PWM problem. Every formulation provides a system of equations, obtained through the Fourier series expansion, which can be used to calculate the firing angles which eliminate the lower-order harmonics and control the fundamental frequency.

3.2.1.1 Quarter Wave Symmetry

Regarding the phase output voltage depicted at Fig. 3.2, the current formulation for SHE-PWM problem with quarter-wave (QW) symmetry is given by (3.1), (3.2), (3.3) and (3.4) [11, 12]. V_L is the step voltage, θ_k is the identifier of

every firing angle, l is the total number of firing angles in the first QW and n is the identifier of every odd harmonic (due to the odd symmetry, the waveform in three-phase systems only contains odd non-triple harmonics). On the other hand, as it can be noticed at (3.3), the search range of every firing angle is [0,π/2].

$$v_{a0} = \sum_{n=1,3,5,7,...}^{\infty} b_n sin(n\omega t), \tag{3.1}$$

$$b_n = \frac{4V_L}{n\pi} \sum_{k=1}^{l} m_k cos(n\theta_k), \tag{3.2}$$

$$0 \leq \theta_1 < \theta_2 < ... < \theta_l \leq \frac{\pi}{2}, \tag{3.3}$$

$$m_k = \left\{ \begin{array}{c} 1 \ \forall \ positive \ \ step, \\ -1 \ \forall \ \ negative \ \ step, \end{array} \right\}, \tag{3.4}$$

As it given by (3.2), the Fourier series expansion only contains b_n coefficients which depend on the sign of every step, m_k. In this way, l equations must be solved to control l harmonics. Therefore, QW symmetry provides lower computational load, due to its greater simplicity, to eliminate equal number of harmonics than HW symmetry or non-symmetry [127]. In this way, QW symmetry is an interesting option in case of eliminating a high number of harmonics, all of them with equal phase value [108, 126].

The equation system to be solved, which eliminates the lower order harmonics and controls the amplitude of the fundamental frequency, is given by (3.3), (3.4), (3.5) and (3.6) [126].

$$\begin{array}{c} \frac{4}{\pi(L-1)}(m_k \cos(\theta_1) + m_k \cos(\theta_2) + ... + m_k \cos(\theta_l)) - \frac{m_a}{2} = 0, \\ \vdots \\ \frac{4}{n\pi(L-1)}(m_k \cos(n\theta_1) + m_k \cos(n\theta_2) + ... + m_k \cos(n\theta_l)) = 0, \end{array} \tag{3.5}$$

$$0 < m_a < 1.15, \tag{3.6}$$

As it is given by (3.5), the equation system predefines the m_k values and therefore, the sign of every step. In this way, the waveform must be defined beforehand, hindering significantly the searching task in case of multilevel converters, where the number of possible waveforms is high.

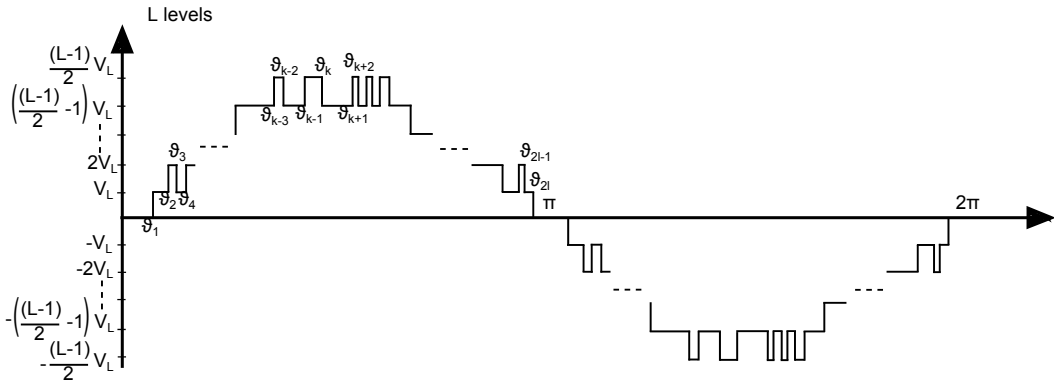

Figure 3.3. Switching scheme of SHE-PWM with HW symmetry.

3.2.1.2 Half Wave Symmetry

The scheme of a SHE-PWM waveform with HW symmetry is depicted at Fig. 3.3, whose Fourier series expansion is given by (3.7), where a_n and b_n are the Fourier series coefficients and ω is the fundamental frequency [108, 127, 152]. This waveform, in case of three phase systems, contains odd non-triplen harmonics besides the fundamental frequency.

$$v_{a0} = \sum_{n=1,3,5,7,\ldots}^{\infty} a_n cos(n\omega t) + \sum_{n=1,3,5,7,\ldots}^{\infty} b_n sin(n\omega t), \tag{3.7}$$

With the aim of solving the SHE-PWM problem, the firing angles located in the first half fundamental cycle must be calculated to control the lower-order harmonics. SHE-PWM with HW symmetry provides twice as many different firing angles as SHE-PWM with QW symmetry [108]. However, unlike QW symmetry, both a_n and b_n must be controlled and therefore, $2l$ angles must be calculated to eliminate l harmonics. In this way, the number of controlled harmonics are equal for both symmetries, although HW one could provide harmonics with different phase values, obtaining a wider variety of solutions.

As it has been provided by [152], the equations of a_n and b_n are given by (3.8), (3.9), (3.10) and (3.11). According to the Fig. 3.3, L is the number of levels, V_L is the step voltage, θ_k are the firing angles, $2l$ is the number of firing angles over the HW period. As it is given by (3.11), the search range of every firing angle is [0,π].

$$a_n = -\frac{2V_L}{n\pi}\sum_{k=1}^{2l} m_k sin(n\theta_k), \tag{3.8}$$

$$b_n = \frac{2V_L}{n\pi}\sum_{k=1}^{2l} m_k cos(n\theta_k), \tag{3.9}$$

$$m_k = \left\{ \begin{array}{l} 1 \ \forall \ raising \ \ edge, \\ -1 \ \forall \ \ falling \ \ edge, \end{array} \right\} \tag{3.10}$$

$$0 \leq \theta_1 < \theta_2 < ... < \theta_{2l} \leq \pi, \tag{3.11}$$

HW symmetry offers a wider variety of solutions than QW one, providing the possibility of obtaining better harmonic performance, besides different phases at every harmonic [127, 152].

The equation system to be solved is given by (3.10), (3.11), (3.12), (3.13), (3.14) and (3.15) [152].

$$\begin{array}{l} \frac{2}{\pi(L-1)}(-m_k \sin(\theta_1) - m_k \sin(\theta_2) - ... - m_k \sin(\theta_{2l})) - X_1 = 0, \\ \qquad\qquad\qquad\qquad\qquad\qquad \vdots \\ \frac{2}{n\pi(L-1)}(-m_k \sin(n\theta_1) - m_k \sin(n\theta_2) - ... - m_k \sin(n\theta_{2l})) = 0, \end{array} \tag{3.12}$$

$$\begin{array}{l} \frac{2}{\pi(L-1)}(m_k \cos(\theta_1) + m_k \cos(\theta_2) + ... + m_k \cos(\theta_{2l})) - Y_1 = 0, \\ \qquad\qquad\qquad\qquad\qquad\qquad \vdots \\ \frac{2}{n\pi(L-1)}(m_k \cos(n\theta_1) + m_k \cos(n\theta_2) + ... + m_k \cos(n\theta_{2l})) = 0, \end{array} \tag{3.13}$$

$$\sqrt{X_1^2 + Y_1^2} = \frac{m_a}{2}, \ \ 0 < m_a < 1.15, \tag{3.14}$$

$$\phi_1 = arctg\left(\frac{Y_1}{X_1}\right), \tag{3.15}$$

Like QW symmetry, the equation system predefines the m_k values and therefore, the sign of every step.

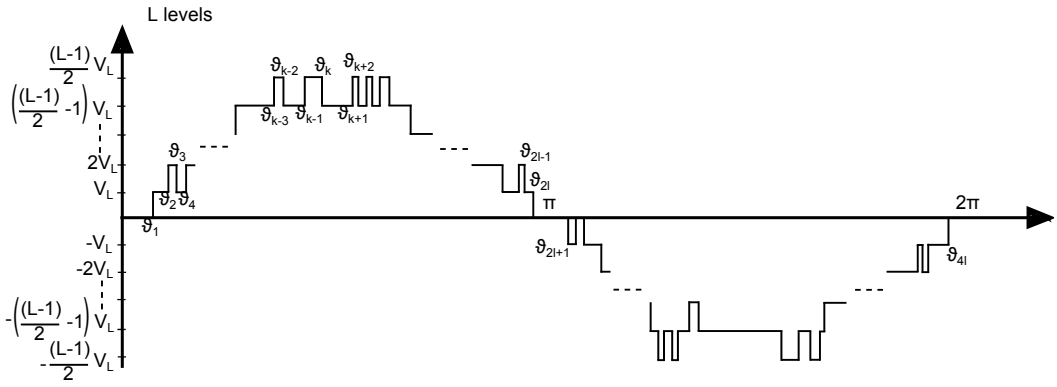

Figure 3.4. Switching scheme of SHE-PWM with non-symmetry (NS).

3.2.1.3 Non-Symmetry

The SHE-PWM with non-symmetry, whose scheme is depicted at Fig. 3.4, contains the Fourier series expansion given by (3.16).

$$v_{a0} = a_0 + \sum_{n=1,2,3,4...}^{\infty} a_n cos(n\omega t) + \sum_{n=1,2,3,4...}^{\infty} b_n sin(n\omega t), \tag{3.16}$$

The a_0, a_n and b_n coefficients are given by (3.17), (3.18), (3.19), (3.20) and (3.21). As it can be noticed, the search range for every firing angles is [0, 2π].

$$a_0 = \frac{V_L}{2\pi} \sum_{k=1}^{4l} m_k \theta_k, \tag{3.17}$$

$$a_n = -\frac{2V_L}{n\pi} \sum_{k=1}^{4l} m_k sin(n\theta_k), \tag{3.18}$$

$$b_n = \frac{2V_L}{n\pi} \sum_{k=1}^{4l} m_k cos(n\theta_k), \tag{3.19}$$

$$m_k = \left\{ \begin{array}{l} 1 \ \forall \ raising \ \ edge, \\ -1 \ \forall \ \ falling \ \ edge, \end{array} \right\} \tag{3.20}$$

$$0 \leq \theta_1 < \theta_2 < ... < \theta_{4l} \leq 2\pi, \tag{3.21}$$

This waveform provides $4l$ firing angles over the fundamental period. In this way, regarding the same switching frequency, non-symmetry provides twice and four-fold as many firing angles as HW and QW symmetries, respectively. However, besides the requirement of controlling the a_0, a_n and b_n values, the even harmonics must also be eliminated. Therefore, $4l$ firing angles must be calculated to control $l-2$ harmonics. In this way, this kind of waveform is the least appealing due to its non-optimum harmonic content, utilizing the same switching frequency and its higher computational load [108, 127, 153, 154].

3.2.2 Selective Harmonic Elimination for Modular Multilevel Converter

Regarding the MMC scheme depicted at Fig. 2.5-(c), two different SHE-PWM waveforms can be obtained at the phase output voltage. On the one hand, N+1 levels can be obtained switching simultaneously at the upper and lower arms. On the other hand, if the upper and lower arm commutations are alternated, the MMC will provide a waveform with 2N+1 levels.

3.2.2.1 (N+1) Selective Harmonic Elimination

The switching scheme of SHE-PWM waveform with N+1 levels is depicted at Fig. 3.5 [11, 12]. As it can be noticed, at every firing angle two switchings, one at every arm, happens simultaneously. In this way, the amplitude of every phase output voltage step is given by (3.22), where V_{DC} is the DC input voltage and N is the number of SMs at every arm. In addition, the differential voltage in the arm inductances is always closed to zero, only depending on the SM capacitor voltages and their associated ripple.

$$V_L = \frac{V_{DC}}{N} \tag{3.22}$$

This technique requires a i_{circ} control technique which does not disturb the phase output voltage.

3.2.2.2 (2N+1) Selective Harmonic Elimination

(2N+1) SHE-PWM modulation presents the switching scheme depicted at Fig. 3.6, where the amplitude of every phase output voltage step is given by (3.23). As

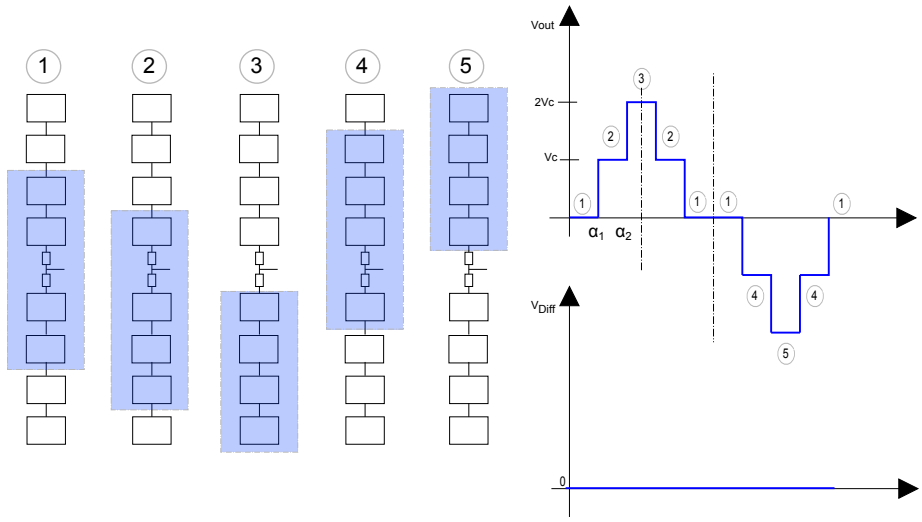

Figure 3.5. Switching scheme of (N+1) SHE-PWM modulation, for $N = 4$.

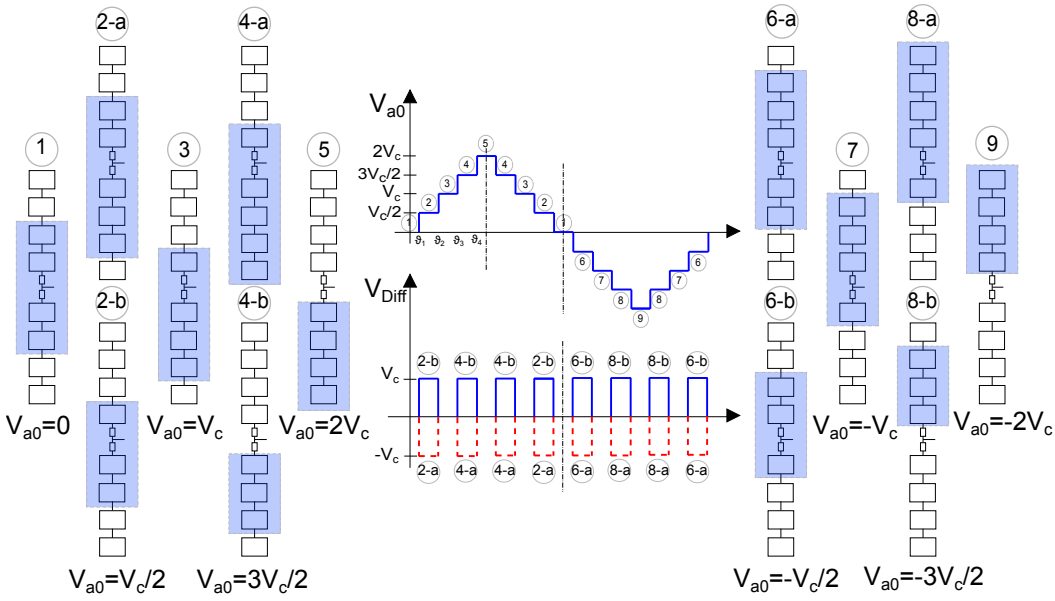

Figure 3.6. Switching scheme of (2N+1) SHE-PWM modulation, for $N = 4$.

it can be noticed, (2N+1) SHE-PWM alternates the switchings of the upper and lower arms and moving from one state to the next only requires one commutation, unlike (N+1) SHE-PWM [11, 12]. In this way, twice as many firing angles as (N+1) SHE-PWM, with equal number of commutations over the fundamental period, are available. Therefore, (2N+1) SHE-PWM is able to eliminate twice as many harmonics as (N+1) SHE-PWM with equal switching frequency, providing a significantly lower THD. In other words, equal THD can be achieved with lower switching losses.

$$V_L = \frac{V_{DC}}{2N} \tag{3.23}$$

The main drawback inherent to this technique is its high i_{circ} ripple, due to the alternation of commutations. As it can be noticed in Fig. 3.6, there are several phase output voltage levels which provide positive or negative differential voltage. In this way, a i_{circ} control and a i_{circ} ripple limitation are required to operate the MMC.

3.3 Solution to the SHE-PWM Problem

Several calculation algorithms have been published in the technical literature to solve the equation systems which solve the SHE-PWM problem [108]. As it has been commented, regardless of the utilized symmetry, the present equation systems depend on the sing of every step. In this way, present calculation methods utilize predefined switching patterns to start the search of firing angles [108]. The selection of this pattern is particularly relevant in case of multilevel converters where different patterns are required throughout the m_a range. It may happen that a particular waveform is not useful to solve the SHE-PWM problem for a particular m_a value. For this reason, several methods have been presented which provide techniques to obtain a suitable pattern for a particular m_a value and its corresponding initial solution [126, 152, 155]. In case that pattern is not valid, another one must be tried again, until a valid solution is obtained.

With the aim of implementing the SHE-PWM, this section describes the most relevant calculation algorithms and selects one of them to solve the equation systems.

3.3.1 Calculation Algorithms

Several algorithms have been presented in previous works with the aim of solving the non-linear equation system which describes the SHE-PWM problem. The most relevant algorithms are iterative approaches, Walsh functions, theory of resultants, equal area criteria - based four equation method and optimization algorithms[108, 127, 153]. All of these techniques are designed to be applied off-line, except for the equal area criteria which can also be applied on-line. Regarding other on-line techniques, the neural network, modulation based algorithm, simplex homotopic fixed-point algorithm and model predictive control are the most relevant. However, low accuracy, low number of controlled harmonics [108] or higher switching losses [156–158] are the main drawbacks of on-line techniques.

3.3.1.1 Newton-Raphson

The Newton-Raphson method utilizes the derivative of the equation system given by (3.5), in case of QW symmetry. In this way, it is possible to obtain the switching trajectories of the firing angles for a particular m_a value and therefore, to obtain the solution for another closed m_a value [159]. This challenge is met utilizing an iterative approach. However, this dependence on the derivative can make the algorithm provide a local minimum rather than the global minimum. In addition, this technique depends largely on the starting solution [109], whose prediction may not be possible in case of a high number of firing angles or in case of multilevel waveforms [108]. Predictive [159], equal area [160] or genetic algorithms [161] can help to search these initial values.

3.3.1.2 Walsh Functions

Walsh functions transform the Fourier Series equation system on an algebraic system, providing a reduction in the computational load [128]. However, this method is dependent on the initial solution as it happens with Newton-Raphson method.

3.3.1.3 Theory of Resultants

Theory of resultants converts the initial equation system into an equivalent polynomial equation system which can be solved through the resultants method [129]. This technique does not depend on the initial solution and it is able to find all the solutions. However, the main problem of this technique is the high degree of

the polynomials in case of a high number of levels, resulting in high computational cost [109]. The theory of symmetric polynomials and the theory of power sums may decrease this computational load [130, 162]. Recently, another method has been presented which is based on the symmetrical polynomial theory and Groeβner bases [163]. This technique provides higher calculation efficiency than the theory of resultants. However, when the number of firing angles is increased, the computational cost is still high, controlling 9 harmonics at the most.

3.3.1.4 Equal Area Criteria - Based Four Equation Method

This technique is able to control groups of four harmonics independently. In this way, it is not required to operate with the whole equation system given by (3.5). This method divides (3.5) in groups of four equations and is based on the equal area criteria. In this way, through this criteria and utilizing a predefined switching pattern, modifications in the reference fundamental amplitude make every group of four equations independent among each other. Therefore, the computational load is reduced, providing more flexibility to increase the number of firing angles. However, this technique provides a reduced number of switching patterns due to the predefined waveforms and requires more firing angles to eliminate the same number of harmonics than other methods. In this way, the switching losses provided by this technique are higher. Finally, the accuracy in the elimination of harmonics, for several m_a values, is lower than other methods, such as Newton-Raphson, theory of resultants or optimization techniques [164].

3.3.1.5 Modulation based algorithm

The modulation based algorithm is a real-time technique which does not require the solution of the equation system given by (3.5) to eliminate lower-order harmonics. This method compares the sinusoidal reference waveform with a modified carrier. Utilizing this carrier, whose frequency is f_c, the harmonics lower than f_c are eliminated. In this way, this technique is simpler than other techniques. However, due to the elimination of triplen harmonics, in case of three-phase systems this method provides higher switching losses than other methods, which are able to leave the triplen harmonics uncontrolled [156].

3.3.1.6 Simplex Homotopic Fixed-Point Algorithm

The simplex homotopic fixed-point algorithm provides the initial values to search the firing angles using polynomial equations, which are previously obtained from

the Fourier series equations. Once the initial values are obtained, they are refined through a cubic iteration [165]. This technique is proposed to operate on-line, using several processors in parallel. However, due to the dependence on the initial values, more solutions could be valid which are not provided by the method.

3.3.1.7 Neural Networks

This technique utilizes a generalized Hopfield neural network (GHNN) to minimize an objective function that solves the SHE-PWM problem. The associated differential equations are solved by the Runge-Kutta fourth-order method. This technique obtains the solutions in real-time [166]. However, it only provides a reduced number of controlled harmonics.

3.3.1.8 Model Predictive Control

The model predictive control is an on-line technique which provides the firing angles that eliminate the lower-order harmonics. In particular, an objective function, which considers the DC component, the fundamental harmonic amplitude, the amplitude of the harmonics to be eliminated (including the even harmonics) and the number of commutations over the fundamental period, is utilized. The main drawbacks of this technique are the higher switching losses, the reduced number of harmonics that can be controlled and lower accuracy than off-line techniques [157, 158].

3.3.1.9 Optimization Algorithms

Optimization algorithms are well suited for finding solutions in spaces that are not well defined or have a large number of local minimums, which greatly hinder the searching task of traditional methods of calculation [109]. Due to their intrinsic ability to use randomly distributed initial population, managing large amounts of data simultaneously, avoiding local minima and solving complex problems, optimization algorithms are a good solution to the problem of SHE modulation [131]. The most relevant optimization algorithms are genetic algorithms (GAs)[132, 167], differential evolution algorithms (DE)[133, 168] and particle swarm optimization algorithms (PSO)[134]. On the other hand, there are also algorithms which combine GAs with random search to obtain the sets of angles [109, 169–171] or to obtain the initial values which can be used by Newton-Raphson method [153, 154, 161, 172].

These techniques, due to the utilization of randomly distributed initial population, can provide different solutions to the SHE-PWM problem after several executions [132, 133]. Therefore, despite the fact that these methods are not able to ensure that all the existing solutions will be found, they are able to obtain a high number of them. In addition, different published works have proved their validity to control a high number of harmonics [11, 12, 102], unlike the theory of resultants.

3.3.2 Search Algorithm Selection

With the aim of controlling the MMC under variable operating conditions, with variable fundamental frequency and m_a values, a high number of harmonics must be controlled throughout the m_a range. Furthermore, it is required that the selected algorithm provides several different solutions, for every m_a value, with the aim of improving the design regarding the THD or the amplitudes of the first non-eliminated harmonic [102, 154].

Firstly, considering the number of controlled harmonics, only Newton-Raphson, optimization techniques, modulation based algorithm, based four-equations method and Walsh functions are able to eliminate a high number of undesired harmonics. Newton-Raphson, Walsh functions and four-equations method depend strongly on the initial values, which are difficult to be found in case of a high number of firing angles and multilevel inverters. In addition, based four-equations method and modulation based algorithm provide higher switching losses than optimization algorithms or Newton-Raphson methods.

Regarding the ability to provide several solutions for every m_a value, without depending on initial values, only optimization algorithms and theory of resultants are able to provide this feature. However, the theory of resultants are not able to calculate a high number of firing angles.

Therefore, considering these two constraints, optimization techniques are considered suitable to solve the SHE-PWM problem for MMCs. The existing optimization techniques differ in the selection, crossover and mutation processes, besides the management of inequalities and all of them can be used to solve the SHE-PWM problem. However, due to their dependence on the objective function, the most optimum method can not be clearly determined beforehand. Moreover, all of the methods have acquired features over the years which were characteristic of others, resulting in different versions of every optimizing algorithm [173].

In this way, because of their proven effectiveness in the technical literature [11, 12, 102, 109, 132, 153, 154, 161, 167, 169–175], GAs have been selected to solve

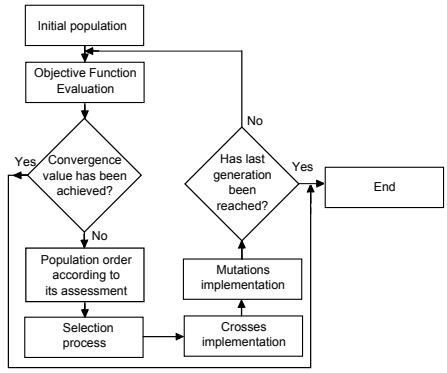

Figure 3.7. Flow diagram of genetic algorithms (GAs).

the SHE-PWM problem. They are stochastic optimization techniques of general purpose and do not need to know the derivative of the objective function to get to the optimal solution. Every solution depends on the optimization variables which in case of SHE-PWM problem are the firing angles.

GAs are based on the flux diagram of fig. 4.8-(a) and on the following concepts [132]:

- Initial population: Set of possible values for every firing angle on which to evaluate the objective function. The population must be defined within the limit values, search range, of every variable.
- Objective function: This function represents the problem to be solved and hence, the goal is to find the set of variables that minimize its value.
- Generations: The evaluation of the objective function according to the current population of every variable is implemented as many times as number of generations. The aim is achieving an existing population, for every variable, which provides a better objective function solution from one generation to the next.
- Selection: The selection process, which can be developed in different ways, determines which elements of a population will be chosen as parents for the next generation. The best solutions will persist, but these solutions are not the only ones selected, since the algorithm can get stuck in a local minimum soon. Among all selected parents, a percentage of the children is created by crosses and the remaining by mutations.
- Crossover: In the crossover process, the values of both parents are used

to generate the value of a child. In this work, arithmetic crossover has been utilized which returns a child value located randomly in between the parents values.

- Mutations: After making the crossovers, mutations are made. This process is interesting since it can generate very different solutions from those previously existing and it can prevent the algorithm from being trapped in a local minimum.

3.4 Conclusion

The SHE-PWM technique is able to provide simultaneously tight control of lower-order harmonics and low switching losses. Therefore, it is a suitable technique to reduce the switching losses of MMCs when they are applied in medium voltage applications where the number of SMs at every arm is not high. QW symmetry can be used to control a high number of harmonics, due to its reduced computational load and HW symmetry can be utilized to optimize the solution, considering the THD or the first non-eliminated harmonic. In this way, both symmetries have been studied in this thesis.

Considering the two possible waveforms of SHE-PWM provided by MMCs, the (N+1) SHE-PWM provides a lower circulating current ripple than (2N+1) SHE-PWM, but the latter is able to provide a lower THD under the same switching frequency. Therefore, both waveforms have been considered in this thesis.

In addition, regarding the existing methods to solve the SHE-PWM problem, the optimization algorithms have been selected in this thesis, due to their ability to control a high number of harmonics and to obtain several solutions for every m_a. In this way, it is possible to operate the MMC under different operating conditions. In particular, GAs have been selected due to their proven effectiveness in the technical literature.

Finally, the study of current formulations for both HW and QW symmetries shows that previous works which solve the SHE-PWM problem search the firing angles using a predefined switching pattern. However, in multilevel converters such as MMCs, this switching pattern may not provide a solution to the SHE-PWM problem for a particular m_a value. In that case, the switching pattern must be replaced by another one and the search should be restarted. Moreover, the utilization of different switching patterns is required to find a solution throughout the m_a range. Therefore, a method which is able to calculate simultaneously the switching patterns and the associated firing angles, without using a predefined

waveform, would simplify the search process, particularly when the number of possible switching patterns is significantly high. This thesis proposes a novel method with these characteristics for both QW and HW symmetries.

Chapter 4

Novel Technique to Implement SHE-PWM

4.1 Introduction

Previous works, which solve the SHE-PWM problem, search the firing angles using a predefined switching pattern [108, 109, 127–134, 164, 165, 168, 176]. In multilevel converters such as MMCs, this switching pattern may not provide a solution to the SHE-PWM problem for a particular modulation index, m_a, value. In that case, the switching pattern should be replaced by another one and the search should be restarted. Moreover, the utilization of different switching patterns is required to find a solution throughout the m_a range [11]. Therefore, a method which is able to calculate simultaneously the switching pattern and the associated firing angles, without using a predefined waveform, would simplify the search process, particularly when the number of possible switching patterns is significantly high.

This work presents two mathematical methods which are able to solve the SHE-PWM problem with quarter wave (QW) and half-wave (HW) symmetries, respectively, for multilevel converters [97, 177–179]. The proposed methods utilize unique equation systems which are valid for any possible waveform. Thereby, these techniques are able to provide simultaneously the switching patterns and the firing angles that comply with the solution to the SHE-PWM problem, without using predefined waveforms, throughout the m_a range. In this way, the search process, which is based on optimization algorithms, is simplified and the likeli-

hood to obtain a wider variety of solutions, using the same number of variables than previous methods, is higher. Both methods, in particular the QW method due to its lower computational load, are able to eliminate a significantly high number of harmonics.

4.2 Novel Method to Solve the QW Symmetry SHE-PWM Problem

The new proposed method, which solves the SHE-PWM problem with QW symmetry, provides simultaneously both the switching patterns and the associated firing angles, throughout the m_a range, without using predefined waveforms [97, 177, 179].

4.2.1 Equation System

Regarding a three-phase MMC, where the triplen harmonics are not required to be controlled, the mathematical problem which eliminates the lower-order harmonics and controls the amplitude of the fundamental frequency, is described by (4.1) and (4.2), where L is the number of levels of MMC, n identifies every harmonic, l is the total number of firing angles or controlled harmonics, $\theta_{k,virtual}$ identifies every firing angle and m_a is the modulation index of the phase output voltage.

$$\begin{aligned}
&\frac{4}{\pi(L-1)}(\cos(\theta_{1,virtual})+\cos(\theta_{2,virtual})+...+\cos(\theta_{l,virtual}))-\frac{m_a}{2}=\varepsilon_1,\\
&\frac{4}{5\pi(L-1)}(\cos(5\theta_{1,virtual})+\cos(5\theta_{2,virtual})+...+\cos(5\theta_{l,virtual}))=\varepsilon_5,\\
&\qquad\qquad\qquad\qquad\qquad\qquad\qquad\vdots\\
&\frac{4}{n\pi(L-1)}(\cos(n\theta_{1,virtual})+\cos(n\theta_{2,virtual})+...+\cos(n\theta_{l,virtual}))=\varepsilon_n,
\end{aligned} \tag{4.1}$$

$$0 \leq m_a \leq 1.15, \tag{4.2}$$

Eq. (4.1) has no negative signs which are associated to negative steps in the output voltage waveform. To consider the negative steps, the firing angles are

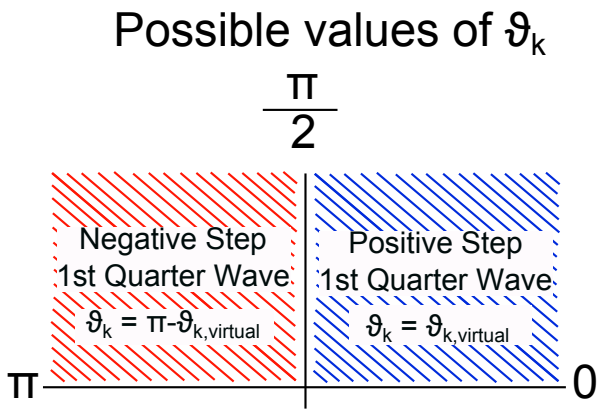

Figure 4.1: Search ranges for firing angles which represent positive and negative steps.

searched in the interval [0, π] (see Fig. 4.1) instead of [0, $\pi/2$] as it is done in previous methods with QW symmetry [109]. In this way, there are two different types of angles:

- Angles $\theta_{k,virtual}$ located in the interval [0, $\pi/2$]. These angles represent positive steps in the output voltage waveform and their corresponding values, θ_k, are given by (4.3).

$$\theta_k = \theta_{k,virtual}, \tag{4.3}$$

- Angles $\theta_{k,virtual}$ located in the interval [$\pi/2$, π]. These are virtual angles that represent negative steps. The virtual angles can be transformed into a real angle included in the interval [0, $\pi/2$], thereby maintaining the QW symmetry, making use of expression (4.4). This fact is justified by means of expression (4.5).

$$\theta_k = \pi - \theta_{k,virtual}, \tag{4.4}$$

$$cos(n(\pi - \theta_{k,virtual})) = cos(n\pi)cos(n\theta_{k,virtual}) = -cos(n\theta_{k,virtual}) \quad \forall n\ odd, \tag{4.5}$$

Therefore, the equation system is unique and valid for any kind of waveforms. Consequently, the algorithm is able to provide simultaneously both the switching

patterns and the associated firing angles for every m_a value, without using a predefined waveform. This technique simplifies the search process in case of a high number of angles and levels where there is a wide variety of possible switching patterns.

Furthermore, with the aim of providing more flexibility to the algorithm to find a solution, there is no constraint in the order of firing angles, as it is given by (4.6). Moreover, crosses between angles are allowed throughout the modulation index range, as it can be seen at Fig. 4.2-(a), and therefore, longer sets of continuous solutions can be obtained.

$$No\ constraint\ in\ the\ order\ of: \theta_1, \theta_2, ..., \theta_l, \tag{4.6}$$

4.2.2 Objective Function

The optimization algorithm used to obtain the sets of firing angles that solve (4.1), utilizes an objective function, F, which will be minimized to find adequate solutions. This objective function is expressed by (4.7), where ε_n is the amplitude error provided by the algorithm for the n^{th} harmonic, whose value is given by (4.1). On the other hand, f_{valid} is a function which checks in the first quarter wave that every solution is valid, with the aim of rejecting invalid solutions. Valid solutions are those that fall between the maximum and minimum voltage limits allowable with the converter, as shown at Figs. 4.2-(b) and 4.2-(d).

$$F = \varepsilon_1^2 + \varepsilon_5^2 + ... + \varepsilon_n^2 + f_{valid}, \tag{4.7}$$

The calculation of f_{valid} requires the following procedure:

- Calculation of $\theta_1, \theta_2, ..., \theta_l$, from $\theta_{1,virtual}, \theta_{2,virtual}, ..., \theta_{l,virtual}$, utilizing (4.3) and (4.4), besides the sign of their corresponding steps.
- Calculation of the ascending order of $\theta_1, \theta_2, ..., \theta_l$.
- Once the order of $\theta_1, \theta_2, ..., \theta_l$ has been obtained, the level, L_i, of the waveform after every consecutive, j, firing angle is given by (4.8) and (4.9), as it is shown at Fig. 4.2-(d).

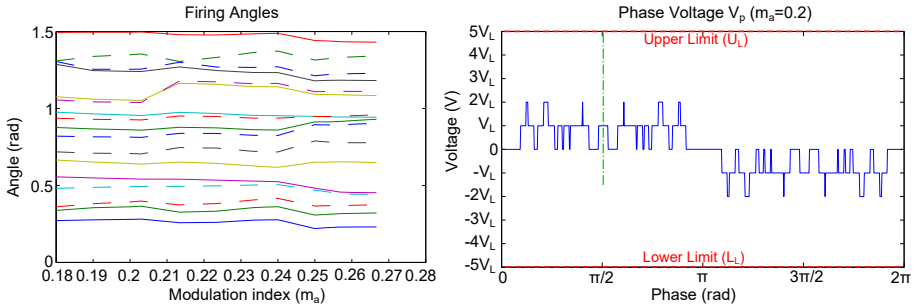

(a) Set of 17 firing angles for the m_a values from 0.18 up to 0.28.

(b) Phase output voltage waveform for m_a equal to 0.2.

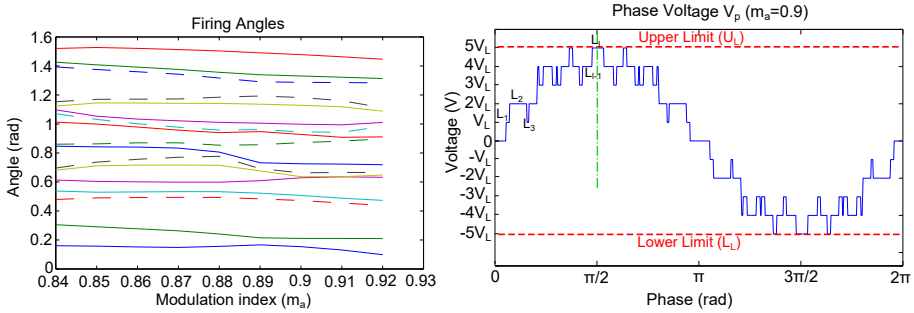

(c) Set of 17 firing angles for the m_a values from 0.84 up to 0.93.

(d) Phase output voltage waveform for m_a equal to 0.9.

Figure 4.2. SHE-PWM implementation for an MMC with 11 levels.

$$L_i = \sum_{j=1}^{i} S_j, \quad 1 \leq i \leq l, \tag{4.8}$$

$$S_j = \left\{ \begin{array}{l} 1 \ \forall \ positive \ \ step, \\ -1 \ \forall \ negative \ \ step, \end{array} \right\} \tag{4.9}$$

- Finally, f_{valid} is given by (4.10), where U_L and L_L are the maximum and minimum allowed levels, respectively.

$$f_{valid} = \left\{ \begin{array}{c} H,\ if\ \{\exists L_i > U_L\ or\ \exists L_i < L_L\}, 1 \leq i \leq l \\ 0,\ if\ \{L_i \leq U_L\ \&\ L_i \geq L_L\}, 1 \leq i \leq l \end{array} \right\}, \tag{4.10}$$

$$H > Convergence\ Threshold\ Value\ (CTV), \tag{4.11}$$

In case the waveform is valid, providing voltage levels which do not exceed the maximum and minimum allowed levels, f_{valid} will return a 0 value and the error provided by (4.7) will be the real error in the harmonic amplitudes. In this way, when valid waveforms are regarded, the optimization algorithm will try to minimize the error in the harmonic amplitudes and it will be possible to find a solution with an error lower than the convergence threshold value (CTV). In case the waveform is not valid, f_{valid} will return a high value, H, higher than the convergence value. In this way, the error provided by (4.7) will also be higher than the convergence value and the optimization algorithm will disregard that solution. Thereby, invalid waveforms will be rejected.

Through (4.7), the algorithm will always provide valid solutions. Moreover, among all the valid solutions that the algorithm is able to find for a particular m_a, (4.7) is used to identify the ones that provide a very low harmonic amplitude error, in particular, an error lower than the threshold value.

4.2.3 Comparison of Traditional and Novel Methods

The proposed method utilizes a unique equation system which can be used with any valid waveform. In this way, it is not required to change the equation system when the switching pattern is modified, simplifying significantly the search process. With the aim of comparing the traditional and novel methods, a MMC with 2 sub-modules per arm is utilized. 2 firing angles, θ_1 and θ_2, are considered and two harmonics, 1^{st} and 5^{th}, are controlled.

Figs. 4.3, 4.4 and 4.5 shows the objective function values, given by (4.7), for different θ_1 and θ_2 values, when a traditional or the proposed novel methods are utilized. Particularly, the traditional method [12, 180, 181], where the firing angles are searched in the range $[0, \pi/2]$, considers two possibilities. On the one hand, the waveform will contain two positive steps, Figs. 4.3-(1) and 4.3-(2), and on the other hand, the switching pattern will contain one positive step and one negative step, Figs. 4.4-(1) and 4.4-(2). Traditional methods include a restriction in the order of the angles. In this case, with the aim of facilitating the study of the objective function space, this restriction will not be applied:

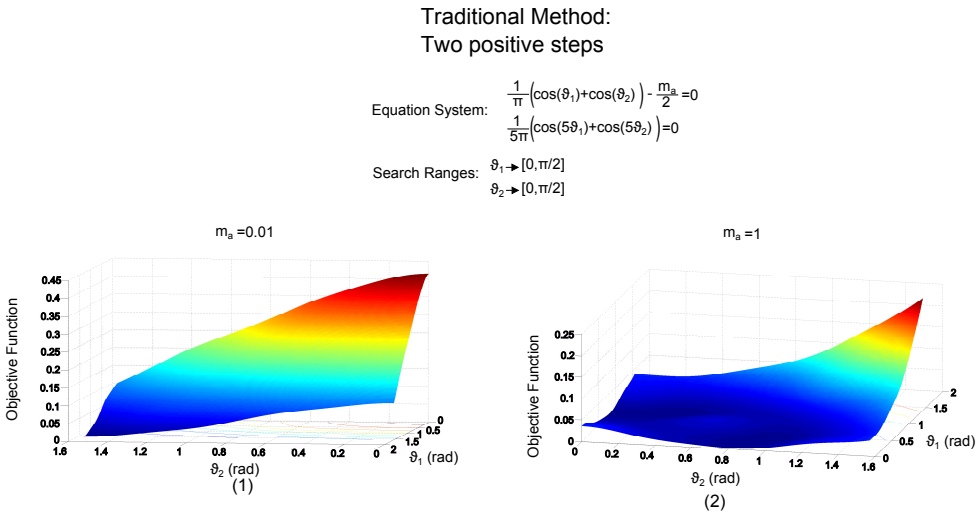

Figure 4.3: SHE-PWM implementation for an MMC with 11 levels (traditional method): Objective function value, considering two positive steps, in case $m_a = 0.01$ (1) and $m_a = 1$ (2).

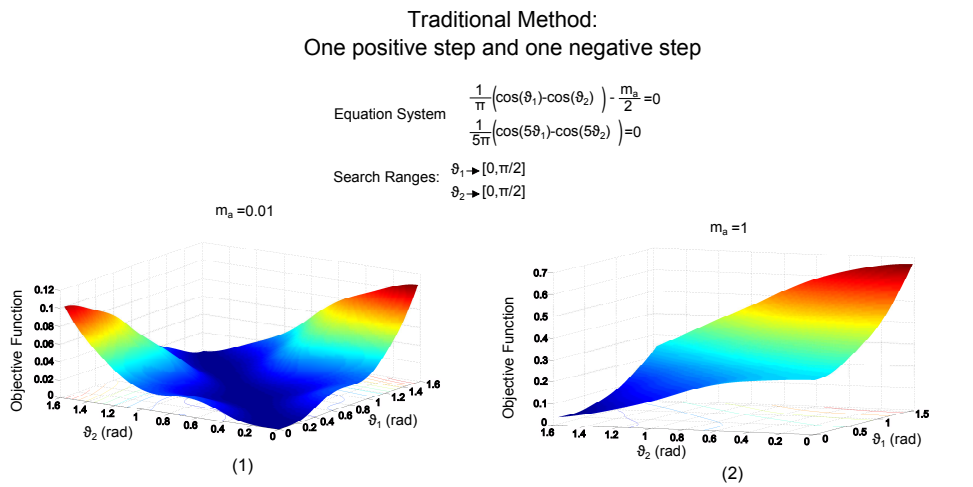

Figure 4.4: SHE-PWM implementation for an MMC with 11 levels (traditional method): Objective function value, one positive step and one negative step, in case $m_a = 0.01$ (1) and $m_a = 1$ (2).

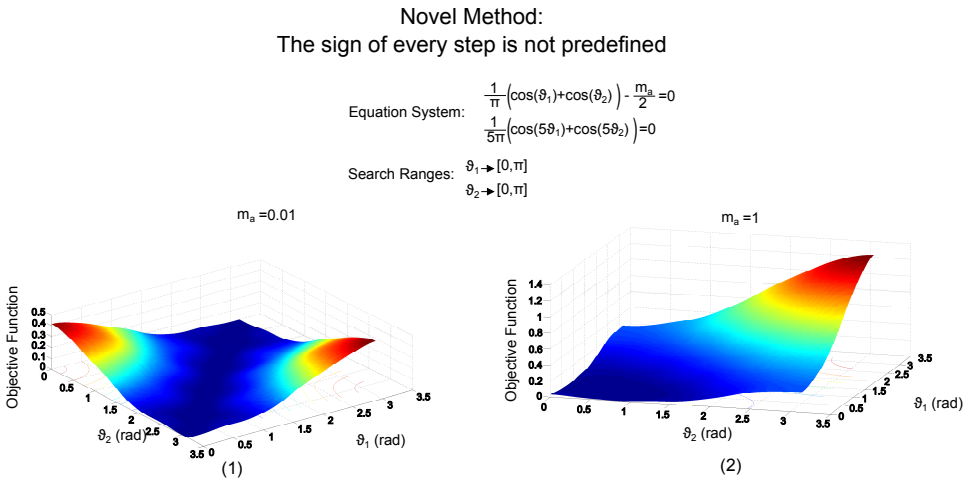

Figure 4.5: SHE-PWM implementation for an MMC with 11 levels (novel method): Objective function value, without any predefined waveform, in case $m_a = 0.01$ (1) and $m_a = 1$ (2).

- Traditional Method - Two positive steps: Fig. 4.3-(1) shows the objective function value for every value of θ_1 and θ_2 when m_a is equal to 0.01. As it can be noticed, there is only one point, located in values closed to $\pi/2$ for both angles, which could solve the equation system. In this way, it is difficult to find the solution and there could be other possible waveforms that could provide better harmonic performances. On the other hand, when the m_a value is equal to 1, as it can be noticed at Fig. 4.3-(2), there are more possible solutions because this switching pattern is suitable for high m_a values.

- Traditional Method - One positive step and one negative step: Fig. 4.4-(1) shows a great number of possible solutions. Therefore, this switching pattern is helpful to provide a solution in case of low m_a values. However, as it can be noticed at Fig. 4.4-(2), in case of high m_a values, this waveform is not able to provide a solution.

Figs. 4.3-(1), 4.3-(2), 4.4-(1) and 4.4-(2) demonstrate that different switching patterns and their corresponding equation systems, must be checked to find a solution throughout the m_a range, in case of traditional methods. Therefore, when the number of levels of the converter or the number of firing angles are high, the searching task is significantly hindered because of the high number of possible switching patterns.

On the other hand, when the novel proposed method is applied, the equation system is unique and the angles θ_1 and θ_2 will be searched in the range $[0, \pi]$. In this way, the switching pattern is not predefined. As it can be noticed at Figs. 4.5-(1) and 4.5-(2), this technique is able to provide solutions for low and high m_a values, respectively, due to its ability to search automatically not only the firing angles, but also the switching patterns. Therefore, considering this feature and the no-requirement of a predefined sequence in the firing angles, the searching task is significantly simplified and the probability of finding more solutions is higher, particularly when the number of possible waveforms is high.

4.3 Novel Method to Solve the HW Symmetry SHE-PWM Problem

The proposed calculation method also solves the SHE-PWM problem with HW symmetry for MCs without using predefined waveforms [178]. Analogously to the proposed QW implementation, it is not required to define different equation systems for every switching pattern, simplifying significantly the search of the solutions. This technique provides modifications in the Fourier series equation system, which is utilized by previous published works [108, 127, 152], and in the method to search the firing angles. The search process is based on genetic algorithms (GAs) due to its proven effectiveness to solve the SHE problem [109, 132].

4.3.1 Equation System and Search Range of every Firing Angle

The proposed equation system, which is valid for any multilevel waveform, only contains the equations related to positive steps, m_k equal to 1. Therefore, based on (3.8) and (3.9), the a_n coefficients will be calculated by (4.12), where L is the number of levels, $\alpha_{k,virtual}$ is the identifier of every firing angle, $2l$ is the total number of firing angles in the half wave and n is the identifier of every odd non-triplen harmonic.

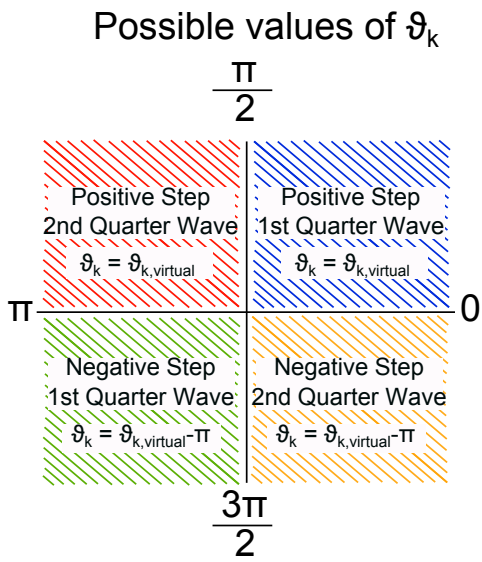

Figure 4.6: Search ranges utilized for firing angles which represent positive and negative steps in both quarter waves.

$$\begin{aligned}
&\frac{2}{\pi(L-1)}(-\sin(\theta_{1,virtual})-\sin(\theta_{2,virtual})-...-\sin(\theta_{2l,virtual}))-X_1=\varepsilon_{a1},\\
&\qquad\qquad\qquad\qquad\qquad\qquad\qquad\qquad\qquad\qquad\vdots\\
&\frac{2}{n\pi(L-1)}(-\sin(n\theta_{1,virtual})-\sin(n\theta_{2,virtual})-...-\sin(n\theta_{2l,virtual}))=\varepsilon_{an},
\end{aligned} \tag{4.12}$$

On the other hand, the b_n coefficients will be obtained by (4.13):

$$\begin{aligned}
&\frac{2}{\pi(L-1)}(\cos(\theta_{1,virtual})+\cos(\theta_{2,virtual})+...+\cos(\theta_{2l,virtual}))-Y_1=\varepsilon_{b1},\\
&\qquad\qquad\qquad\qquad\qquad\qquad\qquad\qquad\qquad\qquad\vdots\\
&\frac{2}{n\pi(L-1)}(\cos(n\theta_{1,virtual})+\cos(n\theta_{2,virtual})+...+\cos(n\theta_{2l,virtual}))=\varepsilon_{bn},
\end{aligned} \tag{4.13}$$

X_1 and Y_1 values must comply with (4.14a) and (4.14b), where m_a is the modulation index and ϕ_1 is the phase of the fundamental harmonic.

$$\sqrt{X_1^2 + Y_1^2} = \frac{m_a}{2}, \;\; 0 < m_a < 1.15, \tag{4.14a}$$

$$\phi_1 = arctg\left(\frac{Y_1}{X_1}\right), \tag{4.14b}$$

The search process provides any kind of switching patterns because the firing angles, $\alpha_{k,virtual}$, will not be searched in the range $[0, \pi]$, as it is done in previous works [152]. In this case, as it can be noticed at Fig. 4.6, the firing angles will be searched in the range $[0, 2\pi]$, maintaining the HW symmetry. In this way:

- The angles $\theta_{k,virtual}$ whose value is located in $[0, \pi/2]$ will represent positive steps in the first quarter wave. The real angle, θ_k, value will be given by $\theta_{k,virtual}$.
- The angles $\theta_{k,virtual}$ whose value is located in $[\pi, 3\pi/2]$ will represent negative steps in the first quarter wave, and the real angle, θ_k, value will be given by $\theta_{k,virtual} - \pi$. This assumption is based on (4.15) and (4.16).
- The angles $\theta_{k,virtual}$ whose value is located in $[\pi/2, \pi]$ will represent positive steps in the second quarter wave. The real angle, θ_k, value will be given by $\theta_{k,virtual}$.
- The angles $\theta_{k,virtual}$ whose value is located in $[3\pi/2, 2\pi]$ will represent negative steps in the second quarter wave, and the real angle, θ_k, value will be given by $\theta_{k,virtual} - \pi$. This assumption is based on (4.15) and (4.16).

$$\begin{aligned} cos(n(\theta_{k,virtual} - \pi)) &= cos(n\theta_{k,virtual})cos(n\pi) = \\ &= -cos(n\theta_{k,virtual}) \;\; \forall n \; odd, \end{aligned} \tag{4.15}$$

$$\begin{aligned} sin(n(\theta_{k,virtual} - \pi)) &= sin(n\theta_{k,virtual})cos(n\pi) = \\ &= -sin(n\theta_{k,virtual}) \;\; \forall n \; odd, \end{aligned} \tag{4.16}$$

$$No\ constraint\ in\ the\ order\ of: \theta_{1,virtual}, \theta_{2,virtual}, ..., \theta_{2l,virtual}, \tag{4.17}$$

Furthermore, as it is detailed at (4.17), there will not be any constraint in the order of firing angles. This fact, combined with (4.15) and (4.16), provides the required flexibility to find different waveforms with only one equation system.

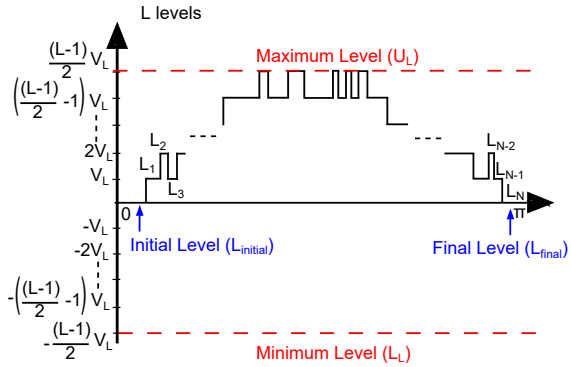

(a) Half-wave with initial value 0.

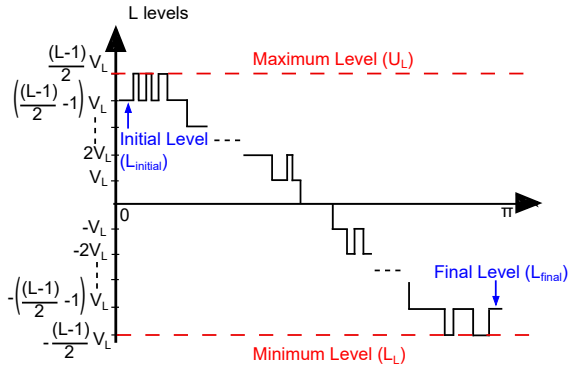

(b) Half-wave with initial value $(((L-1)/2)-1)V_L$.

Figure 4.7. Validity restrictions.

4.3.2 Objective Function

The objective function to be solved by the optimization algorithm is given by (4.18), where f_{valid} is a function which checks the validity of the obtained waveform, considering the number of levels of the converter and the initial, $L_{initial}$ and final, L_{final}, levels of the half wave. These levels must be equal but with opposite signs, as it is shown at Fig. 4.7, and they will be input parameters for the GA.

$$F = \varepsilon_{a1}^2 + \varepsilon_{b1}^2 + \varepsilon_{a5}^2 + \varepsilon_{b5}^2 + ... + \varepsilon_{an}^2 + \varepsilon_{bn}^2 + \\ + f_{valid}(\theta_{1,virtual}, \theta_{2,virtual}, ..., \theta_{2l,virtual}), \tag{4.18}$$

f_{valid} consists of:

- Calculation of $\theta_1, \theta_2, ..., \theta_{2l}$, from $\theta_{1,virtual}, \theta_{2,virtual}, ..., \theta_{2l,virtual}$, and the sign of their corresponding steps, as it is depicted at Fig 4.6.
- Calculation of the order, from lower to higher value, of $\theta_1, \theta_2, ..., \theta_{2l}$.
- Once the order of $\theta_1, \theta_2, ..., \theta_{2l}$ has been calculated, the level, L_i, of the waveform after every consecutive, j, firing angle is given by (4.19a) and (4.19b), as it is shown at Fig. 4.7-(a).

$$L_i = L_{initial} + \sum_{j=1}^{i} S_j, \quad 1 \leq i \leq 2l, \tag{4.19a}$$

$$S_j = \left\{ \begin{array}{l} 1 \ \forall \ raising \ \ edge, \\ -1 \ \forall \ \ falling \ \ edge, \end{array} \right\} \tag{4.19b}$$

- Finally, f_{valid} is given by (4.20), where U_L and L_L are the maximum and minimum allowed levels and $L_{initial}$ is the initial level of the waveform. Therefore, in case the waveform was not valid, this function would return a high value, H, and the genetic algorithm would reject that solution. Otherwise, f_{valid} would return a 0 value. Valid waveforms are those which provide voltage levels that fall between the maximum and minimum allowed levels, besides $L_N = -L_{initial}$ (see Fig. 4.7).

$$f_{valid} = \left\{ \begin{array}{l} H, \ if \ \left\{ \begin{array}{c} \exists L_i > U_L \ or \ \exists L_i < L_L \ or \\ L_N \neq -L_{initial} \end{array} \right\}, 1 \leq i \leq N \\ 0, \ if \ \left\{ \begin{array}{c} L_i \leqq U_L \ \& \ L_i \geq L_L \ \& \\ L_N = -L_{initial} \end{array} \right\}, 1 \leq i \leq N \end{array} \right\}, \tag{4.20}$$

$$H > Convergence \, Threshold \, Value, \tag{4.21}$$

In this way, the algorithm will always provide valid solutions.

4.4 Proposed Search Algorithm

The proposed search algorithm, whose flow diagram is depicted at Fig. 4.8, is based on optimization techniques. Genetic algorithms (GAs) have been selected to solve the SHE-PWM problem due to their demonstrated effectiveness [109, 132]. They are stochastic optimization techniques of general purpose. GAs do not require the derivative of the objective function to get to the optimal solution. Every solution depends on the optimization variables, which in case of SHE-PWM problem, are the firing angles.

The proposed search algorithm, which solves the SHE-PWM problem for a particular m_a value, consists of three different processes: genetic algorithm (GA), optimization process (OP) and initial population definition (IPD), as it can be noticed at Fig. 4.8. The dashed lines highlight which part of the overall flux diagram corresponds to each process.

- **Genetic Algorithm (GA):** The GA is based on the flow diagram depicted at Fig. 4.8, where the initial population contains possible values, which are inside the search range, for every firing angle. The objective function is given by (4.7) or (4.18) for QW or HW symmetries, respectively. At every generation, the objective function will be evaluated utilizing the existing population for every firing angle. When going from one generation to the next, the aim is obtaining an existing population which provides a better objective function solution. The last generation will be reached unless a previous generation provides a solution value lower than the convergence threshold value (CTV). The selection process determines which elements of a population will be chosen as parents for the next generation. The best solutions are more likely to be selected. Finally, the population of the next generation can be created by crossover, generating children with similar values to those of their parents, or mutations, which generate children with values completely different with the aim of avoiding local minimums [125]. The GA configuration is detailed at section 4.6.
- **Optimization Process (OP):** The optimization process (OP), which is depicted at Fig. 4.8, executes the GA over the initial population defined for every variable. Once the GA has finished, with the aim of improving the solution, the GA will be executed again using the resulting population of the previous execution with a reduction by 10% of the search range for every variable. In this way, the search will be focused on the best solution provided by the previous execution [171, 173, 181]. The process will continue iteratively until the improvement is not significant.

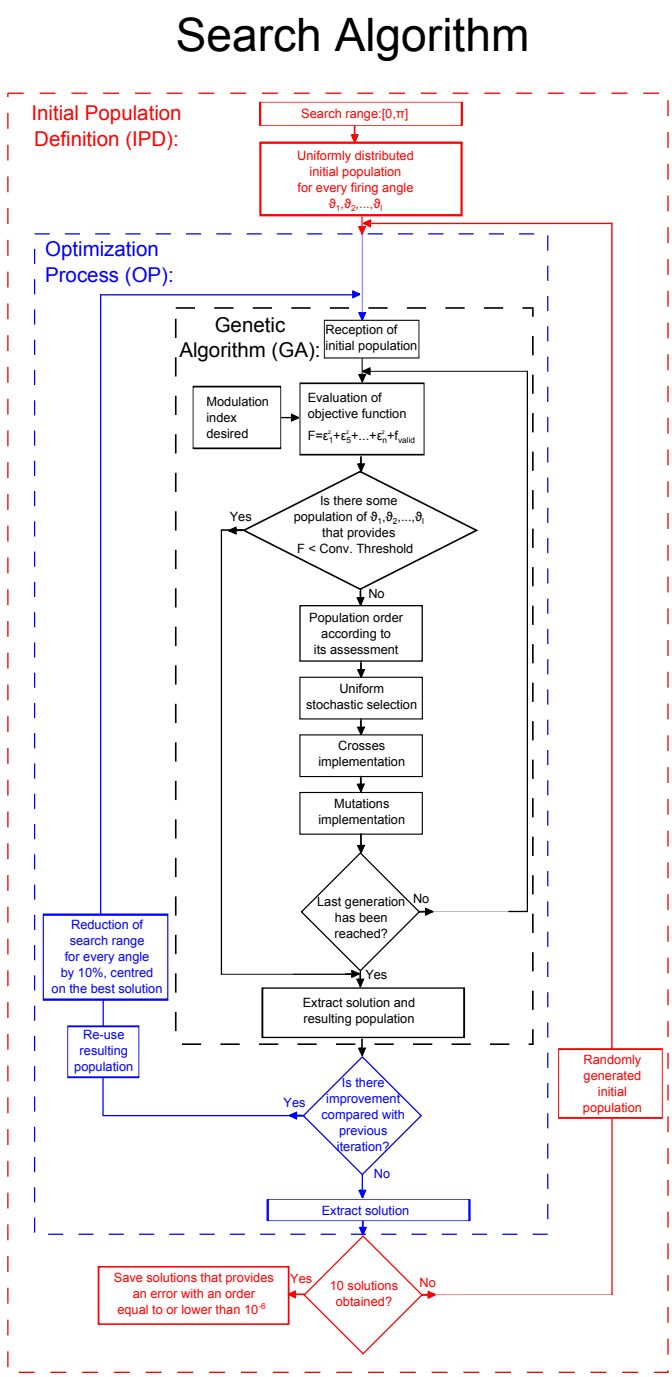

Figure 4.8. Flow diagram of the search algorithm.

- **Initial Population Definition (IPD):** It is required to define the initial population which is used by the OP to execute the GA. As it is depicted at Fig. 4.8, the OP is firstly executed with an uniformly distributed initial population along the search range of every variable, which is [0, π]. Subsequent executions of OP use randomly distributed initial populations with the aim of finding more than one solution for every m_a sample. After 10 executions of OP, the solutions which provide an acceptable error (this value will be defined in section 4.6) in the objective function evaluation will be stored. If the number of executions is incremented, more solutions can be found.

4.5 Proposed Acquisition of Solutions

Firstly, the solutions for 10 samples of m_a will be acquired consecutively between 0.1 and 1.1 values. Subsequently, a local search will be implemented around every calculated solution. In this case, the distance between samples will be 10^{-2}. This local search utilizes an initial population which contains the solution of the previous closest m_a sample. Hence, sets of angles, which are continuous throughout different intervals of the m_a range, are created. In this way, it is possible to obtain solutions throughout the m_a range.

The algorithm calculates the sets of firing angles off-line. Afterwards, these sets will be stored in look-up tables with the aim of utilizing them by a controller in real time. Furthermore, due to the continuity of every set of angles throughout different intervals of the m_a range and the proximity between m_a samples, a linearization technique, such as the one presented in [182], can be applied with high accuracy inside every continuous interval. In this way, any value of m_a can be obtained.

4.6 Genetic Algorithm Configuration

The selected configuration for GA, whose implementation is the one provided by the optimization toolbox of MATLAB software [183], is based on previous work [109, 131, 164, 171, 173] and empirical results:

- Search range: the search range for every firing angle is $[0, \pi]$ or $[0, 2\pi]$ for QW or HW symmetries, respectively.

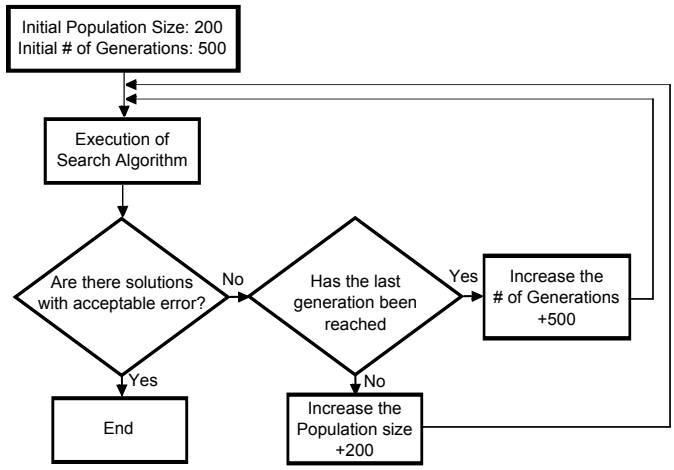

Figure 4.9: Flow diagram to adjust the population size and the number of generations.

- Population format: Floating point has been selected to represent the firing angles. This format provides lower computational load than binary format which requires a high number of bits, particularly when the required accuracy is high [173].

- Population size and number of generations: Both magnitudes will be adjusted empirically utilizing the designing process detailed at Fig. 4.9. As it can be noticed, for a particular value of population size and generations, in case the proposed search algorithm, which is depicted at Fig. 4.8, do not provide solutions with an acceptable error and the total number of generations is reached in the first iteration of the optimization process (OP), the number of generations will be increased. On the other hand, if the total number of generations is not reached and the error provided by the search algorithm is still high, because a local minimum is found, the population size will be increased. This process will continue iteratively until an accepted error is obtained in the solutions.

  With the aim of simplifying the design process, the population size and the number of generations have been calculated for a high number of firing angles, in particular 17. In this way, the obtained values may be utilized successfully when the number of firing angles is lower. In the latter case, lower population size or lower number of generations could be used to reduce the computational cost, but less solutions could also be obtained (there

Table 4.1. Genetic Algorithm Configuration and Execution Time

# of Firing Angles	4	6	8	9	12	17	34
Population Size	1800	1800	1800	1800	1800	1800	1800
# of Generations	4000	4000	4000	4000	4000	4000	10000
Execution Time (Seconds) of GA	10	227	609	610	643	737	3300

could be less successful iterations of IPD). The design process has been repeated for 34 firing angles.

Table 4.1 shows the execution time of the genetic algorithm for different cases, using a processor Intel(R) Core(TM) i7-3520M CPU @ 2.90 GHz. As it can be noticed, under equal population size and number of generations, the execution time increases when the number of firing angles is incremented. For the cases with lower number of firing angels, 4 and 6, a minimum has been obtained before reaching the last generation. When the number of firing angles is higher, this limit is reached. However, through the optimization process (OP) described at section 4.4, it is not required to increase the number of generations beyond 4000 to obtain valid solutions for every m_a. The number of iterations of OP is always lower than 40 and usually lower than 10. Increasing the number of generations beyond 4000 could provide more solutions and reduce the number of iterations of the OP, but the latter is not straightforward and the execution time of GA is significantly increased. In case of 34 firing angles, the number of generations was incremented because with 4000 there was no solution.

- Selection features: The selection function selected is uniform stochastic, whose operation determines that the solutions which offer better value for the objective function will be more likely to be parents of the next generation [183].
- Mutation features: The mutation function selected is *Adaptive Feasible*. It generates random directions, which are adaptive according to whether the last generation has been successful or not. This function is able to satisfy the linear constraints and bounds [183].
- Crossover features: The function which performs the crossings is *Crossover Arithmetic*, which creates a child with a random arithmetic mean that lies between the two parents [171]. On the other hand, based on previous work, the selected percentage of crossings is 80% [131, 183].
- Convergence threshold: The selected maximum accepted error is 10^{-6} and it is also the convergence threshold value (CTV) when the number of firing angles is high. This accepted error is based on the harmonic content ob-

tained in previous works [109, 164, 184]. On the other hand, in case the number of firing angles is low (lower than 12 approximately), it is possible to obtain a high number of solutions, for every m_a value, with a lower error and the convergence threshold value will be 10^{-8}.

4.7 Analysis of Solutions

4.7.1 Performance Evaluation

The proposed search methods are able to find different solutions for every m_a value. In this way, different indicators have been published in the technical literature to classify the solutions with the aim of selecting one of them [154].

- **Harmonic Distortion Factor (HDF)**

  This factor, which is given by (4.22), provides the relevance of the first two non-eliminated harmonics. Regarding three-phase systems, the odd triplen harmonics will not be considered [154, 172].

$$HDF(\%) = 100\frac{\sqrt{V_{1h}^2 + V_{2h}^2}}{V_1}, \tag{4.22}$$

- **Total Harmonic Distortion (THD)**

  The total harmonic distortion (THD) is given by (4.23) [127]. The non-triplen harmonics are not regarded due to the three-phase system.

$$THD(\%) = \frac{100}{V_1}\sqrt{\sum_{n=5,7\ldots}^{\infty} V_n^2}, \tag{4.23}$$

- **Harmonic Loss Factor (HLF)**

  The harmonic loss factor, which is given by (4.24), is proportional to the weighted current total harmonic distortion (WTHD_i) [154].

$$HLF(\%) = \frac{100}{V_1}\sqrt{\sum_{n=5,7\ldots}^{\infty}\left[\frac{V_n}{n}\right]^2}, \tag{4.24}$$

- **Lower-Order Triplen Harmonics**

  Despite the fact that triplen harmonics are eliminated in three-phase systems, these harmonics increment the stress imposed on the insulation of grid transformers or motors [154]. Therefore, the analysis of triplen harmonic amplitudes should be considered. The third and ninth harmonic factors are given by (4.25) and (4.26), respectively.

$$3^{rd}(\%) = 100\frac{V_3}{V_1}, \tag{4.25}$$

$$9^{th}(\%) = 100\frac{V_9}{V_1}, \tag{4.26}$$

4.7.2 Solutions with a Low Number of Controlled Harmonics

Several solutions have been obtained throughout the m_a range for six different cases (where ϕ_1 is the fundamental phase given by (4.14b)):

- Case I: MMC with 7 levels and 4 firing angles with QW symmetry.
- Case II: MMC with 7 levels and 8 firing angles with HW symmetry and $\phi_1 = \pi/2$.
- Case III: MMC with 9 levels and 4 firing angles with QW symmetry.
- Case IV: MMC with 9 levels and 8 firing angles with HW symmetry and $\phi_1 = \pi/2$.
- Case V: MMC with 9 levels and 6 firing angles with QW symmetry.
- Case VI: MMC with 9 levels and 12 firing angles with HW symmetry and $\phi_1 = \pi/2$.

As it has been detailed in Section 4.5, for every case, solutions for 11 samples of m_a have been obtained consecutively between 0.1 and 1.1 values. In particular, the initial population definition (IPD) process included in the search algorithm, detailed at section 4.4, is configured to realize 20 iterations, being able to obtain different solutions with acceptable error for every m_a value (in the best scenario, 20 different solutions would be obtained for every m_a value).

On the other hand, in case of HW symmetry, for every m_a value, the search algorithm will be executed with every possible initial value, L_i, regarding the

levels of the converter. In addition, the fundamental phase utilized is $\phi_1 = \pi/2$, providing a sine wave.

For every solution, the performance indicators detailed at Section 4.7.1 have been obtained. The convergence threshold utilized to obtain the solutions was 10^{-8} and those which provide an error in the objective function lower than 10^{-6} were stored. In this way, all the solutions provide a low error, lower than 10^{-6} and many of them provide errors with an order of 10^{-7}, 10^{-8} or even 10^{-9}. The value H, detailed at sections 4.2 and 4.3, must be higher than the convergence threshold value and the maximum accepted error in case they were different, as it happens in this case.

The analysis of solutions is realized below and some information about these solutions is also included in appendix A.

4.7.2.1 Analysis of Solutions for every Case

Several solutions have been obtained for every case. In addition, for cases II, IV and VI, for every HW solution, there is another symmetric one, with identical harmonic content, whose angle values for positive and negative steps, $\theta_{k,positiveStep-symmetric}$ and $\theta_{k,negativeStep-symmetric}$, are given by (4.27) and (4.28), respectively, where $2l$ is the total number of firing angles in the first HW [154]. An example of these waveforms is depicted at Fig. 4.10

$$\theta_{k,negativeStep-symmetric} = \pi - \theta_{2l-k,positiveStep}, \tag{4.27}$$

$$\theta_{k,positiveStep-symmetric} = \pi - \theta_{2l-k,negativeStep}, \tag{4.28}$$

Summarizing, the results for every case are the following:

- Solutions for case I (Table A.1). For every performance indicator, the solution which provides the lowest value is highlighted in red color. The total number of solutions obtained throughout the m_a range is 29. However, no solutions have been found for $m_a = 1.1$.
- Solutions for case II. Solutions with $L_i = 0$ and $L_i = 1$ have been obtained (Tables A.2 and A.3) throughout the m_a range. For every performance indicator, the solution which provides the lowest value is highlighted in red color. The total number of solutions with $L_i = 0$ and $L_i = 1$ are 36 and 31, respectively. In total, 67 solutions have been found and other 67 symmetric solutions can be obtained through (4.27) and (4.28).

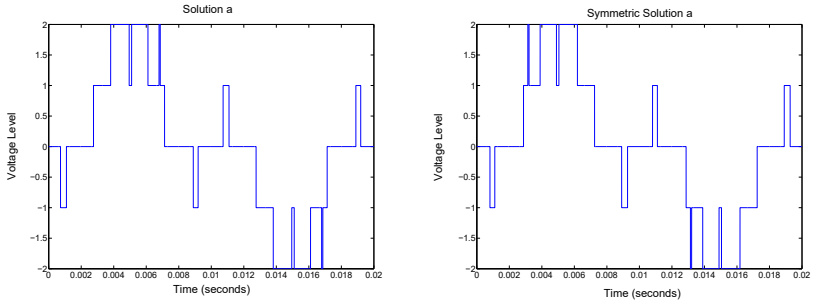

(a) HW solution with $L_i = 0$ and $m_a = 0.3$ (case VI).

(b) Symmetric HW solution with $L_i = 0$ and $m_a = 0.3$ (case VI).

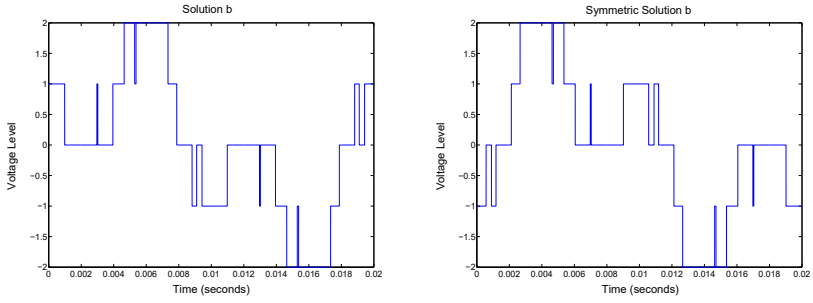

(c) HW solution with $L_i = 1$ and $m_a = 0.3$ (case VI).

(d) Symmetric HW solution with $L_i = -1$ and $m_a = 0.3$ (case VI).

Figure 4.10. Example of symmetrical solutions (amplitude normalized by V_L).

Among the solutions obtained with $L_i = 0$ and $L_i = 1$, the one with lowest HLF for every m_a is highlighted at table A.4. As it can be noticed, depending on m_a, the best solution may be provided by $L_i = 0$ or $L_i = 1$. On the other hand, $L_i = 0$ is the only one which provides a solution for high m_a ($m_a = 1$ and $m_a = 1.1$).

- Solutions for case III: (Table A.5). For every performance indicator, the solution which provides the lowest value is highlighted in red color. The total number of solutions obtained throughout the m_a range is 20. However, no solutions have been found for $m_a = 1.1$.
- Solutions for case IV: Different solutions with $L_i = 0$ and $L_i = 1$ have been obtained and their corresponding performance factors have been detailed at tables A.6 and A.7. The solution which provides the lowest value is

highlighted in red color. The number of solutions obtained throughout the m_a range with $L_i = 0$ and $L_i = 1$ are 22 and 27, respectively. Therefore, the total number of solutions is 49 and the same number of symmetric solutions can be obtained through (4.27) and (4.28).

On the other hand, with the aim of comparing the solutions with the lowest HLF when $L_i = 0$ and $L_i = 1$ for every m_a, all of them are included at table A.8. As it can be noticed, depending on m_a, the lowest HLF (highlighted in red colour) will be provided by $L_i = 0$ or $L_i = 1$. However, for $m_a = 1$ and $m_a = 1.1$ no solutions have been obtained.

- Solutions for case V: (Table A.9). For every indicator, the solution which provides the lowest value is highlighted in red color. The total number of solutions obtained throughout the m_a range is 36. As an example, the solutions obtained with $m_a = 0.3$ are included at Fig. 4.11.

- Solutions for case VI: Different solutions with $L_i = 0$ and $L_i = 1$ have been obtained and their corresponding performance factors have detailed at tables A.10, A.11 and A.12. The solution which provides the lowest value is highlighted in red color. The number of solutions obtained throughout the m_a range with $L_i = 0$ and $L_i = 1$ are 75 and 137, respectively. Therefore, the total number of solutions is 212 and the same number of symmetric solutions can be obtained through (4.27) and (4.28). As an example, the solutions obtained with $m_a = 0.3$ for $L_i = 0$ and $L_i = 1$ are included at Figs. 4.12, 4.13 and 4.14.

  With the aim of comparing the solutions with the lowest HLF when $L_i = 0$ and $L_i = 1$ for every m_a, all of them are included at table A.13. As it can be noticed, depending on m_a, the lowest HLF (highlighted in red colour) will be provided by $L_i = 0$ or $L_i = 1$. In addition, $L_i = 0$ has provided solutions throughout the m_a range. Otherwise, $L_i = 1$ has not provided solutions for $m_a = 1.1$.

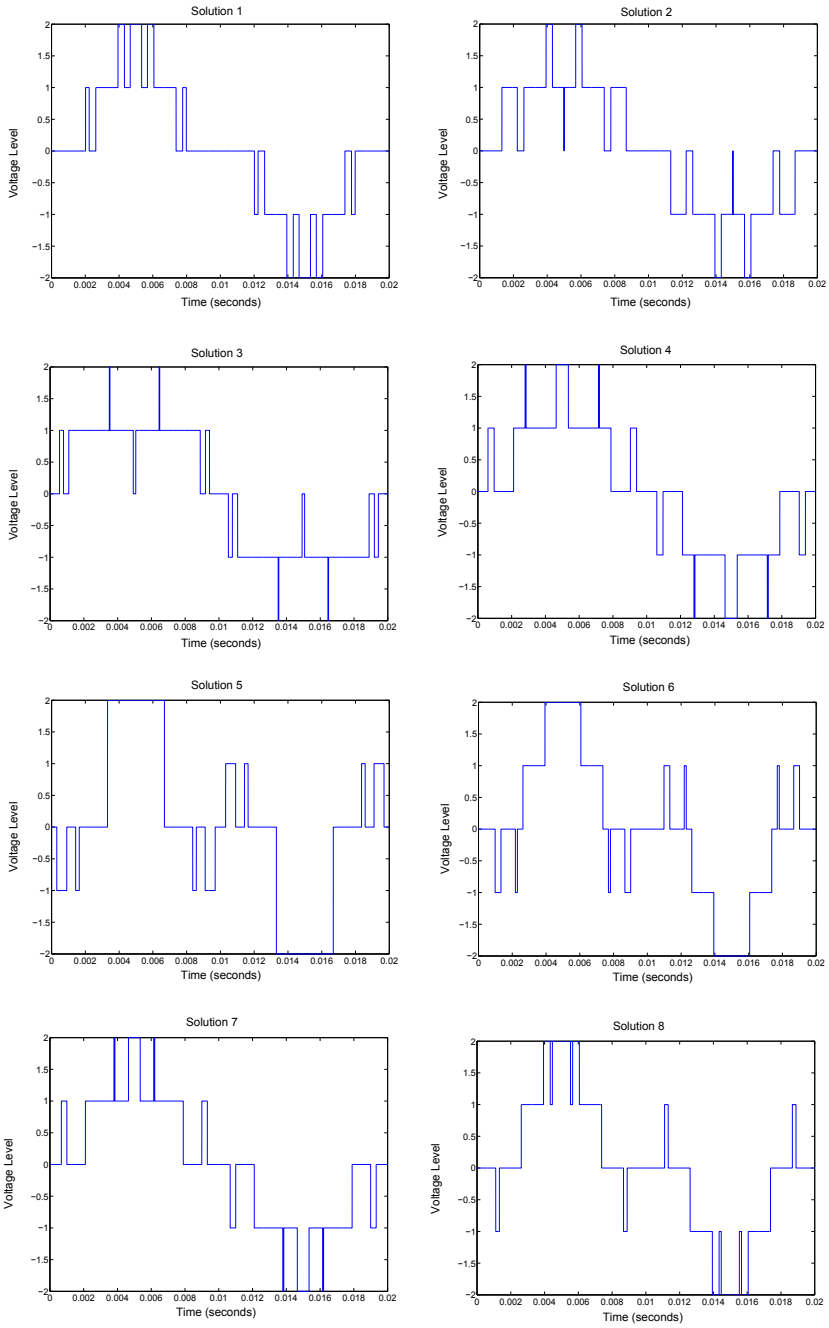

Figure 4.11: QW solutions obtained for case V with $m_a = 0.3$ (amplitude normalized by V_L).

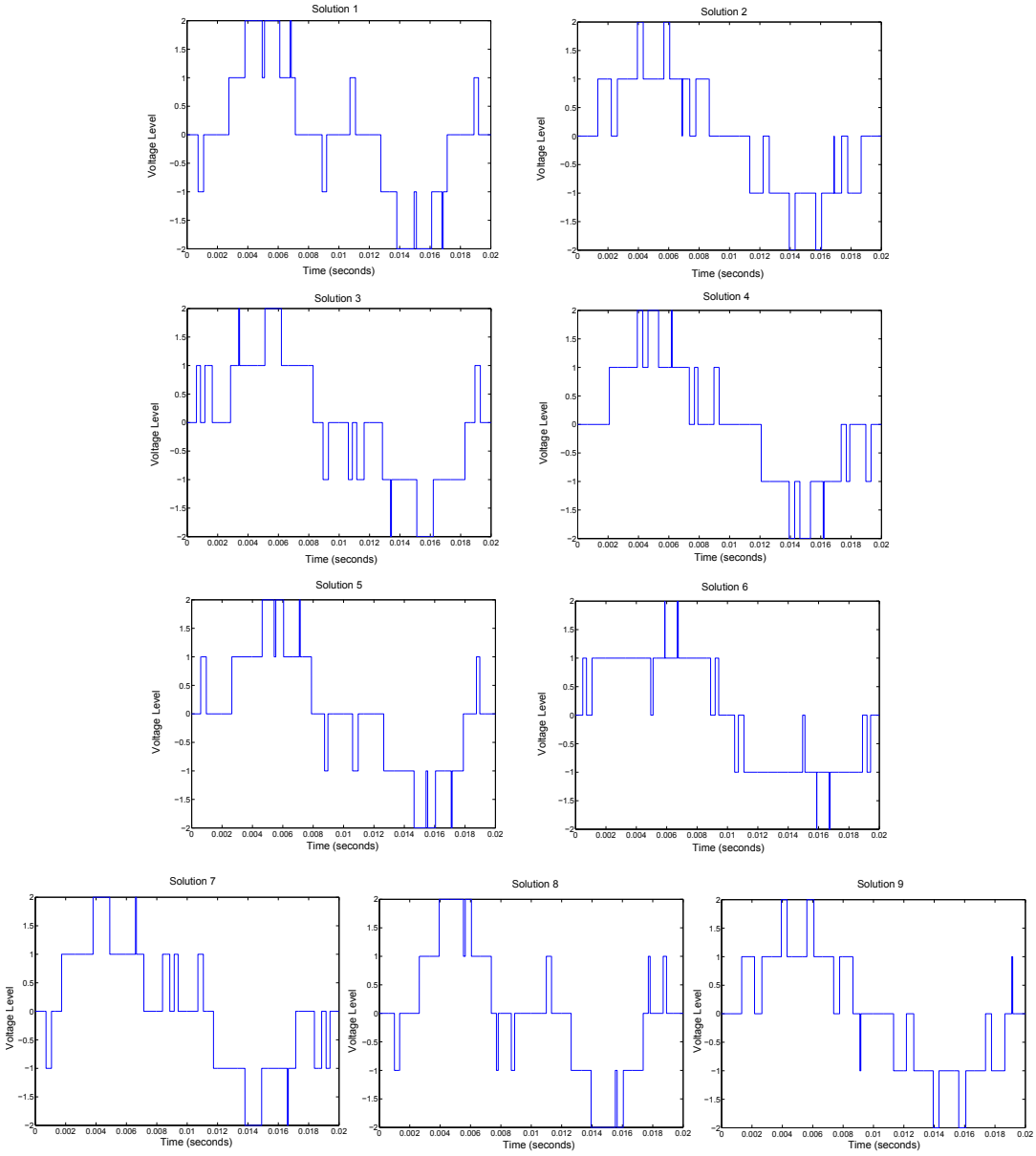

Figure 4.12: HW solutions obtained for case VI with $m_a = 0.3$ and $L_i = 0$ (amplitude normalized by V_L).

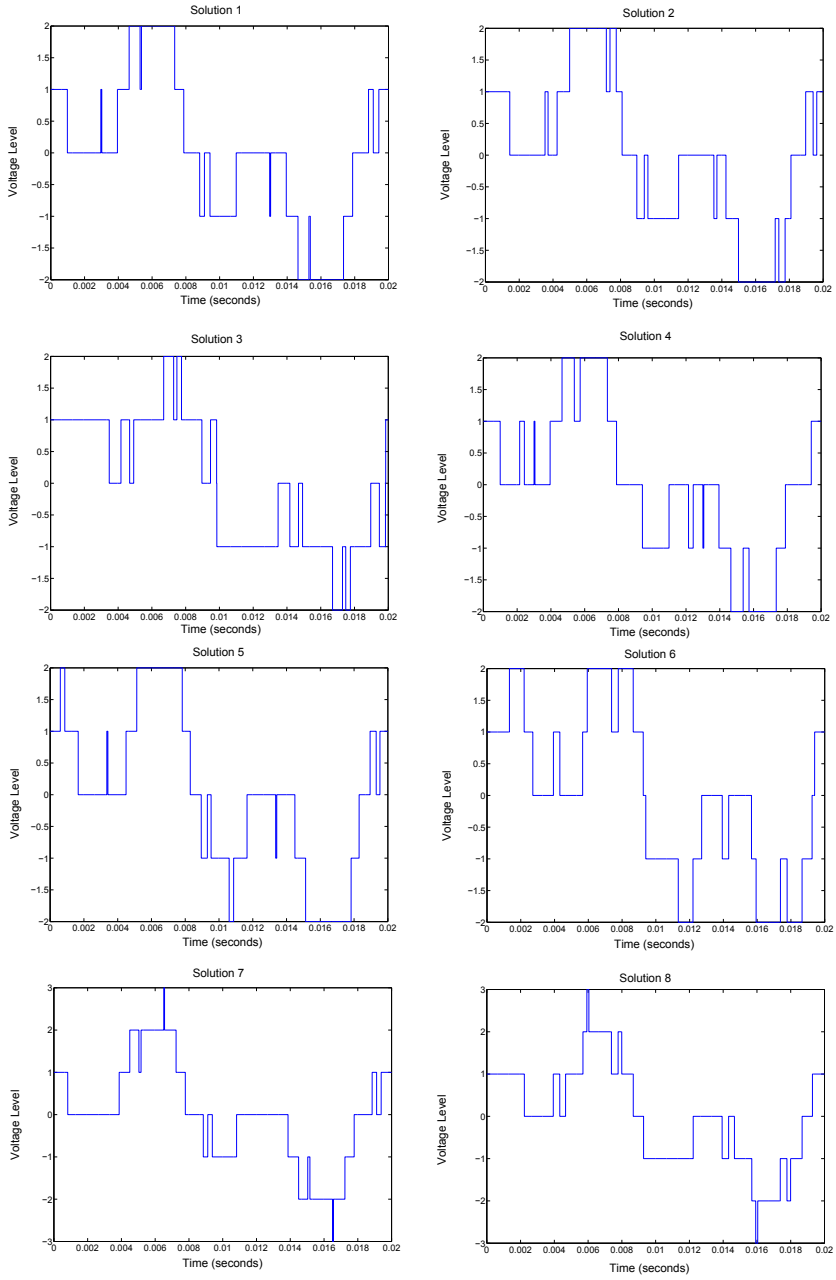

Figure 4.13: HW solutions obtained for case VI with $m_a = 0.3$ and $L_i = 1$ (part 1) (amplitude normalized by V_L).

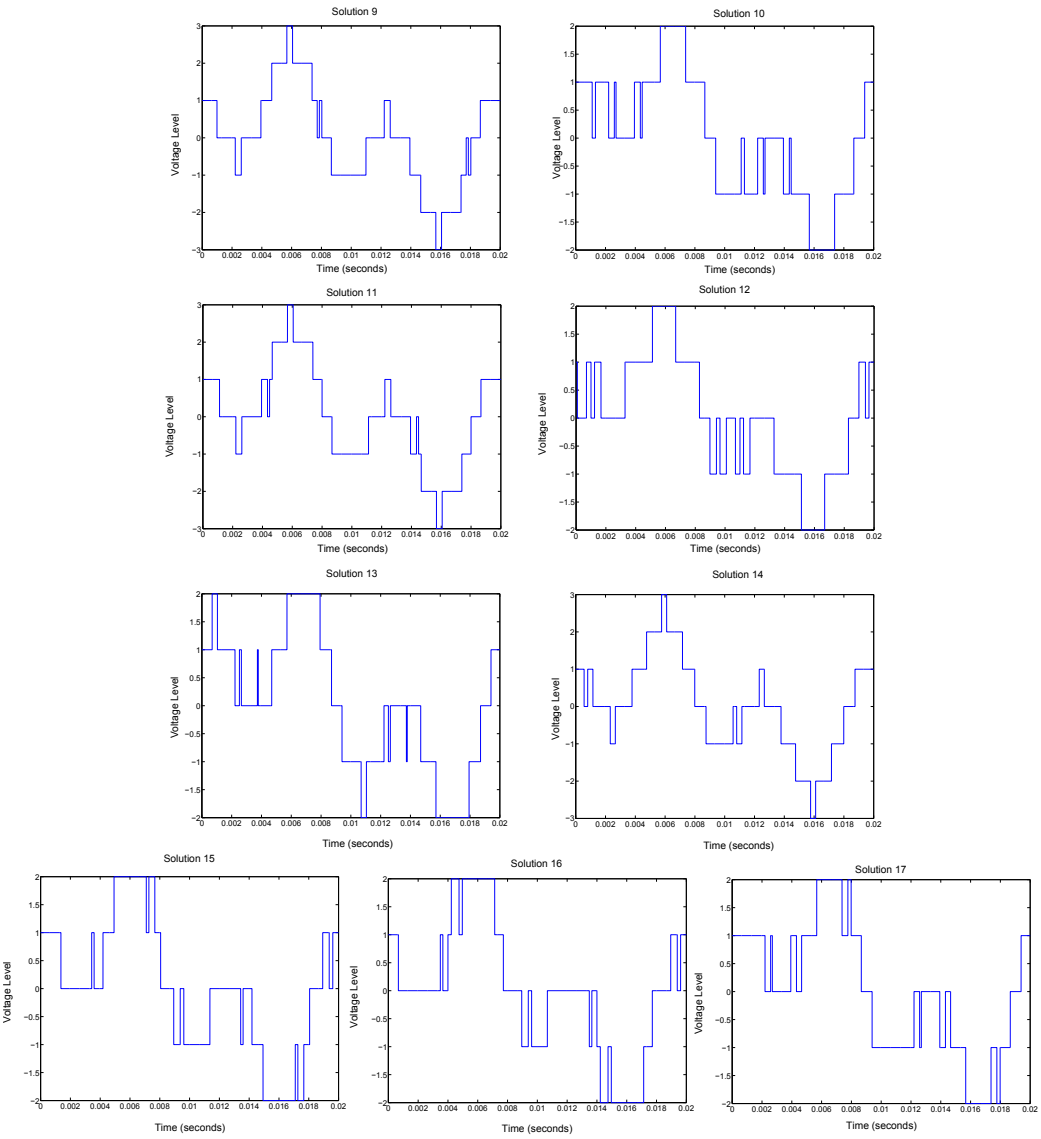

Figure 4.14: HW solutions obtained for case VI with $m_a = 0.3$ and $L_i = 1$ (part 2) (amplitude normalized by V_L).

Based on these results, several conclusions have been extracted. First, unlike in the case of bipolar waveforms [154], the first two non-eliminated harmonics do not concentrate the majority of the harmonic energy. Therefore, under the same THD value, the multilevel waveforms will provide lower HLF values than bipolar waveforms.

Second, among all the solutions obtained for every case, the lowest value for every indicator may be provided by different solutions. In this way, it will be required to determine the selection criteria depending on the application. In this work, with the aim of improving the efficiency of the MMC, the solutions with lowest HLF value will be selected. In case there are several solutions with the same HLF value, the one which provides the lowest third harmonic will be selected. However, depending on the application, a different criteria could be selected [154].

Third, for a fundamental phase $\phi_1 = \pi/2$, which provides a sine waveform, the solutions with HW symmetry have been obtained with initial levels $L_i = 0$ and $L_i = 1$. The rest of L_i values have not provided any solution. On the other hand, the solutions with $L_i = 0$ and $L_i = 1$ will have symmetric ones with $L_i = 0$ and $L_i = -1$, respectively.

Furthermore, the total number of solutions obtained throughout the m_a range, under equal number of levels, tends to increase when the number of firing angles is incremented, as it can be noticed between the QW solutions obtained, regarding 9 levels, with 4 (case III) and 6 (case V) firing angles, which are included at tables A.5 and A.9, respectively. The same effect can be noticed between the HW solutions obtained for 9 levels, with 8 (case IV) firing angles at tables A.6 and A.7 and 12 (case VI) firing angles at tables A.10, A.11 and A.12. This fact can also be noticed between QW and HW solutions with equal number of levels and eliminated harmonics. In this way, the HW solutions require twice as many firing angles to be solved as QW solutions and therefore, the number of HW solutions obtained is higher, as it can be noticed at tables A.5, A.6 and A.7 or A.9, A.10, A.11 and A.12. In addition, the HW symmetry provides a higher number of solutions due to its ability to obtain harmonics with different phase values [152].

On the other hand, under equal number of firing angles, the total number of solutions obtained throughout the m_a range tends to decrease when the number of levels increases. This effect can be noticed when cases I (7 levels) and III (9 levels) or II (7 levels) and IV (9 levels) are compared, as it can be noticed at tables A.1 and A.5 or A.2, A.3, A.6 and A.7, respectively. In addition, when the number of levels increases the lowest THD or HLF obtained for every m_a tends to decrease, due to the multilevel characteristic. This fact can be observed if cases III and V or IV and VI are compared between each other.

Table 4.2. Solutions with lowest HLF for every case (HLF values (%))

Mod. Index	0.1	0.2	0.3	0.4	0.5	0.6	0.7	0.8	0.9	1	1.1
Case I	6.11	1.92	2.12	1.21	1.08	0.5	0.6	0.44	0.63	0.26	-
Case II	5.97	2.42	1.86	1.15	1.1	0.51	0.6	0.41	0.6	0.38	0.5
Case III	4.43	2.21	1.21	1	0.54	0.37	0.33	0.27	0.49	0.33	-
Case IV	4.71	1.84	1.15	0.95	0.79	0.59	0.43	0.47	0.32	-	-
Case V	3.43	1.2	0.68	0.76	0.53	0.39	0.39	0.29	0.17	0.26	0.23
Case VI	3.38	1.22	0.72	0.69	0.5	0.29	0.29	0.29	0.17	0.24	0.24

Table 4.3. Firing angles and sign of every step of solutions selected for case V

m_a	θ_1	θ_2	θ_3	θ_4	θ_5	θ_6
0.1	$\Uparrow$0.7944	$\Downarrow$0.8553	$\Uparrow$1.0672	$\Downarrow$1.1851	$\Uparrow$1.3464	$\Downarrow$1.5111
0.2	$\Downarrow$0.1861	$\Uparrow$0.7538	$\Uparrow$0.9905	$\Uparrow$1.2789	$\Uparrow$1.4053	$\Downarrow$1.4515
0.3	$\Uparrow$0.1756	$\Downarrow$0.2500	$\Uparrow$0.3477	$\Uparrow$1.1019	$\Downarrow$1.1136	$\Downarrow$1.5473
0.4	$\Uparrow$0.0925	$\Uparrow$0.4486	$\Downarrow$0.6782	$\Uparrow$0.7809	$\Downarrow$1.0087	$\Downarrow$1.5322
0.5	$\Uparrow$0.3699	$\Uparrow$0.7986	$\Downarrow$0.8111	$\Uparrow$0.9815	$\Uparrow$1.2888	$\Downarrow$1.3642
0.6	$\Uparrow$0.1739	$\Uparrow$0.4756	$\Downarrow$0.6783	$\Uparrow$0.7350	$\Uparrow$1.2060	$\Downarrow$1.2563
0.7	$\Uparrow$0.6278	$\Uparrow$0.8345	$\Uparrow$1.0973	$\Uparrow$1.0973	$\Downarrow$1.1326	$\Uparrow$1.3406
0.8	$\Uparrow$0.2461	$\Uparrow$0.6104	$\Uparrow$0.9868	$\Uparrow$1.2229	$\Downarrow$1.3143	$\Uparrow$1.4855
0.9	$\Uparrow$0.1034	$\Uparrow$0.2889	$\Uparrow$0.6126	$\Uparrow$1.1067	$\Downarrow$1.1433	$\Uparrow$1.5483
1	$\Uparrow$0.1829	$\Uparrow$0.3951	$\Uparrow$0.6706	$\Downarrow$0.7899	$\Uparrow$0.8463	$\Uparrow$1.0551
1.1	$\Uparrow$0.1116	$\Uparrow$0.2798	$\Uparrow$0.5026	$\Uparrow$0.8015	$\Downarrow$0.8984	$\Uparrow$0.9865

Considering the same number of controlled harmonics and levels, the QW and HW solutions are compared. In this way, cases I, III and V are compared with cases II, IV and VI, respectively. Table 4.2 contains the solutions which provide the lowest HLF for every case. Firstly, the three comparisons show how the lowest HLF may be provided by the QW or HW symmetry depending on the m_a value. In this way, obtaining the solutions with both symmetries is interesting. In addition, if one of the symmetries, QW or HW, does not provide solutions for the highest m_a values, the other symmetry could solve the problem, as it happens with cases I, II, III and IV, where the number of firing angles in the first QW is close to $(L-1)/2$, (where L is the number of levels). In particular, for case I, there are no solutions when $m_a = 1.1$, for case III, when $m_a = 1.1$ and for case IV, when $m_a = 1$ and $m_a = 1.1$. On the other hand, this fact does not happen for cases V and VI where the number of firing angles is higher and both symmetries provide solutions throughout the m_a range.

The firing angles associated to the solutions selected in table 4.2 for cases V and VI, are included at tables 4.3 and 4.5, respectively. The harmonic content associated to every solution is included at tables 4.4 and 4.6, which show a correct

Table 4.4: Harmonic content of solutions selected for case V (% based on fundamental)

m_a	1^{st}	5^{th}	7^{th}	11^{th}	13^{th}	17^{th}
0.1	99.93	0.10	0.09	0.05	0.12	0.00
0.2	99.97	0.02	0.01	0.02	0.00	0.01
0.3	100.05	0.01	0.02	0.03	0.02	0.01
0.4	100.01	0.02	0.01	0.03	0.02	0.02
0.5	99.97	0.01	0.01	0.01	0.02	0.01
0.6	99.98	0.01	0.00	0.01	0.00	0.00
0.7	99.89	0.15	0.06	0.14	0.01	0.06
0.8	99.99	0.01	0.02	0.01	0.03	0.01
0.9	99.98	0.01	0.00	0.01	0.01	0.00
1	100.00	0.01	0.01	0.01	0.03	0.02
1.1	100.00	0.00	0.01	0.00	0.00	0.01

Table 4.5. Firing angles and sign of every step of solutions selected for case VI

m_a	θ_1	θ_2	θ_3	θ_4	θ_5	θ_6	θ_7	θ_8	θ_9	θ_{10}	θ_{11}	θ_{12}	Initial Level
0.1	⇓0.8344	⇓1.1385	⇑1.2775	⇓1.3805	⇑1.4666	⇓1.5949	⇑1.6924	⇑1.9768	⇑2.2906	⇓2.3490	⇓2.8732	⇓3.1327	1
0.2	⇑0.0000	⇓0.2708	⇑0.7089	⇓0.7749	⇑0.9048	⇑1.1119	⇑1.3185	⇑1.5470	⇓1.5937	⇓2.0298	⇓2.2363	⇓2.4315	1
0.3	⇑0.1899	⇓0.2730	⇑0.3639	⇓0.5164	⇑0.8951	⇑1.0622	⇓1.0815	⇑1.6061	⇓1.9467	⇓2.6022	⇓2.8087	⇑2.9206	0
0.4	⇑0.4292	⇓0.7985	⇓1.1163	⇑1.1892	⇓1.5428	⇑1.6777	⇑1.9318	⇓2.4123	⇑2.4973	⇓2.7729	⇓2.9278	⇓3.1196	1
0.5	⇑0.0764	⇓0.2453	⇓1.0919	⇑1.2241	⇑1.3905	⇑1.7790	⇓1.8650	⇑2.0199	⇓2.3430	⇓2.4707	⇓2.7649	⇓3.0553	1
0.6	⇑0.1518	⇓0.5467	⇑1.1435	⇓1.1699	⇑1.4868	⇑1.6529	⇑1.9859	⇓2.0132	⇓2.4993	⇓2.6390	⇓2.7392	⇓2.9877	1
0.7	⇑0.2104	⇑0.8370	⇑1.0678	⇓1.2719	⇑1.3475	⇑1.6559	⇓1.7459	⇑1.7950	⇓1.8439	⇓2.0736	⇓2.5139	⇓2.7222	0
0.8	⇑0.3465	⇓0.3706	⇑0.4518	⇑1.2131	⇑1.8161	⇓1.8970	⇑2.0131	⇓2.1393	⇓2.3576	⇓2.7014	⇓2.8963	⇓3.0821	1
0.9	⇑0.1069	⇑0.2860	⇑0.9422	⇑1.1075	⇓1.1460	⇑1.5662	⇓1.6237	⇑1.6744	⇓2.0257	⇓2.5318	⇓2.7044	⇓2.8551	0
1	⇑0.3277	⇑0.6712	⇓0.8045	⇑0.8651	⇑1.2393	⇓1.3920	⇑1.4551	⇓2.2369	⇓2.5170	⇓2.7472	⇓2.9560	⇓3.1408	1
1.1	⇑0.0985	⇑0.2854	⇑0.4993	⇑0.8185	⇓1.9978	⇑2.1092	⇓2.2548	⇑2.3514	⇓2.3891	⇓2.6362	⇓2.8615	⇓3.1130	0

elimination of the undesired harmonics.

Finally, with the aim of studying the solutions when $\phi_1 \neq \pi/2$, the search algorithm has been executed again for case VI when $m_a = 0.5$, but with $\phi_1 = 0$, providing a cosine waveform. As a result, modifying the fundamental phase does not provide different solutions. The solutions are the same but shifted $\pi/2$.

4.7.2.2 Continuous Sets of Solutions

As an example, for the cases V and VI, continuous sets of solutions have been obtained utilizing the solutions selected and included at table 4.3 and 4.5, respectively. These sets have been provided by the local search detailed at Section 4.5. In this way, the solutions are obtained throughout the m_a range. For every set of angles, the performance indicators are provided.

As it has been detailed for the acquisition of solutions included a tables 4.3 and 4.5, the convergence threshold utilized to obtain the continuous sets of firing angles was 10^{-8}, accepting solutions which provides an error in the objective

Table 4.6: Harmonic content of solutions selected for case VI (% based on fundamental)

m_a	1^{st}	5^{th}	7^{th}	11^{th}	13^{th}	17^{th}
0.1	99.99	0.20	0.15	0.15	0.12	0.02
0.2	100.03	0.06	0.03	0.04	0.06	0.01
0.3	100.04	0.02	0.04	0.02	0.01	0.01
0.4	99.99	0.02	0.02	0.02	0.02	0.01
0.5	100.00	0.02	0.01	0.02	0.02	0.01
0.6	100.02	0.01	0.01	0.01	0.01	0.01
0.7	100.00	0.01	0.01	0.01	0.02	0.02
0.8	100.01	0.01	0.01	0.01	0.01	0.01
0.9	100.00	0.01	0.01	0.01	0.00	0.01
1	100.00	0.02	0.02	0.02	0.02	0.02
1.1	99.99	0.01	0.00	0.01	0.01	0.00

function lower than 10^{-6}. Thereby, all the continuous sets of firing angles provide a low error, lower than 10^{-6} and many of their solutions provide errors with an order of 10^{-7}, 10^{-8} or even 10^{-9}.

Fig. 4.15, 4.16 and 4.17 shows the sets of firing angles obtained for the case V, where the solid and dashed lines represent positive and negative steps, respectively, in the first QW. As it can be noticed, there are several gaps in the m_a range where solutions have not been provided. In this way, intermediate m_a samples have been utilized. In particular, solutions for $m_a = 0.25$, $m_a = 0.64$, $m_a = 0.74$ and $m_a = 0.88$ have been obtained. Afterwards, a local search has been realized utilizing these solutions, eliminating the gaps through the resulting sets of firing angles, except for the range from 1.04 to 1.09 where there is no solution. The intermediate sets of firing angles are depicted at Fig. 4.18.

In addition, as it can be noticed at Figs. 4.15-(a)-(1), 4.15-(b)-(1), 4.15-(c)-(1) and 4.16-(g)-(1), there are several firing angles which change the sign of their corresponding steps in a continuous way, providing longer sets of firing angles. In these cases, the virtual firing angle crosses the threshold $\pi/2$, changing the sign of the step, maintaining the continuity of the angle value. On the other hand, the over-modulation region is characterized by an increment in the third harmonic, as it is shown at Fig. 4.17-(k)-(2).

Furthermore, the solutions obtained from table 4.3 (case V) for $m_a = 0.1$ and $m_a = 0.2$ belong to the same set of firing angles as it shown at Figs. 4.15-(a)-(1) and 4.15-(b)-(1). Otherwise, the set of firing angles obtained through $m_a = 0.3$ provide a different solution for $m_a = 0.5$, from the one included at table 4.3. Thereby, the local search may provide new solutions for different m_a values. Finally, the trend of THD and HLF, as the m_a increases, is decreasing, as it can be observed at Figs. 4.15, 4.16, 4.17 and 4.18, except for particular increments.

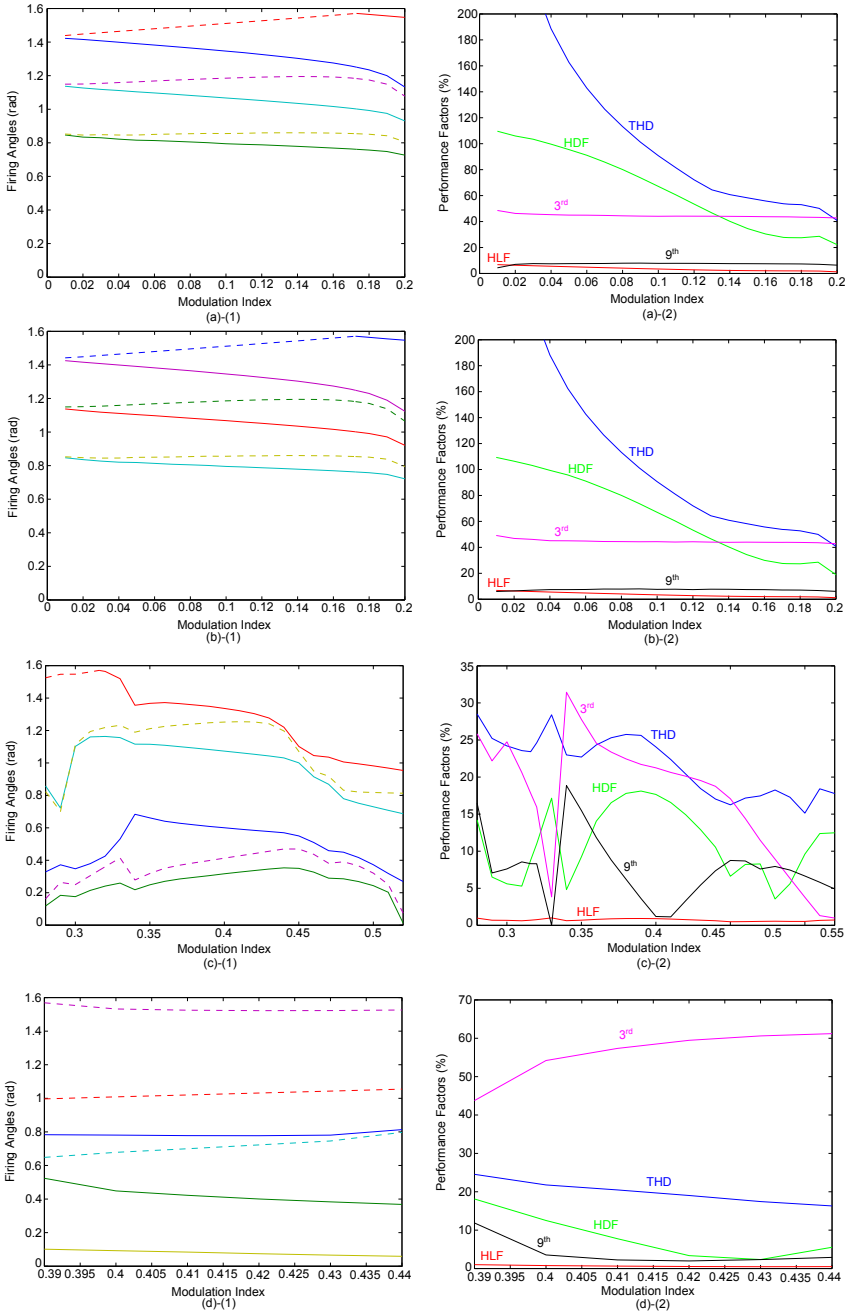

Figure 4.15. Continuous sets of solutions for case V (part 1).

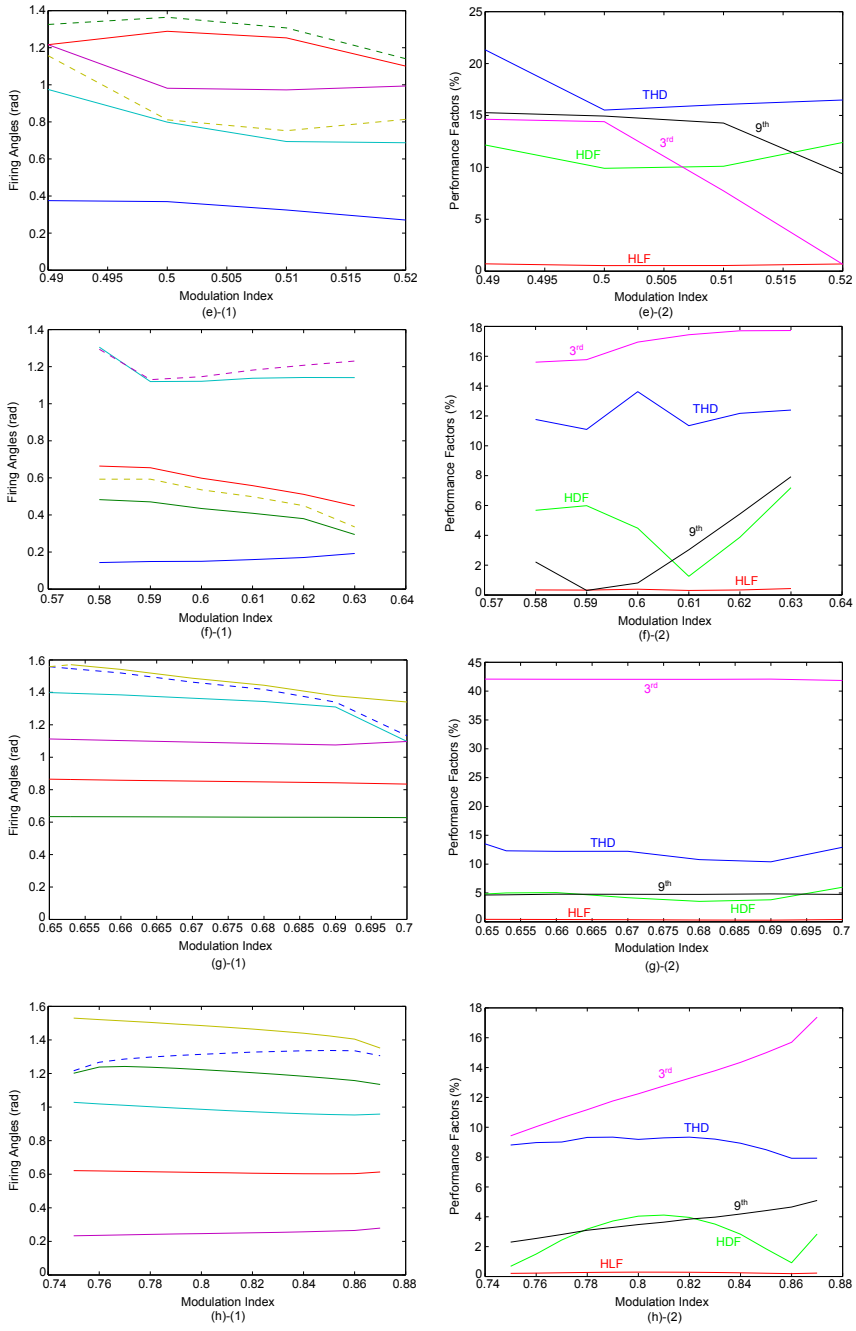

Figure 4.16. Continuous sets of solutions for case V (part 2).

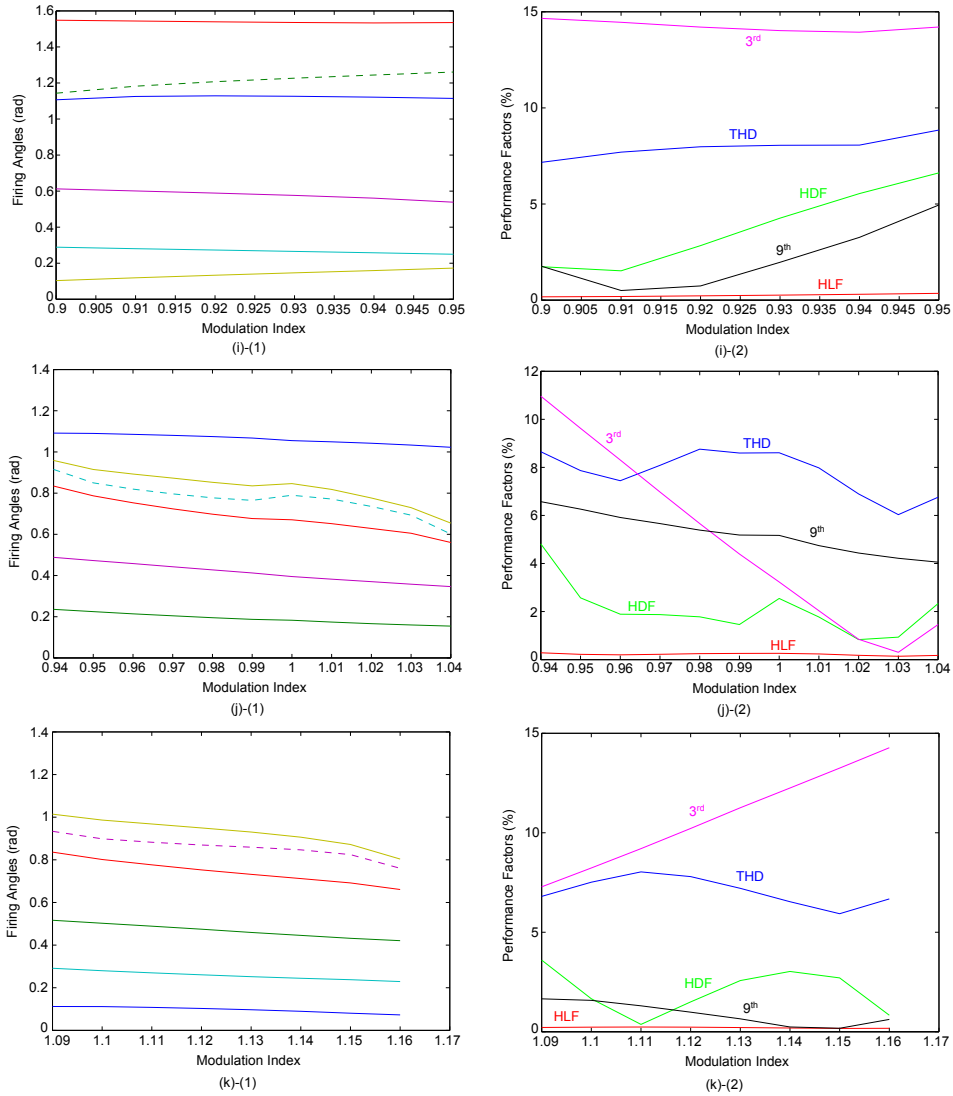

Figure 4.17. Continuous sets of solutions for case V (part 3).

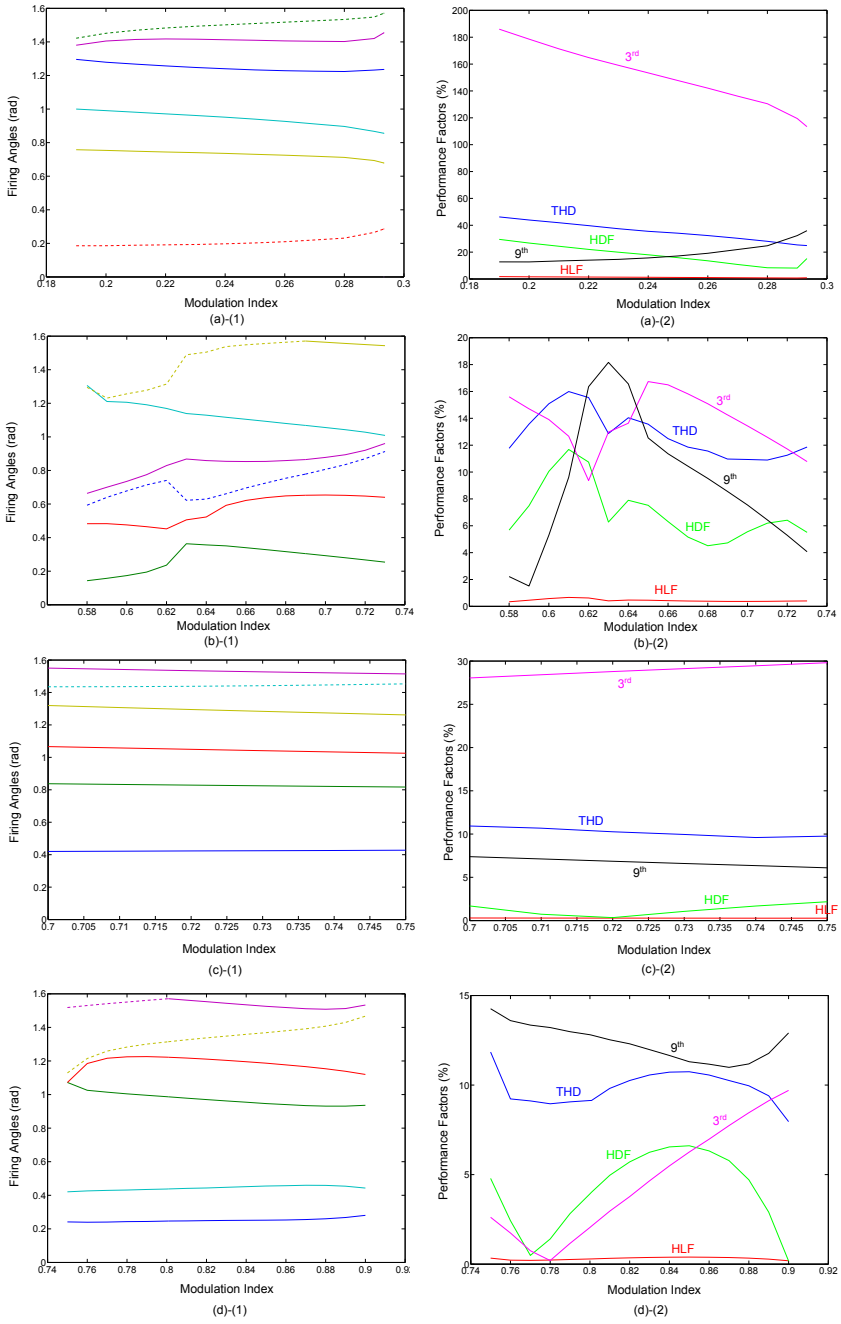

Figure 4.18. Continuous sets of intermediate solutions for case V.

Figs. 4.19, 4.20 and 4.21 shows the continuous sets of firing angles for Case VI, where the solid and dashed lines represent positive and negative steps, respectively, in the first HW. The sets have been calculated through the solutions included at table 4.5. The performance factors have also been depicted for every solution. As it can be noticed, there are several gaps in the m_a range where there is no solution. In this way, several intermediate solutions have been utilized to address this problem. In particular, the solutions for the m_a samples $m_a = 0.18$ $(L_i = 0)$, $m_a = 0.36$ $(L_i = 0)$, $m_a = 0.43$ $(L_i = 1)$, $m_a = 0.66$ $(L_i = 1)$, $m_a = 0.74$ $(L_i = 0)$, $m_a = 1.03$ $(L_i = 0)$ and $m_a = 1.045$ $(L_i = 0)$ have been obtained. Through these solutions, the corresponding continuous sets have been acquired, completing the m_a range, as it is depicted at Figs. 4.22 and 4.23. In this case, the HW symmetry has provided solutions from $m_a = 1.04$ to $m_a = 1.09$, unlike the QW symmetry.

Figs. 4.19, 4.20, 4.21, 4.22 and 4.23 shows how the THD and HLF reduces progressively, except for particular increments, when the m_a is increased. Finally, the over-modulation region provides an increment in the third harmonic, as it is shown at Fig. 4.21-(k)-(2).

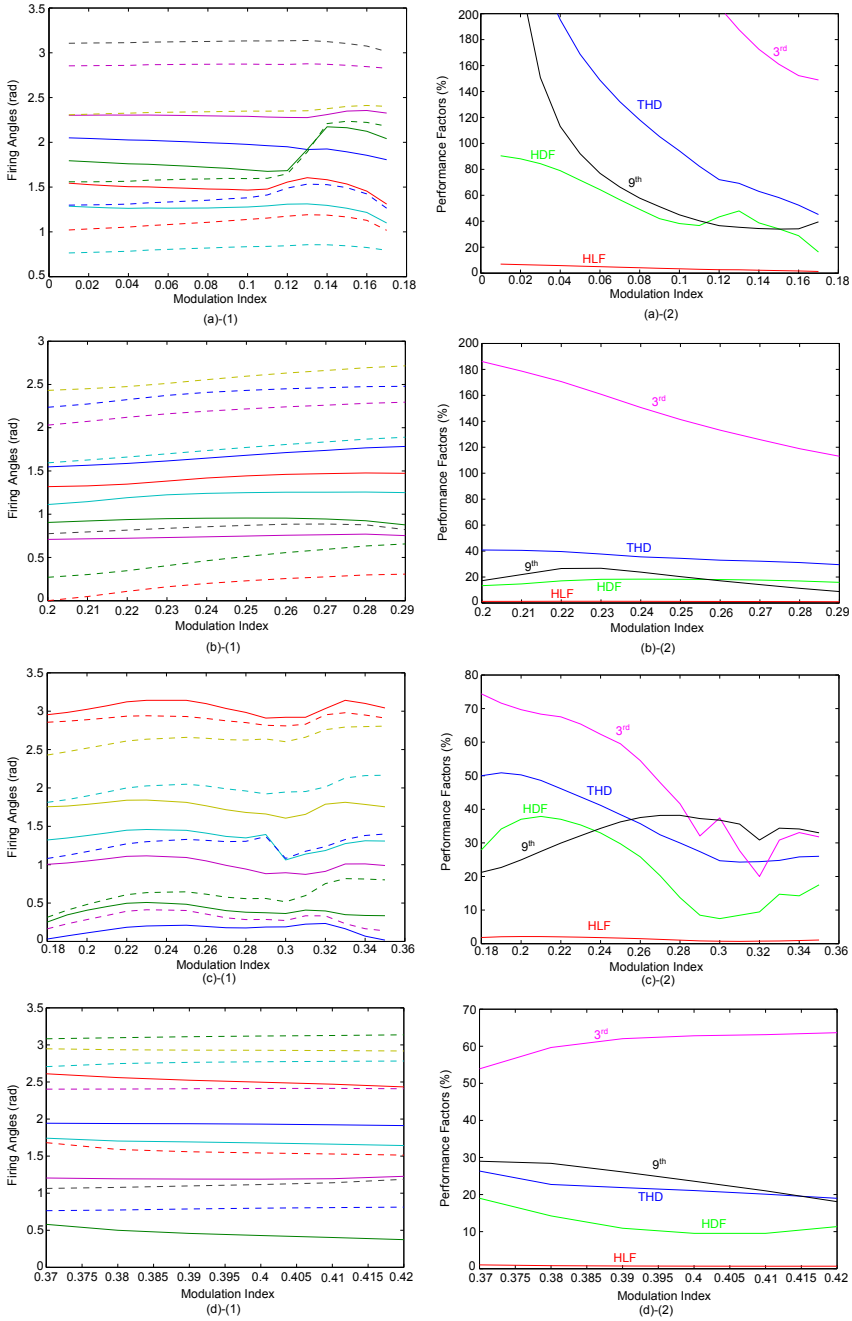

Figure 4.19. Continuous sets of solutions for case VI (part 1).

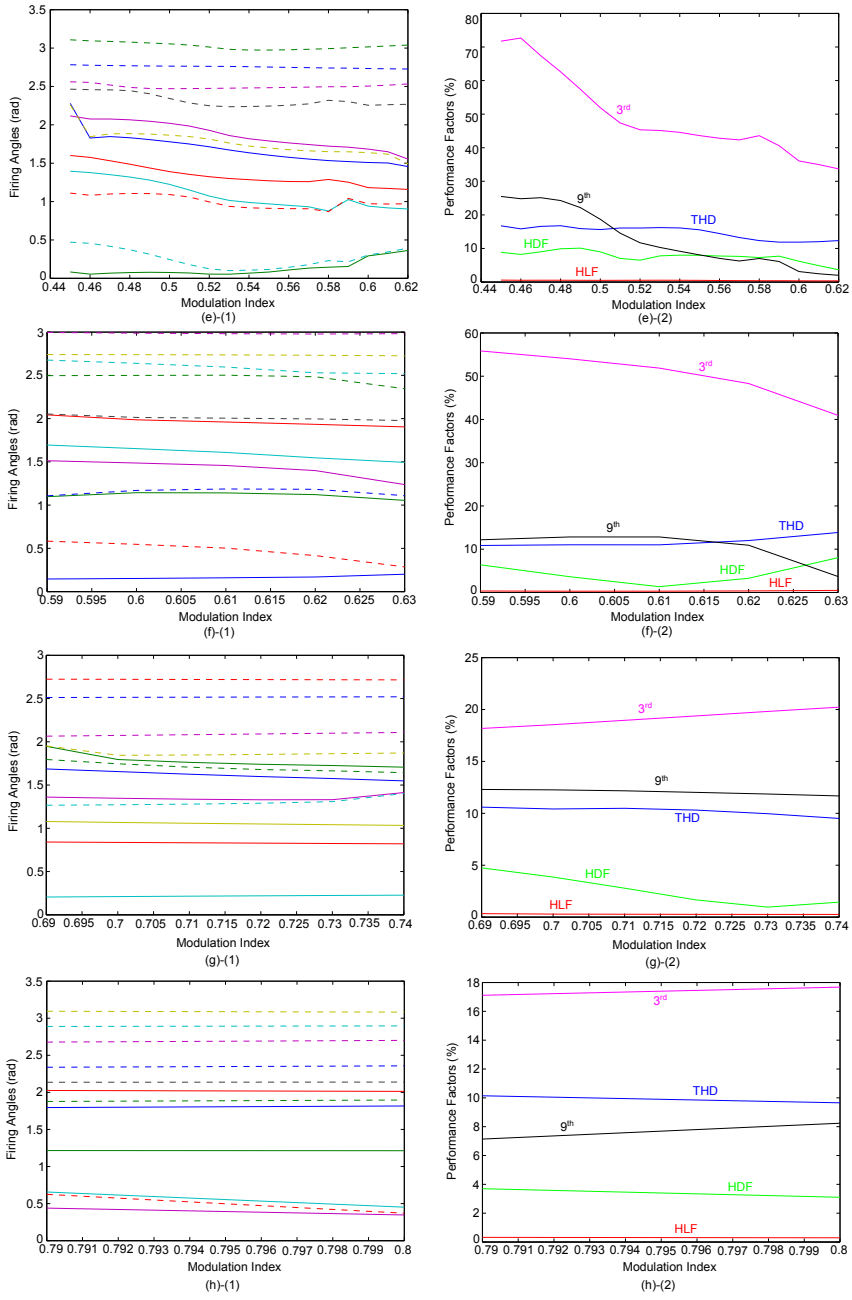

Figure 4.20. Continuous sets of solutions for case VI (part 2).

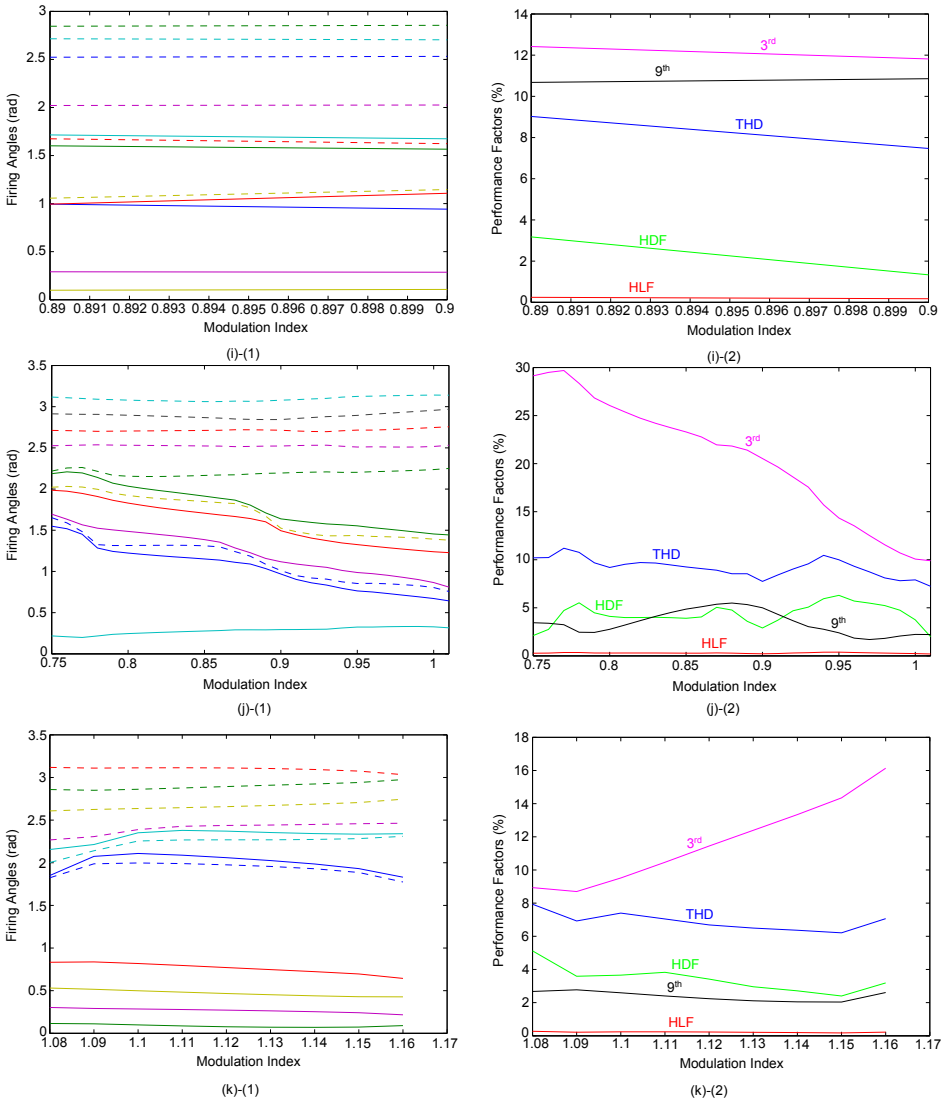

Figure 4.21. Continuous sets of solutions for case VI (part 3).

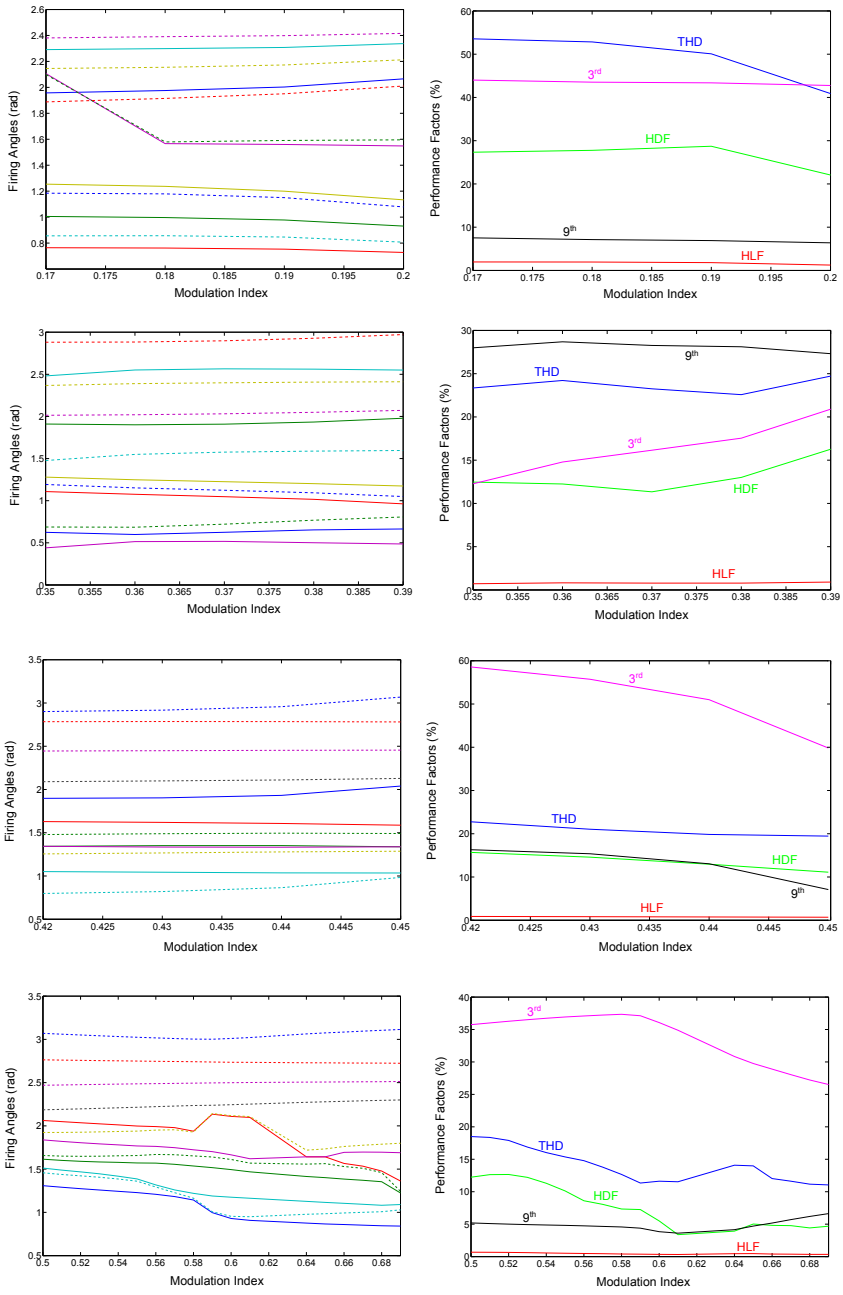

Figure 4.22. Continuous sets of intermediate solutions for case VI (part 1).

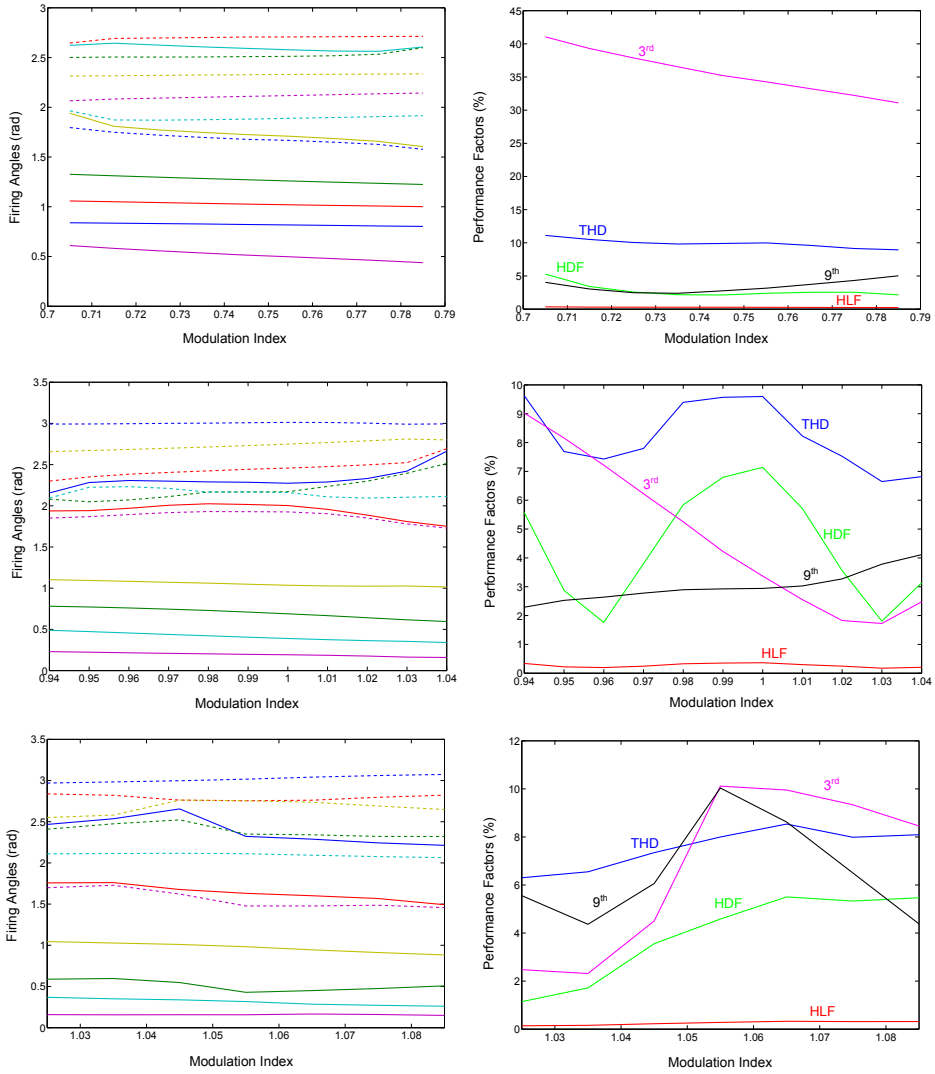

Figure 4.23. Continuous sets of intermediate solutions for case VI (part 2).

Table 4.7: Firing angles and sign of every step of QW solutions (9 firing angles and 11 levels)

m_a	θ_1	θ_2	θ_3	θ_4	θ_5	θ_6	θ_7	θ_8	θ_9
0.1	⇑0.708	⇓0.7436	⇑0.8956	⇓0.9655	⇑1.0855	⇓1.1887	⇑1.28	⇓1.4154	⇑1.483
0.2	⇑0.6762	⇓0.7306	⇑0.8293	⇓0.9369	⇑0.984	⇑1.2993	⇓1.3413	⇑1.4586	⇓1.5313
0.3	⇑0.6594	⇓0.7288	⇑0.7916	⇑1.0162	⇓1.0409	⇑1.1151	⇓1.1937	⇑1.2474	⇑1.5483
0.4	⇑0.6511	⇓0.7698	⇑0.8329	⇑0.8358	⇓0.9148	⇑1.0091	⇑1.2786	⇓1.3559	⇑1.4169
0.5	⇑0.3707	⇓0.4489	⇑0.5083	⇑0.8101	⇓0.8453	⇑0.9106	⇑1.0705	⇓1.1026	⇑1.1692
0.6	⇑0.2007	⇑0.4559	⇓0.5173	⇑0.5873	⇑0.8352	⇓0.8632	⇑1.029	⇓1.3258	⇑1.3481
0.7	⇑0.2736	⇑0.6056	⇑0.9496	⇑1.1351	⇓1.2321	⇑1.245	⇓1.3766	⇑1.4173	⇑1.5586
0.8	⇑0.3055	⇑0.5961	⇑0.8928	⇑1.0538	⇑1.2268	⇓1.3301	⇑1.3809	⇓1.4335	⇑1.4826
0.9	⇑0.0878	⇑0.3322	⇑0.5896	⇑0.8544	⇓0.977	⇑1.0066	⇑1.3131	⇓1.3869	⇑1.5131
1	⇑0.1616	⇑0.3295	⇑0.4794	⇑0.779	⇓0.8447	⇑0.9193	⇑1.0748	⇓1.554	⇓1.564
1.1	⇑0.0983	⇑0.2055	⇑0.227	⇑0.3873	⇑0.596	⇓0.9047	⇑1.0008	⇓1.2542	⇑1.5622

Table 4.8: Harmonic Amplitudes (% based on fundamental harmonic) for QW solutions with 9 firing angles and 11 levels

m_a	1^{st}	5^{th}	7^{th}	11^{th}	13^{th}	17^{th}	19^{th}	23^{th}	25^{th}
0.1	100.05	0.02	0.12	0.10	0.08	0.05	0.06	0.02	0.06
0.2	99.97	0.00	0.05	0.03	0.06	0.02	0.02	0.01	0.04
0.3	100.20	0.20	0.02	0.11	0.21	0.09	0.12	0.09	0.04
0.4	100.04	0.16	0.25	0.21	0.04	0.00	0.13	0.13	0.04
0.5	99.99	0.01	0.03	0.00	0.01	0.01	0.01	0.01	0.01
0.6	100.00	0.07	0.11	0.02	0.01	0.04	0.02	0.07	0.07
0.7	100.00	0.00	0.00	0.02	0.04	0.03	0.01	0.04	0.03
0.8	100.00	0.00	0.01	0.01	0.00	0.03	0.02	0.02	0.02
0.9	100.00	0.00	0.01	0.01	0.00	0.01	0.01	0.00	0.01
1	100.00	0.00	0.01	0.00	0.01	0.01	0.01	0.01	0.00
1.1	100.03	0.03	0.16	0.02	0.03	0.03	0.05	0.08	0.17

4.7.3 Solutions with a High Number of Controlled Harmonics

The proposed search method has been utilized to obtain solutions when the number of controlled harmonics is high (apart from the information included in this section, some additional information related to these solutions is included in appendix B). In this case, the QW symmetry has been utilized due to its lower computational load. In particular, solutions throughout the m_a range, between 0.1 and 1.1, have been obtained with 9 and 17 firing angles, from a converter with $L = 11$. Examples of solutions for different m_a values with 34 firing angles have been provided with the aim of showing the ability of the search method to eliminate a high number of harmonics.

In case of 9 firing angles, as it has been done in section 4.7.2, the maximum accepted error will be 10^{-6} and the convergence threshold value will be 10^{-8} to obtain lower errors in case it is possible. In case of 17 firing angles, the convergence threshold utilized to obtain the solutions was 10^{-6} and this is also

Table 4.9: Firing angles and sign of every step of QW solutions (17 firing angles and 11 levels)

m_a	θ_1	θ_2	θ_3	θ_4	θ_5	θ_6	θ_7	θ_8	θ_9	θ_{10}	θ_{11}	θ_{12}	θ_{13}	θ_{14}	θ_{15}	θ_{16}	θ_{17}
0.1	0.2601⇑	0.3311⇓	0.3692⇑	0.4484⇓	0.5935⇑	0.6868⇓	0.7092⇑	0.8111⇓	0.8866⇑	0.9207⇓	0.9891⇑	1.033⇓	1.0936⇑	1.1469⇓	1.1996⇑	1.2621⇓	1.5274⇑
0.2	0.2796⇑	0.3614⇑	0.3931⇓	0.4924⇓	0.5433⇑	0.643⇑	0.7075⇓	0.8141⇓	0.8619⇑	0.9274⇓	0.9574⇑	1.0403⇓	1.0544⇑	1.2411⇑	1.2547⇓	1.3492⇓	1.4957⇑
0.3	0.4039⇑	0.4464⇑	0.4625⇓	0.5441⇑	0.5751⇓	0.6863⇓	0.7421⇑	0.8097⇓	0.8348⇑	1.0184⇑	1.0453⇓	1.1105⇑	1.1624⇓	1.2037⇑	1.2772⇓	1.2977⇑	1.4512⇓
0.4	0.3091⇑	0.3388⇓	0.3894⇑	0.464⇑	0.6027⇓	0.9025⇑	0.9339⇓	0.9851⇑	1.044⇓	1.066⇑	1.1969⇑	1.2094⇓	1.2684⇑	1.3057⇓	1.3782⇑	1.4053⇓	1.5042⇓
0.5	0.3244⇑	0.41⇑	0.4972⇑	0.571⇓	0.6999⇓	0.7758⇑	0.7923⇓	0.8624⇑	0.9103⇓	0.937⇑	1.0632⇑	1.0817⇓	1.1306⇑	1.1787⇓	1.207⇑	1.3993⇓	1.5106⇓
0.6	0.2778⇑	0.4383⇑	0.4676⇓	0.5238⇑	0.5803⇓	0.6129⇑	0.6948⇓	0.7072⇑	0.8028⇓	0.8456⇑	0.9944⇑	1.034⇓	1.0677⇑	1.1979⇑	1.2152⇓	1.2551⇑	1.298⇓
0.7	0.1263⇑	0.356⇑	0.4653⇓	0.4729⇑	0.5095⇑	0.5395⇓	0.6046⇑	0.6635⇓	0.7032⇑	0.7378⇓	0.7898⇑	0.9528⇓	0.9804⇑	1.1039⇑	1.1377⇓	1.324⇑	1.3644⇓
0.8	0.3614⇑	0.4021⇓	0.4381⇑	0.6019⇑	0.6316⇓	0.6912⇑	0.7504⇓	0.8022⇑	0.8032⇑	0.8383⇓	0.9034⇑	1.0379⇑	1.0782⇓	1.0974⇑	1.1929⇑	1.2238⇓	1.2613⇑
0.9	0.1538⇑	0.2106⇑	0.472⇓	0.5073⇑	0.6288⇑	0.6363⇑	0.663⇓	0.7253⇑	0.8714⇓	0.928⇑	0.9454⇓	0.9983⇑	1.1288⇑	1.1824⇓	1.2869⇓	1.331⇑	1.4783⇑
1	0.1352⇑	0.2296⇑	0.2891⇓	0.3443⇑	0.4957⇑	0.5405⇓	0.5748⇑	0.7041⇑	0.7088⇓	0.7573⇑	0.9148⇓	0.9423⇑	1.0675⇑	1.1511⇓	1.1676⇑	1.2439⇓	1.3039⇑
1.1	⇑0.0858	⇑0.1456	⇑0.2569	⇓0.3486	⇑0.3553	⇑0.5052	⇓0.5173	⇑0.5717	⇑0.6882	⇓0.9630	⇑1.0169	⇓1.1829	⇑1.2502	⇓1.2815	⇑1.3958	⇓1.4355	⇑1.4656

Table 4.10: Harmonic Amplitudes (% based on fundamental harmonic) for QW solutions with 17 firing angles and 11 levels

m_a	1^{st}	5^{th}	7^{th}	11^{th}	13^{th}	17^{th}	19^{th}	23^{th}	25^{th}	29^{th}	31^{th}	35^{th}	37^{th}	41^{th}	43^{th}	47^{th}	49^{th}
0.1	99.90	0.01	0.01	0.08	0.02	0.05	0.02	0.00	0.02	0.02	0.02	0.04	0.06	0.02	0.08	0.09	0.06
0.2	99.83	0.03	0.18	0.12	0.20	0.15	0.09	0.11	0.01	0.08	0.05	0.03	0.08	0.06	0.04	0.09	0.04
0.3	100.01	0.31	0.11	0.19	0.03	0.03	0.18	0.03	0.14	0.04	0.11	0.17	0.06	0.01	0.03	0.05	0.07
0.4	100.03	0.13	0.05	0.04	0.13	0.01	0.12	0.09	0.05	0.11	0.08	0.02	0.10	0.01	0.05	0.06	0.01
0.5	100.02	0.02	0.01	0.01	0.00	0.01	0.02	0.00	0.01	0.00	0.02	0.01	0.00	0.00	0.01	0.01	0.00
0.6	99.98	0.01	0.03	0.03	0.05	0.03	0.02	0.01	0.01	0.00	0.00	0.01	0.03	0.01	0.02	0.00	0.01
0.7	100.03	0.10	0.02	0.10	0.00	0.02	0.04	0.06	0.03	0.00	0.01	0.05	0.00	0.10	0.02	0.04	0.03
0.8	99.99	0.01	0.07	0.06	0.10	0.10	0.02	0.02	0.02	0.01	0.02	0.02	0.05	0.04	0.03	0.04	0.01
0.9	99.98	0.01	0.01	0.00	0.03	0.00	0.04	0.02	0.00	0.02	0.01	0.01	0.02	0.02	0.00	0.01	0.00
1	99.99	0.03	0.00	0.02	0.01	0.02	0.02	0.00	0.02	0.01	0.01	0.02	0.01	0.01	0.00	0.01	0.01
1.1	100.02	0.01	0.04	0.02	0.06	0.04	0.03	0.03	0.00	0.02	0.01	0.06	0.06	0.04	0.08	0.00	0.03

Table 4.11: Firing angles and sign of every step of QW solutions (34 firing angles and 11 levels)

m_a	θ_1	θ_2	θ_3	θ_4	θ_5	θ_6	θ_7	θ_8	θ_9	θ_{10}	θ_{11}	θ_{12}	θ_{13}	θ_{14}	θ_{15}	θ_{16}	θ_{17}
0.2	⇑0.0572	⇑0.2854	⇓0.3009	⇑0.3426	⇓0.3622	⇑0.4001	⇓0.4235	⇑0.4579	⇓0.4849	⇑0.5161	⇓0.5464	⇑0.5745	⇓0.6078	⇑0.6333	⇓0.6693	⇑0.6924	⇓0.7306
0.5	⇑0.1420	⇓0.1798	⇑0.1892	⇑0.2363	⇓0.2879	⇑0.3249	⇓0.3337	⇑0.3709	⇑0.4124	⇓0.4357	⇑0.5630	⇓0.5705	⇑0.5984	⇓0.6583	⇑0.7569	⇓0.8242	⇑0.8675
0.9	⇑0.2246	⇑0.2689	⇑0.3140	⇑0.4108	⇓0.4258	⇑0.4590	⇑0.5062	⇓0.5510	⇑0.6537	⇓0.6652	⇑0.7076	⇓0.7314	⇓0.7403	⇑0.7572	⇓0.7937	⇓0.7940	⇑0.8075
m_a	θ_{18}	θ_{19}	θ_{20}	θ_{21}	θ_{22}	θ_{23}	θ_{24}	θ_{25}	θ_{26}	θ_{27}	θ_{28}	θ_{29}	θ_{30}	θ_{31}	θ_{32}	θ_{33}	θ_{34}
0.2	⇑0.7516	⇓0.7909	⇑0.8223	⇓0.8546	⇑0.8795	⇓0.9189	⇑0.9422	⇑0.9440	⇓0.9510	⇓0.9755	⇓1.0388	⇑1.0471	⇓1.1011	⇑1.2206	⇓1.2269	⇑1.2759	⇓1.2870
0.5	⇓0.8827	⇓0.9406	⇑0.9521	⇑1.0467	⇓1.0563	⇑1.0949	⇓1.1139	⇑1.1420	⇓1.1708	⇓1.2825	⇑1.3287	⇑1.3877	⇓1.3922	⇓1.4355	⇑1.5032	⇓1.5342	⇑1.5502
0.9	⇓0.8471	⇑0.8689	⇓0.9098	⇑0.9125	⇑0.9525	⇓0.9660	⇑0.9916	⇓1.0164	⇑1.0273	⇑1.0994	⇓1.1127	⇑1.1403	⇓1.1698	⇑1.1833	⇓1.2893	⇓1.3489	⇓1.5341

Table 4.12: Harmonic Amplitudes (% based on fundamental harmonic) for QW solutions with 34 firing angles and 11 levels

m_a	1^{st}	5^{th}	7^{th}	11^{th}	13^{th}	17^{th}	19^{th}	23^{th}	25^{th}	29^{th}	31^{th}	35^{th}	37^{th}	41^{th}	43^{th}	47^{th}	49^{th}
0.2	99.81	0.03	0.28	0.20	0.24	0.27	0.07	0.19	0.12	0.06	0.20	0.11	0.19	0.19	0.09	0.17	0.00
0.5	100.00	0.04	0.03	0.05	0.02	0.04	0.01	0.08	0.02	0.03	0.04	0.05	0.02	0.04	0.05	0.01	0.02
0.9	99.83	0.15	0.02	0.03	0.04	0.00	0.06	0.07	0.05	0.21	0.05	0.08	0.09	0.03	0.03	0.09	0.07
m_a	53^{th}	55^{th}	59^{th}	61^{th}	65^{th}	67^{th}	71^{th}	73^{th}	77^{th}	79^{th}	83^{th}	85^{th}	89^{th}	91^{th}	93^{th}	97^{th}	101^{th}
0.2	0.04	0.12	0.03	0.14	0.12	0.09	0.08	0.02	0.07	0.07	0.01	0.11	0.05	0.09	0.05	0.01	0.02
0.5	0.01	0.03	0.02	0.03	0.01	0.01	0.01	0.01	0.02	0.02	0.00	0.02	0.02	0.01	0.01	0.01	0.00
0.9	0.02	0.05	0.02	0.15	0.08	0.06	0.01	0.03	0.07	0.02	0.07	0.02	0.09	0.06	0.11	0.00	0.03

the maximum error accepted for every obtained solution. This threshold has been increased in comparison with the cases with lower number of firing angles, because the number of solutions obtained with an error lower than 10^{-7} was low and therefore, increasing the threshold reduces the computational burden. Tables 4.7, 4.8, 4.9 and 4.10 show the solutions for every m_a value and their corresponding harmonic content, respectively. As it can be noticed, the first 8^{th} and 16^{th} odd and non-triplen harmonics are correctly eliminated.

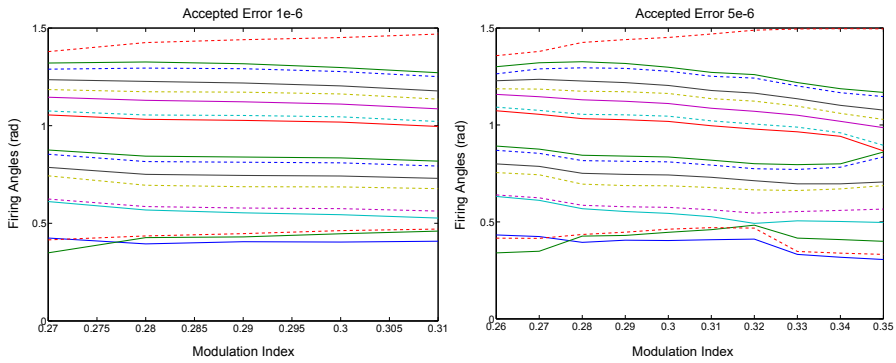

(a) Set of firing angles with accepted error equal to 10^{-6}.

(b) Set of firing angles with accepted error equal to $5(10^{-6})$.

Figure 4.24. Sets of firing angles obtained with different accepted error.

Table 4.13: QW Solutions (firing angles and sign of every step) with 17 firing angles and 11 levels for continuous set ($m_a = 0.26$ to $m_a = 0.35$)

m_a	θ_1	θ_2	θ_3	θ_4	θ_5	θ_6	θ_7	θ_8	θ_9	θ_{10}	θ_{11}	θ_{12}	θ_{13}	θ_{14}	θ_{15}	θ_{16}	θ_{17}
0.26	⇑0.3403	⇓0.4163	⇑0.4328	⇑0.6315	⇓0.6391	⇓0.7545	⇑0.7991	⇓0.8694	⇑0.8911	⇑1.0732	⇓1.0918	⇑1.1576	⇓1.1864	⇑1.2281	⇓1.2636	⇑1.3005	⇓1.3575
0.27	⇑0.3489	⇓0.4152	⇑0.4246	⇑0.6113	⇓0.6243	⇓0.7431	⇑0.7865	⇓0.8537	⇑0.8753	⇑1.0549	⇓1.0753	⇑1.1456	⇓1.1849	⇑1.2353	⇓1.2892	⇑1.3207	⇓1.3792
0.28	⇑0.3947	⇑0.4267	⇓0.4353	⇑0.5681	⇓0.5858	⇓0.6948	⇑0.7506	⇓0.8161	⇑0.8438	⇑1.0326	⇓1.0547	⇑1.1298	⇓1.1738	⇑1.2266	⇓1.2947	⇑1.3261	⇓1.4254
0.29	⇑0.4059	⇑0.4303	⇓0.4471	⇑0.5536	⇓0.5783	⇓0.6875	⇑0.7452	⇓0.8127	⇑0.8394	⇑1.0270	⇓1.0522	⇑1.1221	⇓1.1716	⇑1.2184	⇓1.2916	⇑1.3172	⇓1.4404
0.3	⇑0.4039	⇑0.4464	⇓0.4625	⇑0.5441	⇓0.5751	⇓0.6863	⇑0.7421	⇓0.8097	⇑0.8348	⇑1.0184	⇓1.0453	⇑1.1105	⇓1.1624	⇑1.2037	⇓1.2772	⇑1.2977	⇓1.4512
0.31	⇑0.4083	⇑0.4600	⇓0.4705	⇑0.5268	⇓0.5626	⇓0.6775	⇑0.7300	⇓0.7932	⇑0.8183	⇑0.9960	⇓1.0212	⇑1.0862	⇓1.1359	⇑1.1778	⇓1.2510	⇑1.2711	⇓1.4690
0.32	⇑0.4114	⇓0.4680	⇑0.4834	⇑0.4925	⇓0.5453	⇓0.6654	⇑0.7125	⇓0.7743	⇑0.8003	⇑0.9786	⇓1.0046	⇑1.0706	⇓1.1228	⇑1.1641	⇓1.2417	⇑1.2597	⇓1.4886
0.33	⇑0.3324	⇓0.3477	⇑0.4164	⇑0.5056	⇓0.5535	⇓0.6619	⇑0.6964	⇓0.7705	⇑0.7954	⇑0.9647	⇓0.9888	⇑1.0502	⇓1.0971	⇑1.1351	⇓1.2012	⇑1.2186	⇓1.4951
0.34	⇑0.3177	⇓0.3389	⇑0.4090	⇑0.5024	⇓0.5595	⇓0.6701	⇑0.6964	⇓0.7822	⇑0.7995	⇑0.9414	⇓0.9596	⇑1.0187	⇓1.0598	⇑1.1011	⇓1.1665	⇑1.1869	⇓1.4963
0.35	⇑0.3062	⇓0.3324	⇑0.3999	⇑0.4971	⇓0.5663	⇓0.6873	⇑0.7060	⇓0.8354	⇑0.8604	⇑0.8667	⇓0.8952	⇑0.9861	⇓1.0285	⇑1.0767	⇓1.1463	⇑1.1680	⇓1.4957

Table 4.14: Harmonic Amplitudes (% based on fundamental harmonic) for solutions (QW) with 17 firing angles and 11 levels for continuous set ($m_a = 0.26$ to $m_a = 0.35$)

m_a	1^{st}	5^{th}	7^{th}	11^{th}	13^{th}	17^{th}	19^{th}	23^{th}	25^{th}	29^{th}	31^{th}	35^{th}	37^{th}	41^{th}	43^{th}	47^{th}	49^{th}
0.26	100.31	0.26	0.32	0.25	0.27	0.17	0.24	0.17	0.18	0.13	0.18	0.11	0.15	0.07	0.11	0.02	0.06
0.27	99.92	0.10	0.08	0.06	0.08	0.09	0.04	0.05	0.06	0.06	0.02	0.04	0.03	0.03	0.01	0.02	0.01
0.28	100.09	0.26	0.07	0.25	0.19	0.15	0.21	0.01	0.14	0.09	0.03	0.13	0.04	0.09	0.08	0.03	0.06
0.29	100.01	0.02	0.02	0.02	0.02	0.02	0.00	0.02	0.01	0.01	0.04	0.02	0.00	0.02	0.01	0.00	0.01
0.3	100.01	0.30	0.11	0.19	0.03	0.03	0.19	0.03	0.14	0.05	0.10	0.18	0.06	0.02	0.02	0.04	0.07
0.31	99.96	0.02	0.01	0.02	0.04	0.02	0.02	0.01	0.00	0.03	0.00	0.00	0.01	0.00	0.01	0.00	0.00
0.32	99.62	0.55	0.25	0.18	0.37	0.43	0.14	0.12	0.28	0.13	0.27	0.21	0.10	0.00	0.14	0.13	0.01
0.33	100.00	0.04	0.02	0.02	0.03	0.01	0.01	0.03	0.01	0.02	0.02	0.00	0.01	0.01	0.00	0.01	0.01
0.34	99.91	0.04	0.06	0.07	0.04	0.02	0.07	0.04	0.01	0.00	0.06	0.04	0.02	0.01	0.03	0.03	0.02
0.35	99.73	0.18	0.24	0.32	0.06	0.05	0.23	0.19	0.05	0.11	0.13	0.12	0.09	0.10	0.04	0.07	0.06

In case of 34 firing angles, the convergence threshold was also 10^{-6} and the accepted error was $5(10^{-6})$. Examples of solutions for several m_a values have been included at table 4.11. As it can be noticed at table 4.12, the utilized accepted error provides a correct elimination of the first 33^{th} odd and non-triplen harmonics.

4.7.3.1 Continuous sets of solutions

For the case of 17 firing angles in the first QW, continuous sets of firing angles have been obtained throughout the m_a range. The sets have been acquired through the solutions included at table 4.9. The convergence threshold has been set to 10^{-6}. For the maximum accepted error there are two possibilities. Firstly, it can be 10^{-6}, providing solutions throughout the m_a range, as it can be noticed at table B.1 (where the associated harmonic content is included at table B.2) which contains intermediate solutions that complement the ones included at table 4.9.

However, as it can be seen at Fig. 4.24-(a), this error provides sets of firing angles which are of too short length (this fact happens when the number of firing angles is high). Therefore, the number of required sets is high. This fact hinders the application of converter control techniques along with SHE-PWM because the modification of the m_a command inside the fundamental period provides distortion in the harmonic content. This distortion, for example, may be increased if a light modification of the m_a command implies the utilization of a new set with different switching pattern. Therefore, longer sets of firing angles may provide lower distortion in the phase output voltage. On the other hand, if the modification of the m_a command is restricted to every quarter wave, the lower order harmonics are not affected. In this way, the distortion disappears but the bandwidth of the control is reduced.

Therefore, regarding the length of the sets of firing angles, if the maximum accepted error is $5 * 10^{-6}$, the length of these sets can be increased, as it can be noticed at Fig. 4.24-(b), where the solid and dashed lines represent positive and negative firing angles, respectively. In this way, the continuity in the solutions is increased and the harmonics are still correctly eliminated, as it is detailed at tables 4.14 and B.4, whose corresponding firing angles are included at tables 4.13 and B.3, respectively.

In this way, through the solutions included at table 4.9, utilizing a maximum accepted error of $5 * 10^{-6}$, several continuous sets of firing angles have been obtained throughout the m_a range, as it is shown at Figs. 4.25, 4.26 and 4.27. With the aim of completing the m_a range, several intermediate solutions, in particular for indices $m_a = 0.173$, $m_a = 0.246$, $m_a = 0.366$, $m_a = 0.513$, $m_a = 0.733$, $m_a = 0.766$, $m_a = 0.933$ and $m_a = 1.066$, have been utilized to obtain more continuous sets. These new sets are included at Figs. 4.28 and 4.29.

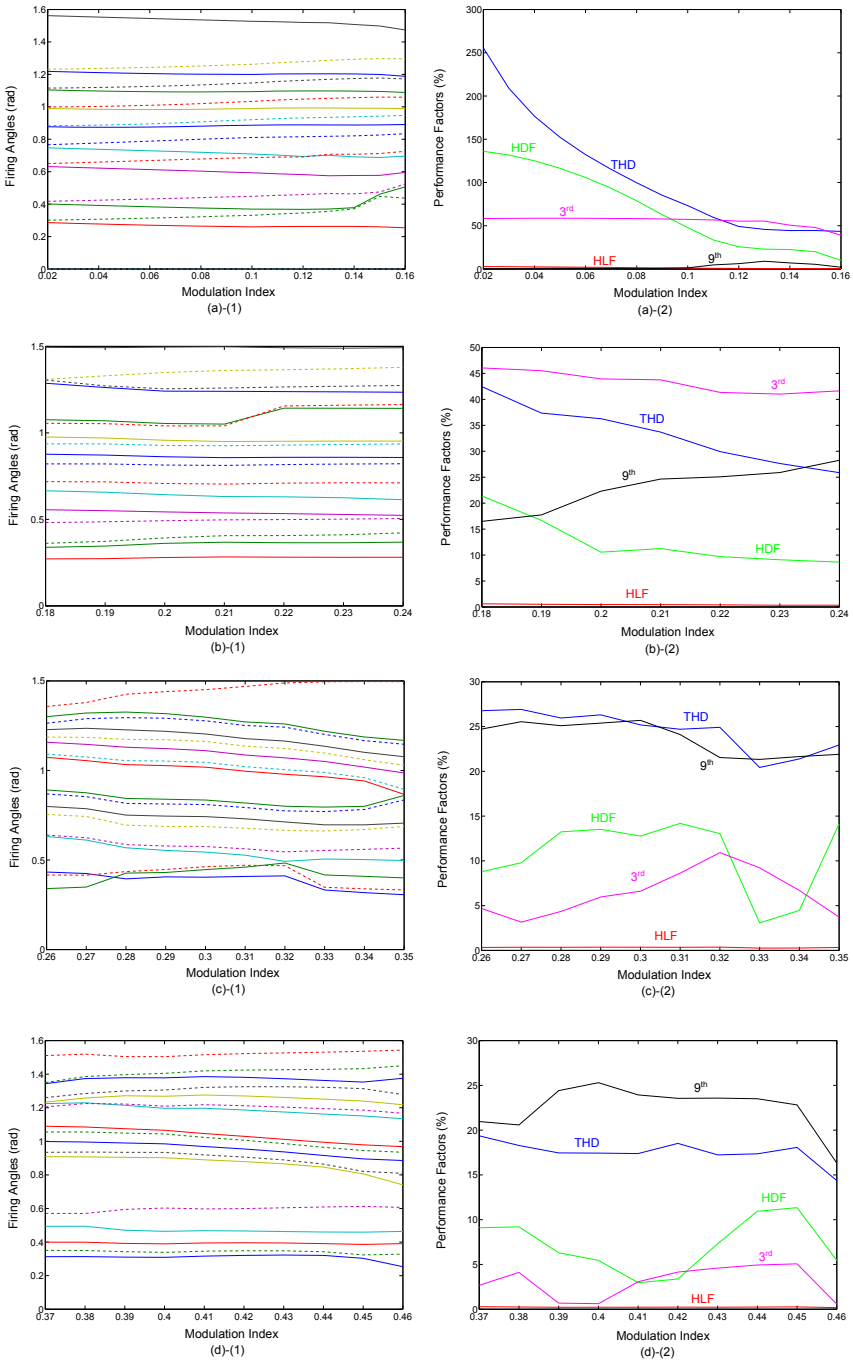

Figure 4.25: Continuous sets of solutions for 17 firing angles and QW symmetry (part 1).

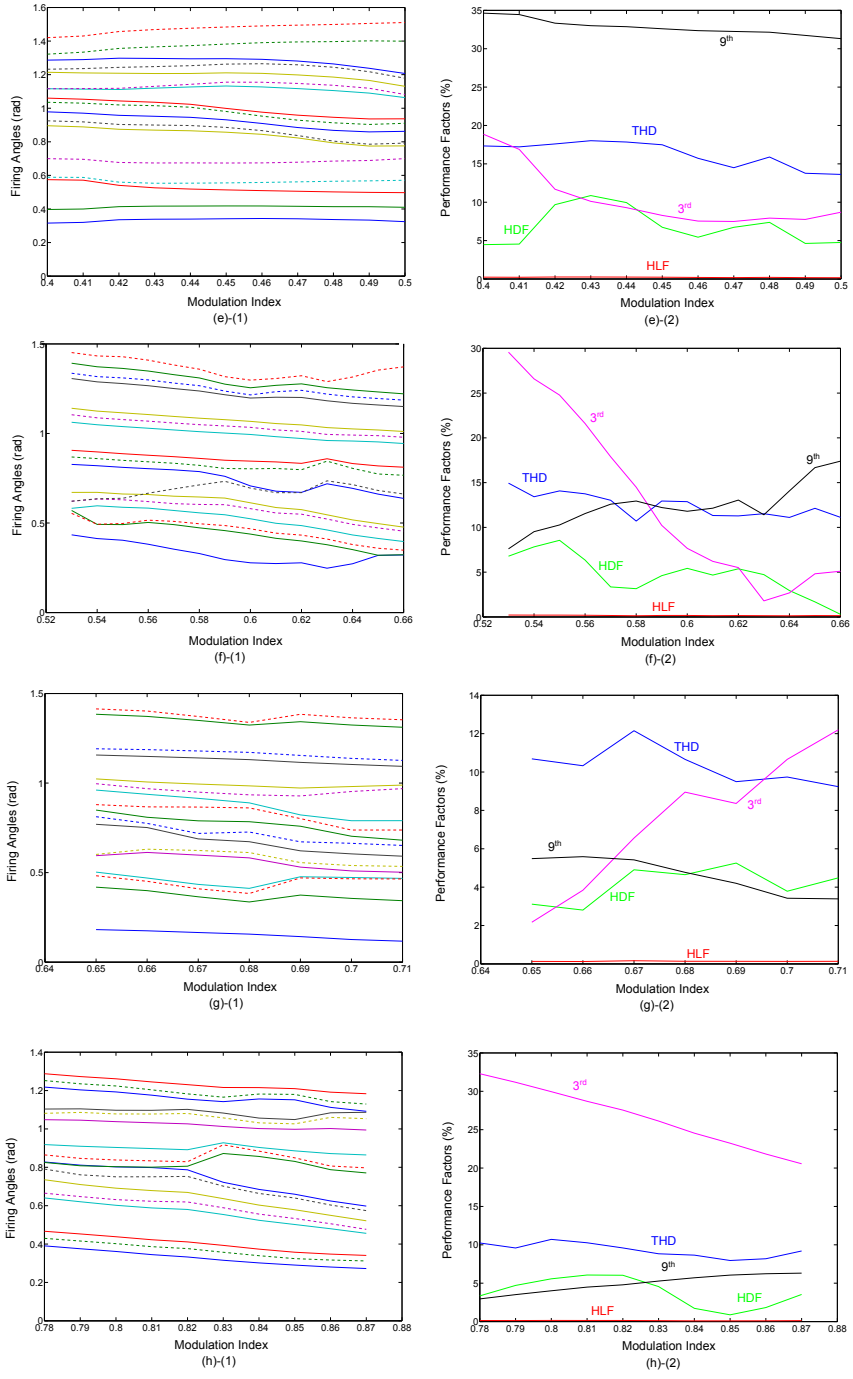

Figure 4.26: Continuous sets of solutions for 17 firing angles and QW symmetry (part 2).

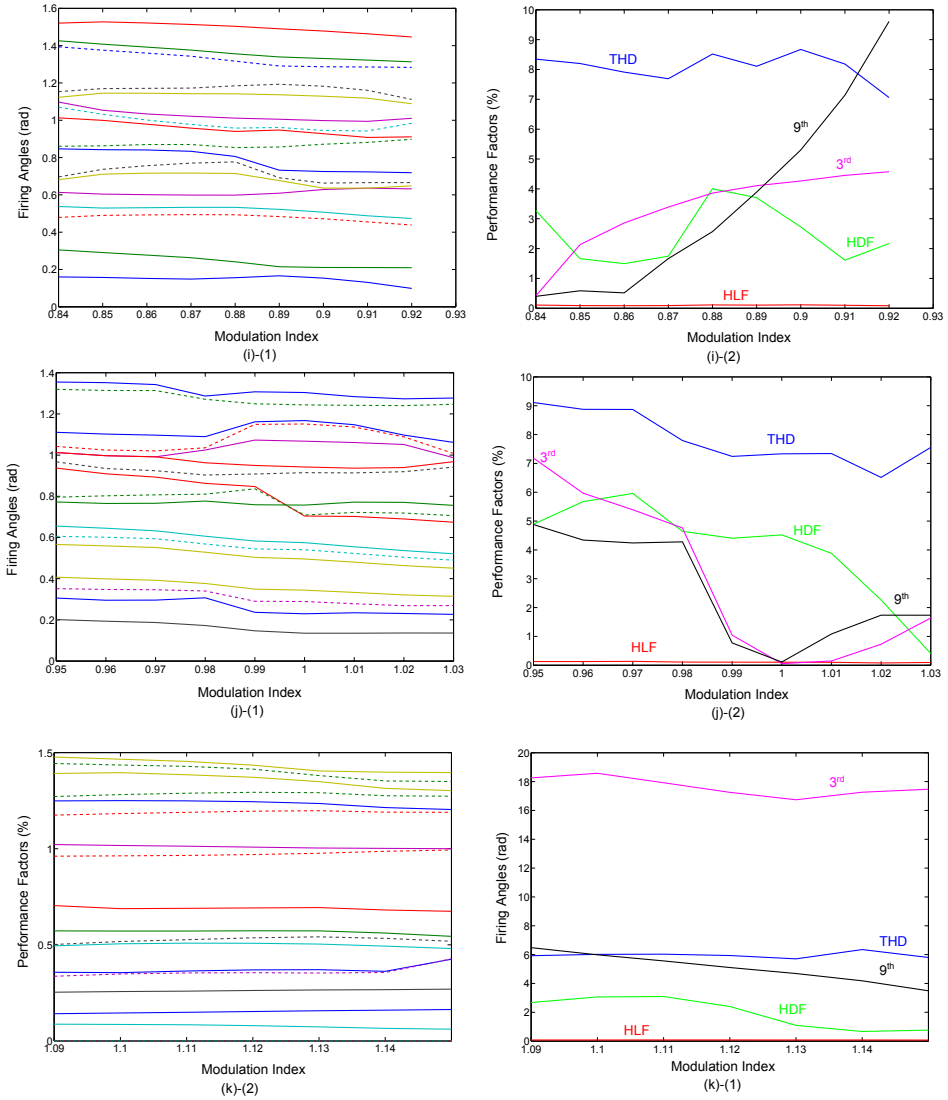

Figure 4.27: Continuous sets of solutions for 17 firing angles and QW symmetry (part 3).

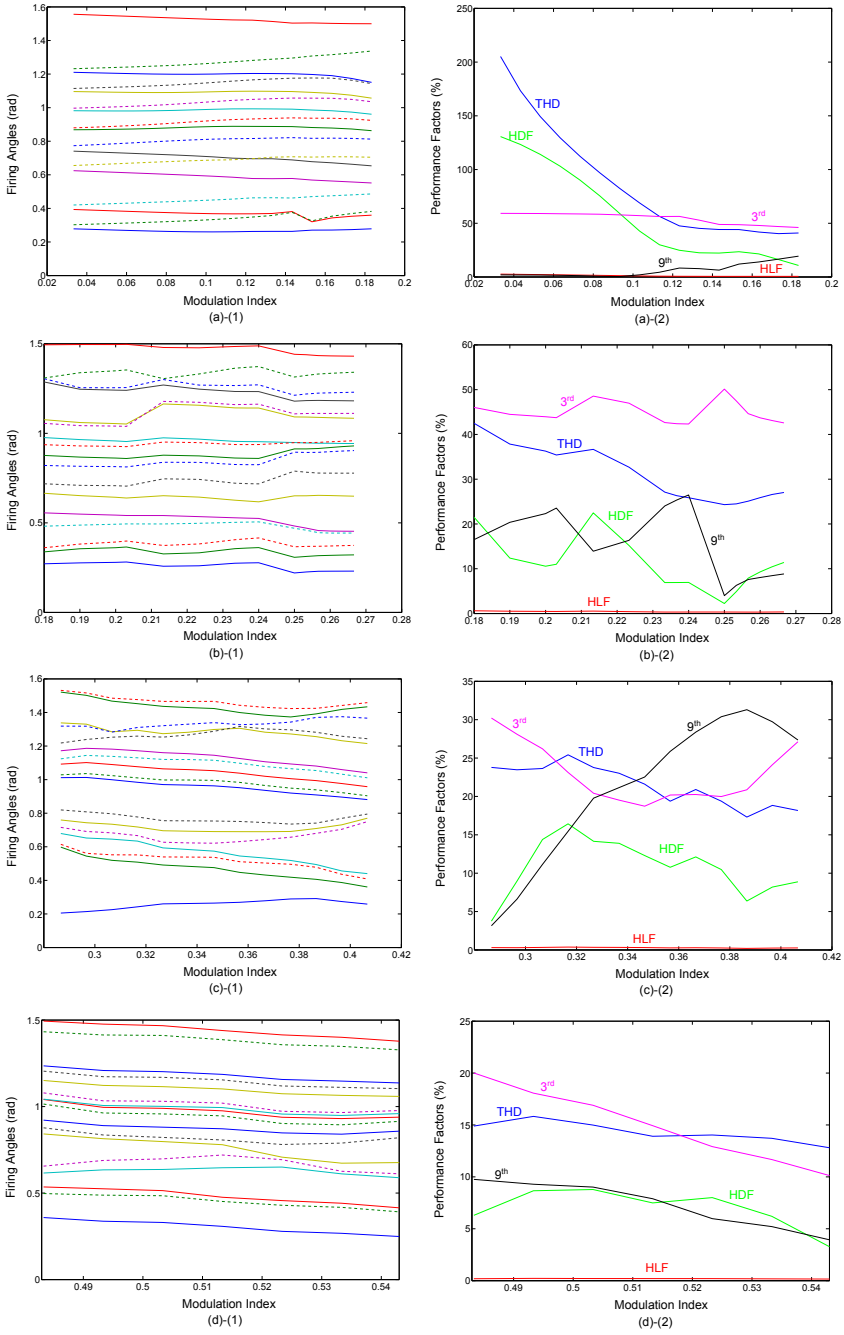

Figure 4.28: Continuous sets of intermediate solutions for 17 firing angles and QW symmetry (part 1).

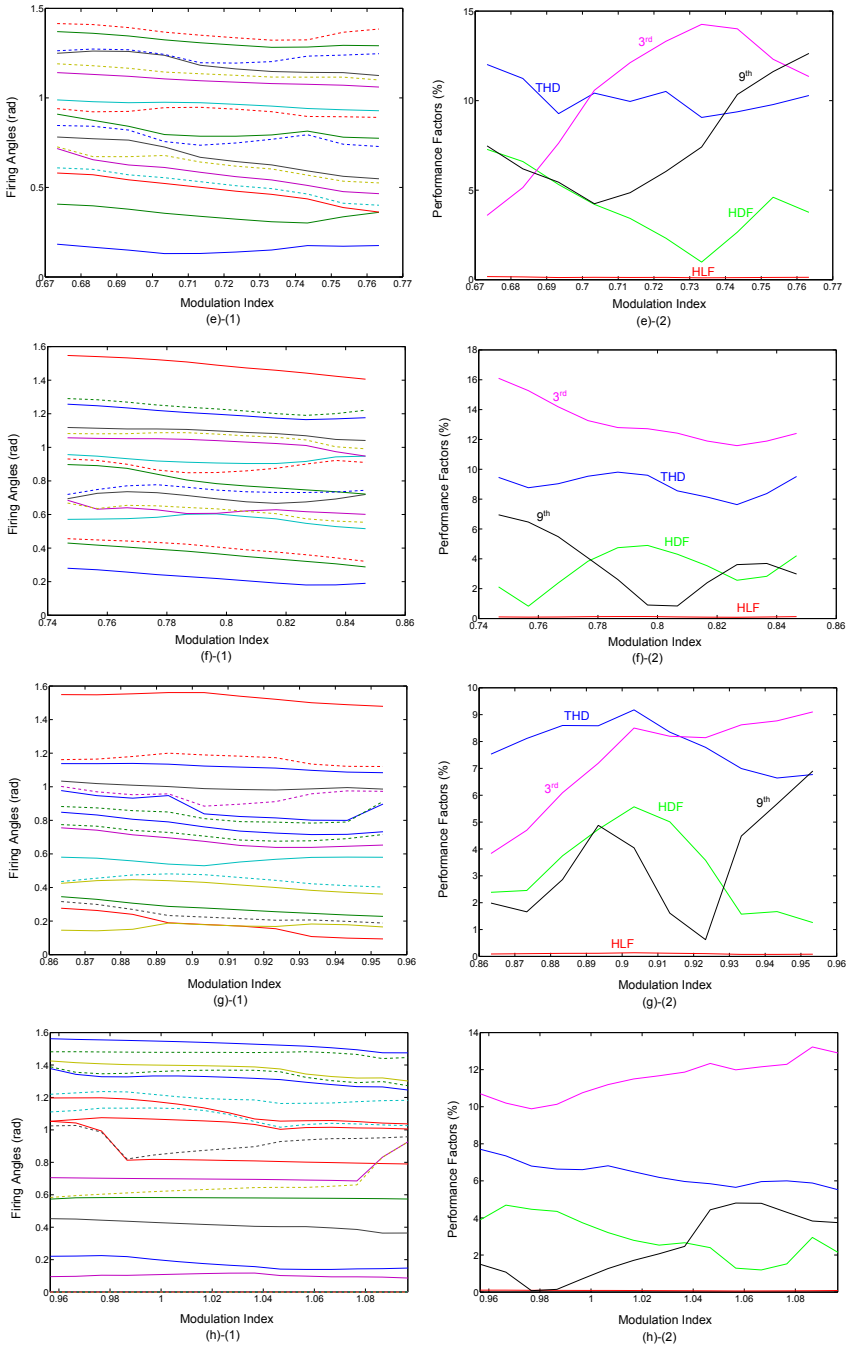

Figure 4.29: Continuous sets of intermediate solutions for 17 firing angles and QW symmetry (part 2).

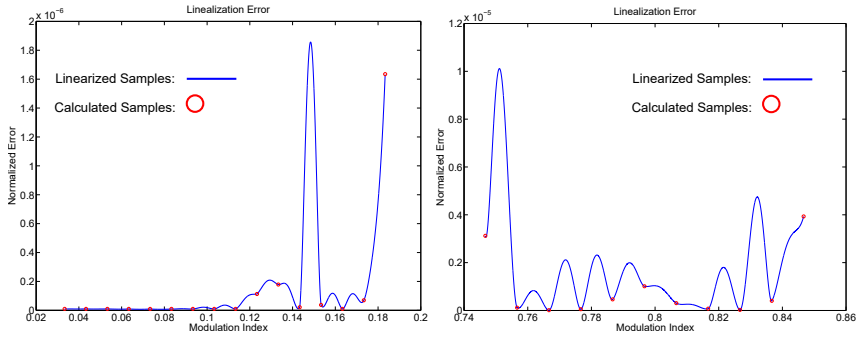

(a) Linearization error from the set of angles with $0.033 < m_a < 0.183$ (depicted at Fig. 4.28-(a)-(1)).

(b) Linearization error from the set of angles with $0.746 < m_a < 0.846$ (depicted at Fig. 4.29-(f)-(1)).

Figure 4.30. Linearization error.

Table 4.15: Solutions obtained with linearization (Firing angles and their corresponding step sign) from the set depicted at Fig. 4.28-(a)-(1)

m_a	θ_1	θ_2	θ_3	θ_4	θ_5	θ_6	θ_7	θ_8	θ_9	θ_{10}	θ_{11}	θ_{12}	θ_{13}	θ_{14}	θ_{15}	θ_{16}	θ_{17}
0.037	⇑0.2769	⇓0.3041	⇑0.3919	⇓0.4219	⇑0.6228	⇓0.6574	⇑0.7390	⇓0.7754	⇑0.8687	⇓0.8814	⇑0.9814	⇓0.9982	⇑1.0952	⇓1.1157	⇑1.2094	⇓1.2335	⇑1.5545
0.047	⇑0.2734	⇓0.3079	⇑0.3879	⇓0.4260	⇑0.6183	⇓0.6623	⇑0.7346	⇓0.7811	⇑0.8697	⇓0.8856	⇑0.9806	⇓1.0018	⇑1.0933	⇓1.1192	⇑1.2066	⇓1.2370	⇑1.5501
0.057	⇑0.2700	⇓0.3117	⇑0.3838	⇓0.4300	⇑0.6138	⇓0.6672	⇑0.7303	⇓0.7870	⇑0.8716	⇓0.8906	⇑0.9804	⇓1.0058	⇑1.0916	⇓1.1230	⇑1.2040	⇓1.2407	⇑1.5457
0.067	⇑0.2667	⇓0.3156	⇑0.3799	⇓0.4341	⇑0.6093	⇓0.6722	⇑0.7258	⇓0.7930	⇑0.8742	⇓0.8964	⇑0.9808	⇓1.0105	⇑1.0904	⇓1.1271	⇑1.2016	⇓1.2447	⇑1.5413
0.077	⇑0.2639	⇓0.3198	⇑0.3762	⇓0.4383	⇑0.6046	⇓0.6770	⇑0.7212	⇓0.7991	⇑0.8777	⇓0.9031	⇑0.9822	⇓1.0161	⇑1.0901	⇓1.1319	⇑1.1999	⇓1.2490	⇑1.5369
0.087	⇑0.2616	⇓0.3244	⇑0.3728	⇓0.4426	⇑0.5998	⇓0.6816	⇑0.7163	⇓0.8048	⇑0.8817	⇓0.9107	⇑0.9848	⇓1.0229	⇑1.0909	⇓1.1378	⇑1.1990	⇓1.2542	⇑1.5327
0.097	⇑0.2604	⇓0.3297	⇑0.3700	⇓0.4471	⇑0.5948	⇓0.6857	⇑0.7107	⇓0.8098	⇑0.8856	⇓0.9185	⇑0.9881	⇓1.0308	⇑1.0929	⇓1.1450	⇑1.1994	⇓1.2604	⇑1.5285
0.107	⇑0.2604	⇓0.3360	⇑0.3681	⇓0.4521	⇑0.5893	⇓0.6886	⇑0.7040	⇓0.8134	⇑0.8881	⇓0.9254	⇑0.9912	⇓1.0388	⇑1.0955	⇓1.1530	⇑1.2009	⇓1.2679	⇑1.5247
0.117	⇑0.2617	⇓0.3435	⇑0.3676	⇓0.4583	⇑0.5826	⇓0.6923	⇑0.6980	⇓0.8155	⇑0.8887	⇓0.9305	⇑0.9928	⇓1.0458	⇑1.0975	⇓1.1611	⇑1.2027	⇓1.2763	⇑1.5221
0.127	⇑0.2629	⇓0.3522	⇑0.3686	⇓0.4630	⇑0.5774	⇓0.6997	⇑0.6959	⇓0.8173	⇑0.8882	⇓0.9342	⇑0.9928	⇓1.0510	⇑1.0979	⇓1.1678	⇑1.2035	⇓1.2844	⇑1.5181
0.137	⇑0.2631	⇓0.3651	⇑0.3743	⇓0.4628	⇑0.5773	⇓0.7060	⇑0.6929	⇓0.8198	⇑0.8876	⇓0.9373	⇑0.9919	⇓1.0550	⇑1.0968	⇓1.1728	⇑1.2027	⇓1.2914	⇑1.5095
0.147	⇑0.2661	⇓0.3559	⇑0.3568	⇓0.4651	⇑0.5744	⇓0.7067	⇑0.6845	⇓0.8198	⇑0.8849	⇓0.9383	⇑0.9890	⇓1.0569	⇑1.0939	⇓1.1761	⇑1.2002	⇓1.3003	⇑1.5040
0.157	⇑0.2707	⇓0.3367	⇑0.3295	⇓0.4722	⇑0.5666	⇓0.7064	⇑0.6755	⇓0.8177	⇑0.8804	⇓0.9371	⇑0.9841	⇓1.0563	⇑1.0886	⇓1.1764	⇑1.1949	⇓1.3109	⇑1.5035
0.167	⇑0.2720	⇓0.3598	⇑0.3472	⇓0.4773	⇑0.5608	⇓0.7073	⇑0.6682	⇓0.8177	⇑0.8763	⇓0.9354	⇑0.9783	⇓1.0532	⇑1.0808	⇓1.1707	⇑1.1840	⇓1.3196	⇑1.5013
0.177	⇑0.2755	⇓0.3746	⇑0.3557	⇓0.4828	⇑0.5551	⇓0.7060	⇑0.6592	⇓0.8151	⇑0.8689	⇓0.9296	⇑0.9684	⇓1.0436	⇑1.0670	⇓1.1553	⇑1.1646	⇓1.3302	⇑1.5000

4.7.4 Linearization

As it has been commented, the sets of angles calculated will be stored in look-up tables to be applied on-line. On the other hand, with the aim of obtaining any m_a value, the linearization technique described at [182] can be applied with accuracy due to the continuity of every set of firing angles. As an example, regarding the sets of angles depicted at Figs. 4.28 and 4.29, the linearization errors provided by two of these sets of angles are depicted at Fig. 4.30. As it can be noticed, the error increases but it is acceptable because the undesired harmonics are still correctly eliminated, as it is shown at tables 4.16 and 4.18. These tables show the harmonic content obtained in intermediate values of those particular sets of angles. The corresponding firing angles are included at tables 4.15 and 4.17, respectively. Finally, the linearization error could be reduced further increasing the number of samples calculated with the local search described at section 4.5.

Table 4.16: Solutions obtained with linearization (Harmonic Amplitudes (% based on fundamental harmonic)) from the set depicted at Fig. 4.28-(a)-(1)

m_a	1^{st}	5^{th}	7^{th}	11^{th}	13^{th}	17^{th}	19^{th}	23^{th}	25^{th}	29^{th}	31^{th}	35^{th}	37^{th}	41^{th}	43^{th}	47^{th}	49^{th}
0.037	99.85	0.22	0.13	0.10	0.12	0.06	0.09	0.10	0.13	0.14	0.13	0.09	0.08	0.10	0.10	0.11	0.19
0.047	99.87	0.19	0.09	0.05	0.08	0.04	0.05	0.04	0.11	0.11	0.12	0.08	0.03	0.09	0.11	0.06	0.12
0.057	99.88	0.16	0.05	0.04	0.05	0.02	0.05	0.04	0.09	0.07	0.09	0.06	0.09	0.06	0.09	0.01	0.08
0.067	99.91	0.09	0.03	0.04	0.03	0.03	0.05	0.03	0.06	0.06	0.06	0.02	0.13	0.05	0.07	0.05	0.05
0.077	99.91	0.05	0.03	0.00	0.02	0.03	0.03	0.03	0.07	0.07	0.04	0.00	0.09	0.07	0.07	0.06	0.01
0.087	99.89	0.05	0.01	0.05	0.02	0.03	0.03	0.04	0.04	0.05	0.03	0.02	0.07	0.06	0.08	0.08	0.10
0.097	99.90	0.04	0.03	0.06	0.02	0.05	0.03	0.03	0.02	0.03	0.02	0.03	0.06	0.02	0.09	0.13	0.18
0.107	99.91	0.03	0.03	0.07	0.03	0.05	0.04	0.04	0.02	0.02	0.01	0.04	0.06	0.01	0.08	0.18	0.23
0.117	99.93	0.02	0.00	0.09	0.15	0.02	0.12	0.18	0.08	0.10	0.20	0.11	0.09	0.16	0.06	0.13	0.09
0.127	99.95	0.07	0.03	0.15	0.25	0.07	0.26	0.06	0.02	0.04	0.10	0.32	0.03	0.38	0.19	0.05	0.10
0.137	99.94	0.01	0.02	0.07	0.13	0.13	0.23	0.13	0.18	0.18	0.14	0.28	0.10	0.27	0.00	0.03	0.15
0.147	99.99	0.03	0.08	0.19	0.07	0.44	0.44	0.12	0.58	0.58	0.08	0.81	0.71	0.30	0.81	0.32	0.07
0.157	100.00	0.05	0.05	0.02	0.04	0.06	0.05	0.06	0.06	0.03	0.06	0.14	0.14	0.07	0.11	0.29	0.02
0.167	99.93	0.04	0.02	0.01	0.05	0.03	0.03	0.05	0.09	0.00	0.02	0.11	0.02	0.11	0.05	0.20	0.26
0.177	99.75	0.11	0.23	0.30	0.08	0.07	0.22	0.25	0.14	0.16	0.06	0.14	0.13	0.04	0.04	0.13	0.15

Table 4.17: Solutions obtained with linearization (Firing angles and their corresponding step sign) from the set depicted at 4.29-(f)-(1)

m_a	θ_1	θ_2	θ_3	θ_4	θ_5	θ_6	θ_7	θ_8	θ_9	θ_{10}	θ_{11}	θ_{12}	θ_{13}	θ_{14}	θ_{15}	θ_{16}	θ_{17}
0.751	⇑0.2761	⇑0.4250	⇓0.4530	⇑0.5717	⇑0.6635	⇓0.6551	⇑0.7068	⇓0.7313	⇑0.8948	⇓0.9273	⇑0.9531	⇑1.0555	⇓1.0816	⇑1.1165	⇑1.2533	⇓1.2877	⇑1.5446
0.761	⇑0.2653	⇑0.4129	⇓0.4460	⇑0.5738	⇑0.6350	⇓0.6432	⇑0.7301	⇓0.7577	⇑0.8845	⇓0.9129	⇑0.9415	⇑1.0526	⇓1.0809	⇑1.1121	⇑1.2427	⇓1.2779	⇑1.5375
0.771	⇑0.2510	⇑0.4010	⇓0.4386	⇑0.5786	⇑0.6352	⇓0.6533	⇑0.7335	⇓0.7735	⇑0.8608	⇓0.8855	⇑0.9270	⇑1.0515	⇓1.0837	⇑1.1095	⇑1.2289	⇓1.2626	⇑1.5286
0.781	⇑0.2373	⇑0.3887	⇓0.4294	⇑0.5906	⇑0.6190	⇓0.6477	⇑0.7234	⇓0.7714	⇑0.8262	⇓0.8585	⇑0.9159	⇑1.0498	⇓1.0872	⇑1.1083	⇑1.2148	⇓1.2470	⇑1.5168
0.791	⇑0.2256	⇑0.3754	⇓0.4166	⇑0.6021	⇑0.6063	⇓0.6387	⇑0.7054	⇓0.7557	⇑0.7969	⇓0.8492	⇑0.9096	⇑1.0446	⇓1.0840	⇑1.1032	⇑1.2034	⇓1.2352	⇑1.5011
0.801	⇑0.2134	⇑0.3597	⇓0.3998	⇑0.5971	⇑0.6129	⇓0.6276	⇑0.6864	⇓0.7414	⇑0.7782	⇓0.8539	⇑0.9055	⇑1.0366	⇓1.0747	⇑1.0943	⇑1.1930	⇓1.2237	⇑1.4831
0.811	⇑0.1999	⇑0.3441	⇓0.3843	⇑0.5821	⇑0.6243	⇓0.6131	⇑0.6720	⇓0.7338	⇑0.7651	⇓0.8660	⇑0.9036	⇑1.0279	⇓1.0650	⇑1.0860	⇑1.1814	⇓1.2098	⇑1.4674
0.821	⇑0.1871	⇑0.3297	⇓0.3700	⇑0.5634	⇑0.6237	⇓0.5928	⇑0.6698	⇓0.7313	⇑0.7536	⇓0.8853	⇑0.9086	⇑1.0181	⇓1.0537	⇑1.0767	⇑1.1703	⇓1.1967	⇑1.4525
0.831	⇑0.1804	⇑0.3151	⇓0.3531	⇑0.5397	⇑0.6137	⇓0.5691	⇑0.6819	⇓0.7322	⇑0.7423	⇓0.9089	⇑0.9269	⇑0.9963	⇓1.0278	⇑1.0602	⇑1.1669	⇓1.1947	⇑1.4349
0.841	⇑0.1844	⇑0.2989	⇓0.3336	⇑0.5231	⇑0.6058	⇓0.5579	⇑0.7031	⇓0.7381	⇑0.7301	⇓0.9172	⇑0.9449	⇑0.9636	⇓0.9986	⇑1.0447	⇑1.1724	⇓1.2089	⇑1.4165

Table 4.18: Solutions obtained with linearization (Harmonic Amplitudes (% based on fundamental harmonic)) from the set depicted at 4.29-(f)-(1)

m_a	1^{st}	5^{th}	7^{th}	11^{th}	13^{th}	17^{th}	19^{th}	23^{th}	25^{th}	29^{th}	31^{th}	35^{th}	37^{th}	41^{th}	43^{th}	47^{th}	49^{th}
0.751	100.12	0.07	0.01	0.13	0.17	0.13	0.26	0.13	0.05	0.23	0.19	0.17	0.24	0.27	0.26	0.47	0.03
0.761	100.01	0.00	0.01	0.01	0.01	0.01	0.00	0.03	0.01	0.01	0.02	0.05	0.05	0.11	0.01	0.04	0.18
0.771	99.99	0.02	0.00	0.01	0.00	0.04	0.03	0.03	0.01	0.02	0.13	0.15	0.11	0.13	0.09	0.08	0.19
0.781	99.98	0.04	0.01	0.02	0.03	0.06	0.05	0.07	0.06	0.04	0.18	0.17	0.06	0.04	0.10	0.00	0.21
0.791	99.98	0.01	0.06	0.06	0.09	0.16	0.04	0.02	0.04	0.01	0.03	0.01	0.18	0.08	0.16	0.04	0.07
0.801	100.00	0.01	0.08	0.07	0.09	0.13	0.01	0.03	0.02	0.00	0.02	0.02	0.08	0.00	0.02	0.08	0.11
0.811	99.99	0.00	0.03	0.03	0.02	0.05	0.00	0.00	0.03	0.04	0.02	0.01	0.01	0.01	0.02	0.03	0.07
0.821	99.98	0.02	0.00	0.02	0.02	0.02	0.02	0.02	0.11	0.13	0.05	0.05	0.02	0.13	0.09	0.17	0.10
0.831	99.98	0.00	0.01	0.03	0.04	0.05	0.03	0.06	0.03	0.13	0.12	0.03	0.18	0.09	0.21	0.15	0.29
0.841	99.92	0.00	0.10	0.07	0.02	0.05	0.03	0.08	0.04	0.10	0.18	0.05	0.12	0.20	0.06	0.01	0.05

4.8 Simulation Results

Simulations results have been obtained from a three phase MMC whose scheme is depicted at Fig. 2.5-(c) and reproduced here for convenience (see Fig. 4.31). The simulation parameters are included at table 4.19. Utilizing the firing angles calculated in section 4.7, QW waveforms and HW waveforms have been obtained from a MMC with 5 and 4 SMs per arm, respectively. In particular, 17 and 9 firing angles (included at tables 4.9 and 4.7, respectively) have been utilized to obtain the results with fundamental frequency $f = 50$ Hz and $f = 100$ Hz, respectively, besides $m_a = 0.9$. In this way, a (2N+1) SHE-PWM waveform with

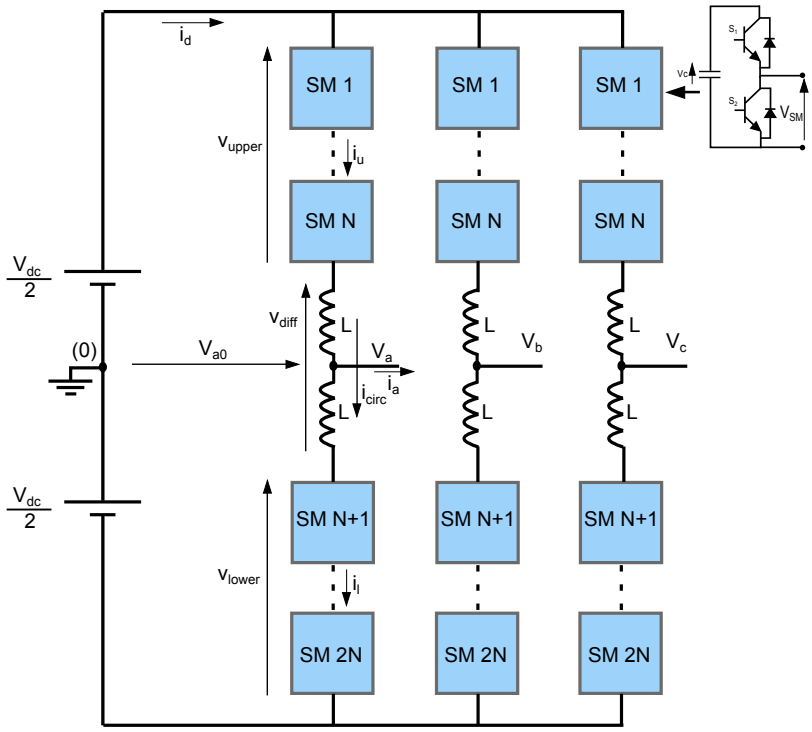

Figure 4.31. Three-phase MMC with HB SMs.

Table 4.19. Simulation Parameters

Parameter	Value		
SM capacitor, C	$4.6mF$		
SM capacitor voltage, V_C	$2250V$		
Arm inductor, L	$9mH$		
Load, R_L and L_L. Star configuration.	12Ω and $40mH$		
# of SMs per arm, N	4	5	
dc link Voltage, V_{dc}	$9000V$	$11250V$	
# of Angles (1^{st} HW/QW) (2N+1) SHE	12-HW	9-QW	17-QW
Fundamental frequency, f	$150Hz$	$100Hz$	$50Hz$
First non-eliminated harmonic	$2850Hz$	$2900Hz$	$2650Hz$
Modulation index, m_a	0.9		

QW symmetry has been obtained.

On the other hand, 12 firing angles with HW symmetry have been utilized with $f = 150$ Hz. The values of f have been selected to obtain a similar switching frequency at every case. This fact will be described deeply in chapter 5. In

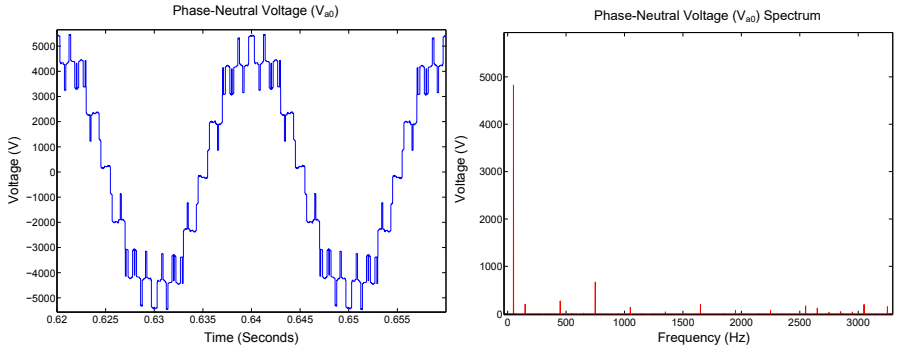

(a) Phase-neutral voltage (v_{a0}). (b) Phase-neutral voltage (v_{a0}) spectrum.

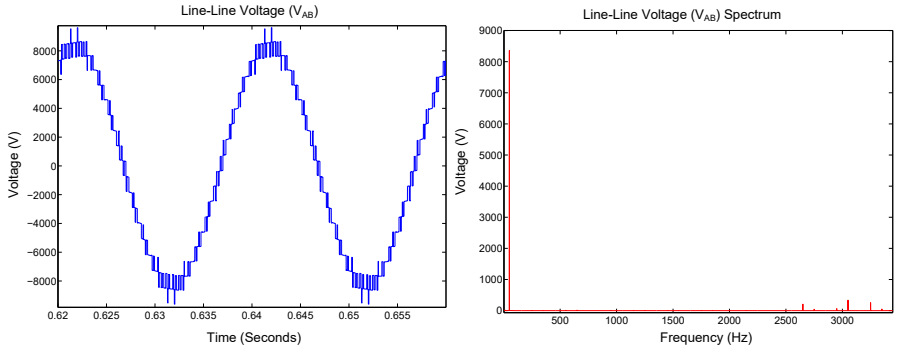

(c) Line-line voltage (V_{AB}). (d) Line-line voltage (V_{AB}) spectrum.

Figure 4.32: Simulation results with 17 firing angles in the first QW and fundamental frequency equal to 50 Hz.

addition, the increase in f implies a decrement in the phase output voltage due to the increase in the voltage drop of the arm inductance, as it can be noticed at Figs. 4.32-(a), 4.33-(a) and 4.34-(a).

Fig. 4.32-(a) shows the phase-neutral voltage (v_{a0}) in case of 17 firing angles and $f = 50$ Hz. The simulation corresponds with the firing angles included at table 4.9 for $m_a = 0.9$. The v_{a0} spectrum depicted at Fig. 4.32-(b) shows the correct elimination of non-desired harmonics up to 2650 Hz, except for the triplen harmonics. These triplen harmonics are eliminated in the line-line voltage (v_{AB}), depicted at Fig. 4.32-(c), as it can be noticed at Fig. 4.32-(d) which shows the v_{AB} spectrum.

On the other hand, in case of 9 firing angles, a fundamental frequency equal

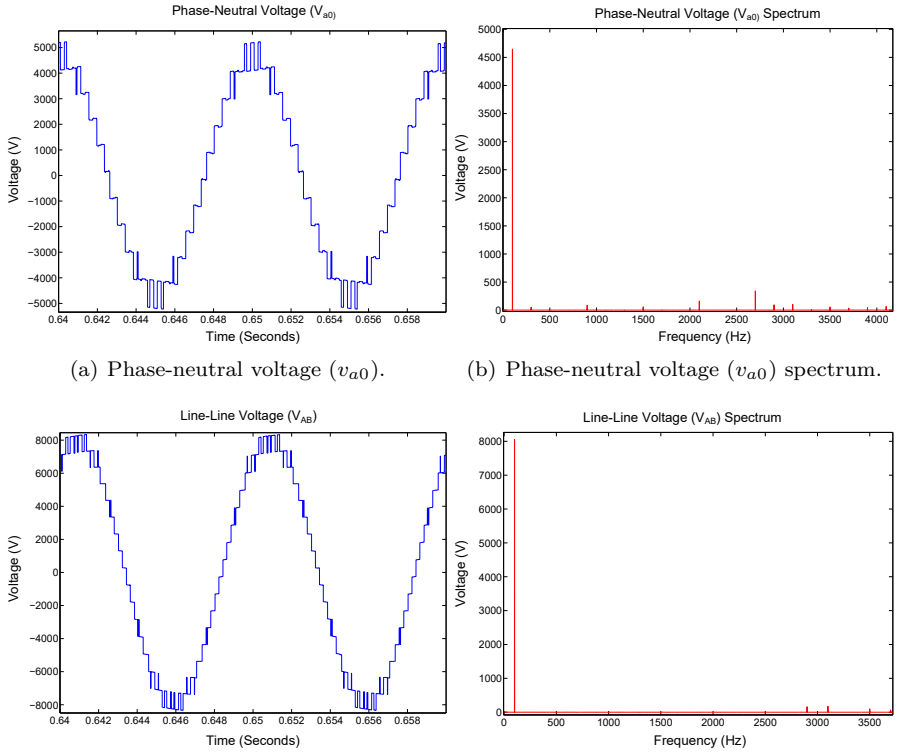

(a) Phase-neutral voltage (v_{a0}).

(b) Phase-neutral voltage (v_{a0}) spectrum.

(c) Line-line voltage (V_{AB}).

(d) Line-line voltage (V_{AB}) spectrum.

Figure 4.33: Simulation results with 9 firing angles in the first QW and fundamental frequency equal to 100 Hz.

to 100 Hz has been utilized. In this way, Fig. 4.33-(a) shows the v_{a0} when $m_a = 0.9$. The simulation corresponds with the firing angles included at table 4.7. Furthermore, the v_{a0} spectrum, which is included at Fig. 4.33-(b), shows the correct elimination of the undesired harmonics up to 2900 Hz, except for the triplen harmonics. However, these harmonics are eliminated in v_{AB}, which is depicted at Fig. 4.33-(c), as it is shown in its corresponding spectrum depicted at Fig. 4.33-(d).

Finally, in case of HW symmetry, 12 firing angles in the first HW (obtained from table 4.5) have been used with $f = 150$ Hz and $m_a = 0.9$. Firstly, v_{a0} can be seen at Fig. 4.34-(a), where its corresponding spectrum, depicted at Fig. 4.34-(b), shows a correct elimination of the undesired harmonics up to 2850 Hz, except

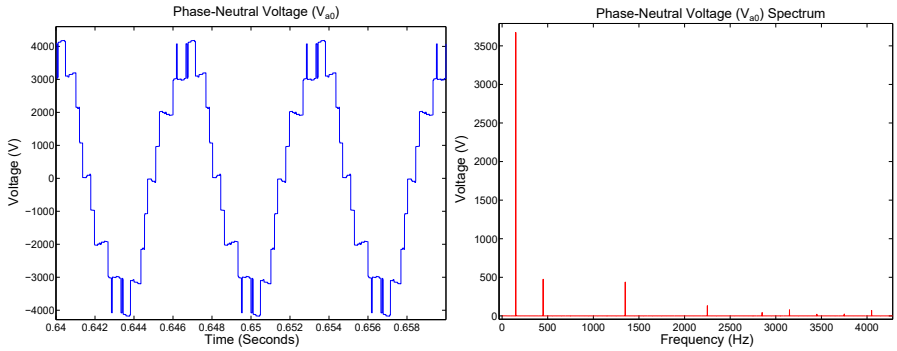

(a) Phase-neutral voltage (v_{a0}).

(b) Phase-neutral voltage (v_{a0}) spectrum.

(c) Line-line voltage (V_{AB}).

(d) Line-line voltage (V_{AB}) spectrum.

Figure 4.34: Simulation results with 12 firing angles in the first HW and fundamental frequency equal to 150 Hz.

for the triplen harmonics, cancelled in the line-line voltage. Figs. 4.34-(c) and 4.34-(d) show the line-line voltage v_{AB} and its spectrum, respectively.

4.9 Experimental Results

Experimental results have been obtained from a prototype of a single-phase MMC, whose details are included at table 4.20, to validate the proposed formulation that solves the SHE-PWM problem. In particular, this MMC, which is deeply described in chapter 5, contains 5 SMs per arm and is controlled utilizing the DSPACE 1103 board [185]. 2N+1 SHE-PWM waveforms with QW symmetry

Table 4.20. Specifications for the Experimental Setup

Parameter	Value	
# of SMs per arm, N	5	
dc link Voltage, V_{dc}	$250V$	
SM capacitor, C	$3.6mF$	
SM capacitor voltage, V_C	$50V$	
Arm inductor, L	$3.6mH$	
Load, R_L and L_L	22Ω and $10mH$	
# of Angles, per QW, for (2N+1) SHE	17	9
Fundamental frequency, f	$50Hz$	$100Hz$
First non-eliminated (non-triple) harmonic	$2650Hz$	$2900Hz$
Modulation index, m_a	0.9	

have been obtained with 9 and 17 firing angles in the first QW.

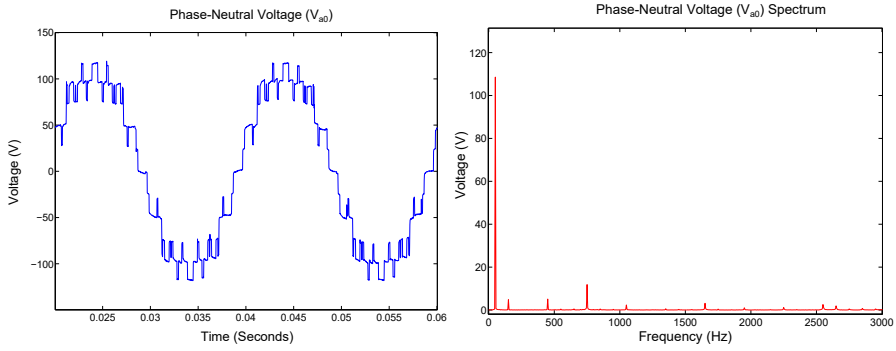

(a) Phase-neutral voltage (v_{a0}). (b) Phase-neutral voltage (v_{a0}) spectrum.

Figure 4.35: Experimental results with 17 firing angles in the first QW and $f = 50$ Hz.

Fig. 4.35-(a) shows the v_{a0} when 17 firing angles are utilized in the first QW. This waveform and its corresponding spectrum, which is depicted at Fig. 4.35-(b), corroborate the simulation results depicted at Figs. 4.32-(a) and 4.32-(b), respectively. As it can be noticed, the first non eliminated (non-triple) harmonic is located at 2650 Hz, as it also happens in the simulation results.

Fig. 4.36-(a) shows the v_{a0} when 9 firing angles are utilized in the first QW. This waveform and its corresponding spectrum, which is depicted at Fig. 4.36-(b), corroborate the simulation results depicted at Figs. 4.33-(a) and 4.33-(b), respectively. As it can be noticed, the first non eliminated (non-triple) harmonic is located at 2900 Hz, as it also happens in the simulation results.

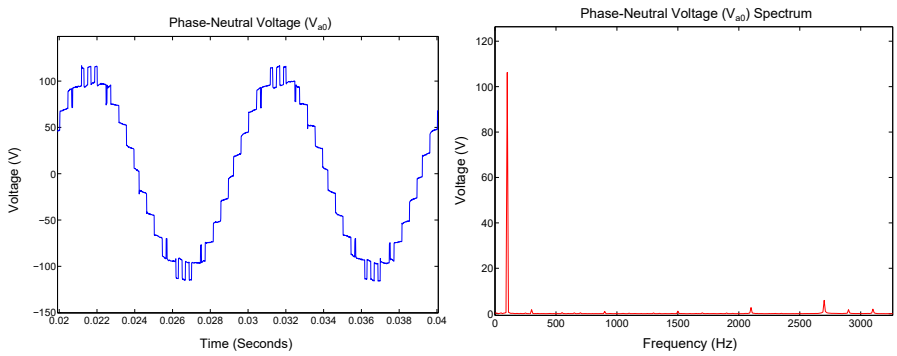

(a) Phase-neutral voltage (v_{a0}). (b) Phase-neutral voltage (v_{a0}) spectrum.

Figure 4.36: Experimental results with 9 firing angles in the first QW and $f = 100$ Hz.

4.10 Conclusion

Two novel formulations to solve the SHE-PWM problem with QW and HW symmetries, respectively, have been presented. These methods are able to calculate simultaneously the switching patterns and the associated firing angles throughout the m_a range, without using predefined waveforms. The mathematical problem has been addressed defining a unique equation system which is valid for any possible waveform. The search algorithm, which is based on genetic algorithms, utilizes a novel objective function which disregards invalid solutions. In addition, the proposed search method is able to find several solutions for the same m_a value. Finally, a local search has been designed, which is able to obtain continuous sets of solutions throughout the m_a range.

Examples of solutions for different numbers of firing angles and converter levels have been obtained throughout the m_a range. In addition, different solutions and waveforms have been obtained for every m_a value and a design process, based on the performance factors of every solution, has been proposed. On the other hand, in case of HW symmetry, it has been demonstrated that the modification of the fundamental phase does not provide different solutions.

Finally, simulation and experimental results validate the waveforms provided by the proposed formulations. In particular, the experimental results have been obtained from a prototype of single-phase MMC.

As a conclusion, the proposed formulations simplify significantly the search pro-

cess with respect to previous works and are able to provide new waveforms which are not predefined beforehand. In this way, the application of SHE-PWM in multilevel converters is simplified and a high number of harmonics can be controlled simultaneously.

Chapter 5

Novel Circulating Current Control Methods for MMC with SHE-PWM

5.1 Introduction

As it has been highlighted at chapter 2, one of the main challenges to be met when SHE-PWM is utilized to operate the MMC is controlling the circulating current, i_{circ}, without disturbing the phase output voltage, v_{a0}. The i_{circ} control is required to reduce the SM capacitor voltage ripple and the MMC losses [82].

This chapter proposes two different i_{circ} controls which can be applied with (N+1) SHE-PWM and (2N+1) SHE-PWM [97, 179], respectively. They adjust the DC component of i_{circ} and the energy stored in the SMs to their references, besides maintaining the energy balance between the upper and lower arms. In this way, it is possible to achieve a low SM capacitor voltage ripple and simultaneously to get benefit from the low switching losses and low THD provided by (N+1) SHE-PWM and (2N+1) SHE-PWM. Both controls have been developed utilizing the three-phase MMC depicted at Fig. 2.5-(c), whose v_{a0} and v_{diff} are given by (2.2) and (2.3), respectively.

The first one is applied with (N+1) SHE-PWM. It employs different m_a values at the upper and lower arms but unlike previous methods, the utilized m_{a-up} and m_{a-low} values are constant over the fundamental period, except for the possibility

of interchanging both values. Therefore, the sign of v_{diff} can be modified without disturbing the lower-order harmonics of v_{a0}. The i_{circ} reference will be followed, determining the sign of v_{diff} according to the relationship between the i_{circ} real and reference values.

The other technique takes the i_{circ} control introduced in [111] for (2N+1) PWM modulations, which utilizes high switching frequency and complements it with a method to limit the i_{circ} ripple. This limitation is required in case of (2N+1) SHE-PWM because of its low switching frequency and the uneven distance between adjacent firing angles.

5.2 Circulating Current Reference Definition

For both proposed control techniques, the circulating current reference has been obtained according to the algorithm described in Section 2.4.1 [82]. In this way, the i_{circ} contains a dc component which ensures the dc and ac side powers balance. Furthermore, the phase energy is adjusted to its reference and the phase arm energies are completely balanced.

5.3 Proposed Circulating Current Control with (N+1) SHE-PWM

5.3.1 Circulating Current Control Principle

The proposed i_{circ} control is able to follow the i_{circ} reference without disturbing the phase output voltage, v_{a0}, when (N+1) SHE-PWM, whose switching scheme is depicted at Fig. 3.5 and reproduced here for convenience (see Fig. 5.1), is utilized. The proposed technique is based on utilizing different m_a values at every arm to follow the i_{circ} reference, but unlike previous methods, these two values, m_{a-up} and m_{a-low}, will be maintained constant over the fundamental period, except for the option of interchanging both values. In this way, it is possible to vary the sign of v_{diff} without disturbing the lower-order harmonics of v_{a0}.

In case of utilizing different m_a values at the upper and lower arms, the switching instants are not simultaneous at both arms, as it is depicted at Fig. 5.2. In this way, the Fourier series development of v_{a0}, when (N+1) SHE-PWM with QW symmetry is utilized, is given by (5.1), (5.2), (5.3), (5.4), (5.5) and (5.6), where

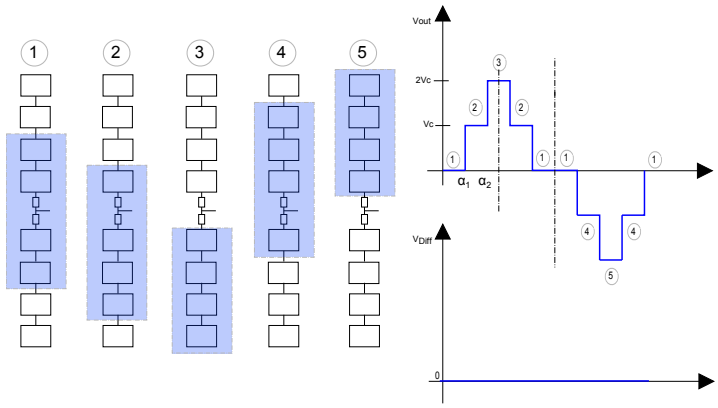

Figure 5.1. Switching scheme of (N+1) SHE-PWM modulation, for $N = 4$.

V_{dc} is the dc bus voltage, N is the number of SMs at every arm, θ_{k-up} is the identifier of every firing angle in the upper arm, θ_{k-low} is the identifier of every firing angle in the lower arm, l is the total number of firing angles in the first QW and n is the identifier of every harmonic. Furthermore, the upper and lower reference values, m_{a-up} and m_{a-low}, fulfil (5.7) and (5.8).

$$v_{a0} = \sum_{n=1,3,5,7,\ldots}^{\infty} b_n sin(n\omega t), \tag{5.1}$$

$$b_n = \frac{2V_c}{n\pi} \sum_{k=1}^{l} f_{k-up} cos(n\theta_{k-up}) + f_{k-low} cos(n\theta_{k-low}), \tag{5.2}$$

$$V_c = \frac{V_{dc}}{N}, \tag{5.3}$$

$$0 \leq \theta_1 < \theta_2 < \ldots < \theta_l \leq \frac{\pi}{2}, \tag{5.4}$$

$$f_{k-up} = \left\{ \begin{array}{c} 1 \ \forall \ positive \ \ step, \\ -1 \ \forall \ \ negative \ \ step, \end{array} \right\}, \tag{5.5}$$

$$f_{k-low} = \left\{ \begin{array}{c} 1 \ \forall \ positive \ \ step, \\ -1 \ \forall \ \ negative \ \ step, \end{array} \right\}, \tag{5.6}$$

$$m_a = \frac{m_{a-up} + m_{a-low}}{2} \tag{5.7}$$

$$0 \leq m_a \leq 1.15, \tag{5.8}$$

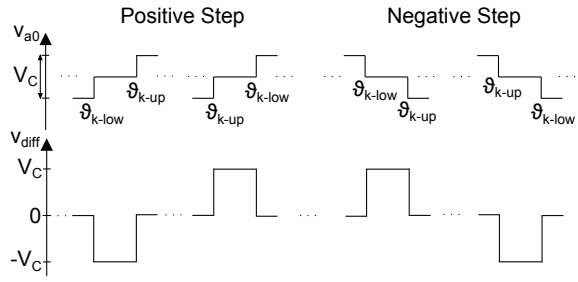

Figure 5.2: Relationship between v_{diff} and v_{a0} according to the order of the upper and lower firing angles.

Eq. (5.2) provides the value of every harmonic. Therefore, the equation system which must be solved to control the fundamental and lower-order harmonics, is given by (5.9). In this way, the obtained sets of angles θ_{k-up} and θ_{k-low} must be executed completely over the fundamental period to avoid disturbing the fundamental and the lower-order harmonics of v_{a0}. However, in case of applying previous i_{circ} control techniques with SHE-PWM, m_{a-up} and m_{a-low} will be varied at every switching instant, utilizing different values of θ_{k-up} and θ_{k-low}, with the aim of following the i_{circ} reference and therefore, v_{a0} will be disturbed [5, 82, 85, 87, 93, 96, 103–106, 144–146]. Furthermore, the i_{circ} control technique proposed by [107] for (N+1) SHE-PWM, which utilizes $m_{a-up} = m_{a-low}$ but introduces opposite variations in θ_{k-up} and θ_{k-low}, through PI controls, could insert disturbances at v_{a0} in case the variations in the firing angles are significant [110].

$$\begin{aligned}
&\tfrac{2}{\pi(L-1)}(f_{1-up}\cos(\theta_{1-up}) + f_{1-low}\cos(\theta_{1-low}) + ... \\
&+f_{l-up}\cos(\theta_{l-up}) + f_{l-low}\cos(\theta_{l-low})) - \tfrac{m_{a-up}+m_{a-low}}{4} = 0, \\
&\tfrac{2}{5\pi(L-1)}(f_{1-up}\cos(5\theta_{1-up}) + f_{1-low}\cos(5\theta_{1-low}) + ... \\
&+f_{l-up}\cos(5\theta_{l-up}) + f_{l-low}\cos(5\theta_{l-low})) = 0, \\
&\vdots \\
&\tfrac{2}{n\pi(L-1)}(f_{1-up}\cos(n\theta_{1-up}) + f_{1-low}\cos(n\theta_{1-low}) + ... \\
&+f_{l-up}\cos(n\theta_{l-up}) + f_{l-low}\cos(n\theta_{l-low})) = 0,
\end{aligned} \tag{5.9}$$

The proposed i_{circ} is also based on utilizing different m_a values at every arm, but unlike previous methods, these two values, m_{a-up} and m_{a-low}, will be maintained constant over the fundamental period and therefore, the lower-order harmonics

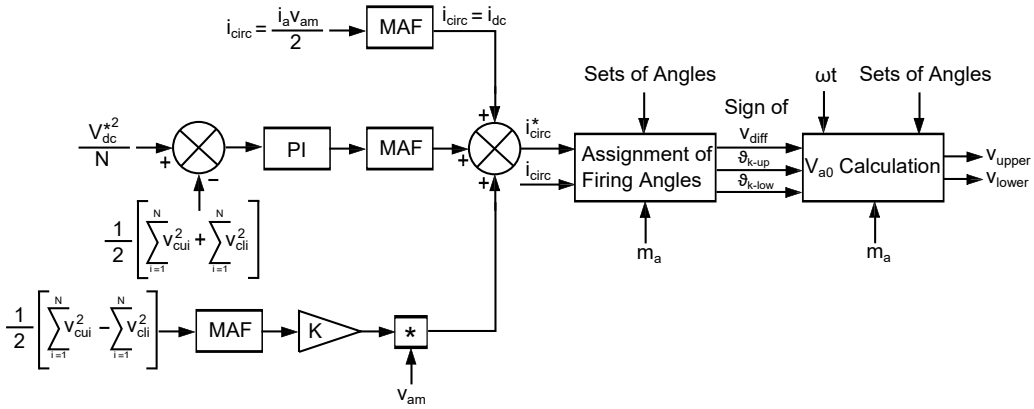

(a) Circulating current control for (N+1) SHE-PWM.

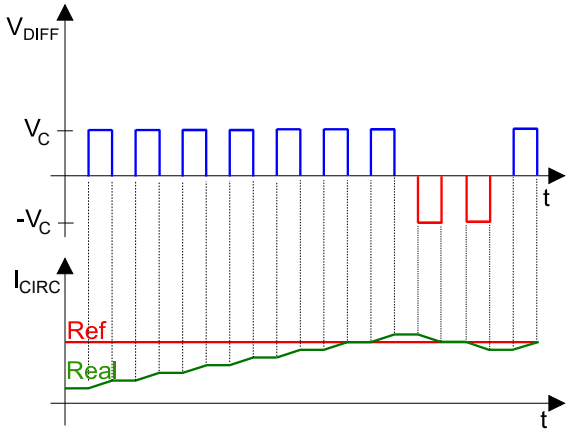

(b) Criteria to define the sign of v_{diff}.

Figure 5.3. Circulating current control for (N+1) SHE-PWM.

of v_{a0} will not be disturbed. As it can be noticed at Fig. 5.2, the firing angles θ_{k-up} and θ_{k-low} could insert a positive or a negative v_{diff}, depending on the sign of their corresponding step and the order of both firing angles. Furthermore, in case m_{a-up} and m_{a-low} utilize the same switching pattern ($f_{k-up} = f_{k-low}$), both modulation indexes could be interchanged, applying θ_{k-up} in the lower arm and θ_{k-low} in the upper arm, without disturbing v_{a0}, as it can be noticed at (5.9), changing the sign of v_{diff}. Therefore, for every pair of θ_{k-up} and θ_{k-low}, it is possible to determine the sign of v_{diff} without disturbing v_{a0}, providing a degree

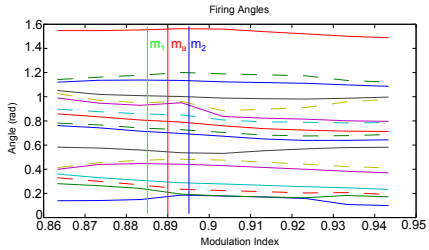

Figure 5.4: Definition of modulation indexes for i_{circ} control over a particular set of angles. The set of 17 firing angles has been calculated for a MMC with 10 SMs at every arm.

of freedom to follow the i_{circ} reference. Furthermore, if m_{a-up} and m_{a-low} are close between each other, the i_{circ} ripple will be low.

The proposed control and the criteria to select the sign of v_{diff} are depicted at Fig. 5.3-(a) and Fig. 5.3-(b), respectively.

5.3.2 Assignment of Firing Angles

The proposed i_{circ} control utilizes two different modulation index values, m_1 and m_2, which will be assigned to m_{a-up} and m_{a-low}, respectively or to the contrary, depending on the v_{diff} requirements. Furthermore, continuous sets of angles over the fundamental period are needed due to the requirement of utilizing the same switching pattern for m_{a-up}, m_{a-low} and m_a. Fig. 5.4 shows the definition of m_1 and m_2 according to m_a. On the other hand, m_1 and m_2 will be closed to m_a with the aim of obtaining a low i_{circ} ripple, whose value is given by (5.10), where L is the arm inductance and f is the fundamental frequency.

$$|\Delta i_{circ}| = \frac{V_c}{4L\pi f}|\theta_{k-up} - \theta_{k-low}|, \tag{5.10}$$

The modulation index assignment for every arm will be made before every switching instant with the aim of following i_{circ} accurately. In this way, the next pair of firing angles $\theta_{k,1}$ and $\theta_{k,2}$ will be assigned to θ_{k-up} and θ_{k-low}, respectively or to the contrary, depending on the required sign of v_{diff}. Fig. 5.5 shows the flow diagram which determines this assignment, which depends on v_{diff}, the sign of the step, f_k and the order of $\theta_{k,1}$ and $\theta_{k,2}$.

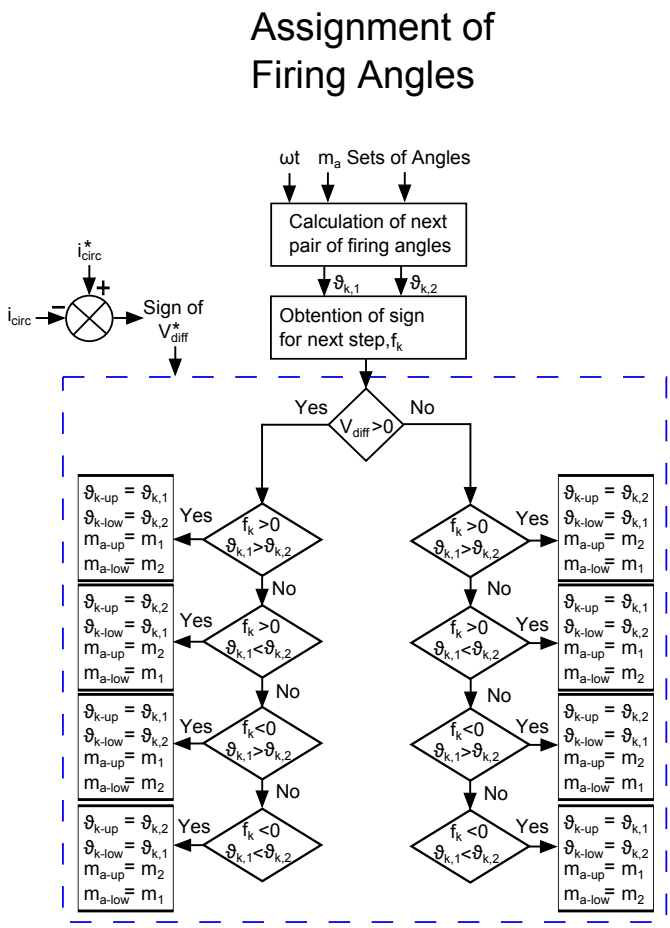

Figure 5.5: Assignment of the next firing angles to the upper and lower arms, depending on the sign of v_{diff}.

5.3.2.1 Management of Close Firing Angles

When two firing angles are very close between each other, $\theta_{k,1}$ or $\theta_{k,2}$ could be fired later than $\theta_{k+1,1}$ or $\theta_{k+1,2}$, as it can be noticed at Figs. 5.6 and 5.7. This fact will be correctly addressed because every pair of firing angles will be managed separately and they will be fired according to the required v_{diff} at the firing instant. Fig. 5.8 shows different cases where there are two consecutive firing angles which are very close or identical between each other. As it has been

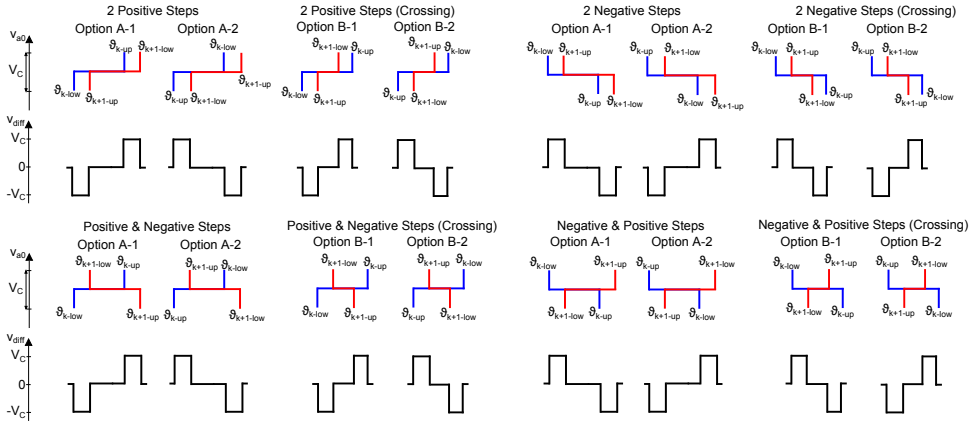

Figure 5.6: Switching schemes when there are two firing angles very close between each other and the required v_{diff} sign is opposite.

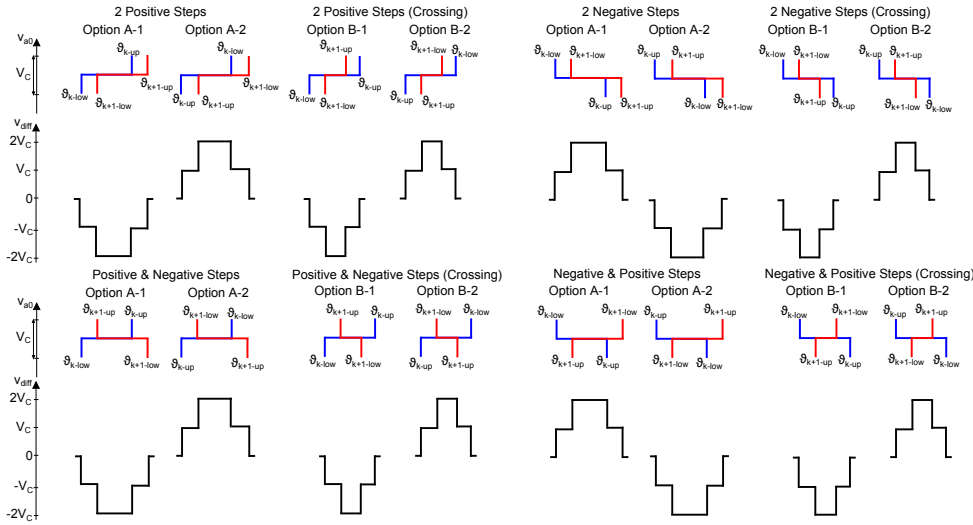

Figure 5.7: Switching schemes when there are two firing angles very close between each other and the required v_{diff} sign is the same. These schemes would provide $v_{diff} = \pm 2V_c$.

commented, all of these cases will be correctly managed, because every pair of $\theta_{k,1}$ and $\theta_{k,2}$ will be managed independently.

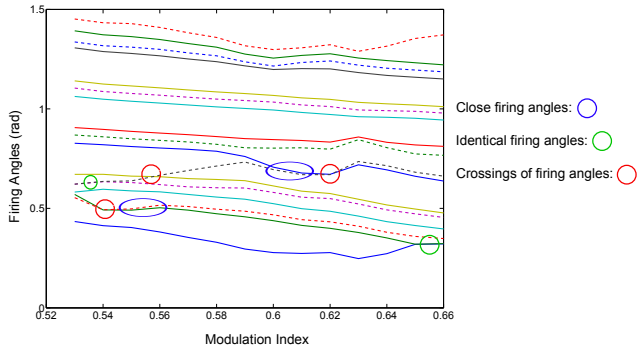

Figure 5.8: Set of firing angles where crossings, close angles and identical angles can be noticed.

However, in case the resulting assignment for a pair of $\theta_{k,1}$ and $\theta_{k,2}$ make v_{upper} or v_{lower} exceed their maximum/minimum limits given by the number of SMs, the final assignment will be the opposite one. In this way, that pair of firing angles will not provide a correct v_{diff}, but the rest of firing angles will allow the control to follow the i_{circ} reference. This issue will be shown at the simulation results.

On the other hand, the exceptional case where $\theta_{k,1}$, $\theta_{k+1,1}$ and $\theta_{k+2,1}$ (or even more firing angles) could be fired before $\theta_{k,2}$ is also considered. In this case, besides regarding the criteria given by Fig. 5.5 and the constraint of not overtaking the maximum/minimum v_{upper} and v_{lower} at every $\theta_{m,1}$, a new constraint must be considered. In this case, if a firing angle $\theta_{m,1}$ precede $\theta_{n,2}$, the assignment of $\theta_{m,1}$ must also regard that $\theta_{n,2}$ does not exceed the maximum/minimum phase voltage limits. Examples of these cases are included at Fig. 5.9. However, due to the proximity between m_1 and m_2, these cases are very uncommon. Cases where the firing angles are close in pairs are much more common, as it is also included in Fig. 5.9.

In addition, as it is shown at Fig. 5.7, close firing angles could provide sates where $v_{diff} = \pm 2V_c$ in case the sign of the required v_{diff} is the same at both firing instants (k and k+1). However, the i_{circ} ripple will not be excessive because of the proximity between m_1 and m_2. On the other hand, in case the required sign of v_{diff} is opposite at both firing instants, the switching schemes of Fig. 5.6 will be given.

Finally, crossings between firing angles over the m_a range can also be noticed at Fig. 5.8. These cases are particular ones of close firing angles and they will be processed in the same way.

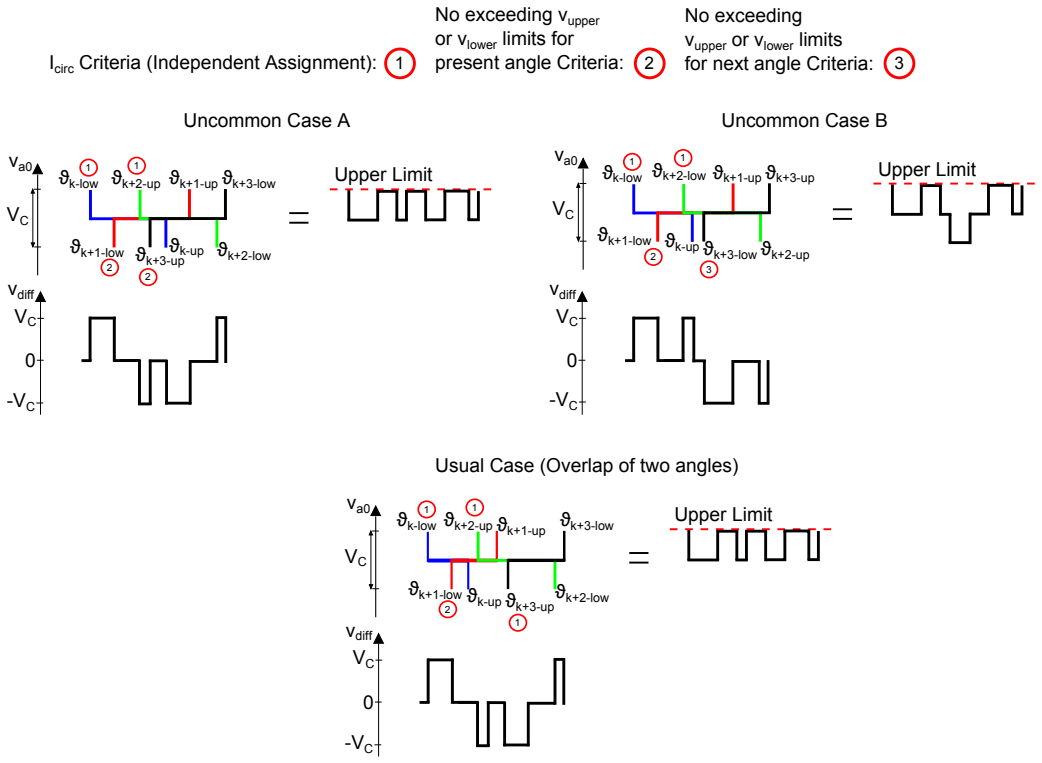

Figure 5.9: Two different uncommon cases where four and three firing angles of m_1, respectively, are fired before the first of m_2. A common case is also presented, where at every instant there is only overlap of two firing angles.

5.3.3 Generation of Upper and Lower Arm Voltages

Fig. 5.10 shows how to combine the SHE-PWM implementation method described in chapter 4 and the (N+1) SHE-PWM circulating current controller described in this section. As Fig. 5.10 discloses, the implementation method calculates the firing angles to generate v_{a0} off-line, regardless the circulating current reference. These firing angles are stored in look-up tables which are utilized by the i_{circ} controller. In this way, according to the desired m_a and phase values, the i_{circ} controller calculates the required v_{upper} and v_{lower}, as it is detailed at Fig. 5.3.

Finally, the balancing algorithm selected in chapter 2 (described in section 2.4.6) is applied. As it has been commented, it operates solely in case there is a change

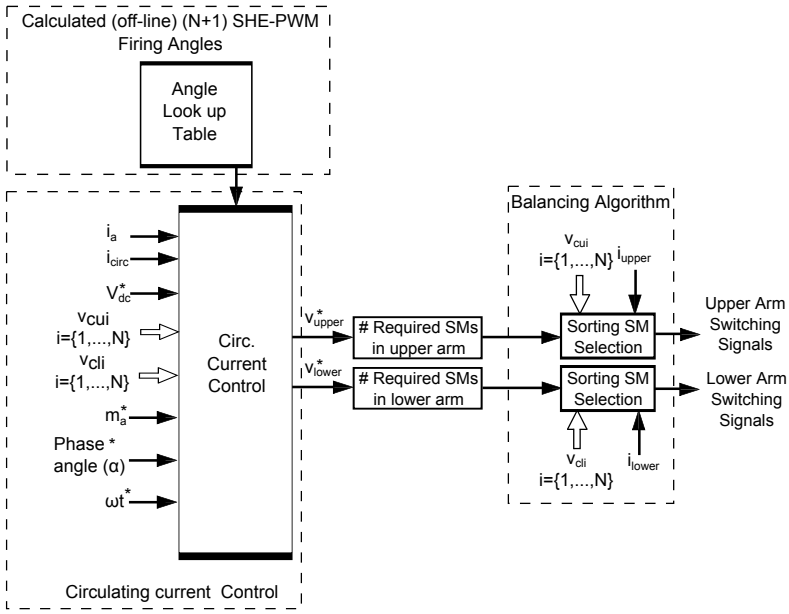

Figure 5.10. Generation of upper and lower arm voltages at every phase.

in the phase output voltage [11, 12, 142]. In this way, the switching losses are not increased due to the balancing algorithm.

5.3.4 Balancing Technique in case of Low Effective Switching Frequency

In case of very low effective switching frequency, $f_{sw-effective}$, approximately when $f_{sw-effective} \leq 2f$, being f the fundamental frequency, the utilized balancing algorithm could not operate correctly for particular current phases. This issue happens when the firing angles are not uniformly distributed over the fundamental period. In this way, for instance, a SM capacitor with the lowest voltage could be inserted when the arm current is positive. However, due to the low number of firing angles, the arm current sign changes before that SM could be short-circuited. In this way, instead of being charged, that capacitor could be discharged.

This issue may be addressed introducing extra-switchings where the balancing algorithm may operate without modifying the phase output voltage. In this

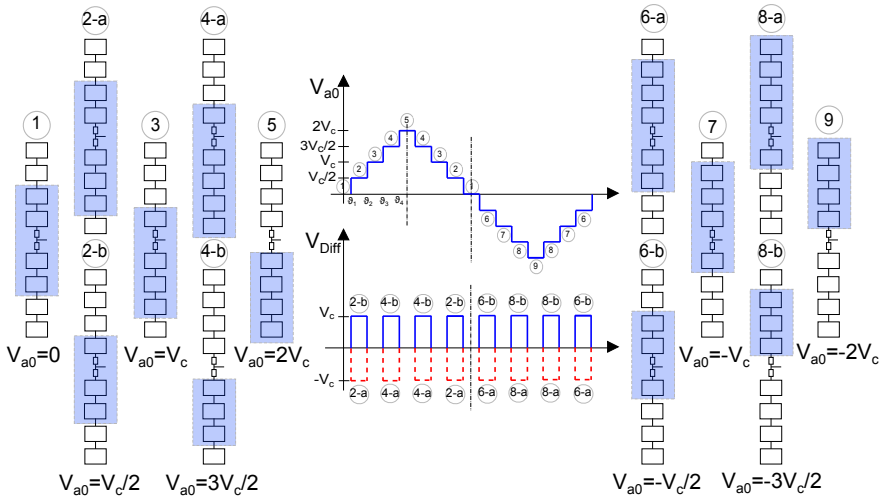

Figure 5.11: Switching scheme of (2N+1) SHE-PWM. v_{diff} **and** v_{a0} **are depicted for every switching state.**

way, uniformly distributed balancing instants are executed over the fundamental phase. In particular, the balancing instants will be 0, $\pi/4$, $\pi/2$, $3\pi/4$, π, $5\pi/4$, $3\pi/2$ and $7\pi/4$. With the aim of avoiding an excessive increase in the switching losses, the maximum number of SMs that can be interchanged inside every arm at every balancing instant is restricted to 2.

5.4 Proposed Circulating Current Control with (2N+1) SHE-PWM

5.4.1 Circulating Current Control Principle

The proposed i_{circ} control technique is based on the concept of redundant switching states provided by (2N+1) SHE-PWM. Fig. 5.11 illustrates this concept [11, 12] when N is even. When the output voltage v_{a0} is an integer multiple of V_c (where V_c is the SM capacitor average voltage), for instance $v_{a0} = rV_c$, there is only one switching state that generates this voltage level. However, when $v_{a0} = (r/2)V_c$, there are two redundant switching states able to generate the voltage level (states (2-a)-(2-b), (4-a)-(4-b), (6-a)-(6-b) and (8-a)-(8-b) in Fig. 5.11). One redundant switching state is characterized by having $N + 1$ SMs inserted

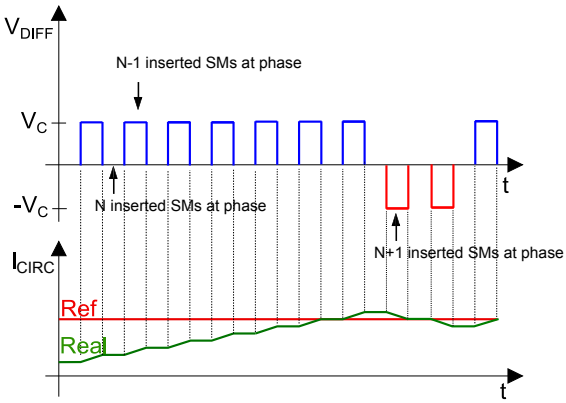

(a) Selection of differential voltage sign and its associated circulating current.

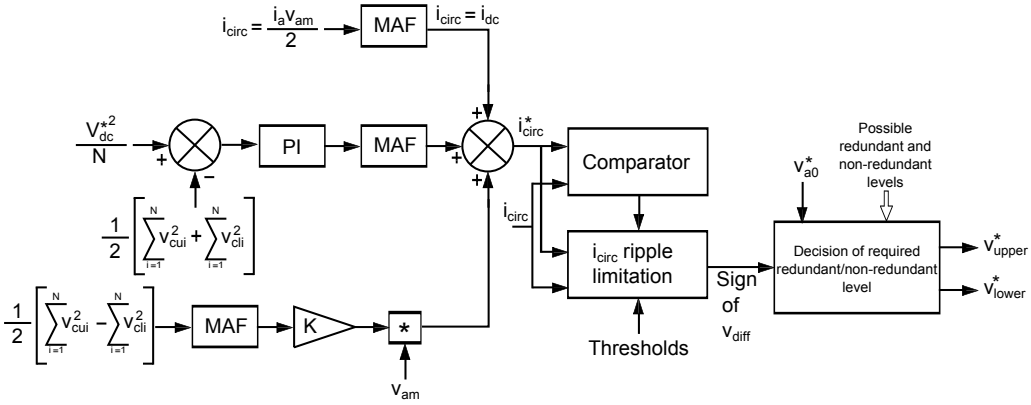

(b) Closed-loop circulating current control for (2N+1) SHE-PWM.

Figure 5.12. Circulating current control for (2N+1) SHE-PWM.

in the whole phase, while the other one contains $N-1$ inserted SMs. Redundant switching states generate the same output voltage, but different values of the differential voltage, v_{diff}, applied to the embedded phase inductances. In particular, redundant switching states with $N+1$ inserted SMs (denoted as $x-a$ with $x = 2, 4, 6, 8$ in Fig. 5.11) generate $v_{diff} = -V_c$ and consequently, make i_{circ} decrease (see Fig. 5.12-(a) for definition of the signs of v_{diff} and i_{circ}). Alternatively, states with $N-1$ inserted SMs (denoted as $x-b$ with $x = 2, 4, 6, 8$ in Fig. 5.11) generate $v_{diff} = V_c$ and make i_{circ} increase. On the other hand, in

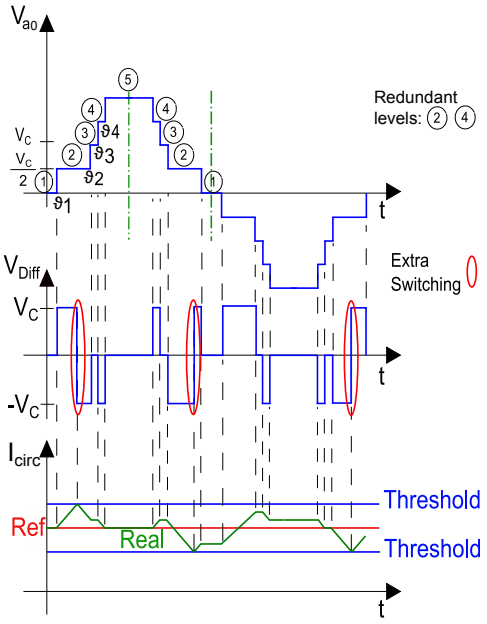

Figure 5.13. Limitation of circulating current ripple.

case N is odd, the redundant and non-redundant voltage levels will be given by $v_{a0} = rV_c$ and $v_{a0} = (r/2)V_c$, respectively.

In this way, making use of the appropriate redundant switching state it is feasible to control i_{circ} and make it follow a reference. Therefore, based on the required v_{a0}, the i_{circ} controller determines the required redundant/non-redundant state and provides the required upper and lower arm voltages. This concept is illustrated in Fig. 5.12-(b).

5.4.2 Circulating Current Ripple Limitation

The proposed control follows the i_{circ} reference with an associated ripple, as it is shown at Fig. 5.13. This ripple value is given by (5.11), where V_c is the SM capacitor voltage, L is the arm inductance, $\Delta\theta$ is the phase distance between two consecutive firing angles and f is the fundamental frequency.

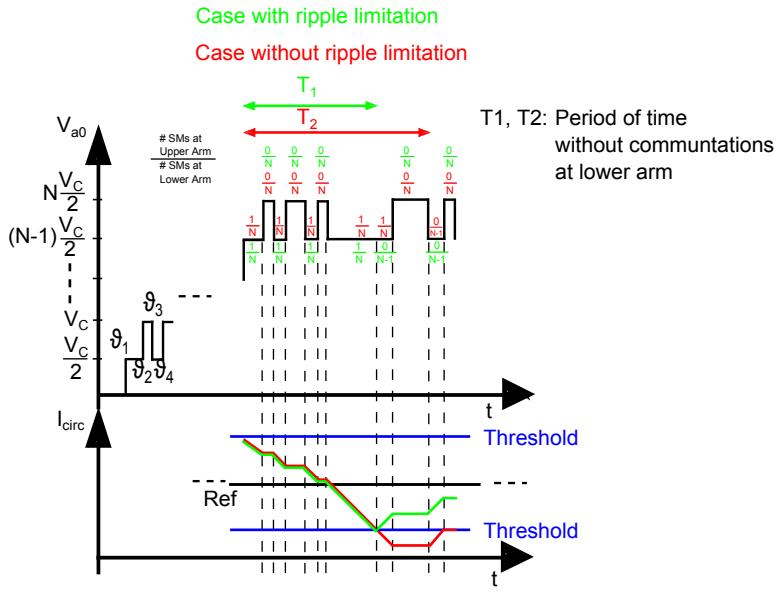

Figure 5.14: Unequal distribution of commutations at upper and lower arms over particular intervals of fundamental period. This issue is mitigated by the extra-switchings.

$$\Delta i_{circ} = \frac{V_c}{4L\pi f}\Delta\theta, \tag{5.11}$$

Due to the low switching frequency and the unequal distance between consecutive firing angles, inherent to SHE-PWM waveforms, $\Delta\theta$ can take high values. Therefore, the i_{circ} ripple will be considerable and the i_{circ} reference will not be correctly followed. With the aim of addressing this problem, a i_{circ} ripple limitation is provided, which consist of employing two thresholds, one above the i_{circ} reference and the other one below it, as it is depicted at Fig. 5.13. In the event that i_{circ} exceeds any of the two thresholds, two simultaneous extra-switchings, one at every arm, will be used to switch from one redundant state to the other one, consequently changing the sign of v_{diff}, without disturbing v_{a0}. In this way, the control will operate correctly regardless of the set of firing angles.

Furthermore, the fact that (2N+1) SHE-PWM alternates the commutations of the upper and lower arms, along with the proposed i_{circ} control, makes the balancing algorithm less effective. This drawback is based on the existence of relatively

long periods of time where there are not commutations in one of the two arms. As an example, Fig. 5.14 shows several consecutive firing angles which are provided by commutations at the upper arm. In this way, the balancing algorithm does not operate at the lower arm over that period of time. This fact would increase the SM capacitor voltage ripple. However, this issue may be mitigated by the extra-switchings, as it is shown at Fig. 5.14, which happen simultaneously at both arms and increase the average switching frequency of the SMs, thus contributing to improve the voltage balance of the SMs. However, the frequency increase causes additional losses. This issue will be analysed in Section 5.5.

5.4.3 Generation of Upper and Lower Arm Voltages at every Phase

Fig. 5.15 shows how to combine the SHE-PWM implementation method described in chapter 4 and the proposed (2N+1) SHE-PWM i_{circ} controller. As it is depicted at Fig. 5.15, the implementation method calculates the firing angles to generate v_{a0} off-line, regardless the circulating current reference. These firing angles are stored in look-up tables. In this way, according to the desired m_a value, the required instantaneous v_{a0} value is sent to the i_{circ} controller. Then, this controller (Fig. 5.12-(b)) calculates in real time the circulating current reference and, whenever possible, it selects the suitable redundant state to track that reference. In case a non-redundant state is required, it will also be provided.

Finally, the balancing algorithm selected for (N+1) SHE-PWM and described at section 2.4.6 [11, 12] is also applied in case of (2N+1) SHE-PWM, not increasing the switching losses. In addition, this modulation does not require the extra balancing instants, utilized by (N+1) SHE-PWM when the effective switching frequency is low, due to the extra-switchings detailed at section 5.4.2.

5.5 Simulation Results

With the aim of validating the (N+1) SHE-PWM and (2N+1) SHE-PWM i_{circ} control techniques described in this section, a Matlab/Simulink model of a three-phase MMC has been developed, whose scheme is depicted at Fig. 2.5-(c) and reproduced here for convenience (see Fig. 5.16). The i_{circ} reference is calculated using the algorithm described in [82].

In case of (N+1) SHE-PWM, the sets of firing angles utilized are the ones obtained in chapter 4 with 17 firing angles and 11 levels. On the other hand, for (2N+1)

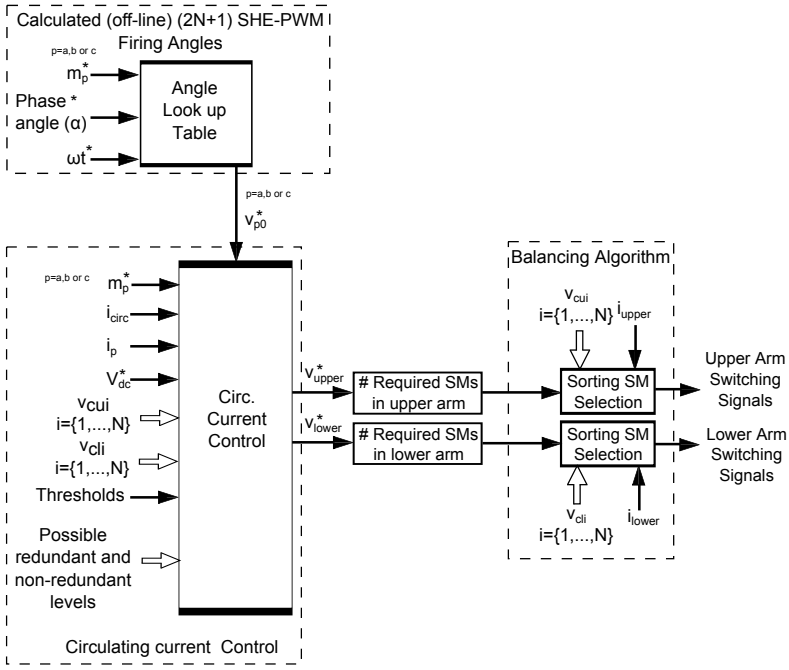

Figure 5.15. Generation of upper and lower arm voltages at every phase.

Table 5.1: Firing angles and sign of every step of QW solutions with 17 firing angles and 21 levels

m_a	θ_1	θ_2	θ_3	θ_4	θ_5	θ_6	θ_7	θ_8	θ_9	θ_{10}	θ_{11}	θ_{12}	θ_{13}	θ_{14}	θ_{15}	θ_{16}	θ_{17}
0,1	⇓0,404	⇑0,4241	⇑0,7214	⇓0,7617	⇑0,8204	⇓0,8805	⇑0,9206	⇓0,9969	⇑1,0186	⇑1,2199	⇓1,2339	⇑1,3244	⇓1,353	⇑1,4238	⇓1,4935	⇑1,5578	⇑1,5579
0,2	⇑0,5972	⇓0,6222	⇑0,6704	⇓0,7198	⇑0,7438	⇑0,8949	⇓0,9215	⇑0,9738	⇓1,0283	⇑1,055	⇑1,2234	⇓1,2494	⇑1,31	⇓1,3604	⇑1,3982	⇓1,4695	⇑1,4861
0,3	⇑0,5893	⇓0,6228	⇑0,6542	⇑0,7831	⇓0,8158	⇑0,8496	⇑0,99	⇓1,0273	⇑1,0639	⇑1,2177	⇓1,2554	⇑1,2985	⇓1,3857	⇑1,3966	⇑1,4516	⇓1,4748	⇑1,5452
0,4	⇑0,1417	⇑0,2089	⇑0,3551	⇑0,5895	⇓0,6594	⇑0,686	⇓0,7389	⇑0,7759	⇓0,8567	⇑1,0373	⇓1,0775	⇑1,0974	⇓1,2168	⇓1,4408	⇑1,4801	⇓1,5693	⇓1,5695
0,5	⇑0,1123	⇑0,1911	⇑0,349	⇑0,5818	⇑0,8154	⇓0,854	⇓0,9702	⇑0,9759	⇑1,0633	⇓1,1298	⇑1,157	⇓1,203	⇑1,3354	⇓1,3602	⇑1,5301	⇓1,5494	⇑1,5633
0,6	⇑0,5717	⇑0,6684	⇑0,7665	⇑0,8674	⇑0,9717	⇑1,0795	⇓1,1401	⇑1,1553	⇑1,1583	⇓1,1816	⇑1,2105	⇑1,3202	⇓1,3644	⇑1,379	⇑1,4466	⇓1,4761	⇑1,5099
0,7	⇑0,4821	⇑0,6476	⇑0,7311	⇑0,8167	⇑0,9037	⇑0,9942	⇑1,09	⇑1,185	⇓1,2038	⇑1,2127	⇑1,2533	⇓1,2602	⇓1,3049	⇑1,4172	⇓1,4639	⇑1,4773	⇓1,5526
0,8	⇑0,1375	⇑0,1942	⇑0,3437	⇑0,4434	⇑0,4831	⇓0,6114	⇑0,6378	⇑0,7799	⇓0,9066	⇑0,9292	⇑1,0124	⇑1,0952	⇓1,2435	⇑1,2818	⇑1,3605	⇓1,3673	⇓1,5159
0,9	⇑0,0934	⇑0,1635	⇑0,2973	⇑0,3624	⇑0,4276	⇑0,556	⇑0,8167	⇑1,0245	⇑1,1045	⇓1,1509	⇑1,1986	⇓1,2298	⇑1,2719	⇓1,3891	⇑1,421	⇓1,4526	⇑1,5555
1	⇑0,1159	⇑0,1241	⇑0,2048	⇑0,3727	⇑0,4426	⇑0,4773	⇑0,5538	⇓0,5661	⇑0,7213	⇑0,791	⇓0,9495	⇑0,9791	⇑1,0352	⇑1,1037	⇓1,159	⇑1,33	⇓1,4969

SHE-PWM, 21 levels and 17 firing angles (see table 5.1) are utilized. In addition, as a reference, a fundamental phase $\phi_1 = 0$ (cosine waveform) is used to provide the phase output voltage waveform of phase A. Therefore, the switching patterns obtained in chapter 4 with sine waveform, are shifted $\pi/2$ radians. In case of using an external control, this initial phase would be given by that control. The rest of phases, B and C, are shifted $4\pi/3$ and $2\pi/3$, respectively, from phase A.

Waveform assessment, THD and efficiency studies have been conducted using the commented MMC model and the following results have been obtained:

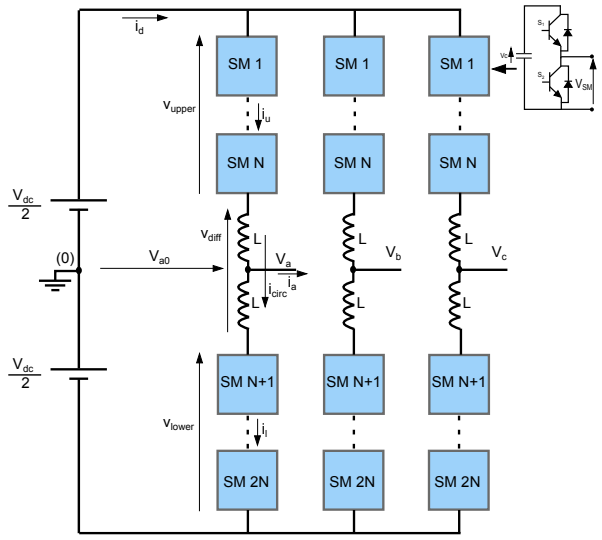

Figure 5.16. Three-phase MMC with HB SMs.

5.5.1 Waveform Assessment

The simulation parameters to assess the waveforms, utilizing a converter with 10 SMs at every arm, are included at table 5.2.

5.5.1.1 Waveform Assessment for (N+1) SHE-PWM Control Technique

The simulation results have been obtained using a fundamental frequency, f, equal to 50 Hz. Firstly, the i_{circ} control operation is detailed in Figs. 5.17, 5.18 and 5.19, utilizing a load of 24Ω and $40mH$ to reduce the effect of the arm inductances in the phase output voltage (with the aim of visualizing clearly the waveforms). Secondly, using the load detailed at table 5.2, two different simulation results have been obtained. The first one, which is included at Fig. 5.20, shows a transitory state where the m_a value is modified from 0.2 to 0.9. The second one, which is depicted at Fig. 5.21, shows a load change from 48Ω and $16mH$ to 24Ω and $8mH$ when $m_a = 0.5$. All these results have been obtained using 17 firing angles in the first QW.

With the aim of adjusting the values of m_1 and m_2, once the m_a is given, several

Table 5.2. Simulation Parameters

Parameter	**Value**
# of SMs per arm, N	10
dc link Voltage, V_{dc}	$22500V$
SM capacitor, C	$4.6mF$
SM capacitor voltage, V_C	$2250V$
Arm inductor, L	$18mH$
Load, R_L and L_L. Star configuration.	24Ω and $8mH$
# of Angles (1^{st} QW) (N+1)/(2N+1) SHE	17
Fundamental frequency, f	$50Hz$
First non-eliminated harmonic	$2650Hz$
Modulation index, m_a	0.2 | 0.5 | 0.9
PI control for DC-link voltage	P=$2.5e^{-9}$, I=$9e^{-8}$
Arm energy balance control, K	$1e^{-5}$

simulation tests have been realized. Fig. 5.17 shows two of them, where the i_{circ} control operation and the i_{circ} ripple are depicted in case of $m_1 = m_a - 0.005$, $m_2 = m_a + 0.005$ and $m_1 = m_a - 0.01$, $m_2 = m_a + 0.01$, respectively. As it can be noticed, the second case provides a faster control but a higher i_{circ} ripple for most of the m_a values. In addition, as it is shown at Fig. 5.17-(c), the i_{circ} ripple depends on the m_a value because of two different reasons. Firstly, different switching patterns provide different Δi_{circ} and secondly, as it is detailed at chapter 2, the second harmonic energy variation at every arm increases when m_a and i_a are increased. Finally, when the distance between m_1 and m_2 is lower than $5e-3$, the i_{circ} is not able to follow the i_{circ} reference correctly. Therefore, regarding the trade-off between the i_{circ} ripple and the control response to transient states, utilizing $m_1 = m_a - 0.005$ and $m_2 = m_a + 0.005$ is a correct option.

On the other hand, the operation of the i_{circ} control can be noticed at Fig. 5.18. In particular, it is possible to notice the utilization of m_1 and m_2 in the differential voltage and the phase output voltage. In the latter, Fig. 5.18-(b), every firing angle consists of two firing angles which are given by m_1 and m_2, respectively. In this way, over short periods of time $v_{diff} \neq 0$ and the i_{circ} is able to follow the i_{circ} reference with an assumed ripple. This fact can be noticed in detail at Figs. 5.18-(b), 5.18-(d) and 5.18-(f). In addition, Figs. 5.18-(c) and 5.18-(e) show the commented second harmonic variation in i_{circ} and v_{diff}, respectively. The i_{circ} control tries to reduce the effect of this variation in i_{circ}, as it can be noticed at Fig. 5.18-(d).

In case there are close firing angles which provide a phase output voltage which exceeds the maximum or minimum allowed levels by the converter, the v_{diff} will have an opposite sign to the desired one. In this way, the i_{circ} will vary in the

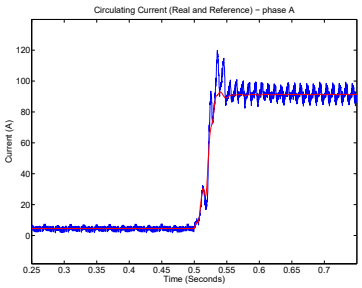

(a) Reference (red) and actual (blue) circulating current when $m_1 = m_a - 0.005$ and $m_2 = m_a + 0.005$.

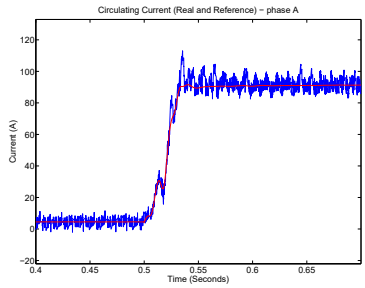

(b) Reference (red) and actual (blue) circulating current when $m_1 = m_a - 0.01$ and $m_2 = m_a + 0.01$.

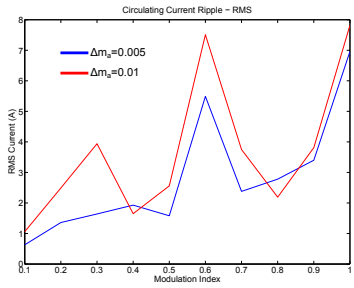

(c) i_{circ} ripple when $m_1 = m_a - 0.005$ and $m_2 = m_a + 0.005$ and when $m_1 = m_a - 0.01$ and $m_2 = m_a + 0.01$.

Figure 5.17: (N+1) SHE-PWM waveforms. Comparison of results with different values of m_1 and m_2.

opposite direction as it can be noticed at Fig. 5.19. However, this fact does not prevent the control from following the i_{circ} reference.

Finally, regarding the m_a transition and the load change at Figs. 5.20 and 5.21, respectively, the results show a correct performance of the converter. In particular Figs. 5.20-(a) and 5.21-(a) show the line-line V_{AB} voltage. The phase currents are depicted at Figs. 5.20-(b) and 5.21-(b). As it can be noticed, the currents are balanced. On the other hand, Figs. 5.20-(c) and 5.21-(c) show the upper and lower arm currents of phase A. Figs. 5.20-(d) and 5.21-(d), which contain the i_{circ} and its corresponding reference, show how the control is able to follow the i_{circ} reference under transient states. The upper and lower SM capacitor

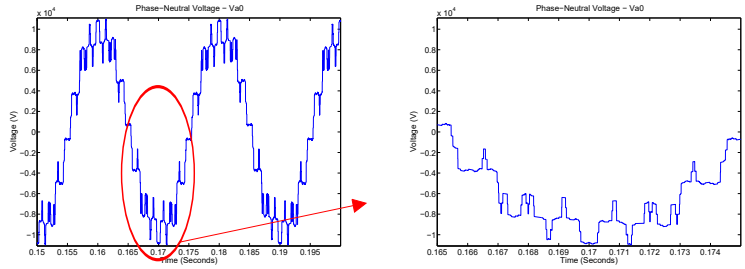

(a) V_{an} waveform. (b) V_{an} waveform in detail.

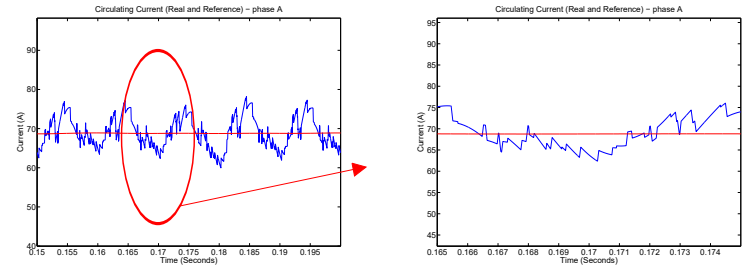

(c) Reference (red) and actual (blue) circulating current. (d) Reference (red) and actual (blue) circulating current in detail.

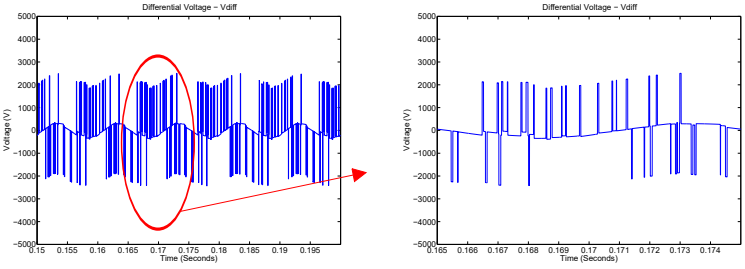

(e) Differential voltage. (f) Differential voltage in detail.

Figure 5.18: (N+1) SHE-PWM waveforms with 17 angles in the first QW, f equal to 50Hz and $m_a = 0.9$.

voltages are depicted at Figs. 5.20-(e), 5.20-(f), 5.21-(e) and 5.21-(f). All of them show an increment in the SM capacitor voltage ripple when the output power is increased. However, despite the transients, all the SM capacitor voltages are balanced and the SM capacitor voltage ripple is always lower than 5%. On the

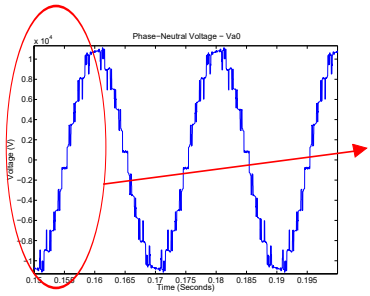

(a) V_{an} waveform.

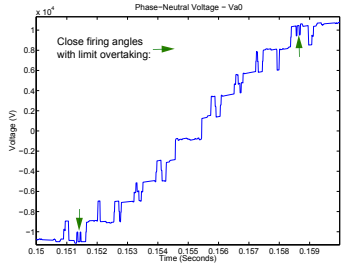

(b) V_{an} waveform in detail.

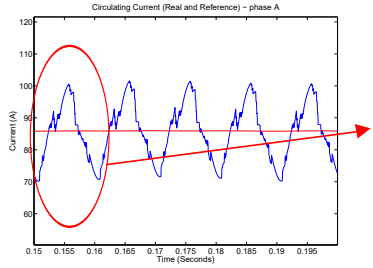

(c) Reference (red) and actual (blue) circulating current.

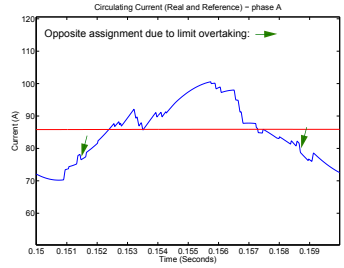

(d) Reference (red) and actual (blue) circulating current in detail.

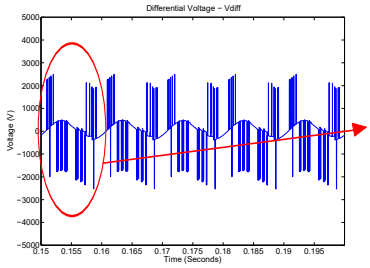

(e) Differential voltage.

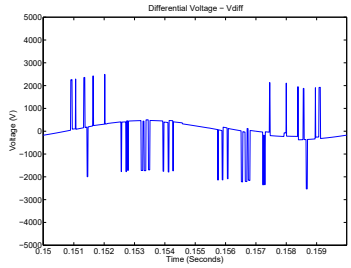

(f) Differential voltage in detail.

Figure 5.19: (N+1) SHE-PWM with 17 angles in 1^{st} QW, $f = 50$Hz and $m_a = 1.01$. There are instants which provide an opposite i_{circ} increase to avoid exceeding the upper and lower output voltage limits. The i_{circ} reference is correctly followed.

other hand, Figs. 5.20-(g), 5.20-(h) and 5.21-(g) show V_{AB} spectrum. Therefore, it is proven how the i_{circ} control does not disturb the phase output voltage. The first undesired harmonic is located at 2650 Hz.

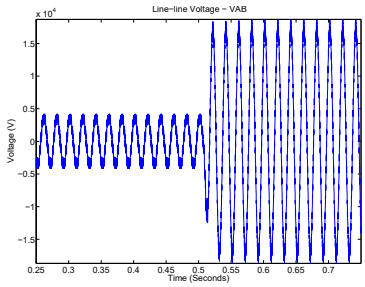

(a) V_{AB} waveform.

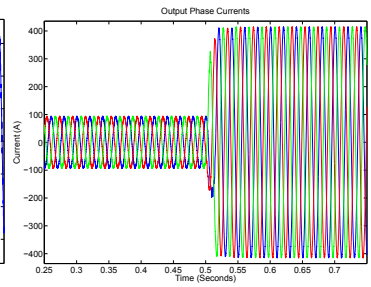

(b) Phase currents.

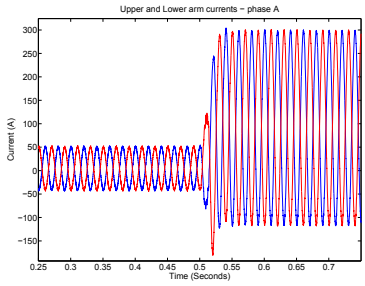

(c) Upper and lower arm currents of phase A.

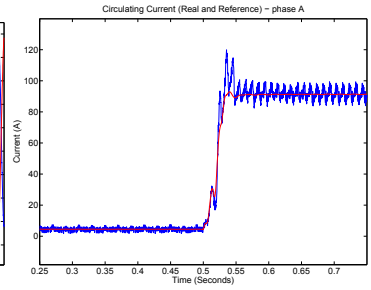

(d) Reference (red) and actual (blue) circulating current.

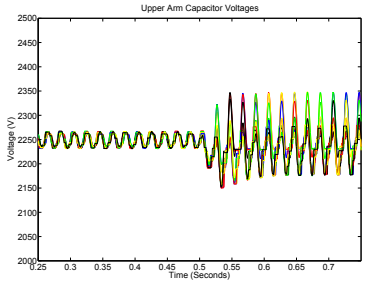

(e) Upper SM capacitor voltages.

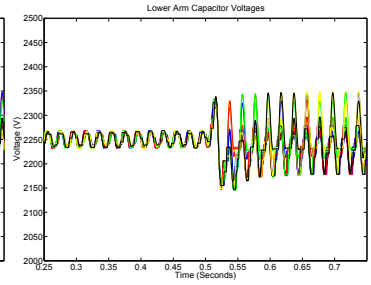

(f) Lower SM capacitor voltages.

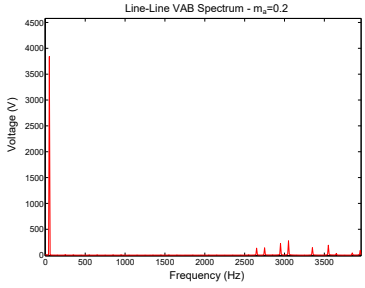

(g) V_{AB} spectrum for $m_a = 0.2$.

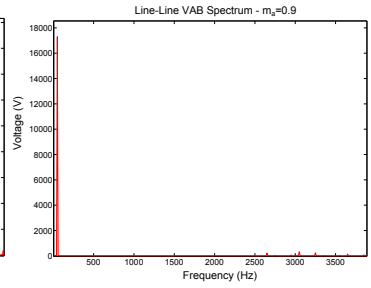

(h) V_{AB} spectrum for $m_a = 0.9$.

Figure 5.20: (N+1) SHE-PWM waveforms with 17 angles in the first QW, f equal to 50Hz and a transition of the m_a value from 0.2 to 0.9.

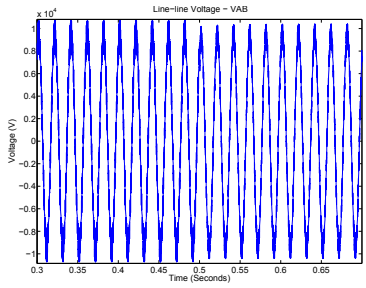

(a) V_{AB} waveform.

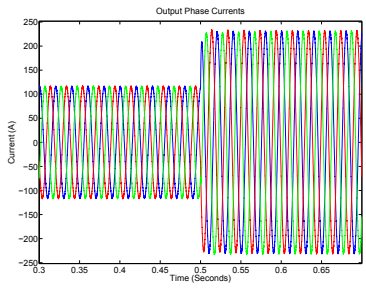

(b) Phase currents.

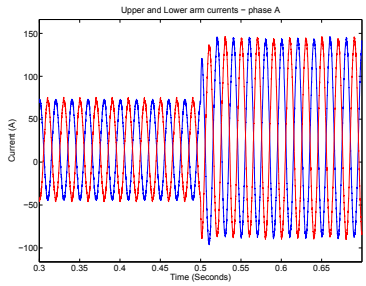

(c) Upper and lower arm currents of phase A.

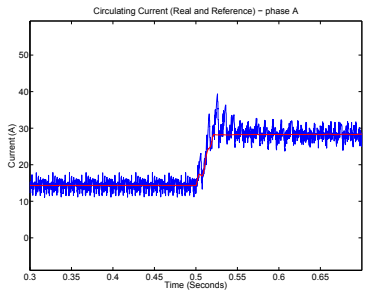

(d) Reference (red) and actual (blue) circulating current.

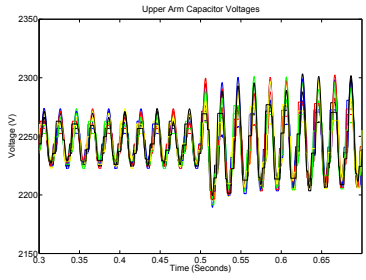

(e) Upper SM capacitor voltages.

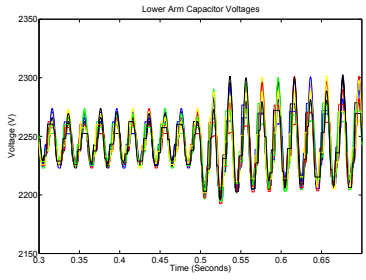

(f) Lower SM capacitor voltages.

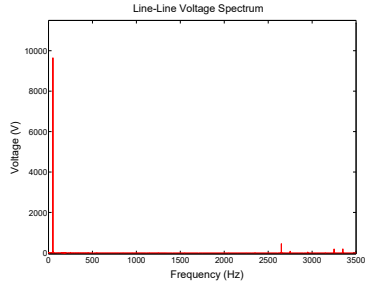

(g) V_{AB} spectrum for $m_a = 0.5$.

Figure 5.21: (N+1) SHE-PWM waveforms with 17 angles in the first QW, f equal to 50Hz and a load change from 48Ω and $16mH$ to 24Ω and $8mH$.

5.5.1.2 Waveform Assessment for (2N+1) SHE-PWM Control Technique

The waveform assessment has been realized regarding the simulation parameters detailed at table 5.2, utilizing a MMC with 10 SMs at every arm.

Fig. 5.22 shows a correct operation of the MMC under a m_a transition from 0.2 to 0.9, utilizing $f = 50$ Hz. In particular, the V_{AB} voltage is depicted at Fig. 5.22-(a). On the other hand, Fig. 5.22-(b) shows the phase currents which are balanced. The arm and circulating currents are included at Figs. 5.22-(c) and 5.22-(d), respectively. As it can be noticed, the i_{circ} is adjusted correctly to its reference. In this case, the i_{circ} ripple threshold has been configured as 15 A. Figs. 5.22-(e) and 5.22-(f) show how the SM capacitor voltages of upper and lower arms are balanced despite the m_a transition. In particular, when $m_a = 0.9$, the SM capacitor voltage ripple is lower than 7%. This ripple is higher than the one provided by (N+1) SHE-PWM (Figs. 5.20-(e) and 5.20-(f)) due to the lower switching frequency and the unequal distribution of upper and lower commutations, commented at section 5.4.2. Finally, the V_{AB} spectra included at Figs. 5.22-(g) and 5.22-(h) provide a correct elimination of the undesired harmonics.

Apart from these results, the study is completed with simulation results which have been obtained using a MMC with 5 SMs at every arm.

5.5.1.2.1 Simulation results utilizing a MMC with 5 SMs at every arm

The simulation parameters are included at table 5.3. In this case, the number of angles are 17 and 34, but the number of levels is 11. The utilized sets of firing angles are the ones calculated at chapter 4.

Figs. 5.23 and 5.24 show the (2N+1) SHE-PWM performance for fundamental frequency, f, equal to 50Hz and 25Hz, respectively. In case of $f = 25$Hz, 34 firing angles in the first QW and a m_a value equal to 0.2 have been used. On the other hand, when $f = 50$Hz, 17 firing angles have been utilized and a transition of the m_a value from 0.5 to 1 has been realized at the instant 0.5s. The number of firing angles is selected to maintain the switching frequency at every arm close to 1 kHz, regardless of the fundamental frequency.

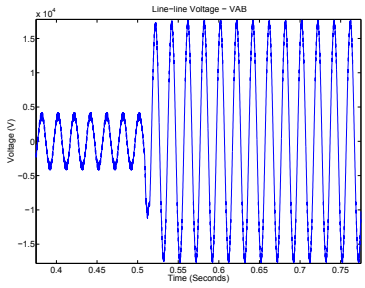

(a) V_{AB} waveform.

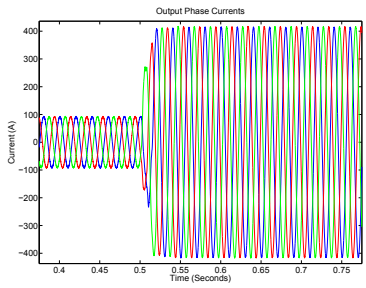

(b) Phase currents.

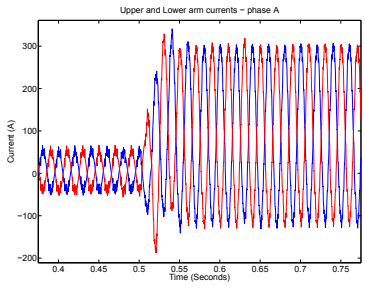

(c) Upper and lower arm currents of phase A.

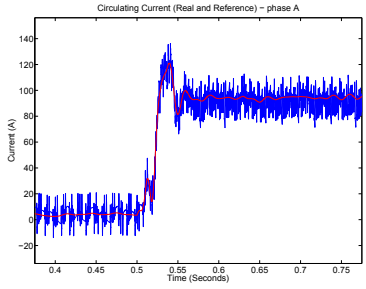

(d) Reference (red) and actual (blue) circulating current.

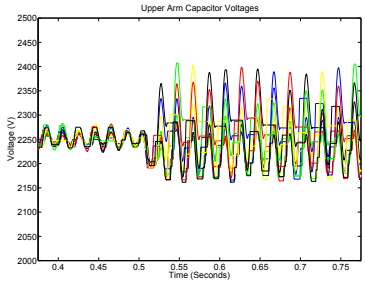

(e) Upper SM capacitor voltages.

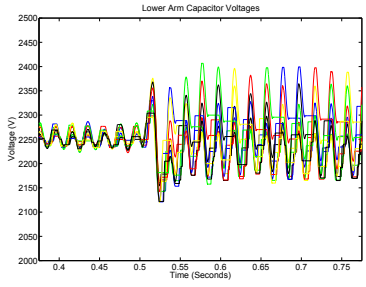

(f) Lower SM capacitor voltages.

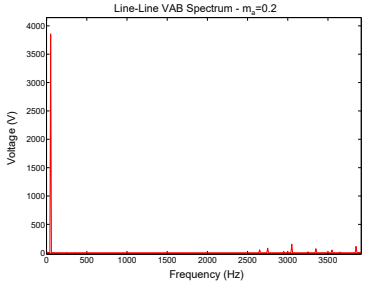

(g) V_{AB} spectrum for $m_a = 0.2$.

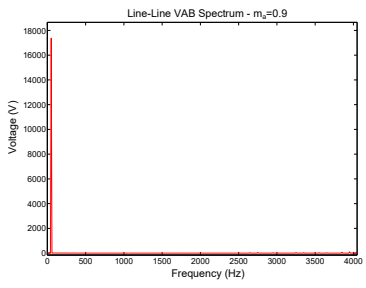

(h) V_{AB} spectrum for $m_a = 0.9$.

Figure 5.22: (2N+1) SHE-PWM waveforms with 17 angles in the first QW, f equal to 50Hz and a transition of the m_a value from 0.2 to 0.9.

Table 5.3. Simulation Parameters

Parameter	Value		
# of SMs per arm, N	5		
dc link Voltage, V_{dc}	$11250V$		
SM capacitor, C	$4.6mF$		
SM capacitor voltage, V_C	$2250V$		
Arm inductor, L	$9mH$		
Load, R_L and L_L. Star configuration.	12Ω and $4mH$		
i_{circ} ripple threshold	$40A$		
# of Angles (1^{st} QW) (2N+1) SHE	17		34
Fundamental frequency, f	$50Hz$		$25Hz$
First non-eliminated harmonic	$2650Hz$		$2575Hz$
Modulation index, m_a	0.5	1	0.2
PI control for DC-link voltage	P=$5e^{-5}$, I=$9e^{-5}$		
Arm energy balance control, K	$2e^{-5}$		

Fig. 5.23-(a) and 5.24-(a) show the line-to-line voltage generated by the converter. The harmonic spectra of these signals are displayed in Figs. 5.23-(b) and 5.24-(b), respectively. The undesired harmonics have been correctly eliminated according to the number of available firing angles.

Fig. 5.23-(c) and 5.24-(c) show the arm currents. To obtain these results, the i_{circ} ripple has been limited utilizing a threshold of 40A, which represents a 15% of the nominal arm current, above and below the i_{circ} reference. It can be noticed how the dc component of i_{circ} is tracked correctly, even during the transient state caused by the change in the m_a value, depicted at Fig. 5.23. This fact is clearly observed at Figs. 5.23-(g) and 5.24-(g), which show the i_{circ} and its corresponding reference. The first one shows the increase in the i_{circ} reference when the m_a is increased and how the controller is able to follow that reference correctly, with an associated ripple. Fig. 5.24-(g) also shows how the i_{circ} reference is tracked correctly. The i_{circ} ripple can also be observed.

Consequently, the SM capacitor voltages are correctly regulated. This is shown in Figs. 5.23-(e), 5.23-(f), 5.24-(e) and 5.24-(f) where the upper and lower arm capacitor voltages are represented. The SM capacitor voltage ripple has resulted lower than 5% for every simulation. Moreover, Figs. 5.23-(e) and 5.23-(f) show how the SM capacitor voltages are correctly balanced despite the increase in their voltage ripple because of the change in the m_a value at 0.5s.

In addition, the SM capacitor voltage ripple shown at these figures is lower than the one provided with 10 SMs at Figs. 5.22-(e) and 5.22-(f), due to the higher effective switching frequency obtained with 5 SMs.

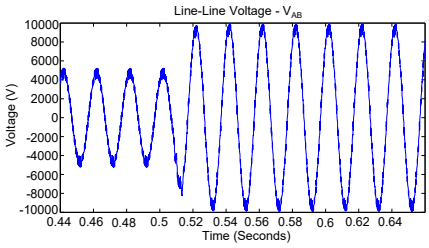

(a) V_{AB} waveform.

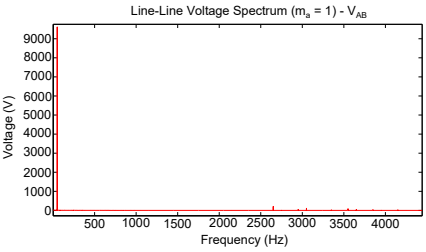

(b) V_{AB} spectrum for m_a equal to 1.

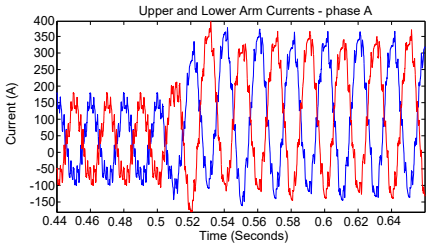

(c) Upper and lower arm currents of phase A.

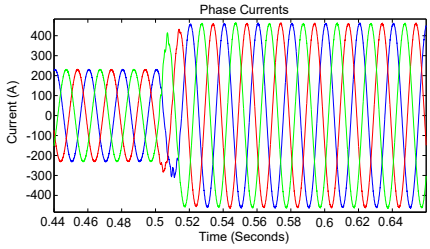

(d) Phase currents.

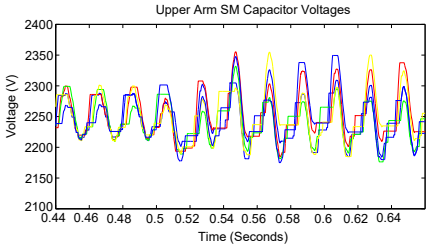

(e) Upper SM capacitor voltages.

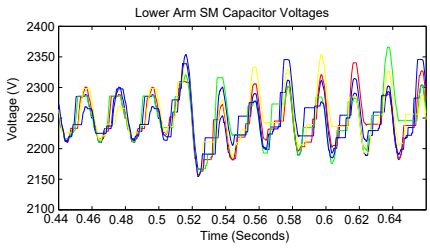

(f) Lower SM capacitor voltages.

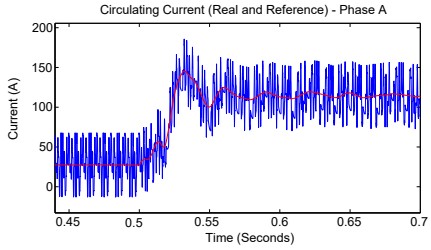

(g) Reference (red) and actual (blue) circulating current.

Figure 5.23: (2N+1) SHE-PWM waveforms with 17 angles in the first QW, f equal to 50Hz and a transition of the m_a value from 0.5 to 1.

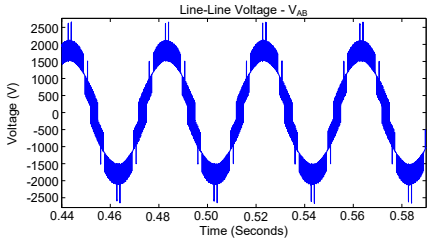

(a) V_{AB} waveform.

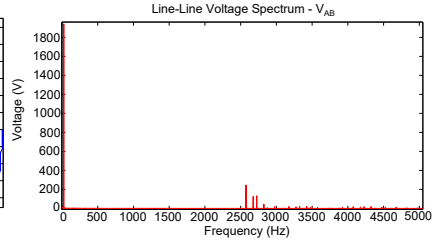

(b) V_{AB} spectrum.

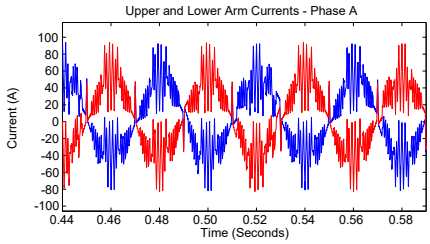

(c) Upper and lower arm currents of phase A.

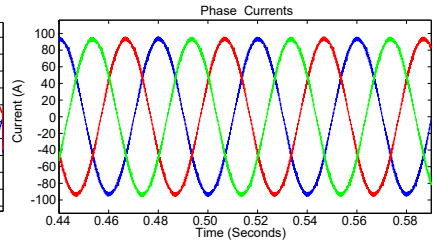

(d) Phase currents.

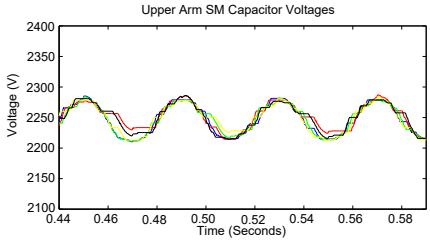

(e) Upper SM capacitor voltages.

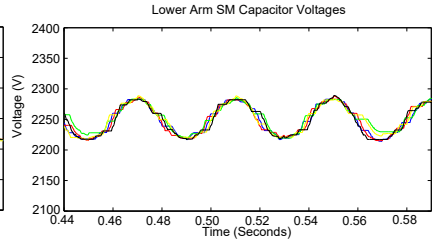

(f) Lower SM capacitor voltages.

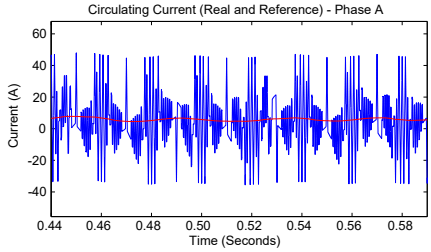

(g) Reference (red) and actual (blue) circulating current.

Figure 5.24: (2N+1) SHE-PWM waveforms with 34 angles in the first QW, f equal to 25Hz and m_a equal to 0.2.

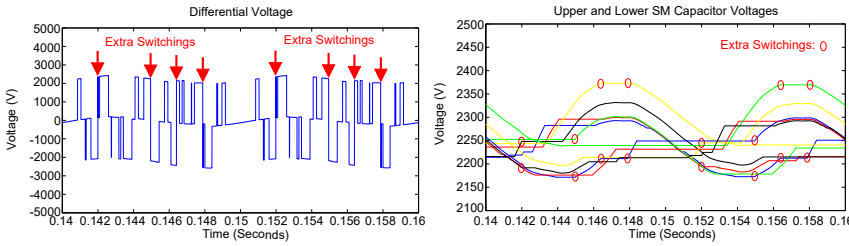

(a) Differential voltage of phase A, where the extra-switchings can be noticed.

(b) Upper and lower SM capacitor voltages, where the extra-switchings can be noticed.

Figure 5.25: (2N+1) SHE-PWM extra-switchings, with 17 angles in the first QW, f equal to 50Hz and m_a value equal to 1.

However, to limit the i_{circ} ripple, extra-switchings between redundant states are allowed. Fig. 5.25 depicts the extra-switchings in case of utilizing 17 firing angles in the first QW, $m_a = 1$ and $f = 50$Hz. In this particular case, the number of extra-switchings increases the switching frequency by 23%, thus worsening the efficiency. However, the i_{circ} ripple is effectively limited within the defined limits. This fact is clearly shown in Figs. 5.26-(a) and 5.26-(b). The first one shows the upper and lower arm currents with and without applying the ripple limitation algorithm. At $t = 0.25$s the ripple limitation algorithm with a threshold of 40A is applied. The effect of the algorithm is clear and the i_{circ} ripple experiences a significant reduction, as it can also be noticed at Fig. 5.26-(b). This figure shows how the i_{circ} reference is correctly followed by the controller when the i_{circ} ripple is reduced. Fig. 5.26-(c) provides the percentage of extra-switchings and the RMS value of the i_{circ} ripple for different threshold values. The i_{circ} ripple on the previous experiments could be reduced below 40A. However, as Fig. 5.26-(c) discloses, an increase in the number of extra-switchings would take place. Consequently, the switching losses would be increased. A trade-off between the switching losses and the i_{circ} ripple should be achieved to reach a proper operation of the MMC.

Considering this trade-off, in case of the MMC with 10 SMs at every arm, it is possible to configure the threshold with a lower value, 15 A, without increasing the switching losses, due to the higher arm inductance provided by the converter with 10 SMs at every arm. When the number of SMs or the DC voltage are increased, the i_{circ} ripple provided by (2N+1) SHE-PWM is lower.

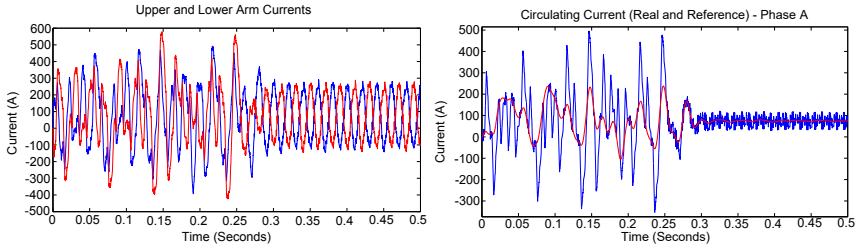

(a) Upper and lower arm currents (i_{circ} ripple limitation, threshold of $40A$, applied at $0.25s$).

(b) Reference (red) and actual (blue) circulating current.

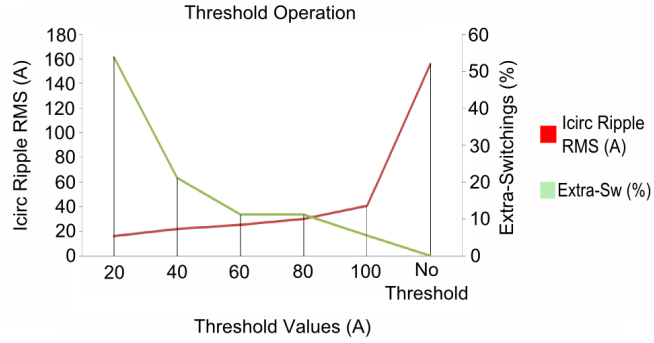

(c) Percentage of extra-switchings and i_{circ} ripple RMS values, depending on the threshold value.

Figure 5.26: Study of the circulating current ripple limitation, when $m_a = 0.8$ and $f = 50$ Hz.

5.5.1.3 Phase Output Voltage and DC Current Spectra Comparison for SHE-PWM and PWM

The phase output voltage and dc input current spectra provided by (N+1) SHE-PWM and (2N+1) SHE-PWM has been obtained. In addition, the study has been increased with the results for PD-PWM and IPD-PWM. In particular, 17 firing angles in the first QW have been used for (N+1) SHE-PWM and (2N+1) SHE-PWM. In this way, the first non-eliminated harmonic is 2650Hz. On the other hand, with the aim of obtaining the first band of harmonics centred in 2650Hz, the carrier frequencies of PD-PWM and IPD-PWM are $f_c = 2650$Hz and $f_c = 1325$Hz, respectively.

As it can be noticed at Fig. 5.27, the spectra provided by (N+1) and (2N+1)

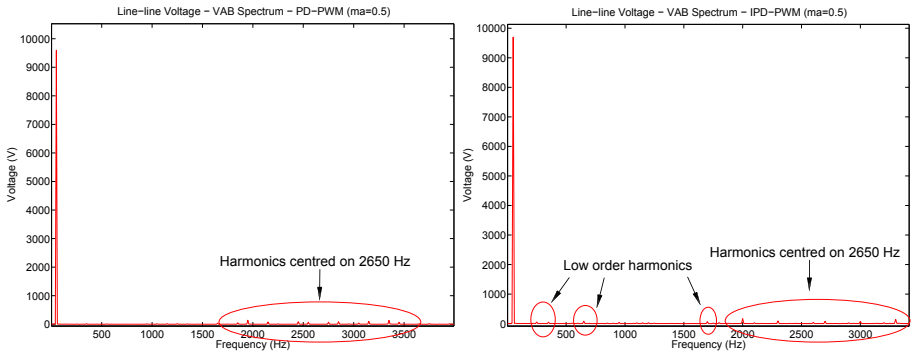

(a) PD-PWM. (b) IPD-PWM.

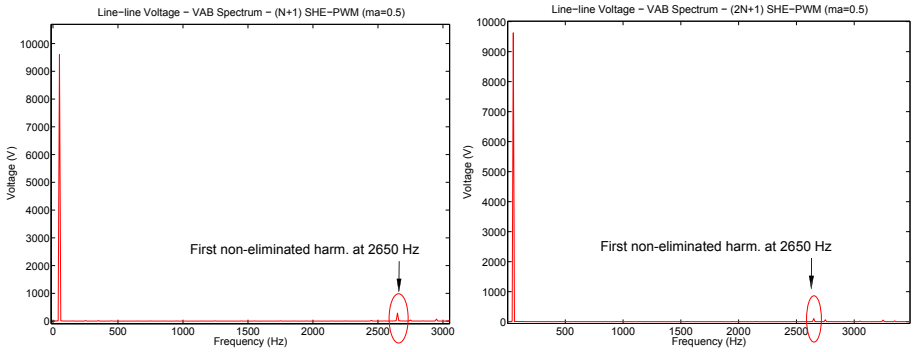

(c) (N+1) SHE-PWM. (d) (2N+1) SHE-PWM.

Figure 5.27. Phase output voltage spectra for $m_a = 0.5$.

SHE-PWM provide the first non-eliminated harmonic located in 2650Hz. On the other hand, PD-PWM and IPD-PWM contains the harmonics centred on 2650Hz, but this band of harmonics is spread up to 1900Hz, approximately, in case of PD-PWM and 1700Hz, in case of IPD-PWM. However, in case of IPD-PWM, low order harmonics appear in the spectrum. [124].

On the other hand, Fig. 5.28 contains the spectrum of the MMC DC input current when different modulations are applied. As it can be noticed, PD-PWM only provides the required DC component. A similar situation happens with (N+1) SHE-PWM. In this case there are other components but with very low amplitude. On the other hand, due to their higher i_{circ} ripple, (2N+1) SHE-PWM and IPD-PWM contain more relevant harmonic components. The first one

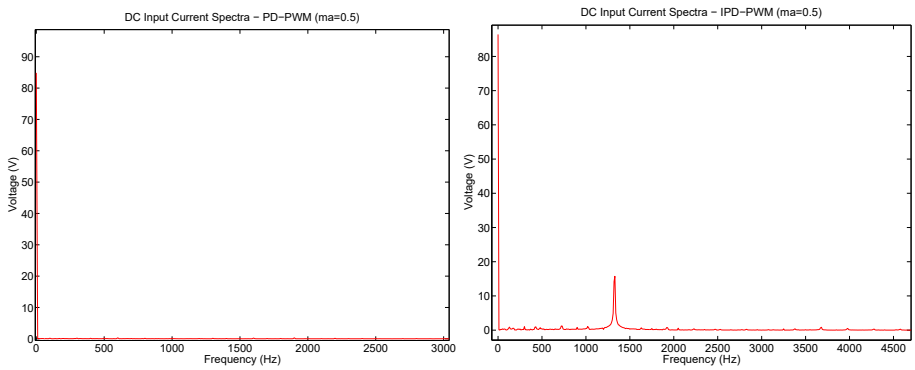

(a) PD-PWM. (b) IPD-PWM.

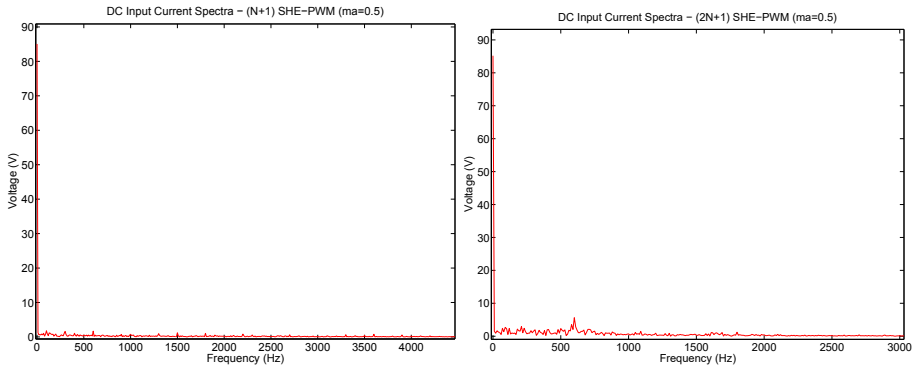

(c) (N+1) SHE-PWM. (d) (2N+1) SHE-PWM.

Figure 5.28. DC input current spectra for $m_a = 0.5$.

provides more components with low amplitude. However, IPD-PWM provides a significantly high harmonic at fc.

5.5.2 Efficiency Study

This section benchmarks the resulting losses provided by (N+1) SHE-PWM and (2N+1) SHE-PWM when the proposed controls are applied against the losses provided by phase disposition pulse width modulation (PD-PWM) and interleaving PD-PWM (IPD-PWM) [118]. To compare the switching losses it is important to define the switching frequency of both modulations. The switching frequency

of (N+1) SHE-PWM, $f_{sw-(N+1)SHE}$ and (2N+1) SHE-PWM, $f_{sw-(2N+1)SHE}$, are given by (5.12) and (5.13), respectively, where l is the number of firing angles in the first QW, f is the fundamental frequency and E_{sw} is the number of extra-switchings in the fundamental period. Alternatively, the switching frequency of PD-PWM, $f_{sw-PDPWM}$ and IPD-PWM, $f_{sw-IPDPWM}$, are given by (5.14), where f_c is the carrier frequency and n_t is the number of transitions between carriers over half fundamental period. The value of n_t is closed to N at high m_a values and it is reduced when m_a is decreased. Therefore, the switching frequency of IPD-PWM and PD-PWM are higher at high m_a values.

$$f_{sw-(N+1)SHE} = 2lf, \tag{5.12}$$

$$f_{sw-(2N+1)SHE} = \frac{(4l + E_{sw})f}{4}, \tag{5.13}$$

$$f_{sw-PDPWM} \approx f_{sw-IPDPWM} \approx f_c + n_t f, \tag{5.14}$$

The simulations have been obtained with 17 firing angles in the first QW for (N+1) SHE-PWM and (2N+1) SHE-PWM. On the other hand, $f_c = 2650$Hz and $f_c = 1325$Hz in case of PD-PWM and IPD-PWM, respectively. In this way, the first harmonic (in case of SHE-PWM) or the first band of harmonics (in case of PWM) will appear at 2650Hz. In addition, the phase current RMS value is 318A and the utilized IGBT is CM600HB-90H of Powerex. Finally, the results have been obtained with a fundamental frequency $f = 50$Hz. The parameters of the MMC are included at table 5.2.

Both switching and conduction losses have been calculated utilizing the method detailed in [1, 186]. For simplification, the junction temperature and the current factor are $T_j = 125°C$ and $k = 1$, respectively [104]. The results have been obtained throughout the m_a and power factor ranges.

5.5.2.1 Efficiency Comparison of (N+1) SHE-PWM and PD-PWM

Fig. 5.29-(a) shows the comparison between the (N+1) SHE-PWM and PD-PWM conduction losses. As it can be noticed, the conduction losses of both modulations are similar, varying its relationship slightly over the m_a and current phase ranges. On the other hand, the switching losses provided by (N+1) SHE-PWM are significantly lower than the ones provided by PD-PWM, as it can be noticed at Fig. 5.29-(b). This fact is particularly relevant for higher m_a values, where the switching frequency of PD-PWM is higher.

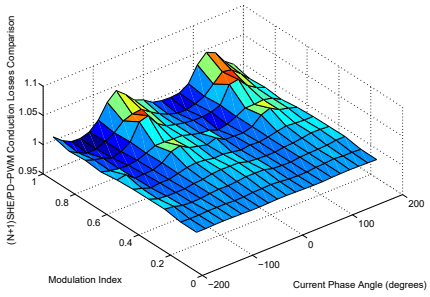

(a) Comparison of conduction losses: (N+1) SHE-PWM / PD-PWM.

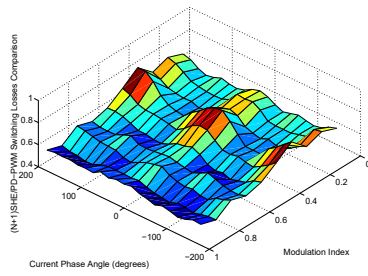

(b) Switching losses comparison: (N+1) SHE-PWM / PD-PWM.

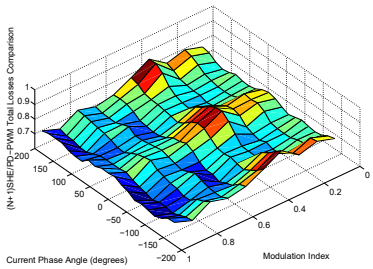

(c) Total losses comparison: (N+1) SHE-PWM / PD-PWM.

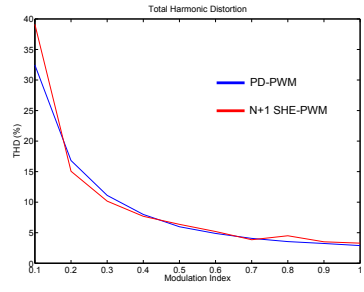

(d) THD comparison between (N+1) SHE-PWM and PD-PWM for a three-phase load of 24Ω & $8mH$.

Figure 5.29. Comparison of losses between (N+1) SHE-PWM and PD-PWM.

Regarding the total losses, (N+1) SHE-PWM is more efficient than PD-PWM throughout the m_a and phase current ranges, highlighting the relevancy of switching losses in a MMC with 10 SMs at every arm. Finally, considering the THD provided by both modulations, included at Fig. 5.29-(d), a similar THD can be obtained but with significantly lower losses if (N+1) SHE-PWM with the proposed control technique is utilized.

5.5.2.2 Efficiency Comparison of (2N+1) SHE-PWM and IPD-PWM

Fig. 5.30-(a) shows similar conduction losses for both (2N+1) SHE-PWM and IPD-PWM. The most efficient modulation depends on the m_a and current phase

values. On the other hand, regarding the switching losses, (2N+1) SHE-PWM is significantly more efficient than IPD-PWM, as it can be noticed at Fig. 5.30-(b). This fact is particularly relevant at high m_a values where the switching frequency of IPD-PWM is higher or at m_a values where the number of extra-switchings is low, as it happens in case of $m_a = 0.5$, regarding the Fig. 5.30-(d). In addition, there are several switching patterns of (2N+1) SHE-PWM, as it can be noticed at table 5.1, where the first firing angle is close to 0.5 or even 0.6 radians ($m_a = 0.1$, $m_a = 0.2$, $m_a = 0.3$, $m_a = 0.6$ and $m_a = 0.7$). In this way, from 5.6 radians up to 0.5 radians there are no switchings for these patterns. Therefore, this fact will make the switching losses of (2N+1) SHE-PWM highly dependant on the current phase, as it can be noticed at Fig. 5.30-(b). In particular, regarding the phase shift of $\pi/2$ realized over the switching patterns, as it has been commented in the beginning of section 5.5, the minimum switching losses are provided when the peak values of the arm current coincide with the intervals of fundamental period without commutations. This situation can be noticed for output current phases equal to $\pm\pi/2$. On the other hand, the dc component of i_{circ}, also influences the switching losses.

Regarding the total losses, as it is shown at Fig. 5.30-(c), (2N+1) SHE-PWM is more efficient than IPD-PWM throughout the m_a and current phase ranges. On the other hand, Fig. 5.30-(e) shows that (2N+1) SHE-PWM provides a lower THD than IPD-PWM throughout the m_a range, except for $m_a = 0.1$, where the THDs are similar.

5.5.2.3 Efficiency Comparison of (N+1) SHE-PWM and IPD-PWM

Fig. 5.31-(a) shows similar conduction losses for both modulation, although depending on the m_a and current phase values the relative efficiency vary. On the other hand, as it can be noticed, for $m_a < 0.6$, the switching losses provided by IPD-PWM are lower than the ones provided by (N+1) SHE-PWM. However, for $m_a > 0.6$ (N+1) SHE-PWM is even more efficient, due to the increase in the switching frequency of IPD-PWM when m_a increases, as it has been commented. This fact can also be noticed in the total losses comparison at Fig. 5.31-(c). In addition, the commented effect of current phase variations on switching and total losses of (N+1) SHE-PWM, due to its unequal distribution of firing angles over the fundamental period, can be noticed at Figs. 5.31-(b) and 5.31-(c). Finally, Fig. 5.31-(d) shows a lower THD provided by IPD-PWM throughout the m_a range.

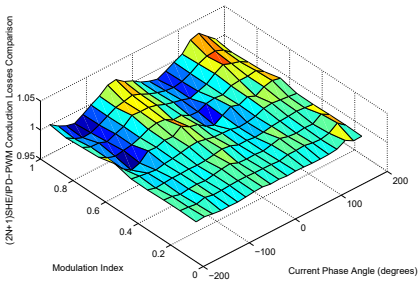

(a) Comparison of conduction losses: (2N+1) SHE-PWM / IPD-PWM.

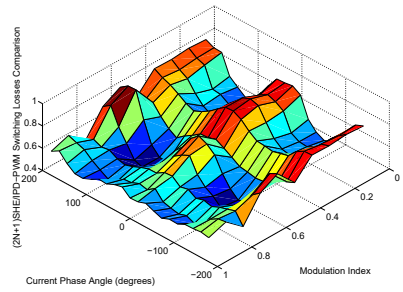

(b) Switching losses comparison: (2N+1) SHE-PWM / IPD-PWM.

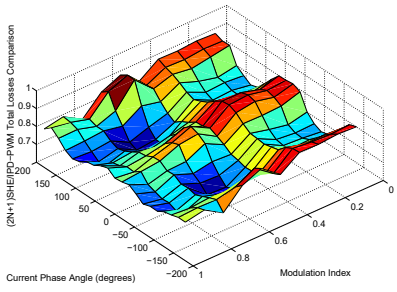

(c) Total losses comparison: (2N+1) SHE-PWM / IPD-PWM.

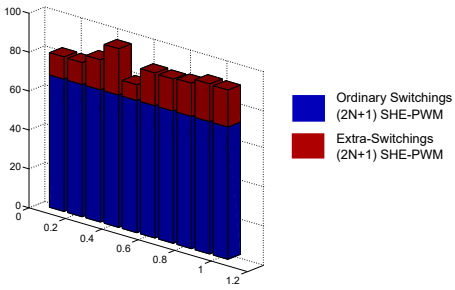

(d) Number of switchings in the fundamental period for (2N+1) SHE-PWM with 17 angles in the first QW, for a three-phase load of 24Ω & $8mH$.

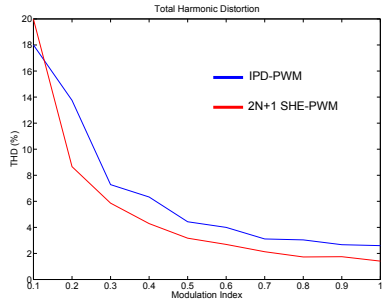

(e) THD comparison between (2N+1) SHE-PWM and IPD-PWM for a three-phase load of 24Ω & $8mH$.

Figure 5.30. Comparison of losses between (2N+1) SHE-PWM and IPD-PWM.

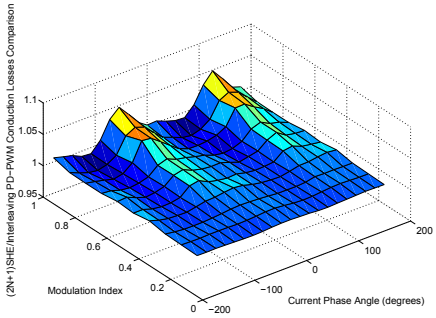

(a) Comparison of conduction losses: (N+1) SHE-PWM / IPD-PWM.

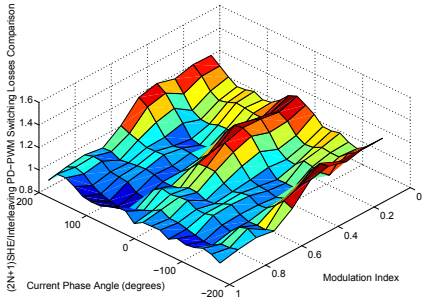

(b) Switching losses comparison: (N+1) SHE-PWM / IPD-PWM.

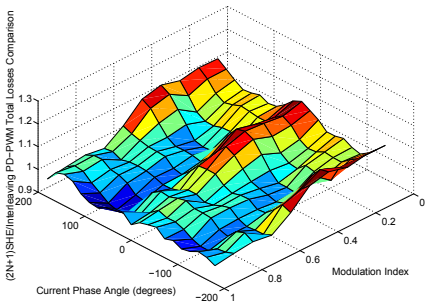

(c) Total losses comparison: (N+1) SHE-PWM / IPD-PWM.

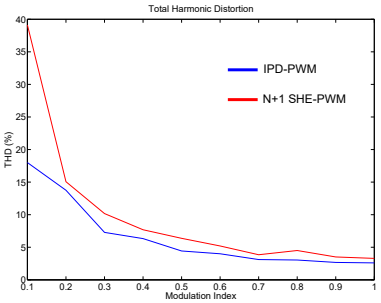

(d) THD comparison between (N+1) SHE-PWM and IPD-PWM for a three-phase load of 24Ω & $8mH$.

Figure 5.31. Comparison of losses between (N+1) SHE-PWM and IPD-PWM.

5.5.2.4 Efficiency Comparison of (N+1) SHE-PWM and (2N+1) SHE-PWM

Fig. 5.32-(a) shows that (N+1) SHE-PWM and (2N+1) SHE-PWM provide similar conduction losses. This relationship depends on the output current phase, the i_{circ} ripple and the percentage of time over the fundamental period where there are $N+1$ or $N-1$ inserted SMs. The latter determines the conduction time of transistors and diodes and therefore, it could modify the conduction losses.

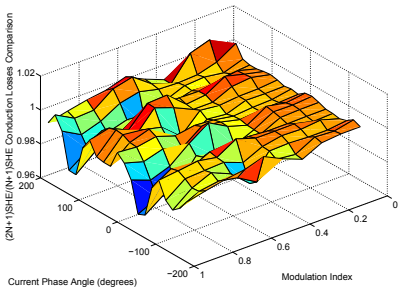

(a) Comparison of conduction losses: (2N+1) SHE-PWM / (N+1) SHE-PWM.

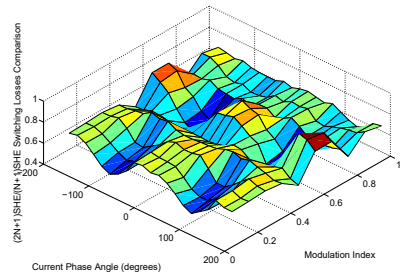

(b) Switching losses comparison: (2N+1) SHE-PWM / (N+1) SHE-PWM.

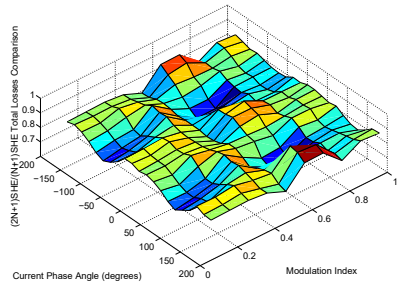

(c) Total losses comparison: (2N+1) SHE-PWM / (N+1) SHE-PWM.

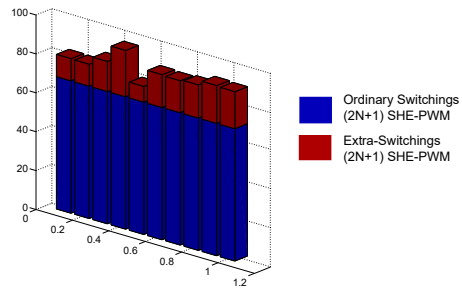

(d) Number of switchings in the fundamental period for (2N+1) SHE-PWM with 17 angles in the first QW, for a three-phase load of 24Ω & $8mH$.

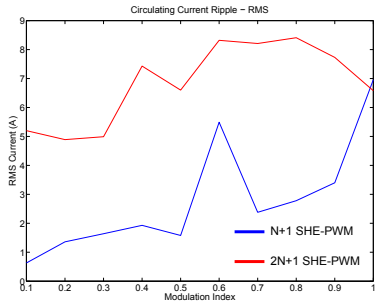

(e) i_{circ} ripple comparison between (2N+1) SHE-PWM and (N+1) SHE-PWM, for a three-phase load of 24Ω & $8mH$.

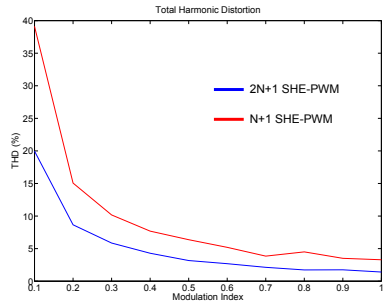

(f) THD comparison between (2N+1) SHE-PWM and (N+1) SHE-PWM for a three-phase load of 24Ω & $8mH$.

Figure 5.32: Comparison of losses between (2N+1) SHE-PWM and (N+1) SHE-PWM, where 17 firing angles have been used.

Regarding the switching losses depicted at Fig. 5.32-(b), (2N+1) SHE-PWM is much more efficient. In addition, the distribution of firing angles at table 5.1 provides a significant variation in the switching losses of (N+1) SHE-PWM when the current phase is modified, as it has been previously commented for $m_a = 0.1$, $m_a = 0.2$, $m_a = 0.3$, $m_a = 0.6$ and $m_a = 0.7$. On the other hand, for $m_a = 0.5$ there is a reduction in the switching losses of (2N+1) SHE-PWM due to the lower number of extra-switchings, which are depicted at Fig. 5.32-(d).

Fig. 5.32-(c) shows how (2N+1) SHE-PWM is more efficient than (N+1) SHE-PWM due to its lower switching losses throughout the m_a and current phase ranges. On the other, as it can be noticed at Fig. 5.32-(f), (2N+1) SHE-PWM also provides a lower THD throughout the m_a range. However, (N+1) SHE-PWM provides a lower i_{circ} ripple, as it is shown at Fig. 5.32-(e).

Finally, in case of a low effective switching frequency, the switching losses of (N+1) SHE-PWM could be higher due to the requirement of extra-switchings, as it was described at section 5.3.4. Fig. 5.33 shows the number of extra-switchings required when 9 firing angles are utilized in the first QW. The extra switchings represent a 30%, approximately, with respect to the ordinary switchings.

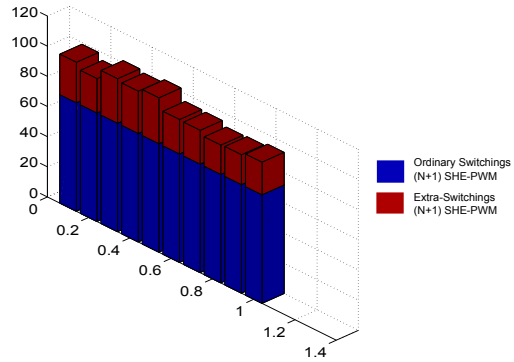

Figure 5.33: Extra switchings to improve the balancing operation of (N+1) SHE-PWM when the effective switching frequency is low ($f_{effective-sw} < 2f$). The number of firing angles in the first QW is 9 and $f = 50$Hz.

5.6 Experimental Results

The i_{circ} control technique proposed for (2N+1) SHE-PWM has been validated experimentally in a laboratory prototype of a single-phase MMC, which is depicted at Figs. 5.34-(a) and 5.34-(b). The set-up features are included at table

Table 5.4. Specifications for the Experimental Setup

Parameter	Value	
# of SMs per arm, N	5	
dc link Voltage, V_{dc}	$250V$	
SM capacitor, C	$3.6mF$	
SM capacitor voltage, V_C	$50V$	
Arm inductor, L	$3.6mH$	
i_{circ} ripple threshold	$2A$	
Initial Load, R_L and L_L	22Ω and $4mH$	
Final Load, R_L and L_L	11Ω and $4mH$	
# of Angles, per QW, for (2N+1) SHE	9	17
Fundamental frequency, f	$100Hz$	$50Hz$
First non-eliminated harmonic	$1900Hz$	$1750Hz$
Modulation index, m_a	0.9	0.9
PI control for dc-link voltage	P=0.0015, I=0.009	
Arm energy balance control, K	0.05	

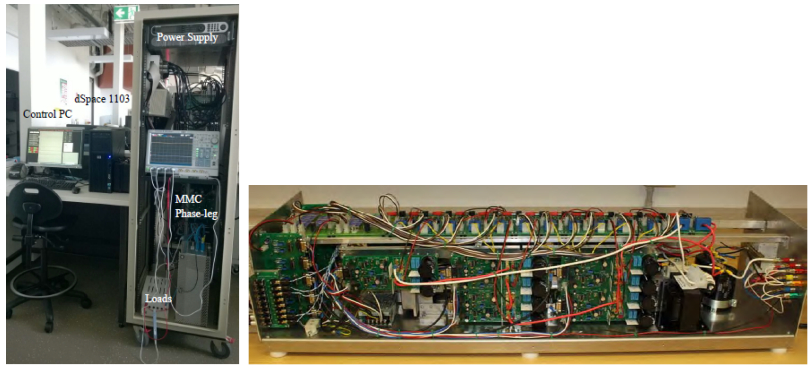

(a) Laboratory set-up. (b) Single phase MMC prototype with 5 SMs at every arm.

Figure 5.34. Prototype of a single-phase MMC.

5.4. The modulation, balancing algorithm and circulating current control are implemented using the dSPACE 1103 board [185]. Due to the utilization of a single-phase system and with the aim of obtaining a high quality output signal, the lower-order odd harmonics will be eliminated, including the triple ones. Two experiments have been realized using an f value equal to 100Hz and 50Hz, respectively. The experimental results are disclosed at Figs. 5.35 and 5.36. To obtain these results, 9 firing angles have been utilized when f = 100Hz. In the same way, 17 angles have been used when f = 50Hz. Therefore, the switching frequency remains the same in both experiments. In addition, a change of load

from 22Ω and 4mH to 11Ω and 4mH has been forced at the instants 0.445s and 1.04s, respectively.

Figs. 5.35-(a) and 5.36-(a) show the phase output voltage generated by the converter. A correct elimination of the undesired harmonics in the output voltage spectrum is demonstrated in Figs. 5.35-(b) and 5.36-(b).

Figs. 5.35-(c) and 5.36-(c) display the arm currents. The DC component of the circulating current reference is tracked correctly, even during the transient state created by the load change. This fact can also be noticed at Figs. 5.35-(g) and 5.36-(g) which show the circulating current, whose DC component is increased when the load current is incremented. At both experiments, the i_{circ} ripple has been limited to 2A.

Figs. 5.35-(e), 5.35-(f), 5.36-(e) and 5.36-(f) show the upper and lower arm capacitor voltages. The SM capacitor voltage ripple is lower than 10%. Moreover, a correct balance between the capacitor voltages is achieved. On the other hand, Figs. 5.35-(e) and 5.35-(f) show a small deviation of the SM capacitor voltages from 50V after the load change. However, this deviation is corrected at instant 0.6s. This effect has happened because, although the proposed i_{circ} control is able to follow the i_{circ} reference correctly, it is not as fast and accurate as other controls based on PWM, which utilize higher switching frequencies and provide lower circulating current ripple. Consequently, after a load change, the SM capacitor voltages experience a slight deviation that is compensated after a transitory period.

Finally, the sampling frequency utilized to measure the arm currents was 40kHz due to the required accuracy to detect the instant when the circulating current exceeds any of the two thresholds, with the aim of not increasing the i_{circ} ripple. However, an analogue detector may be used to detect the instant when the circulating current exceeds the thresholds. In this way, the arm currents should be measured just before every firing angle. Using this technique, a low sampling frequency would be required, whose value would be given by (5.15), where l is the number of firing angles in the first QW and f is the fundamental frequency.

$$f_{sampling} = 2lf, \tag{5.15}$$

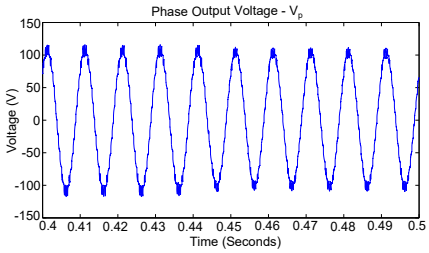

(a) V_a waveform.

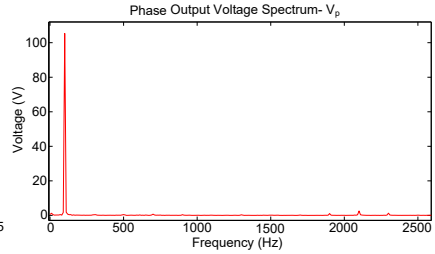

(b) V_a spectrum.

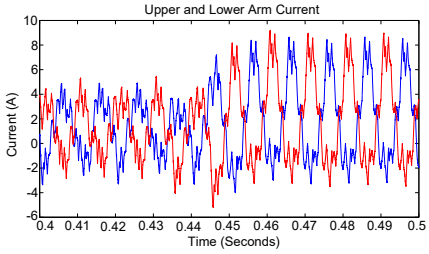

(c) Upper and lower arm currents.

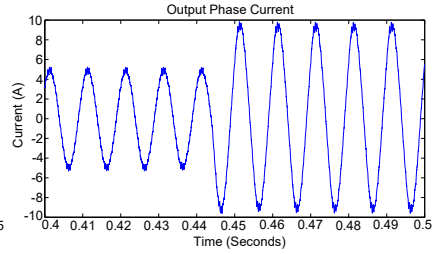

(d) Output phase current.

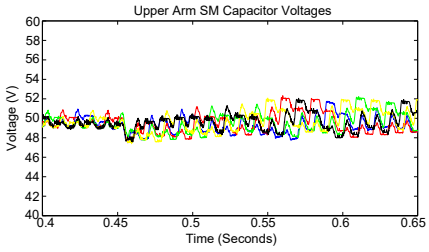

(e) Upper SM capacitor voltages.

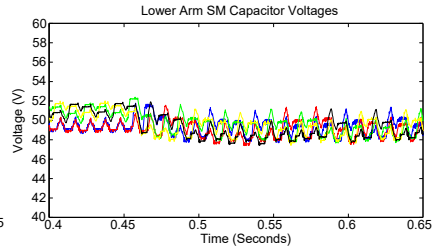

(f) Lower SM capacitor voltages.

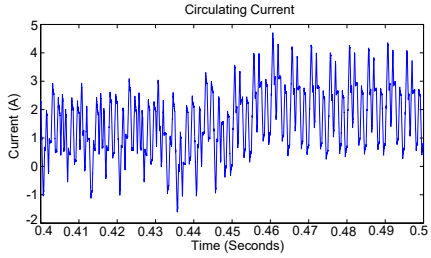

(g) Circulating current.

Figure 5.35: Experimental results for (2N+1) SHE-PWM with 9 angles in the first QW, f equal to 100Hz and m_a equal to 0.9.

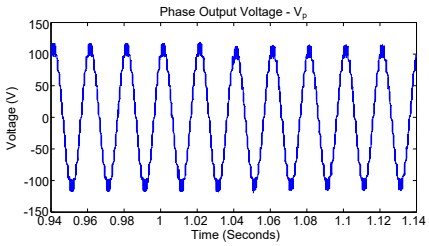

(a) V_a waveform.

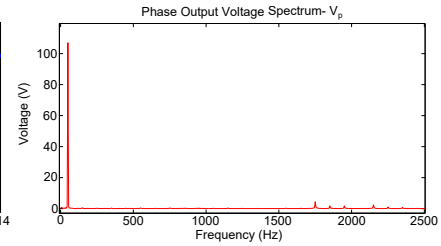

(b) V_a spectrum.

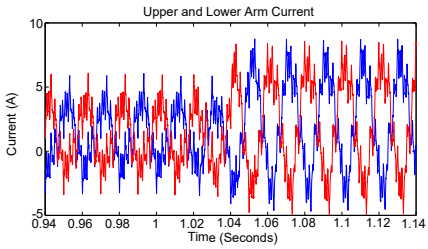

(c) Upper and lower arm currents.

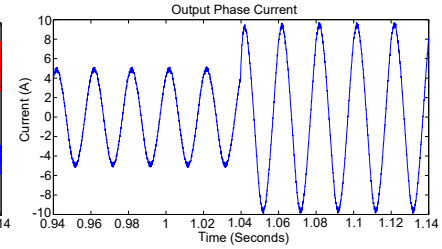

(d) Output phase current.

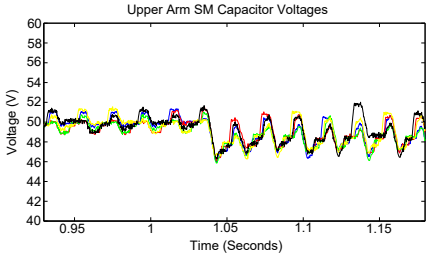

(e) Upper SM capacitor voltages.

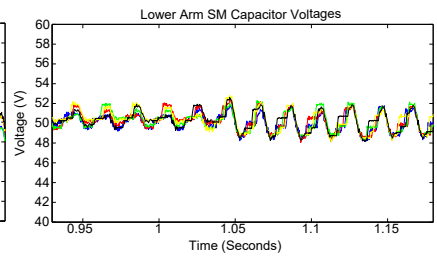

(f) Lower SM capacitor voltages.

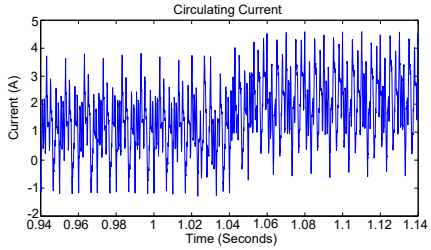

(g) Circulating current.

Figure 5.36: Experimental results for (2N+1) SHE-PWM with 17 angles in the first QW, f equal to 50Hz and m_a equal to 0.9.

5.7 Conclusion

Two circulating current control techniques for MMC, based on (N+1) SHE-PWM and (2N+1) SHE-PWM, respectively, have been presented. These controls are able to track a circulating current reference, regulating the averaged voltage of the SM capacitors and contributing to the energy balance between the converter arms. The first one, which operates along with (N+1) SHE-PWM, utilizes two different modulation indexes, m_1 and m_2, which are applied in the upper or lower arms, generating v_{diff} values which are useful to follow the i_{circ} reference. In addition, due to the utilization of constant values for m_1 and m_2 over the fundamental period, the phase output voltage is not disturbed by the control.

The second i_{circ} control technique, which operates with (2N+1) SHE-PWM, utilizes redundant voltage levels and is able to limit the i_{circ} ripple, regarding the low switching frequency and the uneven distance between adjacent firing angles, which are inherent to (2N+1) SHE-PWM.

Simulation results have been presented that corroborate the correct operation of the proposed algorithms when 34, 17 and 9 firing angles in the first QW are utilized. In case of (2N+1) SHE-PWM, successful experimental results have also been obtained. These facts prove the ability of the proposed methods to control a high number of voltage harmonics under different operating conditions, including different m_a, f and load values.

Regarding the efficiency studies, several conclusions have been extracted. Firstly, the conduction losses are very similar for all the regarded modulations, (N+1) SHE-PWM, (2N+1) SHE-PWM, PD-PWM and IPD-PWM. On the other hand, regarding the switching losses, significant differences between modulations have been found. Firstly, (N+1) SHE-PWM is more efficient than PD-PWM, providing similar THD. Secondly, (2N+1) SHE-PWM is more efficient with respect to IPD-PWM and provides a lower THD. On the other hand, comparing IPD-PWM and (N+1) SHE-PWM, the latter provides a higher efficiency for $m_a > 0.6$ but a higher THD throughout the m_a range. Comparing both (N+1) SHE-PWM and (2N+1) SHE-PWM, the second one is more efficient and provides a lower THD, eliminating the same number of harmonics. In addition, (N+1) SHE-PWM provides higher losses in case the effective switching frequency is lower than $2f$, approximately. However, (N+1) SHE-PWM provides lower SM capacitor voltage, i_{circ} and dc input current ripples than (2N+1) SHE-PWM.

As a result, the most efficient modulation technique is (2N+1) SHE-PWM along with the proposed i_{circ} control. In addition, when the number of SMs increases, the i_{circ} ripple provided by this modulation is reduced. On the other hand, for both (N+1) SHE-PWM and (2N+1) SHE-PWM (it also happens for PWM mo-

dulations), the SM capacitor voltage ripple will be increased in case the effective switching frequency is reduced. This trade-off must be considered in the design process.

All these facts corroborate the suitability of the proposed algorithms to control MMCs with low number of SMs as those used in MV applications.

Chapter 6

Conclusions and Future Work

6.1 Conclusions

Voltage source converters have acquired a high relevance in medium voltage applications, such as medium voltage drives, due to their advantages with respect to current source converters. In particular, VSCs provide lower switching losses than CSC-PWM converters due to the lower number of semiconductors connected in series. Comparing with LCCs, the MVSCs provide several advantages, such as extended operating range, reduced line harmonics, fast and decoupled control of bi-directional active and reactive power flow, black start capability and insensitivity to the strength of the ac network, among others.

Regarding the existing VSCs, multilevel voltage source converters (MVSCs) provide lower effective switching frequency than two level converters, providing a higher efficiency. In addition, a lower total harmonic distortion is obtained due to the multilevel characteristic, which makes it possible for the converter to follow the reference signal more accurately. In addition, lower dV/dt, lower common-mode voltage, smaller and simpler harmonic filters, together with lower insulation requirements make the multilevel topologies a suitable option for medium/high voltage applications.

Among the existing MVSCs, MMCs provide several advantages such as low losses, high scalability and low effective switching frequency due to its modularity, be-

sides mechanical simplicity or transformerless connection. Therefore, it is a suitable converter to be employed in medium voltage (MV) and high power applications. Particularly, the indirect topology can be employed in different medium voltage applications, such as MVDC networks or MV motor drives. In this way, a low switching frequency modulation such as SHE-PWM can improve the MMC performance, providing simultaneously low switching losses and low THD under different operating conditions. Depending on the switching scheme, there are two different kinds of SHE-PWM waveforms provided by the MMC, (N+1) SHE-PWM and (2N+1) SHE-PWM.

Two main challenges must be met to utilize SHE-PWM with indirect MMCs. Firstly, a high number of harmonics must be controlled throughout the m_a range. In this way, a wide range of fundamental frequencies, utilizing a similar switching frequency and different m_a values can be employed. On the other hand, the circulating current must be controlled to improve the efficiency and the operation of the MMC, but without disturbing the phase output voltage. However, the present circulating current controls provide several drawbacks, such as phase output voltage distortion or excessive circulating current ripple, in case they are applied along with SHE-PWM.

As a result, this thesis have addressed both issues:

- **SHE-PWM implementation**: Previous work on SHE-PWM problem searches the firing angles using a predefined switching pattern. In multilevel converters such as MMCs, this switching pattern may not provide a solution to the SHE-PWM problem for a particular m_a. In that case, the switching pattern should be replaced by another one and the search should be restarted. Moreover, the utilization of different switching patterns is required to find a solution throughout the m_a range. Therefore, a method which is able to calculate simultaneously the switching pattern and the associated firing angles without using a predefined waveform would simplify the search process, particularly when the number of possible switching patterns is significantly high.

  In this way, two novel formulations to solve the SHE-PWM problem with QW and HW symmetries, respectively, have been presented. These methods are able to search simultaneously both the firing angles and the switching patterns, throughout the m_a range, without using predefined waveforms. To this end, a universal equation has been defined, which is valid for any possible waveform. The search algorithm, which is based on genetic algorithms, utilizes a novel objective function which disregards invalid solutions. In addition, the proposed search method is able to find several solutions for the same m_a value. Finally, a local search has been

designed, which is able to obtain continuous sets of solutions throughout the m_a range.

As a conclusion, the proposed formulations simplify significantly the search process with respect to previous works and are able to provide a high number of waveforms which are not predefined beforehand. In addition, a high number of harmonics can be controlled simultaneously.

- **Circulating current control techniques**: two circulating current control techniques for MMC, based on (N+1) SHE-PWM and (2N+1) SHE-PWM, respectively, have been presented. These controls are able to track a circulating current reference, regulating the averaged voltage of the SM capacitors and contributing to the energy balance between the converter arms. In addition, the phase output voltage is not disturbed.

  An efficiency study has been realized where (N+1) SHE-PWM, (2N+1) SHE-PWM, PD-PWM and IPD-PWM have been compared. In particular, in this study, (N+1) SHE-PWM and (2N+1) SHE-PWM provide the same first non-eliminated harmonic, f_{harm}. In addition, PD-PWM and IPD-PWM also provide the first band of harmonics located in f_{harm}. The different modulations have been tested under equal operating conditions.

  As a result, several conclusions have been extracted:

  – (2N+1) SHE-PWM, along with the proposed i_{circ} control, provides higher efficiency and lower THD than PD-PWM, IPD-PWM and (N+1) SHE-PWM, throughout the m_a range

  – (N+1) SHE-PWM provides lower SM capacitor voltage ripple, besides lower i_{circ} and dc input current ripples than (2N+1) SHE-PWM

  – (N+1) SHE-PWM, along with its proposed i_{circ} control, provides higher efficiency and similar THD than PD-PWM, throughout the m_a range. In addition, (N+1) SHE-PWM provides higher efficiency than IPD-PWM when $m_a > 0.6$. However, the efficiency of (N+1) SHE-PWM is reduced when the effective switching frequency is approximately lower than $2f$, where f is the fundamental frequency, due to the requirement of extra-switchings to improve the SM capacitor voltage balancing

  Summarizing, under equal number of phase output voltage levels, (N+1) or (2N+1), SHE-PWM techniques provide higher efficiency than PWM techniques. In addition, (2N+1) SHE-PWM is the most efficient modulation technique. However, the modulations which provide (N+1) levels, also provide lower i_{circ} and dc input current ripples. Depending on the application,

if reducing these ripples is required, (N+1) SHE-PWM is an interesting modulation. In this way, both (N+1) SHE-PWM and (2N+1) SHE-PWM are suitable techniques to operate MMCs in medium voltage applications where the number of sub-modules is not high.

Simulation results have validated the proposed SHE-PWM formulations, with QW and HW symmetries, besides the circulating current control techniques proposed for (N+1) SHE-PWM and (2N+1) SHE-PWM. In addition, experimental results, obtained from a prototype of single-phase MMC, have validated the formulation with QW symmetry and the circulating current control proposed for (2N+1) SHE-PWM.

6.2 Main Publications Derived from this Thesis

The main publications derived from this thesis are the following:

- Publications in international journals:

  1. [179] A. Perez-Basante, S. Ceballos, G. Konstantinou, J. Pou, J. Andreu and I. Martinez de Alegria, "(2N+1) Selective Harmonic Elimination-PWM for Modular Multilevel Converters: A Generalized Formulation and A Circulating Current Control Method," in *IEEE Transactions on Power Electronics* , vol.PP, no.99, pp.1-1. Accepted for publication: Feb. 2017. JCR (2015): 4.953. doi: 10.1109/TPEL.2017.2666847

- Publications in international conferences:

  1. [178] A. Pérez-Basante, S. Ceballos, G. Konstantinou, J. Pou, J. Andreu and I. Martinez de Alegria, "A universal formulation for selective harmonic elimination PWM with half-wave symmetry for multilevel voltage source converters," 42^{nd} *Annual Conference of the IEEE Industrial Electronics Society (IECON)*, Florence, 2016, pp. 3207-3212. doi: 10.1109/IECON.2016.7793505

  2. [97] A. Pérez-Basante, S. Ceballos, G. Konstantinou, M. Liserre, J. Pou and I. Martinez de Alegria, "Circulating current control for modular multilevel converter based on selective harmonic elimination with ultra-low switching frequency," *18th European Conference on Power Electronics and Applications (EPE-ECCE)*, Karlsruhe, 2016, pp. 1-10. doi: 10.1109/EPE.2016.7695372

3. [13] A. Perez-Basante, S. Ceballos, J. Pou, A. Gil de Muro, A. Pujana and P. Ibanez, "SiC Modular Multilevel Converters: Sub-Module Voltage Ripple Analysis and Efficiency Estimations," *International Exhibition and Conference for Power Electronics, Intelligent Motion, Renewable Energy and Energy Management (PCIM Europe)*, Nuremberg, Germany, 2014, pp. 1-8.

4. [74] A. Perez-Basante, J. I. Garate, I. Martinez de Alegria, I. Kortabarria and J. Andreu, "Controlled Square Wave High Frequency Rectifier," *International Exhibition and Conference for Power Electronics, Intelligent Motion, Renewable Energy and Energy Management (PCIM Europe)*, Nuremberg, Germany, 2014, pp. 1-8.

- Publications in national conferences:

1. [177] A. Perez-Basante, I. Martinez de Alegria, J. I. Garate, S. Ceballos and J. L. Martin, "Eliminación Selectiva de Armónicos en Convertidores Multinivel Modulares para todo el Rango del Índice de Modulación de Amplitud" *Seminario Anual de Automática, Electrónica Industrial y Automatización (SAAEI)*, Tangier, Morocco, 2014, pp. 1-6

6.3 Future Work

During the progress of this work, several suggestions for future work have arisen:

1. **Circulating current control technique with (N+1) SHE-PWM:** With the aim of validating the proposed circulating current control with (N+1) SHE-PWM, in the near future, experimental results will be obtained. These results will be submitted to a specialized journal.

2. **On-line method to solve SHE-PWM:** The proposed formulations in this thesis to solve the SHE-PWM problem have been used with an off-line technique, such as genetic algorithms. However, the application of these formulations with on-line calculation methods such as neural networks or model predictive control would be interesting. The on-line techniques eliminate the requirement of look-up tables. In this way, a research line based on on-line calculation methods is proposed.

3. **Employment of MMC with SHE-PWM in drive applications:** The MMC could be utilized in drive applications. In this way, a research line is proposed where SHE-PWM, along with the proposed circulating cu-

rrent control techniques, are utilized for a particular fundamental frequency range. The objective would be to increase the efficiency of the MMC. For very low fundamental frequencies, PWM and its associated circulating current control techniques must be applied. The required number of eliminated harmonics at every fundamental frequency should be studied and the external control should be implemented. Finally, the control architecture should be validated in a prototype.

4. **Employment of MMC with SHE-PWM in medium voltage multiterminal direct current networks (MVMTDC):** A research line focused on MVMTDCs, where MMCs are modulated by SHE-PWM, is proposed with the aim of increasing the efficiency of these networks. In this way, the external controls should be implemented and validated along with SHE-PWM and the proposed circulating current control techniques. The control architecture should be validated in a MTDC prototype.

6.4 Acknowledgements

This work has been carried out inside de Research and Education Unit UFI11/16 of the UPV/EHU and supported by the Department of Education, Linguistic Policy and Culture of the Basque Government within the fund for research groups of the Basque university system IT978-16. This work has also been supported in part by Zabalduz program, a UPV/EHU PhD scholarship funding and in part by the Basque Government within the research program ELKARTEK under the projects KK-2015/00091-HVDCL-1, KK-2016/00038-HVDCL-2, HVDCLINK-3, KK-2015/00047-KT4TRANS and KK-2016/00061-KT4TRANS and within the research program ETORTEK under the project IE14-389.

Appendix A

Algorithm Results for A Low Number of Controlled Harmonics

This chapter contains the performance factors, defined at section 4.7.1, corresponding to the solutions obtained for the following cases (where ϕ_1 is the fundamental phase given by (4.14b):

- Case I: MMC with 7 levels and 4 firing angles with QW symmetry.
- Case II: MMC with 7 levels and 8 firing angles with HW symmetry and $\phi_1 = \pi/2$.
- Case III: MMC with 9 levels and 4 firing angles with QW symmetry.
- Case IV: MMC with 9 levels and 8 firing angles with HW symmetry and $\phi_1 = \pi/2$.
- Case V: MMC with 9 levels and 6 firing angles with QW symmetry.
- Case VI: MMC with 9 levels and 12 firing angles with HW symmetry and $\phi_1 = \pi/2$.

The analysis of these results has been realized at section 4.7. In particular, every table contains the following data:

- Table A.1: performance indexes of solutions obtained for case I

- Table A.2: performance indexes of solutions obtained for case II, with initial level $L_i = 0$.
- Table A.3: performance indexes of solutions obtained for case II, with initial level $L_i = 1$.
- Table A.4: comparison of HLF values given by the best solutions of case II, with $L_i = 0$ and $L_i = 1$.
- Table A.5: performance indexes of solutions obtained for case III
- Table A.6: performance indexes of solutions obtained for case IV, with initial level $L_i = 0$.
- Table A.7: performance indexes of solutions obtained for case IV, with initial level $L_i = 1$.
- Table A.8: comparison of HLF values given by the best solutions of case IV, with $L_i = 0$ and $L_i = 1$.
- Table A.9: performance indexes of solutions obtained for case V
- Table A.10: performance indexes of solutions obtained for case VI, with initial level $L_i = 0$.
- Table A.11: performance indexes of solutions obtained for case VI, with initial level $L_i = 1$, part I.
- Table A.12: performance indexes of solutions obtained for case VI, with initial level $L_i = 1$, part II.
- Table A.13: comparison of HLF values given by the best solutions of case VI, with $L_i = 0$ and $L_i = 1$.

The best solutions for every performance factor are depicted in red colour.

Table A.1. QW Solutions for 7 levels and 4 firing angles (Case I)

Mod. Index	Peformance Factors	Sol. 1	Sol. 2	Sol. 3	Sol. 4	Sol. 5
	THD (%)	118.94				
	HDF (%)	83.88				
0.1	HLF (%)	6.11				
	3rd Harm. (%)	46.89				
	9th Harm. (%)	17.64				
	THD (%)	47.94	50.58	57.28	51.78	49.75
	HDF (%)	13.79	26.49	35.27	28.47	28.89
0.2	HLF (%)	1.92	2.22	3.12	2.55	2.35
	3rd Harm. (%)	79.99	123.87	46.09	80.00	211.57
	9th Harm. (%)	43.22	36.88	14.97	66.93	29.35
	THD (%)	42.33	38.91	45.64		
	HDF (%)	35.53	28.43	36.81		
0.3	HLF (%)	2.55	2.12	2.78		
	3rd Harm. (%)	93.17	3.89	62.53		
	9th Harm. (%)	26.31	42.15	9.70		
	THD (%)	24.75	25.71	37.64		
	HDF (%)	16.06	14.66	22.65		
0.4	HLF (%)	1.29	1.21	1.99		
	3rd Harm. (%)	34.64	61.58	26.35		
	9th Harm. (%)	10.88	23.90	17.03		
	THD (%)	26.99	22.57	21.77		
	HDF (%)	21.56	16.56	14.19		
0.5	HLF (%)	1.74	1.08	1.16		
	3rd Harm. (%)	85.74	3.54	34.12		
	9th Harm. (%)	11.37	20.18	20.97		
	THD (%)	14.03	15.49	14.03	14.25	
	HDF (%)	3.87	4.19	4.21	2.40	
0.6	HLF (%)	0.53	0.59	0.50	0.51	
	3rd Harm. (%)	42.68	17.71	10.26	60.51	
	9th Harm. (%)	5.61	11.03	17.73	4.99	
	THD (%)	14.05	18.24	13.78	14.57	
	HDF (%)	6.28	13.57	5.64	4.51	
0.7	HLF (%)	0.63	1.08	0.60	0.63	
	3rd Harm. (%)	42.53	4.33	17.80	2.61	
	9th Harm. (%)	5.74	3.58	13.56	3.48	
	THD (%)	11.38	17.08			
	HDF (%)	3.93	13.98			
0.8	HLF (%)	0.44	1.09			
	3rd Harm. (%)	21.56	1.75			
	9th Harm. (%)	10.20	3.30			
	THD (%)	13.25	11.65	14.16		
	HDF (%)	10.50	8.76	10.64		
0.9	HLF (%)	0.80	0.63	0.74		
	3rd Harm. (%)	13.29	13.33	30.42		
	9th Harm. (%)	3.85	17.44	8.96		
	THD (%)	8.44				
	HDF (%)	2.44				
1	HLF (%)	0.26				
	3rd Harm. (%)	2.89				
	9th Harm. (%)	12.19				

Table A.2: HW Solutions for 7 levels and 8 firing angles with initial level 0 (Case II)

Mod. Index	Performance Factors	Sol. 1	Sol. 2	Sol. 3	Sol. 4	Sol. 5	Sol. 6	Sol. 7	Sol. 8
	THD (%)	136.14							
	HDF (%)	103.93							
0.1	HLF (%)	7.51							
	3rd Harm. (%)	85.20							
	9th Harm. (%)	46.19							
	THD (%)	53.71	53.68	55.83	52.05				
	HDF (%)	32.49	32.41	33.13	31.84				
0.2	HLF (%)	2.49	2.48	2.55	2.42				
	3rd Harm. (%)	72.32	147.76	92.20	101.76				
	9th Harm. (%)	29.12	19.82	22.94	37.18				
	THD (%)	43.20	44.26						
	HDF (%)	34.96	36.66						
0.3	HLF (%)	2.61	2.71						
	3rd Harm. (%)	21.64	19.61						
	9th Harm. (%)	24.13	21.33						
	THD (%)	30.03	26.13						
	HDF (%)	19.25	14.44						
0.4	HLF (%)	1.58	1.15						
	3rd Harm. (%)	44.86	17.86						
	9th Harm. (%)	11.22	2.53						
	THD (%)	23.85	23.89	23.02	23.99				
	HDF (%)	15.39	15.77	17.14	13.76				
0.5	HLF (%)	1.31	1.20	1.32	1.23				
	3rd Harm. (%)	30.76	55.50	27.74	35.01				
	9th Harm. (%)	7.78	8.31	24.45	11.66				
	THD (%)	14.13	14.40	16.01	14.03	14.50	15.83	14.08	14.02
	HDF (%)	4.07	4.32	9.68	3.88	4.12	9.53	3.92	4.11
0.6	HLF (%)	0.53	0.54	0.75	0.53	0.54	0.74	0.53	0.51
	3rd Harm. (%)	32.86	30.90	40.72	42.68	11.32	40.65	32.15	10.26
	9th Harm. (%)	8.44	6.60	7.95	5.61	17.41	7.80	8.84	17.74
	THD (%)	13.97	14.62	14.04	14.35	16.78	16.52		
	HDF (%)	5.07	6.48	6.25	6.43	12.81	12.60		
0.7	HLF (%)	0.60	0.65	0.63	0.64	1.00	0.98		
	3rd Harm. (%)	10.50	43.31	42.57	43.33	57.16	9.11		
	9th Harm. (%)	14.65	6.61	5.73	6.54	3.44	8.62		
	THD (%)	11.39	14.84						
	HDF (%)	2.98	9.43						
0.8	HLF (%)	0.41	0.80						
	3rd Harm. (%)	7.61	12.86						
	9th Harm. (%)	10.55	9.97						
	THD (%)	13.25	12.63						
	HDF (%)	10.51	9.44						
0.9	HLF (%)	0.80	0.67						
	3rd Harm. (%)	13.23	25.79						
	9th Harm. (%)	3.84	5.01						
	THD (%)	11.19	10.74	12.62	9.28				
	HDF (%)	5.63	5.53	9.77	4.03				
1	HLF (%)	0.49	0.48	0.74	0.38				
	3rd Harm. (%)	3.86	3.84	10.45	26.58				
	9th Harm. (%)	6.12	6.13	8.24	8.09				
	THD (%)	9.88							
	HDF (%)	6.85							
1.1	HLF (%)	0.50							
	3rd Harm. (%)	9.42							
	9th Harm. (%)	4.05							

Table A.3: HW Solutions for 7 levels and 8 firing angles with initial level $L_i = 1$ ($L_i = -1$ for symmetric solutions) (Case II)

Mod. Index	Performance Factors	Sol. 1	Sol. 2	Sol. 3	Sol. 4	Sol. 5	Sol. 6
	THD (%)	119.10					
	HDF (%)	78.31					
0.1	HLF (%)	5.97					
	3rd Harm. (%)	192.80					
	9th Harm. (%)	128.04					
	THD (%)	50.54	53.65	55.90	55.72		
	HDF (%)	28.64	32.41	33.21	32.51		
0.2	HLF (%)	2.43	2.49	2.53	2.50		
	3rd Harm. (%)	162.68	70.55	116.11	126.79		
	9th Harm. (%)	46.32	53.26	31.64	47.00		
	THD (%)	41.04	44.64	40.10	41.39	38.48	
	HDF (%)	34.15	36.90	32.65	27.97	24.16	
0.3	HLF (%)	2.51	2.83	2.34	2.34	1.86	
	3rd Harm. (%)	106.81	85.38	140.99	77.19	93.52	
	9th Harm. (%)	12.50	23.44	18.66	29.30	26.79	
	THD (%)	25.95	25.21				
	HDF (%)	15.47	16.07				
0.4	HLF (%)	1.22	1.28				
	3rd Harm. (%)	87.71	88.46				
	9th Harm. (%)	13.86	5.80				
	THD (%)	22.82	23.19	24.17	24.54		
	HDF (%)	16.50	13.39	18.86	18.76		
0.5	HLF (%)	1.29	1.10	1.46	1.47		
	3rd Harm. (%)	56.73	47.65	56.06	41.44		
	9th Harm. (%)	17.71	12.90	14.25	2.45		
	THD (%)	14.13	14.06	17.08	14.15	17.52	
	HDF (%)	4.08	3.80	8.77	2.99	11.34	
0.6	HLF (%)	0.54	0.53	0.79	0.53	0.88	
	3rd Harm. (%)	71.88	34.52	46.45	42.36	38.14	
	9th Harm. (%)	14.59	5.61	9.97	9.62	7.71	
	THD (%)	14.93	14.17	16.68	15.46	17.30	16.63
	HDF (%)	8.27	6.02	12.74	8.89	12.69	12.68
0.7	HLF (%)	0.67	0.61	1.00	0.79	1.06	1.00
	3rd Harm. (%)	48.19	36.85	57.17	23.94	26.53	9.32
	9th Harm. (%)	8.89	5.64	3.52	19.03	12.21	8.66
	THD (%)	15.57	15.65				
	HDF (%)	7.64	10.49				
0.8	HLF (%)	0.75	0.84				
	3rd Harm. (%)	39.23	34.94				
	9th Harm. (%)	12.16	3.35				
	THD (%)	13.14	12.83				
	HDF (%)	6.81	6.60				
0.9	HLF (%)	0.60	0.63				
	3rd Harm. (%)	23.48	22.35				
	9th Harm. (%)	8.07	4.52				

Table A.4. Solutions with lowest HLF for $L_i = 0$ and $L_i = 1$ for case II

Mod. Index	0.1	0.2	0.3	0.4	0.5	0.6	0.7	0.8	0.9	1	1.1
$L_i = 0$	7.51	2.42	2.61	1.15	1.2	0.51	0.6	0.41	0.67	0.38	0.5
$L_i = 1$	5.97	2.43	1.86	1.22	1.1	0.53	0.61	0.75	0.6	-	-

Table A.5. QW Solutions for 9 levels and 4 firing angles (Case III)

Mod. Index	Peformance Factors	Sol. 1	Sol. 2	Sol. 3	Sol. 4
0.1	THD (%)	90.00	90.18		
	HDF (%)	67.88	36.30		
	HLF (%)	4.91	4.43		
	3rd Harm. (%)	46.64	230.38		
	9th Harm. (%)	16.96	16.79		
0.2	THD (%)	44.98	49.59	52.16	
	HDF (%)	27.46	35.47	40.72	
	HLF (%)	2.21	2.94	3.31	
	3rd Harm. (%)	45.03	79.72	89.43	
	9th Harm. (%)	11.21	6.86	14.44	
0.3	THD (%)	25.72	24.77	37.64	
	HDF (%)	14.64	16.06	22.64	
	HLF (%)	1.21	1.28	1.99	
	3rd Harm. (%)	61.60	34.66	26.35	
	9th Harm. (%)	23.85	10.95	17.03	
0.4	THD (%)	20.85			
	HDF (%)	15.64			
	HLF (%)	1.00			
	3rd Harm. (%)	1.93			
	9th Harm. (%)	19.83			
0.5	THD (%)	15.97	14.63		
	HDF (%)	5.84	2.26		
	HLF (%)	0.71	0.54		
	3rd Harm. (%)	42.54	16.06		
	9th Harm. (%)	5.58	15.10		
0.6	THD (%)	11.00	17.08	11.36	
	HDF (%)	1.75	13.98	3.89	
	HLF (%)	0.37	1.09	0.43	
	3rd Harm. (%)	42.25	1.76	21.60	
	9th Harm. (%)	5.28	3.30	10.21	
0.7	THD (%)	9.77	10.83	11.37	
	HDF (%)	1.18	7.86	8.28	
	HLF (%)	0.33	0.60	0.66	
	3rd Harm. (%)	42.13	12.33	33.78	
	9th Harm. (%)	5.12	3.06	10.19	
0.8	THD (%)	8.47			
	HDF (%)	1.68			
	HLF (%)	0.27			
	3rd Harm. (%)	30.99			
	9th Harm. (%)	5.13			
0.9	THD (%)	9.18			
	HDF (%)	6.12			
	HLF (%)	0.49			
	3rd Harm. (%)	13.87			
	9th Harm. (%)	0.57			
1	THD (%)	7.17			
	HDF (%)	4.38			
	HLF (%)	0.33			
	3rd Harm. (%)	2.81			
	9th Harm. (%)	3.24			

Table A.6: HW Solutions for 9 levels and 8 firing angles with initial level 0 (Case IV)

Mod. Index	Performance Factors	Sol. 1	Sol. 2	Sol. 3	Sol. 4
	THD (%)	103.78			
	HDF (%)	79.39			
0.1	HLF (%)	5.80			
	3rd Harm. (%)	84.16			
	9th Harm. (%)	43.72			
	THD (%)	45.90	49.27	46.03	
	HDF (%)	30.82	39.41	23.49	
0.2	HLF (%)	2.63	2.92	2.35	
	3rd Harm. (%)	79.20	30.79	65.49	
	9th Harm. (%)	32.62	16.99	25.00	
	THD (%)	26.47	30.03	28.66	26.14
	HDF (%)	11.60	19.25	18.50	14.44
0.3	HLF (%)	1.20	1.58	1.37	1.15
	3rd Harm. (%)	16.04	44.86	37.44	17.85
	9th Harm. (%)	22.09	11.22	16.24	2.52
	THD (%)	22.29	23.91	21.72	
	HDF (%)	14.47	16.45	15.54	
0.4	HLF (%)	1.08	1.37	1.05	
	3rd Harm. (%)	24.16	44.44	49.83	
	9th Harm. (%)	16.05	16.37	6.31	
	THD (%)	16.46	19.29		
	HDF (%)	9.18	12.59		
0.5	HLF (%)	0.80	0.98		
	3rd Harm. (%)	47.48	8.82		
	9th Harm. (%)	10.67	9.51		
	THD (%)	14.77	13.19		
	HDF (%)	9.27	7.02		
0.6	HLF (%)	0.79	0.59		
	3rd Harm. (%)	12.98	18.65		
	9th Harm. (%)	10.09	12.67		
	THD (%)	10.84	10.64	11.25	
	HDF (%)	7.85	5.62	7.65	
0.7	HLF (%)	0.60	0.51	0.61	
	3rd Harm. (%)	12.33	13.22	16.72	
	9th Harm. (%)	3.05	9.91	6.96	
	THD (%)	9.61	9.75	9.59	
	HDF (%)	5.69	5.80	5.32	
0.8	HLF (%)	0.51	0.52	0.50	
	3rd Harm. (%)	19.97	5.34	7.62	
	9th Harm. (%)	7.69	5.26	7.42	
	THD (%)	7.84			
	HDF (%)	4.60			
0.9	HLF (%)	0.32			
	3rd Harm. (%)	17.77			
	9th Harm. (%)	2.00			

Table A.7: HW Solutions for 9 levels and 8 firing angles with initial level $L_i = 1$ ($L_i = -1$ for symmetric solutions) (Case IV)

Mod. Index	Performance Factors	Sol. 1	Sol. 2	Sol. 3	Sol. 4	Sol. 5
	THD (%)	90.17				
	HDF (%)	63.28				
0.1	HLF (%)	4.71				
	3rd Harm. (%)	135.97				
	9th Harm. (%)	87.73				
	THD (%)	45.87	40.34	50.09		
	HDF (%)	30.89	24.21	37.28		
0.2	HLF (%)	2.63	1.84	3.10		
	3rd Harm. (%)	79.49	50.03	81.73		
	9th Harm. (%)	33.07	31.02	18.72		
	THD (%)	30.72	25.78	25.06	32.82	
	HDF (%)	18.57	14.95	16.11	22.70	
0.3	HLF (%)	1.60	1.20	1.29	1.68	
	3rd Harm. (%)	84.38	88.02	88.44	40.16	
	9th Harm. (%)	25.10	14.09	6.17	18.50	
	THD (%)	20.35	24.06	23.71	20.80	
	HDF (%)	11.43	17.36	16.97	13.66	
0.4	HLF (%)	0.95	1.44	1.40	0.97	
	3rd Harm. (%)	47.33	34.82	53.64	42.05	
	9th Harm. (%)	15.37	5.59	5.37	8.72	
	THD (%)	18.18	17.22	16.95	18.91	
	HDF (%)	11.91	9.35	11.38	12.15	
0.5	HLF (%)	0.94	0.79	0.88	1.01	
	3rd Harm. (%)	56.69	36.49	51.75	27.33	
	9th Harm. (%)	6.60	6.37	8.97	12.34	
	THD (%)	15.57	16.13			
	HDF (%)	7.64	10.51			
0.6	HLF (%)	0.75	0.84			
	3rd Harm. (%)	39.24	34.96			
	9th Harm. (%)	12.16	3.33			
	THD (%)	13.12	13.90	10.57	13.03	10.47
	HDF (%)	9.21	9.86	5.42	8.92	3.91
0.7	HLF (%)	0.72	0.82	0.46	0.75	0.43
	3rd Harm. (%)	40.25	14.07	26.04	13.52	18.35
	9th Harm. (%)	7.58	12.22	8.19	12.46	6.37
	THD (%)	9.34	9.50	9.43		
	HDF (%)	5.08	5.25	5.38		
0.8	HLF (%)	0.47	0.49	0.49		
	3rd Harm. (%)	18.63	32.52	10.88		
	9th Harm. (%)	9.23	3.86	5.49		
	THD (%)	8.77				
	HDF (%)	4.91				
0.9	HLF (%)	0.41				
	3rd Harm. (%)	20.62				
	9th Harm. (%)	7.69				

Table A.8. Solutions with lowest HLF for $L_i = 0$ and $L_i = 1$ for case IV

Mod. Index	0.1	0.2	0.3	0.4	0.5	0.6	0.7	0.8	0.9	1	1.1
$L_i = 0$	5.8	2.35	1.15	1.05	0.8	0.59	0.51	0.5	0.32	-	-
$L_i = 1$	4.71	1.84	1.2	0.95	0.79	0.75	0.43	0.47	0.41	-	-

Table A.9. QW Solutions for 9 levels and 6 firing angles (Case V)

Mod. Index	Peformance Factors	Sol. 1	Sol. 2	Sol. 3	Sol. 4	Sol. 5	Sol. 6	Sol. 7	Sol. 8	Sol. 9
	THD (%)	90.76	93.39							
	HDF (%)	67.11	70.33							
0.1	HLF (%)	3.43	3.78							
	3rd Harm. (%)	44.07	36.40							
	9th Harm. (%)	7.80	71.24							
	THD (%)	40.84	44.54	48.40	49.12	48.88	45.60	40.82	43.91	43.51
	HDF (%)	18.94	12.39	33.80	37.73	30.67	17.19	13.94	26.77	10.29
0.2	HLF (%)	1.20	1.44	1.84	2.01	1.85	1.53	1.22	1.63	1.36
	3rd Harm. (%)	42.80	41.95	5.42	100.29	58.21	41.34	42.71	178.57	42.29
	9th Harm. (%)	6.08	4.34	31.36	14.99	39.04	3.63	5.61	12.69	4.81
	THD (%)	26.67	26.77	24.20	26.73	33.05	26.37	24.69	27.41	
	HDF (%)	15.58	15.31	5.60	14.66	19.84	15.52	12.02	16.04	
0.3	HLF (%)	0.96	0.96	0.68	0.89	1.16	0.94	0.77	0.99	
	3rd Harm. (%)	40.84	6.65	24.75	17.28	88.10	71.27	18.60	60.40	
	9th Harm. (%)	3.24	26.21	7.61	32.63	34.33	7.54	26.33	9.35	
	THD (%)	21.78	22.59							
	HDF (%)	12.52	16.29							
0.4	HLF (%)	0.76	0.90							
	3rd Harm. (%)	54.20	70.56							
	9th Harm. (%)	3.53	17.23							
	THD (%)	15.52	15.07	15.02						
	HDF (%)	9.91	9.94	9.80						
0.5	HLF (%)	0.54	0.53	0.53						
	3rd Harm. (%)	14.40	16.03	16.01						
	9th Harm. (%)	14.94	16.88	16.92						
	THD (%)	13.63	15.08							
	HDF (%)	4.48	10.05							
0.6	HLF (%)	0.39	0.58							
	3rd Harm. (%)	16.95	13.91							
	9th Harm. (%)	0.81	5.30							
	THD (%)	12.92								
	HDF (%)	5.99								
0.7	HLF (%)	0.39								
	3rd Harm. (%)	41.85								
	9th Harm. (%)	4.75								
	THD (%)	9.78	9.19							
	HDF (%)	3.63	4.04							
0.8	HLF (%)	0.29	0.29							
	3rd Harm. (%)	30.07	12.24							
	9th Harm. (%)	3.26	3.48							
	THD (%)	7.96	7.96	7.17	7.59					
	HDF (%)	1.25	0.18	1.74	3.67					
0.9	HLF (%)	0.18	0.19	0.17	0.23					
	3rd Harm. (%)	16.64	9.70	14.66	24.29					
	9th Harm. (%)	7.62	12.91	1.76	6.81					
	THD (%)	8.61	8.70							
	HDF (%)	2.54	6.76							
1	HLF (%)	0.26	0.33							
	3rd Harm. (%)	3.23	0.56							
	9th Harm. (%)	5.17	0.65							
	THD (%)	7.52								
	HDF (%)	1.66								
1.1	HLF (%)	0.23								
	3rd Harm. (%)	8.23								
	9th Harm. (%)	1.58								

Table A.10: HW Solutions for 9 levels and 12 firing angles with initial level 0 (Case VI)

Mod. Index	Performance Factors	Sol. 1	Sol. 2	Sol. 3	Sol. 4	Sol. 5	Sol. 6	Sol. 7	Sol. 8	Sol. 9	Sol. 10
	THD (%)	99.27	98.63	99.77	95.16	90.79	93.32	95.75	99.19	99.78	
	HDF (%)	74.20	72.85	76.15	73.46	67.00	70.27	61.69	73.18	72.30	
0.1	HLF (%)	3.82	3.74	4.13	3.54	3.39	3.78	3.58	3.81	3.90	
	3rd Harm. (%)	66.16	113.75	48.37	327.23	107.59	36.59	122.98	139.18	61.82	
	9th Harm. (%)	21.88	84.89	109.48	19.51	62.71	71.26	66.29	28.14	62.05	
	THD (%)	45.16	53.99	44.85	47.19	49.10	44.97	47.19	49.65	49.50	52.79
	HDF (%)	22.46	38.91	31.93	23.76	37.09	32.77	25.87	34.62	36.67	39.05
0.2	HLF (%)	1.38	2.08	1.74	1.73	1.97	1.77	1.74	2.02	1.96	2.11
	3rd Harm. (%)	46.88	49.45	57.04	73.16	32.03	110.75	62.81	52.44	33.43	53.79
	9th Harm. (%)	11.74	12.86	38.35	22.26	43.10	27.62	18.56	39.34	5.79	54.83
	THD (%)	25.25	26.93	24.69	25.34	27.91	24.93	24.69	27.05	26.52	
	HDF (%)	7.60	15.95	7.46	13.16	15.42	8.01	7.59	15.75	15.10	
0.3	HLF (%)	0.77	0.99	0.72	0.83	0.94	0.75	0.73	0.96	0.92	
	3rd Harm. (%)	68.13	7.80	37.46	31.56	43.42	25.18	38.12	66.08	10.96	
	9th Harm. (%)	9.63	25.69	36.77	19.48	28.78	6.92	36.72	10.29	27.54	
	THD (%)	22.03	26.50	23.98	22.24						
	HDF (%)	9.85	19.92	16.65	12.54						
0.4	HLF (%)	0.71	1.09	0.97	0.72						
	3rd Harm. (%)	42.89	27.76	46.37	45.89						
	9th Harm. (%)	22.42	22.96	16.08	9.47						
	THD (%)	17.83	15.55	15.19	16.09	16.87	15.67	15.76			
	HDF (%)	11.13	8.75	10.02	10.29	8.21	10.39	10.46			
0.5	HLF (%)	0.61	0.49	0.54	0.56	0.57	0.56	0.56			
	3rd Harm. (%)	9.22	61.62	15.20	14.07	45.81	7.70	42.27			
	9th Harm. (%)	16.23	16.39	15.83	14.97	8.18	14.36	15.05			
	THD (%)	11.34	13.67	11.47	12.36	11.94	12.81	11.56	12.63	11.59	13.17
	HDF (%)	5.08	5.87	6.03	5.54	4.19	5.56	2.50	7.37	5.94	6.04
0.6	HLF (%)	0.32	0.44	0.36	0.36	0.34	0.41	0.30	0.41	0.35	0.39
	3rd Harm. (%)	28.50	27.26	41.21	15.19	15.21	36.54	15.87	20.73	42.13	42.15
	9th Harm. (%)	13.50	8.27	5.05	14.97	16.29	2.69	12.93	3.44	4.95	4.95
	THD (%)	10.94	12.36	10.42	12.06	10.14	11.27	12.17	11.83	12.45	11.88
	HDF (%)	1.84	7.16	3.86	5.69	4.18	6.50	8.06	6.88	5.63	7.02
0.7	HLF (%)	0.30	0.40	0.29	0.37	0.30	0.40	0.43	0.39	0.41	0.40
	3rd Harm. (%)	28.03	38.00	18.54	41.57	5.28	20.43	26.75	12.41	20.92	27.04
	9th Harm. (%)	7.38	7.22	12.26	4.52	0.02	8.16	3.46	8.37	11.92	8.90
	THD (%)	9.41	9.39	10.62							
	HDF (%)	3.94	4.00	5.72							
0.8	HLF (%)	0.30	0.30	0.35							
	3rd Harm. (%)	2.43	3.16	9.80							
	9th Harm. (%)	12.95	9.08	3.08							
	THD (%)	8.04	9.70	8.77	7.28	8.93	7.47	8.36			
	HDF (%)	0.76	5.01	3.67	1.66	4.81	1.33	4.44			
0.9	HLF (%)	0.19	0.33	0.27	0.18	0.31	0.17	0.28			
	3rd Harm. (%)	14.63	17.65	7.69	15.23	24.30	11.82	14.50			
	9th Harm. (%)	8.80	1.80	10.47	3.38	5.71	10.86	6.82			
	THD (%)	9.73	8.15								
	HDF (%)	7.15	3.64								
1	HLF (%)	0.37	0.24								
	3rd Harm. (%)	3.37	18.09								
	9th Harm. (%)	2.94	6.89								
	THD (%)	7.40	9.04	7.55	7.33						
	HDF (%)	3.66	6.17	4.18	4.16						
1.1	HLF (%)	0.24	0.33	0.26	0.25						
	3rd Harm. (%)	9.52	8.95	12.17	12.66						
	9th Harm. (%)	2.59	2.45	6.82	3.31						

Table A.11: HW Solutions for 9 levels and 12 firing angles with initial level $L_i = 1$ ($L_i = -1$ for symmetric solutions) - Part I (Case VI)

Mod. Index	Performance Factors	Sol. 1	Sol. 2	Sol. 3	Sol. 4	Sol. 5	Sol. 6	Sol. 7	Sol. 8	Sol. 9	Sol. 10
	THD (%)	106.27	99.86	94.27	98.47	95.71	94.50				
	HDF (%)	80.58	72.52	38.24	60.89	73.51	75.39				
0.1	HLF (%)	4.25	3.90	3.38	3.60	3.53	3.58				
	3rd Harm. (%)	91.35	63.60	255.00	218.19	325.09	249.65				
	9th Harm. (%)	33.67	58.91	44.97	86.32	20.52	88.95				
	THD (%)	44.21	48.82	41.50	46.38	48.19	41.07	48.54	42.27	50.21	40.84
	HDF (%)	27.92	35.16	17.44	31.71	35.13	25.26	36.06	27.67	37.72	13.35
0.2	HLF (%)	1.52	1.88	1.27	1.85	1.84	1.36	1.94	1.49	2.01	1.22
	3rd Harm. (%)	77.87	160.59	138.27	204.86	118.16	119.56	130.92	106.54	69.81	186.12
	9th Harm. (%)	56.69	37.07	39.89	14.79	16.11	30.38	18.53	18.41	49.36	17.17
	THD (%)	25.49	29.83	34.01	25.81	24.77	26.83	24.45	27.37	27.13	27.20
	HDF (%)	13.95	18.06	23.50	15.17	7.58	15.68	8.59	16.00	15.99	15.88
0.3	HLF (%)	0.83	1.09	1.26	0.87	0.73	0.97	0.69	0.99	0.98	0.98
	3rd Harm. (%)	87.12	88.51	56.48	75.76	98.50	99.63	87.67	85.16	108.51	75.34
	9th Harm. (%)	20.83	16.27	19.60	30.91	23.87	48.80	21.29	19.95	6.89	20.36
	THD (%)	22.61	22.33	21.44	21.08	23.35	24.13	23.48	22.19	23.87	22.92
	HDF (%)	16.24	5.85	11.57	9.53	17.50	16.84	15.80	14.73	18.31	16.08
0.4	HLF (%)	0.85	0.74	0.74	0.69	0.88	0.85	0.94	0.78	0.97	0.92
	3rd Harm. (%)	92.75	44.20	43.11	62.83	52.53	45.76	53.63	87.26	48.51	75.10
	9th Harm. (%)	16.05	2.96	23.20	23.60	10.42	15.22	20.32	11.66	6.42	8.79
	THD (%)	15.53	16.35	16.30	16.02	15.64	15.40	17.59	15.02	16.01	16.68
	HDF (%)	9.98	8.16	8.03	8.65	8.98	10.10	9.02	9.63	10.39	10.73
0.5	HLF (%)	0.54	0.56	0.55	0.51	0.50	0.54	0.58	0.53	0.55	0.58
	3rd Harm. (%)	49.90	65.24	29.74	27.22	51.90	26.88	33.52	48.85	48.33	71.85
	9th Harm. (%)	12.50	14.16	12.72	22.04	18.69	16.91	9.77	19.05	19.82	5.87
	THD (%)	13.01	12.03	11.36	12.27	11.02	11.24	11.86	12.45	12.00	11.84
	HDF (%)	5.41	7.43	5.79	5.64	4.43	4.99	3.85	5.17	4.77	5.16
0.6	HLF (%)	0.37	0.38	0.33	0.36	0.30	0.32	0.34	0.34	0.35	0.34
	3rd Harm. (%)	35.77	40.50	37.84	58.41	37.54	37.98	38.25	37.79	37.00	53.27
	9th Harm. (%)	3.56	1.74	4.89	13.57	4.52	5.09	8.75	4.98	11.75	9.33
	THD (%)	10.73	11.95	10.53	12.23	10.81	11.74	12.07	11.75	10.43	11.63
	HDF (%)	5.02	7.21	5.63	7.17	5.99	6.94	8.34	4.94	5.44	6.82
0.7	HLF (%)	0.33	0.40	0.34	0.40	0.35	0.39	0.48	0.35	0.33	0.38
	3rd Harm. (%)	19.98	33.65	43.47	37.68	43.07	31.08	22.21	32.56	38.44	21.71
	9th Harm. (%)	9.10	8.27	7.13	10.61	7.16	8.87	8.57	11.40	4.12	8.87
	THD (%)	9.68	9.46	10.89	9.62	10.07	9.20	9.33	9.66	11.07	10.02
	HDF (%)	4.20	3.86	4.84	4.80	3.92	4.10	3.68	3.10	6.93	5.17
0.8	HLF (%)	0.30	0.30	0.37	0.29	0.31	0.29	0.29	0.29	0.43	0.32
	3rd Harm. (%)	17.19	24.05	34.13	33.59	17.55	30.89	23.18	17.68	28.36	33.84
	9th Harm. (%)	9.35	13.80	3.02	2.60	8.05	8.42	14.95	8.24	3.77	1.81
	THD (%)	8.30	7.42	11.07	9.48	8.97	7.42	7.28	8.65		
	HDF (%)	3.48	1.66	6.41	5.79	5.13	1.50	1.64	4.90		
0.9	HLF (%)	0.25	0.18	0.38	0.35	0.32	0.18	0.18	0.30		
	3rd Harm. (%)	21.07	21.24	20.45	19.81	30.22	20.88	17.43	31.21		
	9th Harm. (%)	6.64	3.10	7.16	5.50	4.89	4.73	8.39	5.30		
	THD (%)	8.69	7.99	8.66	8.16	8.73	8.64	8.45	7.91	7.60	8.20
	HDF (%)	4.34	3.85	4.31	4.21	5.57	4.34	4.33	3.75	3.80	3.45
1	HLF (%)	0.28	0.25	0.28	0.26	0.33	0.27	0.27	0.24	0.24	0.24
	3rd Harm. (%)	16.06	24.38	8.52	24.37	9.04	27.66	9.67	10.07	16.92	17.94
	9th Harm. (%)	5.10	2.82	5.29	5.46	5.19	5.31	5.23	2.23	8.10	6.50

Table A.12: HW Solutions for 9 levels and 12 firing angles with initial level $L_i = 1$ ($L_i = -1$ for symmetric solutions) - Part II (Case VI)

Mod. Index	Performance Factors	Sol. 11	Sol. 12	Sol. 13	Sol. 14	Sol. 15	Sol. 16	Sol. 17	Sol. 18	Sol. 19	Sol. 20	Sol. 21
	THD (%)	49.64	43.65	41.72	46.59							
	HDF (%)	37.25	30.39	25.77	28.00							
0.2	HLF (%)	1.97	1.61	1.38	1.73							
	3rd Harm. (%)	162.20	154.03	69.98	119.62							
	9th Harm. (%)	9.21	13.72	44.48	41.63							
	THD (%)	27.44	26.66	26.23	25.82	29.15	29.35	26.86				
	HDF (%)	16.18	11.31	13.39	11.02	18.46	18.21	15.64				
0.3	HLF (%)	1.00	0.84	0.85	0.81	1.06	1.07	0.97				
	3rd Harm. (%)	108.94	59.82	96.45	101.31	88.05	83.45	81.75				
	9th Harm. (%)	12.55	28.64	5.07	7.52	17.24	19.03	15.44				
	THD (%)	24.13	22.53									
	HDF (%)	16.04	15.53									
0.4	HLF (%)	0.83	0.85									
	3rd Harm. (%)	37.02	69.23									
	9th Harm. (%)	6.25	17.99									
	THD (%)	15.72	20.48	15.09	17.42	15.90	15.05	15.48	19.03	15.57	15.66	17.37
	HDF (%)	10.43	15.86	9.87	11.43	8.06	9.83	9.99	13.45	10.18	10.33	11.85
0.5	HLF (%)	0.56	0.85	0.54	0.67	0.50	0.53	0.54	0.72	0.55	0.56	0.66
	3rd Harm. (%)	60.79	51.52	54.42	64.82	71.21	47.27	47.45	33.65	47.56	68.62	31.31
	9th Harm. (%)	15.88	8.32	6.52	14.90	3.23	17.01	16.86	6.69	16.77	9.24	8.94
	THD (%)	11.70	12.64	11.02	12.73	11.98	13.35					
	HDF (%)	4.67	6.14	3.64	5.78	6.17	6.48					
0.6	HLF (%)	0.33	0.41	0.29	0.37	0.38	0.45					
	3rd Harm. (%)	31.44	52.88	54.02	36.53	45.43	41.94					
	9th Harm. (%)	14.10	7.32	12.83	11.91	20.22	2.76					
	THD (%)	11.55	12.49	11.47	11.91	11.78	11.67	12.07	12.41	11.00	11.94	11.04
	HDF (%)	6.02	7.40	7.30	7.03	7.06	6.43	7.06	4.97	5.11	7.08	5.06
0.7	HLF (%)	0.37	0.41	0.43	0.40	0.39	0.35	0.39	0.38	0.34	0.40	0.35
	3rd Harm. (%)	23.30	45.02	16.57	18.48	18.91	35.88	35.75	35.25	28.27	27.75	39.20
	9th Harm. (%)	8.99	6.90	7.09	7.59	7.68	7.60	11.49	8.19	3.13	7.48	3.52
	THD (%)	9.23	9.17									
	HDF (%)	4.01	4.06									
0.8	HLF (%)	0.29	0.29									
	3rd Harm. (%)	37.32	26.02									
	9th Harm. (%)	12.16	2.75									

Table A.13. Solutions with lowest HLF for $L_i = 0$ and $L_i = 1$ for case VI

Mod. Index	0.1	0.2	0.3	0.4	0.5	0.6	0.7	0.8	0.9	1	1.1
$L_i = 0$	3.39	1.38	0.72	0.71	0.56	0.3	0.29	0.3	0.17	0.24	0.24
$L_i = 1$	3.38	1.22	0.73	0.69	0.5	0.29	0.33	0.29	0.18	0.24	-

Appendix B

Algorithm Results for A High Number of Controlled Harmonics

This chapter contains solutions obtained when 17 harmonics are controlled in case of a MMC with 11 levels. In particular, the firing angles for different m_a values and their corresponding step sign, are included at tables B.1 and B.3. In addition, the associated harmonic content is included at tables B.2 and B.4, respectively. All of these results are analysed at section 4.7.

Table B.1: Intermediate QW solutions (firing angles and sign of every step) with 17 firing angles and 11 levels

m_a	θ_1	θ_2	θ_3	θ_4	θ_5	θ_6	θ_7	θ_8	θ_9	θ_{10}	θ_{11}	θ_{12}	θ_{13}	θ_{14}	θ_{15}	θ_{16}	θ_{17}
0.033	⇑0.2783	⇓0.3026	⇑0.3934	⇓0.4202	⇑0.6245	⇓0.6555	⇑0.7408	⇓0.7732	⇑0.8684	⇓0.8798	⇑0.9818	⇓0.9968	⇑1.0960	⇓1.1144	⇑1.2106	⇓1.2321	⇑1.5563
0.067	⇑0.2669	⇓0.3153	⇑0.3802	⇓0.4338	⇑0.6095	⇓0.6718	⇑0.7262	⇓0.7926	⇑0.8738	⇓0.8958	⇑0.9806	⇓1.0100	⇑1.0904	⇓1.1267	⇑1.2017	⇓1.2443	⇑1.5416
0.133	⇑0.2595	⇓0.3512	⇑0.3628	⇓0.4477	⇑0.5920	⇑0.7014	⇓0.7110	⇓0.8223	⇑0.8900	⇓0.9379	⇑0.9933	⇓1.0540	⇑1.0974	⇓1.1701	⇑1.2020	⇓1.2855	⇑1.4981
0.167	⇑0.2714	⇑0.3472	⇓0.3595	⇓0.4769	⇑0.5613	⇑0.6690	⇓0.7078	⇓0.8183	⇑0.8772	⇓0.9364	⇑0.9795	⇓1.0547	⇑1.0825	⇓1.1731	⇑1.1865	⇓1.3185	⇑1.5012
0.233	⇑0.2747	⇑0.3559	⇓0.4057	⇓0.5028	⇑0.5284	⇑0.6266	⇓0.7217	⇓0.8259	⇑0.8622	⇓0.9373	⇑0.9551	⇑1.1419	⇓1.1604	⇑1.2337	⇓1.2667	⇓1.3635	⇑1.4849
0.267	⇑0.2306	⇑0.3214	⇓0.3743	⇓0.4432	⇑0.4531	⇑0.6490	⇓0.7776	⇓0.9036	⇑0.9297	⇑0.9432	⇓0.9588	⇑1.0841	⇓1.1115	⇑1.1813	⇓1.2295	⇓1.3411	⇑1.4308
0.333	⇑0.3272	⇑0.4193	⇓0.4558	⇑0.5119	⇓0.5638	⇑0.6057	⇓0.6707	⇓0.7789	⇑0.8004	⇑0.9503	⇓0.9691	⇑1.0289	⇓1.0697	⇑1.1116	⇓1.1760	⇑1.1976	⇓1.3934
0.367	⇑0.2785	⇑0.4318	⇓0.5033	⇑0.5329	⇓0.6431	⇑0.6900	⇓0.7443	⇑0.9361	⇓0.9652	⇑1.0200	⇓1.0781	⇑1.1064	⇑1.2826	⇓1.3021	⇓1.3315	⇑1.3834	⇓1.4305
0.433	⇑0.3229	⇓0.3470	⇑0.3937	⇑0.4617	⇓0.6059	⇑0.8606	⇓0.8822	⇑0.9304	⇓0.9791	⇑1.0060	⇑1.1706	⇓1.2009	⇑1.2583	⇓1.3244	⇑1.3697	⇓1.4270	⇓1.5281
0.467	⇑0.3427	⇑0.4170	⇑0.5067	⇓0.5599	⇓0.6763	⇑0.8365	⇓0.8553	⇑0.8974	⇓0.9402	⇑0.9664	⇑1.1203	⇓1.1500	⇑1.2013	⇓1.2602	⇑1.2836	⇓1.3942	⇓1.4935
0.533	⇑0.2674	⇓0.4175	⇑0.4414	⇑0.6111	⇓0.6259	⇑0.6727	⇓0.7889	⇑0.8403	⇓0.8945	⇑0.9305	⇑0.9486	⇓0.9655	⇑1.0647	⇓1.1109	⇑1.1472	⇓1.3479	⇑1.4005
0.567	⇑0.4141	⇑0.5595	⇓0.5803	⇓0.6851	⇑0.6955	⇑0.7925	⇓0.8268	⇑0.8670	⇑1.0216	⇓1.0624	⇑1.1008	⇑1.2650	⇓1.3032	⇑1.3512	⇓1.4399	⇑1.4915	⇓1.5123
0.633	⇑0.2800	⇑0.4377	⇓0.4943	⇑0.5232	⇓0.6433	⇑0.6586	⇓0.7984	⇑0.8316	⇑0.9640	⇓0.9980	⇑1.0319	⇑1.1738	⇓1.2085	⇑1.2483	⇓1.3203	⇑1.4026	⇓1.4279
0.667	⇑0.1694	⇑0.3862	⇓0.4339	⇑0.4527	⇑0.6070	⇓0.6318	⇑0.7160	⇓0.7335	⇑0.7914	⇓0.8644	⇑0.9198	⇓0.9522	⇑0.9968	⇑1.1424	⇓1.1817	⇑1.3640	⇓1.3931
0.733	⇑0.1507	⇑0.3083	⇑0.4614	⇓0.4933	⇑0.5419	⇓0.6031	⇑0.6258	⇓0.7688	⇑0.7932	⇓0.9230	⇑0.9542	⇑1.0799	⇓1.1163	⇑1.1475	⇓1.2026	⇑1.2823	⇓1.3223
0.767	⇑0.2571	⇑0.4059	⇓0.4420	⇑0.5754	⇑0.6402	⇓0.6545	⇑0.7358	⇓0.7710	⇑0.8747	⇓0.8992	⇑0.9325	⇑1.0515	⇓1.0814	⇑1.1096	⇑1.2349	⇓1.2695	⇑1.5328
0.833	⇑0.1787	⇑0.3090	⇑0.3885	⇑0.5377	⇓0.5705	⇑0.6193	⇓0.6728	⇓0.9276	⇑0.9481	⇑0.9790	⇓1.0096	⇑1.0511	⇑1.1682	⇓1.1962	⇓1.3899	⇑1.4125	⇓1.4218
0.867	⇑0.1709	⇑0.2162	⇓0.3509	⇑0.3664	⇓0.4820	⇑0.5326	⇑0.6105	⇑0.7379	⇓0.8451	⇑0.9932	⇓1.0235	⇑1.0407	⇑1.1460	⇓1.1895	⇓1.2805	⇑1.3450	⇑1.5045
0.933	⇑0.1077	⇑0.1825	⇓0.2068	⇑0.2461	⇑0.3829	⇓0.4220	⇑0.5794	⇑0.6389	⇓0.6783	⇑0.7152	⇓0.7836	⇑0.8011	⇓0.9580	⇑0.9875	⇑1.0978	⇓1.1349	⇑1.5006
0.967	⇑0.1868	⇑0.2645	⇓0.3545	⇑0.3967	⇑0.5536	⇓0.5949	⇑0.6351	⇑0.7365	⇓0.8144	⇑0.8971	⇓0.9253	⇑0.9834	⇑1.0049	⇓1.0239	⇑1.0979	⇓1.2958	⇑1.3674

Table B.2: Harmonic Amplitudes (% based on fundamental harmonic) for intermediate solutions (QW) with 17 firing angles and 11 levels

m_a	1^{st}	5^{th}	7^{th}	11^{th}	13^{th}	17^{th}	19^{th}	23^{th}	25^{th}	29^{th}	31^{th}	35^{th}	37^{th}	41^{th}	43^{th}	47^{th}	49^{th}
0.033	99.83	0.25	0.13	0.10	0.14	0.07	0.13	0.15	0.15	0.14	0.12	0.09	0.12	0.11	0.13	0.17	0.20
0.067	99.88	0.09	0.03	0.00	0.04	0.03	0.04	0.09	0.08	0.04	0.03	0.04	0.07	0.07	0.11	0.11	0.11
0.133	100.04	0.08	0.06	0.10	0.08	0.12	0.09	0.12	0.10	0.09	0.10	0.06	0.08	0.03	0.04	0.00	0.01
0.167	99.93	0.02	0.03	0.04	0.02	0.01	0.04	0.03	0.01	0.02	0.02	0.02	0.03	0.03	0.02	0.02	0.01
0.233	99.80	0.18	0.16	0.13	0.12	0.12	0.13	0.14	0.14	0.09	0.07	0.04	0.06	0.07	0.08	0.07	0.05
0.267	99.76	0.17	0.17	0.15	0.15	0.15	0.24	0.07	0.24	0.00	0.03	0.00	0.01	0.00	0.13	0.02	0.08
0.333	100.07	0.00	0.03	0.05	0.08	0.02	0.07	0.03	0.04	0.06	0.07	0.03	0.01	0.04	0.03	0.02	0.02
0.367	100.04	0.14	0.27	0.21	0.19	0.07	0.01	0.05	0.18	0.07	0.15	0.05	0.01	0.02	0.07	0.01	0.07
0.433	99.99	0.01	0.01	0.00	0.01	0.01	0.02	0.01	0.02	0.00	0.01	0.01	0.00	0.01	0.01	0.01	0.01
0.467	99.99	0.01	0.01	0.01	0.01	0.00	0.01	0.00	0.01	0.03	0.00	0.00	0.01	0.01	0.00	0.02	0.00
0.533	99.96	0.04	0.05	0.04	0.03	0.03	0.03	0.03	0.04	0.03	0.02	0.01	0.01	0.01	0.02	0.01	0.01
0.567	99.98	0.01	0.01	0.00	0.00	0.01	0.01	0.00	0.02	0.00	0.01	0.00	0.00	0.00	0.01	0.00	0.01
0.633	100.00	0.01	0.01	0.01	0.02	0.01	0.01	0.00	0.01	0.00	0.00	0.00	0.00	0.01	0.00	0.01	0.00
0.667	99.98	0.04	0.00	0.02	0.02	0.00	0.05	0.03	0.00	0.01	0.00	0.01	0.01	0.00	0.03	0.02	0.00
0.733	99.99	0.01	0.00	0.00	0.01	0.01	0.01	0.01	0.01	0.01	0.00	0.00	0.01	0.00	0.00	0.00	0.00
0.767	99.99	0.01	0.00	0.00	0.01	0.01	0.00	0.00	0.01	0.00	0.00	0.01	0.00	0.00	0.00	0.01	0.00
0.833	100.00	0.04	0.02	0.04	0.05	0.01	0.01	0.02	0.03	0.03	0.03	0.00	0.02	0.01	0.00	0.01	0.03
0.867	99.98	0.01	0.01	0.00	0.00	0.02	0.01	0.01	0.02	0.00	0.01	0.01	0.00	0.01	0.01	0.00	0.01
0.933	100.04	0.03	0.01	0.02	0.01	0.03	0.03	0.00	0.01	0.00	0.01	0.02	0.03	0.01	0.01	0.02	0.01
0.967	99.91	0.09	0.01	0.07	0.06	0.12	0.00	0.04	0.00	0.05	0.01	0.02	0.08	0.03	0.04	0.02	0.02

Table B.3: QW Solutions (firing angles and sign of every step) with 17 firing angles and 11 levels for continuous set ($m_a = 0.84$ to $m_a = 0.92$)

m_a	θ_1	θ_2	θ_3	θ_4	θ_5	θ_6	θ_7	θ_8	θ_9	θ_{10}	θ_{11}	θ_{12}	θ_{13}	θ_{14}	θ_{15}	θ_{16}	θ_{17}
0.84	⇑0.1602	⇑0.3052	⇓0.4793	⇑0.5376	⇑0.6135	⇑0.6816	⇓0.6961	⇑0.8467	⇓0.8605	⇑1.0128	⇓1.0702	⇑1.0975	⇑1.1230	⇓1.1533	⇓1.3938	⇑1.4260	⇑1.5209
0.85	⇑0.1575	⇑0.2909	⇓0.4900	⇑0.5294	⇑0.6040	⇑0.7110	⇓0.7369	⇑0.8423	⇓0.8628	⇑0.9994	⇓1.0318	⇑1.0537	⇑1.1452	⇓1.1698	⇓1.3756	⇑1.4078	⇑1.5275
0.86	⇑0.1520	⇑0.2772	⇓0.4927	⇑0.5312	⇑0.6010	⇑0.7164	⇓0.7564	⇑0.8407	⇓0.8699	⇑0.9790	⇓1.0012	⇑1.0336	⇑1.1447	⇓1.1711	⇓1.3600	⇑1.3922	⇑1.5214
0.87	⇑0.1486	⇑0.2632	⇓0.4940	⇑0.5333	⇑0.5989	⇑0.7167	⇓0.7703	⇑0.8336	⇓0.8701	⇑0.9577	⇓0.9777	⇑1.0216	⇑1.1423	⇓1.1725	⇓1.3433	⇑1.3761	⇑1.5133
0.88	⇑0.1559	⇑0.2412	⇓0.4935	⇑0.5332	⇑0.5986	⇑0.7148	⇓0.7768	⇑0.8060	⇓0.8537	⇑0.9401	⇓0.9579	⇑1.0113	⇑1.1417	⇓1.1846	⇓1.3168	⇑1.3562	⇑1.5036
0.89	⇑0.1662	⇑0.2149	⇓0.4838	⇑0.5225	⇑0.6088	⇑0.6767	⇓0.6919	⇑0.7324	⇓0.8566	⇑0.9474	⇓0.9614	⇑1.0053	⇑1.1366	⇓1.1929	⇓1.2910	⇑1.3395	⇑1.4903
0.9	⇑0.1538	⇑0.2106	⇓0.4720	⇑0.5073	⇑0.6288	⇑0.6363	⇓0.6630	⇑0.7253	⇓0.8714	⇑0.9280	⇓0.9454	⇑0.9983	⇑1.1288	⇓1.1824	⇓1.2869	⇑1.3310	⇑1.4783
0.91	⇑0.1310	⇑0.2104	⇓0.4551	⇑0.4878	⇑0.6359	⇑0.6361	⇓0.6658	⇑0.7232	⇓0.8813	⇑0.9079	⇓0.9427	⇑0.9942	⇑1.1184	⇓1.1605	⇓1.2857	⇑1.3226	⇑1.4633
0.92	⇑0.0985	⇑0.2097	⇓0.4382	⇑0.4732	⇑0.6322	⇑0.6481	⇓0.6658	⇑0.7188	⇓0.8980	⇑0.9112	⇓0.9837	⇑1.0103	⇑1.0885	⇓1.1120	⇓1.2834	⇑1.3132	⇑1.4465

Table B.4: Harmonic Amplitudes (% based on fundamental harmonic) for solutions (QW) with 17 firing angles and 11 levels for continuous set ($m_a = 0.84$ to $m_a = 0.92$)

m_a	1^{st}	5^{th}	7^{th}	11^{th}	13^{th}	17^{th}	19^{th}	23^{th}	25^{th}	29^{th}	31^{th}	35^{th}	37^{th}	41^{th}	43^{th}	47^{th}	49^{th}
0.84	100.06	0.03	0.00	0.01	0.06	0.02	0.05	0.04	0.03	0.00	0.01	0.05	0.01	0.03	0.02	0.01	0.02
0.85	100.01	0.00	0.00	0.00	0.00	0.00	0.01	0.00	0.01	0.00	0.01	0.01	0.01	0.01	0.01	0.00	0.00
0.86	100.00	0.01	0.01	0.00	0.01	0.00	0.00	0.00	0.01	0.00	0.00	0.01	0.01	0.00	0.00	0.00	0.00
0.87	100.00	0.00	0.01	0.01	0.01	0.00	0.01	0.01	0.01	0.00	0.01	0.00	0.01	0.00	0.01	0.00	0.00
0.88	100.01	0.03	0.01	0.01	0.02	0.01	0.01	0.02	0.02	0.02	0.01	0.00	0.00	0.00	0.02	0.01	0.00
0.89	100.01	0.03	0.01	0.01	0.03	0.01	0.02	0.03	0.02	0.02	0.02	0.01	0.01	0.01	0.01	0.02	0.01
0.9	99.98	0.01	0.01	0.00	0.03	0.01	0.04	0.02	0.00	0.02	0.01	0.01	0.02	0.02	0.01	0.01	0.00
0.91	100.00	0.02	0.05	0.03	0.10	0.02	0.10	0.04	0.04	0.04	0.02	0.03	0.00	0.06	0.03	0.02	0.02
0.92	99.96	0.02	0.00	0.01	0.01	0.01	0.01	0.00	0.01	0.01	0.02	0.02	0.00	0.00	0.01	0.02	0.01

Bibliography

[1] S. Rohner, S. Bernet, M. Hiller, and R. Sommer, "Modulation, losses, and semiconductor requirements of modular multilevel converters," *IEEE Transactions on Industrial Electronics*, vol. 57, no. 8, pp. 2633 – 2642, Aug 2010.

[2] J. Rodriguez, S. Bernet, B. Wu, J. Pontt, and S. Kouro, "Multilevel voltage-source-converter topologies for industrial medium-voltage drives," *IEEE Transactions on Industrial Electronics*, vol. 54, no. 6, pp. 2930 – 2945, Dec 2007.

[3] J. Rodriguez, L. Franquelo, S. Kouro, J. Leon, R. Portillo, M. Prats, and M. Perez, "Multilevel converters: An enabling technology for high-power applications," *Proceedings of the IEEE*, vol. 97, no. 11, pp. 1786 – 1817, Nov 2009.

[4] J. Glasdam, J. Hjerrild, L. Kocewiak, and C. Bak, "Review on multi-level voltage source converter based hvdc technologies for grid connection of large offshore wind farms," in *Proc. of IEEE International Conference on Power System Technology (POWERCON)*, Oct 2012, pp. 1 – 6.

[5] A. Antonopoulos, L. Angquist, and H.-P. Nee, "On dynamics and voltage control of the modular multilevel converter," in *Proc. of European Conference on Power Electronics and Applications*, Sept 2009, pp. 1–10.

[6] A. Nami, J. Liang, F. Dijkhuizen, and G. Demetriades, "Modular multilevel converters for hvdc applications: Review on converter cells and functionalities," *IEEE Transactions on Power Electronics*, vol. 30, no. 1, pp. 18 – 36, Jan 2015.

[7] R. Marquardt, A. Lesnicar, and J. Hildinger, "Modulares stromrichterkonzept für netzkupplungsan-wendungen bei hohen spannungen," in *ETG-Fachtagung*, 2002.

[8] D. Siemaszko, A. Antonopoulos, K. Ilves, M. Vasiladiotis, L. Angquist, and H.-P. Nee, "Evaluation of control and modulation methods for modular multilevel converters," in *Proc. of International Power Electronics Conference (IPEC)*, June 2010, pp. 746 – 753.

[9] A. Antonopoulos, L. Angquist, S. Norrga, K. Ilves, and H.-P. Nee, "Modular multilevel converter ac motor drives with constant torque form zero to nominal speed," in *In Proc. of IEEE Energy Conversion Congress and Exposition (ECCE)*, Sept 2012, pp. 739 – 746.

[10] J. Huber and A. Korn, "Optimized pulse pattern modulation for modular multilevel converter high-speed drive," in *Proc. of Power Electronics and Motion Control Conference (EPE/PEMC)*, Sept 2012, pp. LS1a–1.4–1 – LS1a–1.4–7.

[11] G. Konstantinou, M. Ciobotar, and V. Agelidis, "Operation of a modular multilevel converter with selective harmonic elimination pwm," in *Proc. of Power Electronics and ECCE Asia (ICPE ECCE)*, May 2011, pp. 999 – 1004.

[12] G. Konstantinou, M. Ciobotaru, and V. Agelidis, "Selective harmonic elimination pulse-width modulation of modular multilevel converters," *IET Power Electronics*, vol. 6, no. 1, pp. 96 – 107, Jan 2013.

[13] A. Perez-Basante, S. Ceballos, J. Pou, A. G. d. Muro, A. Pujana, and P. Ibanez, "Sic modular multilevel converters: Sub-module voltage ripple analysis and efficiency estimations," in *Proc. of Conference for Power Electronics, Intelligent Motion, Renewable Energy and Energy Management (PCIM Europe)*, May 2014, pp. 1 – 8.

[14] A. Persson and L. Carlsson, "New technologies in hvdc converter design," in *Proc. of AC and DC Power Transmission*, Apr 1996, pp. 387 – 392.

[15] N. Flourentzou, V. Agelidis, and G. Demetriades, "Vsc-based hvdc power transmission systems: An overview," *IEEE Transactions on Power Electronics*, vol. 24, no. 3, pp. 592 – 602, March 2009.

[16] R. Emery and J. Eugene, "Harmonic losses in lci-fed synchronous motors," *IEEE Transactions on Industry Applications*, vol. 38, no. 4, pp. 948 – 954, Jul 2002.

[17] Suroso and T. Noguchi, "Common-emitter topology of multilevel current-source pulse width modulation inverter with chopper-based dc current sources," *IET Power Electronics*, vol. 4, no. 7, pp. 759 – 766, Aug 2011.

[18] C. Klumpner and F. Blaabjerg, "Using reverse blocking igbts in power

converters for adjustable speed drives," in *Proc. of Industry Applications Conference (IAS)*, vol. 3, Oct 2003, pp. 1516 – 1523.

[19] M. Winkelnkemper, A. Korn, and P. Steimer, "A modular direct converter for transformerless rail interties," in *Proc. of IEEE International Symposium on Industrial Electronics (ISIE)*, July 2010, pp. 562 – 567.

[20] R. Torres-Olguin, M. Molinas, and T. Undeland, "Offshore wind farm grid integration by vsc technology with lcc-based hvdc transmission," *IEEE Transactions on Sustainable Energy*, vol. 3, no. 4, pp. 899 – 907, Oct 2012.

[21] A. Lesnicar and R. Marquardt, "An innovative modular multilevel converter topology suitable for a wide power range," in *Proc. of Power Tech Conference Proceedings*, vol. 3, June 2003, p. 6.

[22] M. Glinka and R. Marquardt, "A new ac/ac multilevel converter family," *IEEE Transactions on Industrial Electronics*, vol. 52, no. 3, pp. 662 – 669, June 2005.

[23] A. Korn, M. Winkelnkemper, and P. Steimer, "Low output frequency operation of the modular multi-level converter," in *Proc. of IEEE Energy Conversion Congress and Exposition (ECCE)*, Sept 2010, pp. 3993 – 3997.

[24] L. Angquist, A. Antonopoulos, D. Siemaszko, K. Ilves, M. Vasiladiotis, and H.-P. Nee, "Open-loop control of modular multilevel converters using estimation of stored energy," *IEEE Transactions on Industry Applications*, vol. 47, no. 6, pp. 2516 – 2524, Nov 2011.

[25] H. Akagi, "Classification, terminology, and application of the modular multilevel cascade converter (mmcc)," *IEEE Transactions on Power Electronics*, vol. 26, no. 11, pp. 3119 – 3130, Nov 2011.

[26] E. Solas, G. Abad, J. Barrena, S. Aurtenetxea, A. Carcar, and L. Zajac, "Modular multilevel converter with different submodule concepts - part i: Capacitor voltage balancing method," *IEEE Transactions on Industrial Electronics*, vol. 60, no. 10, pp. 4525 – 4535, Oct 2013.

[27] E. Solas, G. Abad, J. Barrena, S. Aurtenetxea, A. Carcar, and Zajac, "Modular multilevel converter with different submodule concepts - part ii: Experimental validation and comparison for hvdc application," *IEEE Transactions on Industrial Electronics*, vol. 60, no. 10, pp. 4536 – 4545, Oct 2013.

[28] B. Jacobson, P. Karlsson, G. Asplund, L. Harnefors, and T. Jonsson, "Vsc-hvdc transmission with cascaded two-level converters," in *Proc. of Cigré session*, 2010, pp. B4 – B110.

[29] S. Kenzelmann, "Modular dc/dc converter for dc distribution and collection networks," Ph.D. dissertation, École Polytechnique Fédérale de Lausanne, 2012.

[30] G. Adam, S. Finney, and B. Williams, "Hybrid converter with ac side cascaded h-bridge cells against h-bridge alternative arm modular multilevel converter: steady-state and dynamic performance," *IET Generation, Transmission & Distribution*, vol. 7, no. 3, pp. 318 – 328, March 2013.

[31] C. Oates and C. Davidson, "A comparison of two methods of estimating losses in the modular multi-level converter," in *Proc. of European Conference on Power Electronics and Applications (EPE)*, Aug 2011, pp. 1 – 10.

[32] S. Kouro, M. Malinowski, K. Gopakumar, J. Pou, L. Franquelo, B. Wu, J. Rodriguez, M. Perez, and J. Leon, "Recent advances and industrial applications of multilevel converters," *IEEE Transactions on Industrial Electronics*, vol. 57, no. 8, pp. 2553 – 2580, Aug 2010.

[33] M. Hagiwara and H. Akagi, "Control and experiment of pulsewidth-modulated modular multilevel converters," *IEEE Transactions on Power Electronics*, vol. 24, no. 7, pp. 1737 – 1746, July 2009.

[34] S. Rohner, S. Bernet, M. Hiller, and R. Sommer, "Pulse width modulation scheme for the modular multilevel converter," in *Proc. of European Conference on Power Electronics and Applications (EPE)*, Sept 2009, pp. 1 – 10.

[35] S. Allebrod, R. Hamerski, and R. Marquardt, "New transformerless, scalable modular multilevel converters for hvdc-transmission," in *Proc. of IEEE Power Electronics Specialists Conference*, June 2008, pp. 174 – 179.

[36] M. Hagiwara, K. Nishimura, and H. Akagi, "A medium-voltage motor drive with a modular multilevel pwm inverter," *IEEE Transactions on Power Electronics*, vol. 25, no. 7, pp. 1786 – 1799, July 2010.

[37] A. Antonopoulos, L. Angquist, S. Norrga, K. Ilves, L. Harnefors, and H.-P. Nee, "Modular multilevel converter ac motor drives with constant torque from zero to nominal speed," *IEEE Transactions on Industry Applications*, vol. 50, no. 3, pp. 1982 – 1993, May 2014.

[38] A. Antonopoulos, K. Ilves, L. A?ngquist, and H.-P. Nee, "On interaction between internal converter dynamics and current control of high-performance high-power ac motor drives with modular multilevel converters," in *Proc.*

of IEEE Energy Conversion Congress and Exposition (ECCE), Sept 2010, pp. 4293 – 4298.

[39] C. Heising, T. Schrader, R. Bartelt, V. Staudt, and A. Steimel, "Pole-restraining control for modular multilevel converters in electric-ship applications," in *Proc. of IEEE Electric Ship Technologies Symposium (ESTS)*, April 2013, pp. 366 – 371.

[40] M. Spichartz, V. Staudt, and A. Steimel, "Modular multilevel converter for propulsion system of electric ships," in *Proc. of IEEE Electric Ship Technologies Symposium (ESTS)*, April 2013, pp. 237 – 242.

[41] M. Hagiwara, R. Maeda, and H. Akagi, "Theoretical analysis and control of the modular multilevel cascade converter based on double-star chopper-cells (mmcc-dscc)," in *Proc. of International Power Electronics Conference (IPEC)*, June 2010, pp. 2029 – 2036.

[42] E. Behrouzian and M. Bongiorno, "Investigation of negative-sequence injection capability of cascaded h-bridge converters in star and delta configuration," *IEEE Transactions on Power Electronics*, vol. PP, no. 99, pp. 1 – 1, 2016.

[43] E. Behrouzian, M. Bongiorno, and H. Z. D. L. Parra, "Investigation of negative sequence injection capability in h-bridge multilevel statcom," in *Proc. of European Conference on Power Electronics and Applications (EPE-ECCE Europe)*, Aug 2014, pp. 1 – 10.

[44] A. J. Korn, M. Winkelnkemper, P. Steimer, and J. W. Kolar, "Direct modular multi-level converter for gearless low-speed drives," in *Proc. European Conference on of Power Electronics and Applications (EPE-ECCE)*, Aug 2011, pp. 1 – 7.

[45] P. Jones and C. Davidson, "Calculation of power losses for mmc-based vsc hvdc stations," in *Proc. of European Conference on Power Electronics and Applications (EPE)*, Sept 2013, pp. 1 – 10.

[46] A. Nami, L. Wang, F. Dijkhuizen, and A. Shukla, "Five level cross connected cell for cascaded converters," in *Proc. of European Conference on Power Electronics and Applications (EPE)*, Sept 2013, pp. 1 – 9.

[47] R. Marquardt, "Modular multilevel converter: An universal concept for hvdc-networks and extended dc-bus-applications," in *Proc. of International Power Electronics Conference (IPEC)*, June 2010, pp. 502 – 507.

[48] ABB. (2017) Acs 6000c cycloconverter. [Online]. Available:

https://library.e.abb.com/public/2abc426982e203e6c1256e4d004deb49/ACS%206000c%20Cycloconverter.pdf

[49] Siemens. (2017) Simovert d cycloconverter. [Online]. Available: http://www.industry.siemens.com/services/global/en/z_archive/cross_industry_solutions/drives/simovert_d/pages/default.aspx

[50] A. K. Chattopadhyay, "Alternating current drives in the steel industry," *IEEE Industrial Electronics Magazine*, vol. 4, no. 4, pp. 30 – 42, Dec 2010.

[51] ABB. (2017) Acs 6000. [Online]. Available: http://new.abb.com/drives/medium-voltage-ac-drives/acs6000

[52] SIEMENS. (2017) Sinamics sm150. [Online]. Available: http://www.industry.siemens.com/drives/global/en/converter/mv-drives/Pages/sinamics-sm150.aspx

[53] Ingeteam. (2017) Ingedrive-mv500. [Online]. Available: http://www.ingeteam.com/es-es/convertidores-de-frecuencia-e-inversores/convertidores-de-potencia/pc28_6_173/ingedrive-mv500.aspx

[54] ——. (2017) Ingeteam: Power converters. [Online]. Available: www.ingeteam.com

[55] ABB. (2017) Megadrive-lci. [Online]. Available: http://new.abb.com/drives/medium-voltage-ac-drives/megadrive-lci

[56] Siemens. (2017) Sinamics-gl150. [Online]. Available: http://www.industry.siemens.com/drives/global/en/converter/mv-drives/Pages/sinamics-gl150.aspx

[57] R. Automation. (2017) Powerflex-7000. [Online]. Available: http://ab.rockwellautomation.com/es/Drives/Medium-Voltage/PowerFlex-7000

[58] E. P. Wiechmann, P. Aqueveque, R. Burgos, and J. Rodriguez, "On the efficiency of voltage source and current source inverters for high-power drives," *IEEE Transactions on Industrial Electronics*, vol. 55, no. 4, pp. 1771 – 1782, April 2008.

[59] G. Sydnor, R. Bhatia, H. Krattiger, J. Mylius, D. Schäfer, and E. Carpenter, "Fifteen years of operation at nasa's national transonic facility with the world's largest adjustable speed drive," in *Proc. of IET International Conference on Power Electronics, Machines and Drives (PEMD)*, March 2012, pp. 1 – 10.

[60] H. Schlunegger and A. Thoni, "100 mw full-size converter in the grimsel 2 pumped-storage plant," in *Proc. of Hydro conference*, 2013, pp. 1 – 5.

[61] Y. Chen, Z. Li, S. Zhao, X. Wei, and Y. Kang, "Design and implementation of a modular multilevel converter with hierarchical redundancy ability for electric ship mvdc system," *IEEE Journal of Emerging and Selected Topics in Power Electronics*, vol. 5, no. 1, pp. 189 – 202, March 2017.

[62] P. Blaszczyk, M. Steurer, D. Soto, F. Bogdan, J. Hauer, M. Sloderbeck, and K. Schoder, "Modular multilevel converter based test bed for mvdc applications - a case study with a 12 kv, 5 mw setup," in *Proc. of IEEE International Power Electronics and Motion Control Conference (PEMC)*, Sept 2016, pp. 139 – 145.

[63] J. Carr, J. Li, D. Das, and J. Pan, "Wind turbine drivetrain for direct mvdc connection," in *Proc. of IEEE Symposium on Power Electronics and Machines for Wind and Water Applications*, July 2014, pp. 1 – 6.

[64] J. Carr, D. Das, J. Li, J. Pan, S. Ebner, and O. Apeldoorn, "Modular multilevel converter for direct mvdc connection of offshore wind farms," in *Proc. of IEEE Energy Conversion Congress and Exposition (ECCE)*, Sept 2015, pp. 976 – 982.

[65] M. Saeedifard and R. Iravani, "Dynamic performance of a modular multilevel back-to-back hvdc system," *IEEE Transactions on Power Delivery*, vol. 25, no. 4, pp. 2903 – 2912, Oct 2010.

[66] TNEI, "Mvdc technology study – market opportunities and economic impact," TNEI, Tech. Rep., Feb 2015.

[67] I. Martinez de Alegria, "Study on full direct current offshore wind farm," Ph.D. dissertation, University of the Basque Country UPV/EHU, Bilbao, Spain, 2012.

[68] F. Mura and R. W. D. Doncker, "Design aspects of a medium-voltage direct current (mvdc) grid for a university campus," in *Proc. of International Conference on Power Electronics - ECCE Asia*, May 2011, pp. 2359 – 2366.

[69] M. E. Baran and N. R. Mahajan, "Dc distribution for industrial systems: opportunities and challenges," *IEEE Transactions on Industry Applications*, vol. 39, no. 6, pp. 1596–1601, Nov 2003.

[70] N. Doerry and J. Amy, "Mvdc shipboard power system considerations for electromagnetic railguns," in *Proc. of EM Railgun Workshop*, Sep 2015.

[71] ——, "The road to mvdc," in *Proc. of Intelligent Ships Symp. (ASNE)*, 2015.

[72] M. Butcher, R. Maltby, and P. S. Parvin, "Compact dc power and propul-

sion systems - the definitive solution?" in *Proc. of Electric Ship Technologies Symposium*, April 2009, pp. 521 – 528.

[73] S. Lundberg, "Wind farm configuration and energy efficiency studies – series dc versus ac layouts," Ph.D. dissertation, Chalmers University of Technology, 2006.

[74] A. Perez-Basante, J. I. Garate, I. M. d. Alegria, I. Kortabarria, and J. Andreu, "Controlled square wave high frequency rectifier," in *Proc. of International Exhibition and Conference for Power Electronics, Intelligent Motion, Renewable Energy and Energy Management (PCIM Europe)*, May 2014, pp. 1 – 8.

[75] L. Max and S. Lundberg, "System efficiency of a dc/dc converter based wind farm," *Wind Energy*, vol. 11, no. 1, pp. 109 – 120, 2008.

[76] M. Barnes and A. Beddard, "Voltage source converter hvdc links – the state of the art and issues going forward," *Energy Procedia*, vol. 24, pp. 108 – 122, 2012.

[77] X. Pei, O. Cwikowski, D. S. Vilchis-Rodriguez, M. Barnes, A. C. Smith, and R. Shuttleworth, "A review of technologies for mvdc circuit breakers," in *Proc. of Annual Conference of the IEEE Industrial Electronics Society (IECON)*, Oct 2016, pp. 3799 – 3805.

[78] M. Liserre, R. Cardenas, M. Molinas, and J. Rodriguez, "Overview of multi-mw wind turbines and wind parks," *IEEE Transactions on Industrial Electronics*, vol. 58, no. 4, pp. 1081 – 1095, April 2011.

[79] H. Li, Z. Chen, and H. Polinder, "Optimization of multibrid permanent-magnet wind generator systems," *IEEE Transactions on Energy Conversion*, vol. 24, no. 1, pp. 82 – 92, March 2009.

[80] G. P. Adam and B. W. Williams, "Half- and full-bridge modular multilevel converter models for simulations of full-scale hvdc links and multiterminal dc grids," *IEEE Journal of Emerging and Selected Topics in Power Electronics*, vol. 2, no. 4, pp. 1089 – 1108, Dec 2014.

[81] M. Hagiwara, I. Hasegawa, and H. Akagi, "Startup and low-speed operation of an adjustable-speed motor driven by a modular multilevel cascade inverter (mmci)," in *Proc. of IEEE Energy Conversion Congress and Exposition (ECCE)*, Sept 2012, pp. 718 – 725.

[82] J. Pou, S. Ceballos, G. Konstantinou, V. Agelidis, R. Picas, and J. Zaragoza, "Circulating current injection methods based on instantaneous

information for the modular multilevel converter," *IEEE Transactions on Industrial Electronics*, vol. 62, no. 2, pp. 777 – 788, Feb 2015.

[83] M. A. Pérez and J. Rodríguez, "Generalized modeling and simulation of a modular multilevel converter," in *Proc. of IEEE International Symposium on Industrial Electronics*, June 2011, pp. 1863 – 1868.

[84] S. Ceballos, J. Pou, S. Choi, M. Saeedifard, and V. Agelidis, "Analysis of voltage balancing limits in modular multilevel converters," in *Proc. of IEEE Conference of Industrial Electronics (IECON)*, Nov 2011, pp. 4397 – 4402.

[85] S. Engel and R. De Doncker, "Control of the modular multi-level converter for minimized cell capacitance," in *Proc. of European Conference on Power Electronics and Applications (EPE)*, Aug 2011, pp. 1 – 10.

[86] M. Vasiladiotis, N. Cherix, and A. Rufer, "Accurate capacitor voltage ripple estimation and current control considerations for grid-connected modular multilevel converters," *IEEE Transactions on Power Electronics*, vol. 29, no. 9, pp. 4568 – 4579, Sept 2014.

[87] J. Qin and M. Saeedifard, "Predictive control of a modular multilevel converter for a back-to-back hvdc system," *IEEE Transactions on Power Delivery*, vol. 27, no. 3, pp. 1538 – 1547, July 2012.

[88] Q. Tu, Z. Xu, and J. Zhang, "Circulating current suppressing controller in modular multilevel converter," in *Proc. of Annual Conference on IEEE Industrial Electronics Society (IECON)*, Nov 2010, pp. 3198 – 3202.

[89] M. A. Perez, S. Bernet, J. Rodriguez, S. Kouro, and R. Lizana, "Circuit topologies, modeling, control schemes, and applications of modular multilevel converters," *IEEE Transactions on Power Electronics*, vol. 30, no. 1, pp. 4 – 17, Jan 2015.

[90] S. Debnath, J. Qin, B. Bahrani, M. Saeedifard, and P. Barbosa, "Operation, control, and applications of the modular multilevel converter: A review," *IEEE Transactions on Power Electronics*, vol. 30, no. 1, pp. 37 – 53, Jan 2015.

[91] R. Darus, J. Pou, G. Konstantinou, S. Ceballos, R. Picas, and V. Agelidis, "A modified voltage balancing algorithm for the modular multilevel converter: Evaluation for staircase and phase-disposition pwm," *IEEE Transactions on Power Electronics*, vol. 30, no. 8, pp. 4119 – 4127, Aug 2015.

[92] L. Franquelo, J. Rodriguez, J. Leon, S. Kouro, R. Portillo, and M. Prats,

"The age of multilevel converters arrives," *IEEE Industrial Electronics Magazine*, vol. 2, no. 2, pp. 28 – 39, June 2008.

[93] R. Picas, J. Pou, S. Ceballos, J. Zaragoza, G. Konstantinou, and V. Agelidis, "Optimal injection of harmonics in circulating currents of modular multilevel converters for capacitor voltage ripple minimization," in *Proc. of ECCE Asia Downunder*, June 2013, pp. 318 – 324.

[94] R. Picas, J. Pou, S. Ceballos, V. G. Agelidis, and M. Saeedifard, "Minimization of the capacitor voltage fluctuations of a modular multilevel converter by circulating current control," in *Proc. of Annual Conference on IEEE Industrial Electronics Society (IECON)*, Oct 2012, pp. 4985 – 4991.

[95] D. Soto-Sanchez and T. C. Green, "Control of a modular multilevel converter-based hvdc transmission system," in *Proc. of European Conference on Power Electronics and Applications (EPE)*, Aug 2011, pp. 1 – 10.

[96] R. Darus, J. Pou, G. Konstantinou, S. Ceballos, and V. G. Agelidis, "Circulating current control and evaluation of carrier dispositions in modular multilevel converters," in *Proc. of International Power Electronics and Motion Control Conference (ECCE Asia)*, June 2013, pp. 332 – 338.

[97] A. Perez-Basante, S. Ceballos, J. Pou, M. Liserre, G. Konstantinou, and I. M. de Alegria, "Circulating current control for modular multilevel converter based on selective harmonic elimination with ultra-low switching frequency," in *Proc. of European Conference on Power Electronics and Applications (EPE-ECCE)*, Sept 2016.

[98] Q. Tu, Z. Xu, and L. Xu, "Reduced switching-frequency modulation and circulating current suppression for modular multilevel converters," *IEEE Transactions on Power Delivery*, vol. 26, no. 3, pp. 2009 – 2017, July 2011.

[99] S. Li, X. Wang, Z. Yao, T. Li, and Z. Peng, "Circulating current suppressing strategy for mmc-hvdc based on nonideal proportional resonant controllers under unbalanced grid conditions," *IEEE Transactions on Power Electronics*, vol. 30, no. 1, pp. 387 – 397, Jan 2015.

[100] K. Ilves, A. Antonopoulos, L. Harnefors, S. Norrga, and H.-P. Nee, "Circulating current control in modular multilevel converters with fundamental switching frequency," in *Proc. of International Power Electronics and Motion Control Conference (IPEMC)*, vol. 1, June 2012, pp. 249 – 256.

[101] G. Konstantinou, J. Pou, S. Ceballos, R. Picas, J. Zaragoza, and V. G. Agelidis, "Control of circulating currents in modular multilevel converters

through redundant voltage levels," *IEEE Transactions on Power Electronics*, vol. 31, no. 11, pp. 7761 – 7769, Nov 2016.

[102] G. Konstantinou, "Harmonic elimination pulse width modulation of modular and hybrid multilevel converter topologies," Ph.D. dissertation, The University of New South Wales (UNSW), 2012.

[103] J. Böcker, B. Freudenberg, A. The, and S. Dieckerhoff, "Experimental comparison of model predictive control and cascaded control of the modular multilevel converter," *IEEE Transactions on Power Electronics*, vol. 30, no. 1, pp. 422 – 430, Jan 2015.

[104] Q. Tu, Z. Xu, and L. Xu, "Reduced switching-frequency modulation and circulating current suppression for modular multilevel converters," *IEEE Transactions on Power Delivery*, vol. 26, no. 3, pp. 2009 – 2017, July 2011.

[105] J. W. Moon, C. S. Kim, J. W. Park, D. W. Kang, and J. M. Kim, "Circulating current control in mmc under the unbalanced voltage," *IEEE Transactions on Power Delivery*, vol. 28, no. 3, pp. 1952 – 1959, July 2013.

[106] S. Li, X. Wang, Z. Yao, T. Li, and Z. Peng, "Circulating current suppressing strategy for mmc-hvdc based on nonideal proportional resonant controllers under unbalanced grid conditions," *IEEE Transactions on Power Electronics*, vol. 30, no. 1, pp. 387 – 397, Jan 2015.

[107] K. Ilves, A. Antonopoulos, L. Harnefors, S. Norrga, and H.-P. Nee, "Circulating current control in modular multilevel converters with fundamental switching frequency," in *Proc. of International Power Electronics and Motion Control Conference (IPEMC)*, vol. 1, June 2012, pp. 249 – 256.

[108] M. Dahidah, G. Konstantinou, and V. Agelidis, "A review of multilevel selective harmonic elimination pwm: Formulations, solving algorithms, implementation and applications," *IEEE Transactions on Power Electronics*, vol. 30, no. 8, pp. 4091 – 4106, Aug 2015.

[109] M. S. A. Dahidah and V. Agelidis, "Selective harmonic elimination pwm control for cascaded multilevel voltage source converters: A generalized formula," *IEEE Transactions on Power Electronics*, vol. 23, no. 4, pp. 1620 – 1630, July 2008.

[110] S. Du, J. Liu, and T. Liu, "Modulation and closed-loop-based dc capacitor voltage control for mmc with fundamental switching frequency," *IEEE Transactions on Power Electronics*, vol. 30, no. 1, pp. 327 – 338, Jan 2015.

[111] G. Konstantinou, J. Pou, S. Ceballos, R. Picas, J. Zaragoza, and V. G. Agelidis, "Control of circulating currents in modular multilevel converters

through redundant voltage levels," *IEEE Transactions on Power Electronics*, vol. 31, no. 11, pp. 7761 – 7769, Nov 2016.

[112] L. Angquist, A. Antonopoulos, D. Siemaszko, K. Ilves, M. Vasiladiotis, and H.-P. Nee, "Inner control of modular multilevel converters - an approach using open-loop estimation of stored energy," in *Proc. of International Power Electronics Conference (IPEC)*, June 2010, pp. 1579 – 1585.

[113] J. J. Jung, H. J. Lee, and S. K. Sul, "Control of the modular multilevel converter for variable-speed drives," in *Proc. of IEEE International Conference on Power Electronics, Drives and Energy Systems (PEDES)*, Dec 2012, pp. 1 – 6.

[114] S. Rodrigues, R. Teixeira, and P. Bauer, *Dynamic Modeling and Control of VSC-based Multi-terminal DC Networks*, L. L. A. Publishing, Ed. Lap Lambert Academic Publishing, 2012.

[115] T. M. Haileselassie, "Control, dynamics and operation of multi-terminal vsc-hvdc transmission systems," Ph.D. dissertation, Norwegian University of Science and Technology, Faculty of Information Technology, 2012.

[116] A. Yazdani and R. Iravani, "A unified dynamic model and control for the voltage-sourced converter under unbalanced grid conditions," *IEEE Transactions on Power Delivery*, vol. 21, no. 3, pp. 1620 – 1629, July 2006.

[117] G. Carrara, S. Gardella, M. Marchesoni, R. Salutari, and G. Sciutto, "A new multilevel pwm method: a theoretical analysis," *IEEE Transactions on Power Electronics*, vol. 7, no. 3, pp. 497 – 505, Jul 1992.

[118] R. Darus, G. Konstantinou, J. Pou, S. Ceballos, and V. G. Agelidis, "Carrier interleaved pwm techniques in modular multilevel converters: A comparison based on same voltage level waveforms," in *Proc. of Energy Conversion Congress and Exposition (ECCE)*, Sept 2014, pp. 3725 – 3730.

[119] J. Mei, K. Shen, B. Xiao, L. M. Tolbert, and J. Zheng, "A new selective loop bias mapping phase disposition pwm with dynamic voltage balance capability for modular multilevel converter," *IEEE Transactions on Industrial Electronics*, vol. 61, no. 2, pp. 798 – 807, Feb 2014.

[120] G. S. Konstantinou and V. G. Agelidis, "Performance evaluation of half-bridge cascaded multilevel converters operated with multicarrier sinusoidal pwm techniques," in *Proc. of IEEE Conference on Industrial Electronics and Applications (ICIEA)*, May 2009, pp. 3399 – 3404.

[121] Y. Li, Y. Wang, and B. Q. Li, "Generalized theory of phase-shifted carrier pwm for cascaded h-bridge converters and modular multilevel converters,"

IEEE Journal of Emerging and Selected Topics in Power Electronics, vol. 4, no. 2, pp. 589 – 605, June 2016.

[122] G. Konstantinou, J. Pou, S. Ceballos, R. Darus, and V. G. Agelidis, "Switching frequency analysis of staircase-modulated modular multilevel converters and equivalent pwm techniques," *IEEE Transactions on Power Delivery*, vol. 31, no. 1, pp. 28 – 36, Feb 2016.

[123] S. Kouro, R. Bernal, H. Miranda, C. Silva, and J. Rodriguez, "High-performance torque and flux control for multilevel inverter fed induction motors," *IEEE Transactions on Power Electronics*, vol. 22, no. 6, pp. 2116 – 2123, Nov 2007.

[124] H. Liu, G. H. Cho, and S. Park, "Optimal pwm design for high power three-level inverter through comparative studies," *IEEE Transactions on Power Electronics*, vol. 10, no. 1, pp. 38 – 47, Jan 1995.

[125] K. El-Naggar and T. H. Abdelhamid, "Selective harmonic elimination of new family of multilevel inverters using genetic algorithms," *Energy Conversion and Management*, vol. 49, no. 1, pp. 89 – 95, July 2008.

[126] W. Fei, X. Ruan, and B. Wu, "A generalized formulation of quarter-wave symmetry she-pwm problems for multilevel inverters," *IEEE Transactions on Power Electronics*, vol. 24, no. 7, pp. 1758 – 1766, July 2009.

[127] M. Dahidah, G. Konstantinou, N. Flourentzou, and V. Agelidis, "On comparing the symmetrical and non-symmetrical selective harmonic elimination pulse-width modulation technique for two-level three-phase voltage source converters," *Power Electronics, IET*, vol. 3, no. 6, pp. 829 – 842, Nov 2010.

[128] T. Liang, R. O'Connell, and R. Hoft, "Inverter harmonic reduction using walsh function harmonic elimination method," *IEEE Transactions on Power Electronics*, vol. 12, no. 6, pp. 971 – 982, Nov 1997.

[129] J. Chiasson, L. Tolbert, K. McKenzie, and Z. Du, "A new approach to solving the harmonic elimination equations for a multilevel converter," in *Proc. of Industry Applications Conference (38th IAS Annual Meeting)*, vol. 1, Oct 2003, pp. 640 – 647.

[130] J. N. Chiasson, L. M. Tolbert, Z. Du, and K. J. McKenzie, "The use of power sums to solve the harmonic elimination equations for multilevel converters," *European Power Electronics and Drives Journal*, vol. 15, no. 1, pp. 19 – 27, February 2005.

[131] A. I. Maswood, S. Wei, and M. Rahman, "A flexible way to generate pwm-she switching patterns using genetic algorithm," in *Proc. of Applied Power*

Electronics Conference and Exposition (APEC), vol. 2, 2001, pp. 1130 – 1134.

[132] K. El-Naggar and T. Abdelhamid, "Selective harmonic elimination of new family of multilevel inverters using genetic algorithms," *Energy Conversion and Management*, vol. 49, no. 1, pp. 89 – 95, 2008.

[133] Z. Salam, A. Majed, and A. Amjad, "Design and implementation of 15-level cascaded multi-level voltage source inverter with harmonics elimination pulse-width modulation using differential evolution method," *IET Power Electronics*, vol. 8, no. 9, pp. 1740 – 1748, 2015.

[134] H. Taghizadeh and M. Hagh, "Harmonic elimination of cascade multilevel inverters with nonequal dc sources using particle swarm optimization," *IEEE Transactions on Industrial Electronics*, vol. 57, no. 11, pp. 3678 – 3684, Nov 2010.

[135] J. Pou, S. Ceballos, G. Konstantinou, G. J. Capella, and V. G. Agelidis, "Control strategy to balance operation of parallel connected legs of modular multilevel converters," in *Proc. of International Symposium on Industrial Electronics (ISIE)*, May 2013, pp. 1 – 7.

[136] M. Saeedifard and R. Iravani, "Dynamic performance of a modular multilevel back-to-back hvdc system," *IEEE Transactions on Power Delivery*, vol. 25, no. 4, pp. 2903 – 2912, Oct 2010.

[137] K. Ilves, A. Antonopoulos, S. Norrga, and H.-P. Nee, "A new modulation method for the modular multilevel converter allowing fundamental switching frequency," *IEEE Transactions on Power Electronics*, vol. 27, no. 8, pp. 3482 – 3494, Aug 2012.

[138] A. Lesnicar and R. Marquardt, "An innovative modular multilevel converter topology suitable for a wide power range," in *Proc. of IEEE Power Tech Conference Proceedings*, vol. 3, June 2003, p. 6.

[139] F. Deng and Z. Chen, "A control method for voltage balancing in modular multilevel converters," *IEEE Transactions on Power Electronics*, vol. 29, no. 1, pp. 66 – 76, Jan 2014.

[140] K. Ilves, L. Harnefors, S. Norrga, and H.-P. Nee, "Predictive sorting algorithm for modular multilevel converters minimizing the spread in the submodule capacitor voltages," *IEEE Transactions on Power Electronics*, vol. 30, no. 1, pp. 440 – 449, Jan 2015.

[141] S. Fan, K. Zhang, J. Xiong, and Y. Xue, "An improved control system for modular multilevel converters with new modulation strategy and voltage

balancing control," *IEEE Transactions on Power Electronics*, vol. 30, no. 1, pp. 358 – 371, Jan 2015.

[142] ——, "An improved control system for modular multilevel converters featuring new modulation strategy and voltage balancing control," in *IEEE Energy Conversion Congress and Exposition (ECCE)*, Sept 2013, pp. 4000 – 4007.

[143] Q. Tu, Z. Xu, H. Huang, and J. Zhang, "Parameter design principle of the arm inductor in modular multilevel converter based hvdc," in *Proc. of International Conference on Power System Technology (POWERCON)*, Oct 2010, pp. 1 – 6.

[144] B. Chen, Y. Chen, C. Tian, J. Yuan, and X. Yao, "Analysis and suppression of circulating harmonic currents in a modular multilevel converter considering the impact of dead time," *IEEE Transactions on Power Electronics*, vol. 30, no. 7, pp. 3542 – 3552, July 2015.

[145] L. He, K. Zhang, J. Xiong, and S. Fan, "A repetitive control scheme for harmonic suppression of circulating current in modular multilevel converters," *IEEE Transactions on Power Electronics*, vol. 30, no. 1, pp. 471 – 481, Jan 2015.

[146] Z. Li, P. Wang, Z. Chu, H. Zhu, Y. Luo, and Y. Li, "An inner current suppressing method for modular multilevel converters," *IEEE Transactions on Power Electronics*, vol. 28, no. 11, pp. 4873 – 4879, Nov 2013.

[147] H. Aggrawal, J. I. Leon, L. G. Franquelo, S. Kouro, P. Garg, and J. Rodríguez, "Model predictive control based selective harmonic mitigation technique for multilevel cascaded h-bridge converters," in *Proc. of Conference on IEEE Industrial Electronics Society (IECON)*, Nov 2011, pp. 4427 – 4432.

[148] A. Marzoughi and H. Imaneini, "An optimal selective harmonic mitigation for cascaded h-bridge converters," in *Proc. of International Conference on Environment and Electrical Engineering (EEEIC)*, May 2012, pp. 752 – 757.

[149] M. Najjar, A. Moeini, M. K. Bakhshizadeh, F. Blaabjerg, and S. Farhangi, "Optimal selective harmonic mitigation technique on variable dc link cascaded h-bridge converter to meet power quality standards," *IEEE Journal of Emerging and Selected Topics in Power Electronics*, vol. 4, no. 3, pp. 1107 – 1116, Sept 2016.

[150] Y. Liu, H. Hong, and A. Huang, "Real-time algorithm for minimizing thd

in multilevel inverters with unequal or varying voltage steps under staircase modulation," *IEEE Transactions on Industrial Electronics*, vol. 56, no. 6, pp. 2249 – 2258, June 2009.

[151] Y. Liu, H. Hong, and A. Q. Huang, "Real-time calculation of switching angles minimizing thd for multilevel inverters with step modulation," *IEEE Transactions on Industrial Electronics*, vol. 56, no. 2, pp. 285 – 293, Feb 2009.

[152] W. Fei, X. Du, and B. Wu, "A generalized half-wave symmetry she-pwm formulation for multilevel voltage inverters," *IEEE Transactions on Industrial Electronics*, vol. 57, no. 9, pp. 3030 – 3038, Sept 2010.

[153] G. S. Konstantinou and V. G. Agelidis, "Bipolar switching waveform: Novel solution sets to the selective harmonic elimination problem," in *Proc. of IEEE International Conference on Industrial Technology (ICIT)*, March 2010, pp. 696 – 701.

[154] G. Konstantinou and V. Agelidis, "On re-examining symmetry of two-level selective harmonic elimination pwm: Novel formulations, solutions and performance evaluation," *Electric Power Systems Research*, vol. 108, pp. 185 – 197, 2014, "".

[155] W. Fei, B. Wu, and Y. Huang, "Half-wave symmetry selective harmonic elimination method for multilevel voltage source inverters," *IET Power Electronics*, vol. 4, no. 3, pp. 342 – 351, March 2011.

[156] J. R. Wells, X. Geng, P. L. Chapman, P. T. Krein, and B. M. Nee, "Modulation-based harmonic elimination," *IEEE Transactions on Power Electronics*, vol. 22, no. 1, pp. 336 – 340, Jan 2007.

[157] R. P. Aguilera, P. Lezana, G. Konstantinou, P. Acuna, B. Wu, S. Bernet, and V. G. Agelidis, "Closed-loop she-pwm technique for power converters through model predictive control," in *Industrial Electronics Society, IECON 2015 - 41st Annual Conference of the IEEE*, Nov 2015, pp. 5261–5266.

[158] R. Aguilera, P. Acuna, P. Lezana, G. Konstantinou, B. Wu, S. Bernet, and V. Agelidis, "Selective harmonic elimination model predictive control for multilevel power converters," *IEEE Transactions on Power Electronics*, vol. PP, no. 99, pp. 1–1, 2016.

[159] J. Sun and H. Grotstollen, "Solving nonlinear equations for selective harmonic eliminated pwm using predicted initial values," in *Proc. of IEEE*

Conference of Industrial Electronics (IECON), Nov 1992, pp. 259 – 264 vol.1.

[160] J. Chen, T. Liang, and S. Wang, "A novel design and implementation of programmed pwm to eliminate harmonics," in *Proc. of IEEE Industrial Electronics Society (IECON)*, Nov 2005, p. 6.

[161] V. G. Agelidis, A. Balouktsis, and I. Balouktsis, "On applying a minimization technique to the harmonic elimination pwm control: the bipolar waveform," *IEEE Power Electronics Letters*, vol. 2, no. 2, pp. 41 – 44, June 2004.

[162] J. N. Chiasson, L. M. Tolbert, K. J. McKenzie, and Z. Du, "Elimination of harmonics in a multilevel converter using the theory of symmetric polynomials and resultants," *IEEE Transactions on Control Systems Technology*, vol. 13, no. 2, pp. 216 – 223, March 2005.

[163] K. Yang, Q. Zhang, R. Yuan, W. Yu, J. Yuan, and J. Wang, "Selective harmonic elimination with groebner bases and symmetric polynomials," *IEEE Transactions on Power Electronics*, vol. 31, no. 4, pp. 2742 – 2752, April 2016.

[164] D. Ahmadi, K. Zou, C. Li, Y. Huang, and J. Wang, "A universal selective harmonic elimination method for high-power inverters," *IEEE Transactions on Power Electronics*, vol. 26, no. 10, pp. 2743 – 2752, Oct 2011.

[165] H. Huang, S. Hu, and D. Czarkowski, "A novel simplex homotopic fixed-point algorithm for computation of optimal pwm patterns," in *Proc. of Power Electronics Specialists Conference (PESC)*, vol. 2, June 2004, pp. 1263 – 1267.

[166] M. Balasubramonian and V. Rajamani, "Design and real-time implementation of shepwm in single-phase inverter using generalized hopfield neural network," *IEEE Transactions on Industrial Electronics*, vol. 61, no. 11, pp. 6327 – 6336, Nov 2014.

[167] B. Ozpineci, L. M. Tolbert, and J. N. Chiasson, "Harmonic optimization of multilevel converters using genetic algorithms," *IEEE Power Electronics Letters*, vol. 3, no. 3, pp. 92 – 95, Sept 2005.

[168] S. G. Rosu, C. Radoi, A. Florescu, P. Guglielmi, and M. Pastorelli, "The analysis of the solutions for harmonic elimination pwm bipolar waveform with a specialized differential evolution algorithm," in *Proc. of International Conference on Optimization of Electrical and Electronic Equipment (OPTIM)*, May 2012, pp. 814 – 821.

[169] M. S. A. Dahidah and V. G. Agelidis, "A hybrid genetic algorithm for selective harmonic elimination control of a multilevel inverter with non-equal dc sources," in *Proc. of International Conference on Power Electronics and Drives Systems ((PEDS))*, vol. 2, 2005, pp. 1205 – 1210.

[170] ——, "Generalized formulation of multilevel selective harmonic elimination pwm: Case i -non-equal dc sources," in *Proc. of IEEE Power Electronics Specialists Conference (PESC)*, June 2006, pp. 1 – 6.

[171] M. S. A. Dahidah and M. V. C. Rao, "A hybrid genetic algorithm for selective harmonic elimination pwm ac/ac converter control," *Electrical Engineering*, vol. 89, no. 4, pp. 285 – 291, 2007.

[172] V. G. Agelidis, A. Balouktsis, I. Balouktsis, and C. Cossar, "Multiple sets of solutions for harmonic elimination pwm bipolar waveforms: analysis and experimental verification," *IEEE Transactions on Power Electronics*, vol. 21, no. 2, pp. 415 – 421, March 2006.

[173] Z. Michalewicz, *Genetic algorithms + Data structures = Evolution programs*. Springer Science & Business Media, 1996.

[174] V. G. Agelidis, A. I. Balouktsis, and C. Cossar, "On attaining the multiple solutions of selective harmonic elimination pwm three-level waveforms through function minimization," *IEEE Transactions on Industrial Electronics*, vol. 55, no. 3, pp. 996 – 1004, March 2008.

[175] J. Kumar, B. Das, and P. Agarwal, "Selective harmonic elimination technique for a multilevel inverter," in *Proc. of Fifteenth National Power Systems Conference (NPSC)*, Bombay, India, 2008.

[176] F. Filho, H. Maia, T. Mateus, B. Ozpineci, L. Tolbert, and J. Pinto, "Adaptive selective harmonic minimization based on anns for cascade multilevel inverters with varying dc sources," *IEEE Transactions on Industrial Electronics*, vol. 60, no. 5, pp. 1955 – 1962, May 2013.

[177] A. Perez-Basante, I. M. de Alegria, S. C. J. I. Garate, and J. L. Martín, "Eliminación selectiva de armónicos en convertidores multinivel modulares para todo el rango del Índice de modulación de amplitud," in *Proc. of Seminario Anual de Automática, Electrónica Industrial y Automatización*, 2014, pp. 1 – 6.

[178] A. Perez-Basante, S. Ceballos, G. Konstantinou, J. Pou, J. Andreu, and . M. de Alegría, "A universal formulation for selective harmonic elimination pwm with half-wave symmetry for multilevel voltage source converters," in *Proc.*

of Annual Conference of the IEEE Industrial Electronics Society (IECON), Oct 2016, pp. 3207 – 3212.

[179] A. Perez-Basante, S. Ceballos, G. Konstantinou, J. Pou, J. Andreu, and I. M. de Alegria, "(2n+1) selective harmonic elimination-pwm for modular multilevel converters: A generalized formulation and a circulating current control method," *IEEE Transactions on Power Electronics*, vol. PP, no. 99, pp. 1 – 1, 2017.

[180] S. Sirisukprasert, J.-S. Lai, and T.-H. Liu, "Optimum harmonic reduction with a wide range of modulation indexes for multilevel converters," *IEEE Transactions on Industrial Electronics*, vol. 49, no. 4, pp. 875 – 881, Aug 2002.

[181] M. Dahidah and V. Agelidis, "Selective harmonic elimination pwm control for cascaded multilevel voltage source converters: A generalized formula," *IEEE Transactions on Power Electronics*, vol. 23, no. 4, pp. 1620 – 1630, July 2008.

[182] A. Maswood, M. Rashid, and L. Jian, "Optimal pwm-she switching on npc inverter: a winning match for high power conversion," *Electric Power Systems Research*, vol. 48, no. 1, pp. 19 – 24, 1998.

[183] (2017) Mathworks. [Online]. Available: https://es.mathworks.com/products/matlab.html

[184] H. Taghizadeh and M. T. Hagh, "Harmonic elimination of cascade multilevel inverters with nonequal dc sources using particle swarm optimization," *IEEE Transactions on Industrial Electronics*, vol. 57, no. 11, pp. 3678 – 3684, Nov 2010.

[185] (2017) dspace 1103, solutions for control. [Online]. Available: http://www.dspace.com/ww/en/pub/home.cfm

[186] S. S. Fazel, S. Bernet, D. Krug, and K. Jalili, "Design and comparison of 4-kv neutral-point-clamped, flying-capacitor, and series-connected h-bridge multilevel converters," *IEEE Transactions on Industry Applications*, vol. 43, no. 4, pp. 1032 – 1040, July 2007.